Measurement of conductivity of intumescing materials

Anne Beth Auklend Krohn

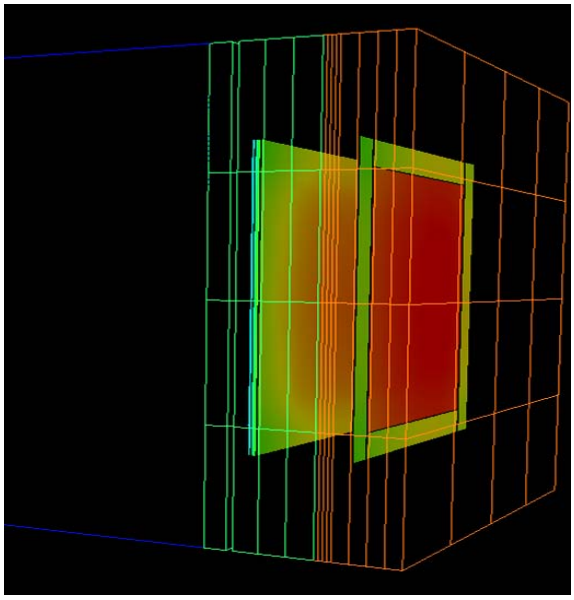

Submitted in partial fulfilment of the requirements for the degree of
Master of Science in Process Technology – Safety Technology
June 2009

Faculty of Mathematics and Natural Sciences,
University of Bergen

The picture at the front page on the left side is from a personal archive showing the furnace while performing one of the experiments done as a part of this thesis. The picture on the right side is from the visualizing programme GL View showing the simulated furnace.

Preface

All graduating students from the master programme process technology from the University of Bergen need to submit a master thesis as a part of their degree. Standardized workload for the master thesis is 60 credit points, which corresponds to approximately 40 working weeks.

The theme for this thesis was given by the company Petrell AS in co-operation with Sintef NBL AS. The project's aim was to develop a test method for finding the thermal conductivity of intumescing materials, including both experiments and numerical simulations. Petrell AS contributed by giving access to the simulation programme Brilliant whilst the physical experiments were performed at Sintef NBL AS.

Throughout the completion of this thesis several people have been of great help, and I would especially like to thank:

- Geir Berge, Petrell AS, for guidance and professional advise
- Kristen Opstad, Petrell AS, for guidance and professional advise
- Bjørn Egil Rossebø, Sintef NBL AS, for technical assistance with the test equipment
- Anne Elise Steen Hansen, Sintef NBL AS, for professional advice
- Petrell AS for supplying office space
- Employees at the Norwegian Fire Resource Centre for technical assistance and for letting me be present at several interesting fire tests

Trondheim, 2. June 2009

Anne Beth Auklend Krohn

Table of contents

Table of figures

Abstract

The main objective of this thesis was to develop a test method for finding the thermal conductivity of intumescing materials to be used in numerical simulations. When simulating for instance fire exposure to a construction protected by a Passive Fire Protection (PFP) material, the physical properties of the PFP materials are very often unknown. Many PFP materials have physical properties that vary with temperature and the accuracy and availability of these data is often inadequate.

This thesis is based on previous work by Sintef NBL AS and Petrell AS, where a furnace was developed and built for use in experiments (1) (2). The principle of this furnace was to expose a PFP material mounted onto a steel plate to a known heat flux given by three vertical radiation foils. Temperatures were measured on the unexposed side of the steel plate to see how much heat had been transmitted. Data obtained from experiments was used as input to the numerical simulation programme Brilliant. Results from the experiments would then be compared with the simulated values. A summary of the experiments that were simulated together with the essential results are shown in chapter 4, Table 6, while an overview of all the experiment and simulations performed are shown in Appendix A.

Experiments without PFP materials were first carried out to see if the furnace could be used to yield reliable results and whether the experiments were repeatable. A carbon steel plate was used as the test specimen. The input power was decided by measuring the surface temperature on one of the radiation foils. This method was concluded to be insufficient, because the experiments kept resulting in very different power curves. Three independent bits of foil were then installed in the furnace for the purpose of controlling the input power based on measuring the temperature on one of them. As these bits of foil were not connected to any power supplies, it was possible to weld thermocouples onto them, which gave more accurate measurements. The experiments became reproducible and the measured temperatures matched the simulated results.

After improving the furnace, experiments were performed with both dead and intumescing isolation protecting the carbon steel plate. Thermal conductivities for the dead materials were given by the manufacturer, and resulted in good correspondences between measured and numerically simulated values. As the thermal properties of the intumescing PFP material were unknown, these values had to be guessed and put into the simulation programme. The resulting simulated temperatures on the unexposed side of the steel plate were then compared to the measured temperatures. When the data became comparable, the correct thermal conductivities were found. This procedure is shown as a flow diagram in Figure 1.

The developed test method has been used to find the thermal conductivity of four different test specimens of intumescing materials, for temperatures from 20 °C to 800 °C. These values may be applied in numerical simulations within the same temperature range.

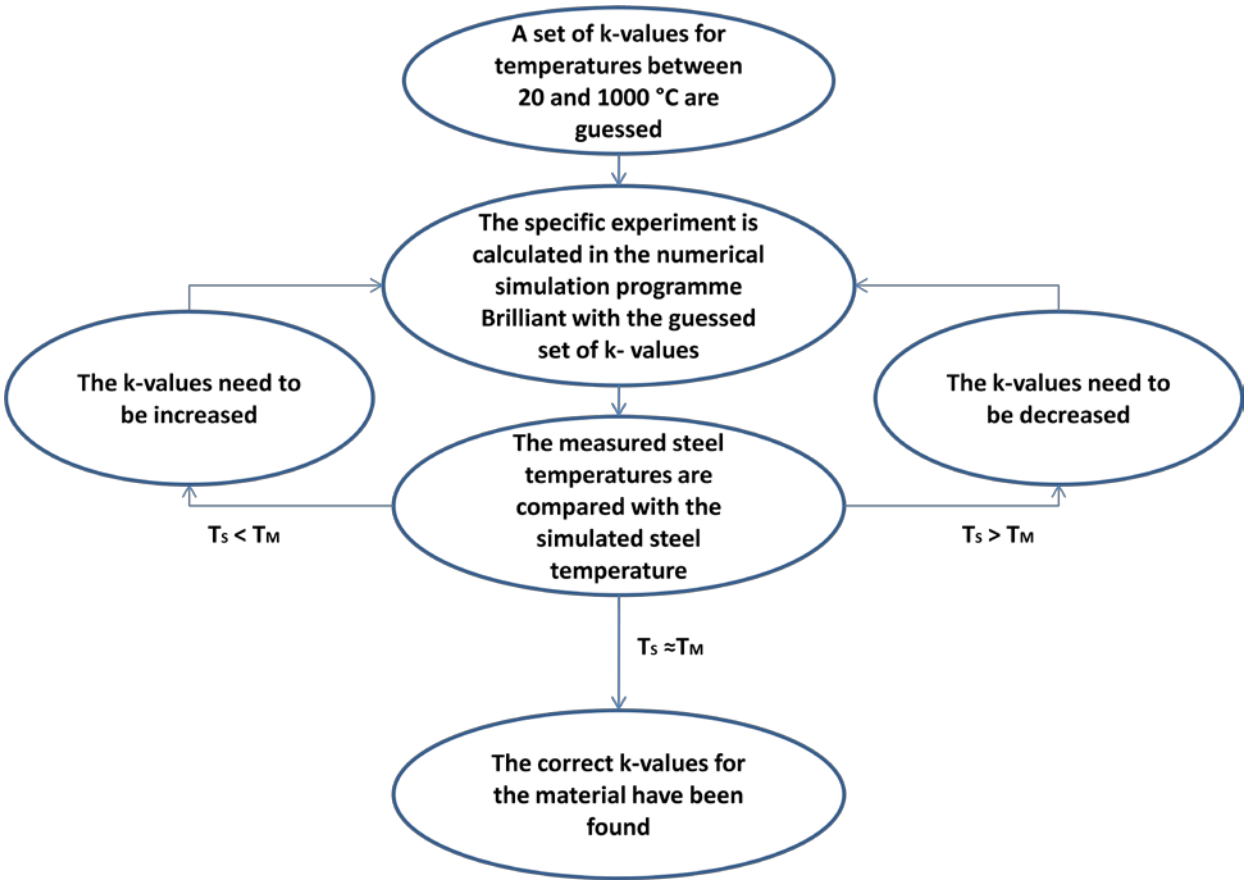

Figure 1 shows a flow diagram for finding the thermal conductivity of intumescing materials. T_s denotes the simulated steel temperature, while T_m denotes the measured steel temperature.

Some issues still remain in the development of the furnace. Foil breakages represent a recurring problem. There is also a desire to obtain a higher heat flux, so that k-values for temperatures up to 1100 °C can be found.

This work demonstrates the many challenges related to numerical simulations and physical experiments. The number of experiments that have been performed without reproducibility indicates how sensitive test apparatus can be and how difficult it is to achieve good measured results.

1 Introduction

This chapter will include the background for this project, its aim and limitations. It will also include a list of symbols used in the report together with some definitions.

1.1 Background

The use of numerical simulation tools in the oil and gas industry has increased during the last years. It is very common to use simulation tools in this type of industry in affiliation with developing and verification studies concerning safety and hazards. A challenge with using simulation tools is the access of reliable input data, which is of great importance in numerical simulations. Fire and heat flux loadings in physical simulation models may be reasonably realistic, but as long as the thermal properties of the materials are unknown and partly guessed, the final simulation results are less reliable (1).

Several types of passive fire protection (PFP) materials have physical properties that vary with temperature (See Table 1, part 2.1.1). Constructions that are protected with fire protection materials represent an area in which simulation input data is limited. Based on this lack of material data, the goal for this project is to develop a method for measuring the thermal conductivity for PFP materials.

Sintef NBL AS and Petrell AS have already been working on developing a measuring method aimed at finding the thermal conductivity of PFP materials. Two reports based on this work are published (1) (2). A part of the work involved the development and building of a testing apparatus, consisting of a control panel, a thyristor, a transformer and a test furnace, which was then used for experiments. The principle of the test furnace was to expose a PFP material mounted onto a steel plate to a known heat flux. The temperature was measured on the unexposed side of the steel plate to see how much heat had been transmitted. Then it would be possible to calculate the thermal conductivity of the PFP material with help from the numerical simulation programme Brilliant. Some initial experiments were performed (2). The next step will be to perform new experiments and subsequently simulate those experiments for comparison and possibly develop the furnace further.

This project is relevant for all fire engineering work where steel constructions need to be protected against fire. It is especially important to use isolation with low thermal conductivity around critical steel constructions where the risk of exposure to hydrocarbon fire is high.

1.2 Objectives

The first objective of this project is to find out whether the current test apparatus, developed by Sintef NBL AS and Petrell AS, can provide reliable thermal properties data for PFP materials. This involves ensuring that experiments are reproducible, and that there is a good correspondence between the experimental and simulated results. A deviance of less

than 5 % in the steady state between experiments and between experiments and simulations will be considered a very good result. See end of part 2.3 for further explanation.

The second objective is, if reasonable, to improve the method of assessment of the thermal properties, both in terms of calculations and experimental setup. The effect of making a simple, but credible testing method would be of great value, both to save money on materials and to save time on performing tests.

1.3 Limitations on the scope of work

Since most PFP on structures are installed to protect against the first occurrence of a fire situation, the test specimens will only be tested once. Testing will be limited to test specimen of a fixed dimension of (0.45x0.45) m^2.

The test method in general and the data obtained from the method will be discussed. However the test specimens' suitability as PFP materials will not be evaluated in terms of adhesion and other essential properties.

The Brilliant code is considered as a numerical simulation tool to be used by the author to derive thermal properties of test specimen from tests. Any improvements, if necessary, of the numerical simulation tool are considered to be outside the scope of work.

1.4 Symbols and definitions

Symbols

A	Area	$[m^2]$
k	Coefficient of thermal conductivity	$\left[W/m \cdot K\right]$
$\dot{q}''_c$	Heat flux convection	$\left[W/m^2\right]$
I	Current	$[A]$
h	Convective heat transfer coefficient	$\left[W/m^2 \cdot K\right]$
ρ	Density	$\left[kg/m^3\right]$
ε	Emissivity	$[-]$
P	Energy	$[J]$
$\dot{q}$	Heat flow (power)	$[W]$
$\dot{q}''$	Heat flux	$\left[W/m^2\right]$
$\dot{q}''_r$	Heat flux radiation	$\left[W/m^2\right]$

$\dot{q}_t''$	Heat flux transmission	$\left[W/m^2\right]$
J	Joule, energy	$\left[kg \cdot m^2/s^2\right]$
C_p	Specific heat capacity	$\left[J/kg \cdot K\right]$
σ	Stefan Boltzmann constant	$\left[5.669 \cdot 10^{-8} W/m^2 \cdot K^4\right]$
T	Temperature	$[K]$
ΔT	Temperature difference	$[K]$
Δx	Thickness	$[m]$
U	Voltage difference	$[V]$
V	Volume	$[m^3]$

SI-units have been used in this report.

Term	**Definition**
Adiabatic	In an adiabatic system there is no energy exchange with the surroundings.
Benarx F Flexi Roll	A PFP material, based on solid epoxy compounds, developed by Beerenberg Corp. AS (3)
Brilliant	A CFD-code (Computational Fluid Dynamics) based on object technology for analysis of transient and stationary phenomena (4).
Chartek 7	Chartek 7 is a high performance epoxy intumescent fire protection coating system developed by International Protective Coatings (5)
Control volume	A mathematical abstraction employed in the process of creating mathematical models of physical processes. A control volume is an object with maximum eight corners and minimum four. It is a geometrical physical volume. All characteristics like temperature and velocity is in the control volume. Control volumes are in this project used in the simulation programme Brilliant.
Dead material	Dead materials are in this report defined as passive fire protection materials that maintain their physical dimensions when exposed to heat.
Delivered power	The delivered power is defined in this report as the power delivered to the furnace, which is the power registered from the control panel less heat loss to the copper plates holding the radiation foils in place.
Epoxy	Epoxy is a plastic material where the molecules will polymerize when mixed with a catalyzing agent like heat. Epoxies are often used as

	intumescing isolation materials (6).
Firemaster	Product name of a ‘dead’ isolation material produced by Morgan Thermal Ceramics. It is manufactured from alkaline earth silicate fibres suitable for use in both cellulosic, hydrocarbon and jet fire protection applications (7).
GL View	GL View is a visualizing programme that can for instance read files and show results from the CFD code Brilliant.
Heat Release Rate (HRR)	The rate at which heat is generated by fire measured in Watts.
Intumescing material	A passive fire protection material that expands when exposed to fire. There are various types of intumescents (8).
Kaowool	Product name of a ‘dead’ isolation material produced by Morgan Thermal ceramics. It is a vacuum mould plate built up from ceramic fibres (9).
Knufoil	A type of foil made up from stainless steel that consists of nickel and chrome (10). Knufoil is in this project used for heat radiation in the furnace.
Passive fire protection material	PFP material is a material with low thermal conductivity, which purpose is to cover, and thus protect, other materials.
ProTek	ProTek is a product name of an intumescent isolation material produced by Solent Composite Systems (11).
Siporex	A type of light-weight concrete.
Thermal conductivity, k	Characterizes the ability of a material to transfer heat. A low number signifies slow heat transfer. The thermal conductivity of materials may changes as a function of temperature (12).

2 Theory

This chapter will highlight the theory behind the experiments and the numerical simulations, which consists of the following main parts:

- Thermal properties of materials
- Passive fire protection materials
- Measuring the conductivity of fire protection materials
- Temperature reading by means of thermocouples
- Software

The first part will give an overview of the theory regarding general thermal properties, such as conductivity, heat capacity, density and emissivity of materials in general, before discussing carbon steel especially.

2.1 Thermal properties of materials

The following parts will treat the most important thermal properties of passive fire protection (PFP) materials. The fire protecting abilities of PFP materials depend on chemical and physical reactions during heat exposure. The thermal properties of a material may also differ between the first and subsequent (second or third) exposures to heat.

For many materials, the behaviour upon heat exposure will also depend on the heat flux level, rate of heating, thickness, geometrical shape and density of the material, etc. (1).

2.1.1 Thermal conductivity

Conduction is a form of heat transfer. Heat will flow from an area of high temperature towards one of lower temperature. This flow can be expressed as heat flux, which in one direction is given by:

$$\dot{q}''_x = -k \cdot \frac{\Delta T}{\Delta x}$$

Where ΔT is the temperature difference over distance Δx, also called the temperature gradient. This formula is known as Fourier's Law of heat conduction. The constant *k* is the thermal conductivity and has units of $W/m \cdot K$ when $\dot{q}''$ is in W/m^2, T is given in *K*, and x is in meters (*m)*. The constant *k* characterizes the ability of a material to transfer heat. The minus sign in the equation indicates that the direction of heat flow is from hot to cold, or down the temperature gradient.

The thermal conductivity of materials changes as a function of temperature. How much it changes depends on which aggregate state the materials are in. Gases and liquids have atoms and molecules that move relatively free and transfer heat by collisions. In solid materials, it is mainly electrons that make the energy move. Usually, it is easier to move heat

in a solid material than in gases or liquids. This means that the conductivity is usually larger for solids (12).

There is a lack of data on thermal conductivity at different temperatures, especially for intumescing fire protection materials (1).

The thermal conductivity of the materials used in this project is shown in Table 1, (9) (13) (14) (15), except from ProTek which is shown in Appendix G.

Table 1 shows the thermal conductivity of a selection of materials at different temperatures.

Type of material	Temperature [°C]	Thermal conductivity [W/mK]
Carbon steel	20	45.8
	300	41.4
	500	37
	900	28.2
Foamglas	0	0.036
	20	0.04
	120	0.059
	330	0.114
	800	0.8
	1000	1.2
Kaowool 1400	20	0.06
	200	0.06
	300	0.07
	400	0.08
	500	0.09
	600	0.10
	800	0.13
	1000	0.18
	1200	0.23
Siporex	20	0.138
FireMaster607 128	20	0.04
	200	0.04
	400	0.09
	600	0.13
	800	0.19
	1000	0.25

Thermal conductivity in porous materials

In this project porous materials like Siporex, Kaowool and Firemaster have been used. For these materials the measured thermal conductivity *k* will include all the three different types of heat transfer that happens in the material. These are conduction, convection and radiation. *k* is then not a material constant, because the thermal properties of gasses and

liquids residing in the pores will change during exposure to heat. Especially moisture has a great influence.

For calculation the radiation through the material, the emissivity and the temperature difference in the material must be known. There will also be convection in the pores. This takes place in tiny cavities inside the porous material. The total amount of heat transfer in a cavity is:

$$q = q_{tc} + q_d + q_r + q_c$$

The indexes stand for thermal conductivity, diffusion, radiation and convection. The convective heat transfer coefficient *h [W/m^{2}K]* depends on the characteristics of the system, the geometry of the solid and the properties of the fluid including flow parameters, and it is also a function of temperature difference (16).

The total thermal conductivity *k* for a porous material depends on temperature, the material's porosity, moisture content and the gas filling in the pores. All the forms of heat transfer depend on temperature. As a rule, heat transfer with conduction rises with temperature and decreases towards zero when T goes towards zero degrees Kelvin. Convection in the pores rises with high temperatures and the radiation rises with the fourth power of the temperature. A general rule is therefore that *k* rises with temperature for porous materials (16).

Both pore volume and pore structure has an impact of *k*. For most building materials *k* is quite large for the solid part of the material. This value is often around 3-4 W/mK. However the air inside the pores is only 0.025 W/mK. The amount of air in proportion to the solid material therefore has an impact of *k*. Convection increases with increasing the pore sizes, but the increase is small. It is first when the pores and cavities are big that the convection really makes an impact. The heat transfer with radiation is however in inverse ratio with the number of times the radiation gets interrupted. The pore structures impact on *k* is a result of the radiation. *k* decreases when the density of the porous material increases, because the number of radiation transitions rises, but when the material gets more packed, conduction takes over to be the main heat transfer mechanism, and the *k* value start to rise again (16).

As mentioned earlier the moisture content in porous materials has a strong impact on the conductivity. The conductivity of water is 0.6 W/mK and for ice it is 1.7 W/mK. These values are higher than the conductivity of air which is 0.025. The conductivity rises with the moist content. Relatively low moist contents can often give an increase in the k-value far beyond what the ratio of water content to pore volume should call for. What happens is that the smallest pores, which are the ones that isolates the most, get filled with water first. The heat transport rises where the pores are bigger and the water has only moistened the pore walls. The water evaporates on the hottest side of the pore wall and diffuse over to the cooler side

where it condensates. This way, the waters large heat of evaporation, approximately $2.3 \cdot 10^6 \, J / kg$, contributes to the heat transport (16).

When materials are applied as insulation, their purpose is to protect another material and keep it from catching fire. It is the air in between the material structure that principally isolate. As the temperature goes up, the convection increases and so does the radiation. Hence it follows that the conduction increases. An example of this is shown in Figure 2 where the isolation material Kaowool is used as a demonstration (9).

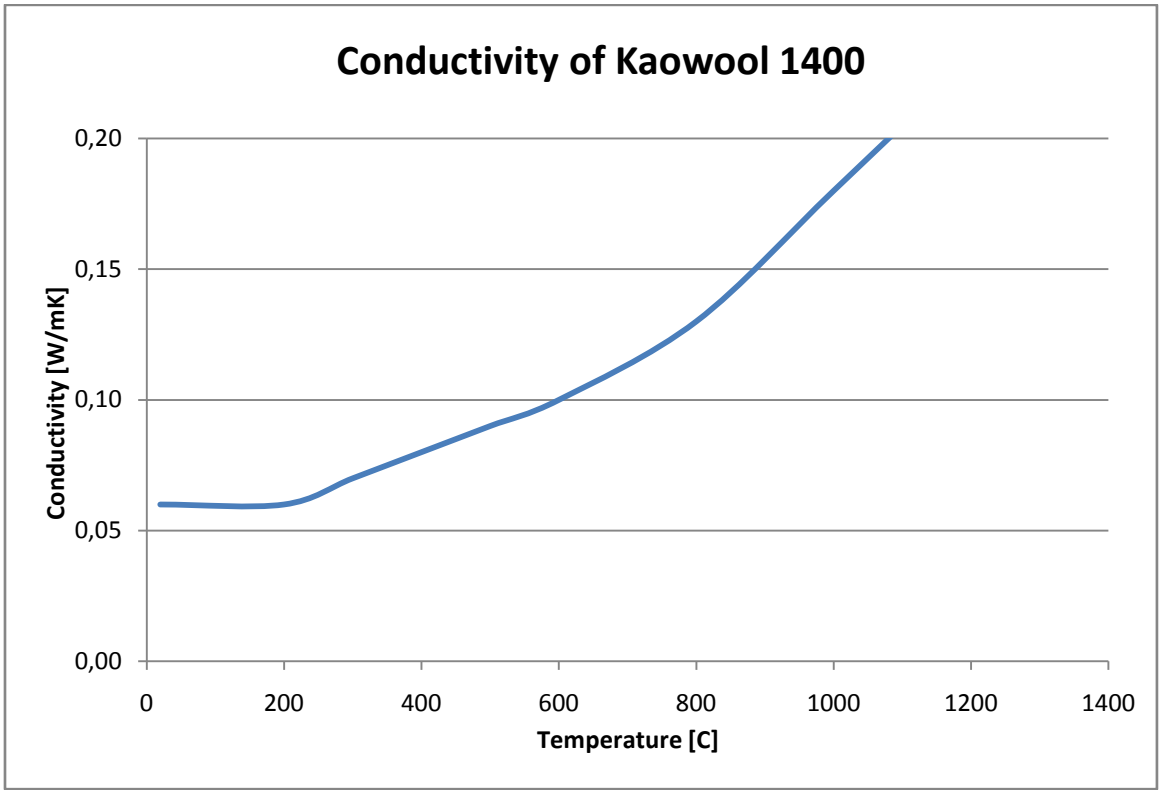

Figure 2 shows the conductivity of the thermal ceramic isolation material Kaowool as a function of temperature (9).

2.1.2 Heat capacity

When a material is to be heated, it must be exposed to some kind of energy. The heat quantity that needs to be supplied to heat one kilo of a material one degree Celsius, is called the heat capacity and it is denoted C_p. The heat capacity is expressed as follows:

$$C = \frac{dQ}{dT}$$

dQ is the energy required to produce a dT temperature change. C_p has the unity $J/_{mole \cdot K}$ and sometimes $J/_{kg \cdot K}$ is used. It is a property that indicates a materials ability to absorb heat from external surroundings. The specific heat capacity is dependent on temperature. At zero degrees Kelvin, the heat capacity is zero. When the temperature rises, the heat capacity rises. At high temperatures, the heat capacity will become almost constant for a material (the specific heat is still subjected to be affected when materials go through phase changes).

The point where the heat capacity goes from being temperature dependent to be constant is called the Debye-temperature. Since the heat capacity is dependent on temperature at temperatures below the Debye-temperature, it is difficult to measure the total energy quantity of a material. To avoid this problem, it is possible to look at how stored quantity of energy varies over time. By only concentrating on the changes in the quantity of energy, one may disregard the area where the heat capacity is temperature dependent and assume that the heat capacity is constant (14).

2.1.3 Density

The density of a material is defined as its mass per unit volume,

$$\rho = \frac{m}{V}$$

Density is measured in kg/m^3. The density is dependent on both pressure and temperature. The density of a material will increase by increasing the pressure. Increasing the temperature generally decreases the density, but there are exceptions to this generalisation (16).

2.1.4 Emissivity

A materials emissivity is a dimensionless quantity between 0 and 1. It is dependent on the body's surface, the colour and how shiny or rough it is. The emissivity and the absorption are always of the same size for the same body. When radiation beams hit a body, some of the energy gets reflected, some gets absorbed and some gets transmitted. The ratio between these coefficients is: R+A+T=1. For example, a mirrored surface may reflect 98 % of the energy, while absorbing 2 % of the energy, which will represent an emissivity close to zero. A good black body surface will reverse the ratio, absorbing 98 % of the energy and reflecting only 2 %, which means an emissivity close to 1 (17).

Typical values of ε for solids are given in Table 2 (13).

Table 2 shows the emissivity of different solids (13).

Surface	Temperature [°C]	Emissivity (ε)
Steel, polished	100	0.066
Mild steel		0.2-0.3
Sheet steel, with rough oxide layer	24	0.8-0.9
Asbestos board	24	0.96
Fire brick	1000	0.75
Concrete tiles	1000	0.63

2.1.5 Thermal properties of carbon steel

Steel is often presented with a thermal conductivity of $45 W/m \cdot K$. This number does not take into account the changes that happen to the steel structure when it is exposed to heat. For normal carbon steel the following conclusions applies (14):

$$k = -0.022 \cdot T + 48 \quad \text{For } 0\,^{\circ}\text{C} \le T \le 900\,^{\circ}\text{C}$$
$$k = 28.2 \quad \text{For } T \ge 900\,^{\circ}\text{C}$$

T is the temperature in the steel in °C. For instance, the thermal conductivity of steel at 500 °C is: $k = -0.022 \cdot 500 + 48 = 37 W/m \cdot {}^{\circ}C$.

The thermal conductivity of carbon steel decreases from 45.8 - 28.2 W/mK between 20 and 900°C, as shown in Figure 3. When the temperature reaches 900 °C the conductivity becomes stable (18).

The specific heat capacity of carbon steel varies according to temperature as shown in Figure 4. The specific heat has a peak of 5000 J/kgK at 735 °C. The reason for this is that the steel goes through a chemical change. At higher temperatures the specific heat is stable at 650 J/kgK (18) (19). The specific heat can be calculated as shown below, where θ is the temperature.

$$C_p = \begin{cases} 425 + 7.73 \cdot 10^{-1}\theta - 1.69 \cdot 10^{-3}\theta^2 + 2.22 \cdot 10^{-6}\theta^3 & \text{for } 20^{\circ}\text{C} \le \theta < 600^{\circ}\text{C} \\ 666 + 13002/(738 - \theta) & \text{for } 600^{\circ}\text{C} \le \theta < 735^{\circ}\text{C} \\ 545 + 17820/(\theta - 731) & \text{for } 735^{\circ}\text{C} \le \theta < 900^{\circ}\text{C} \\ 650 & \text{for } 900^{\circ}\text{C} \le \theta \le 1200^{\circ}\text{C} \end{cases}$$

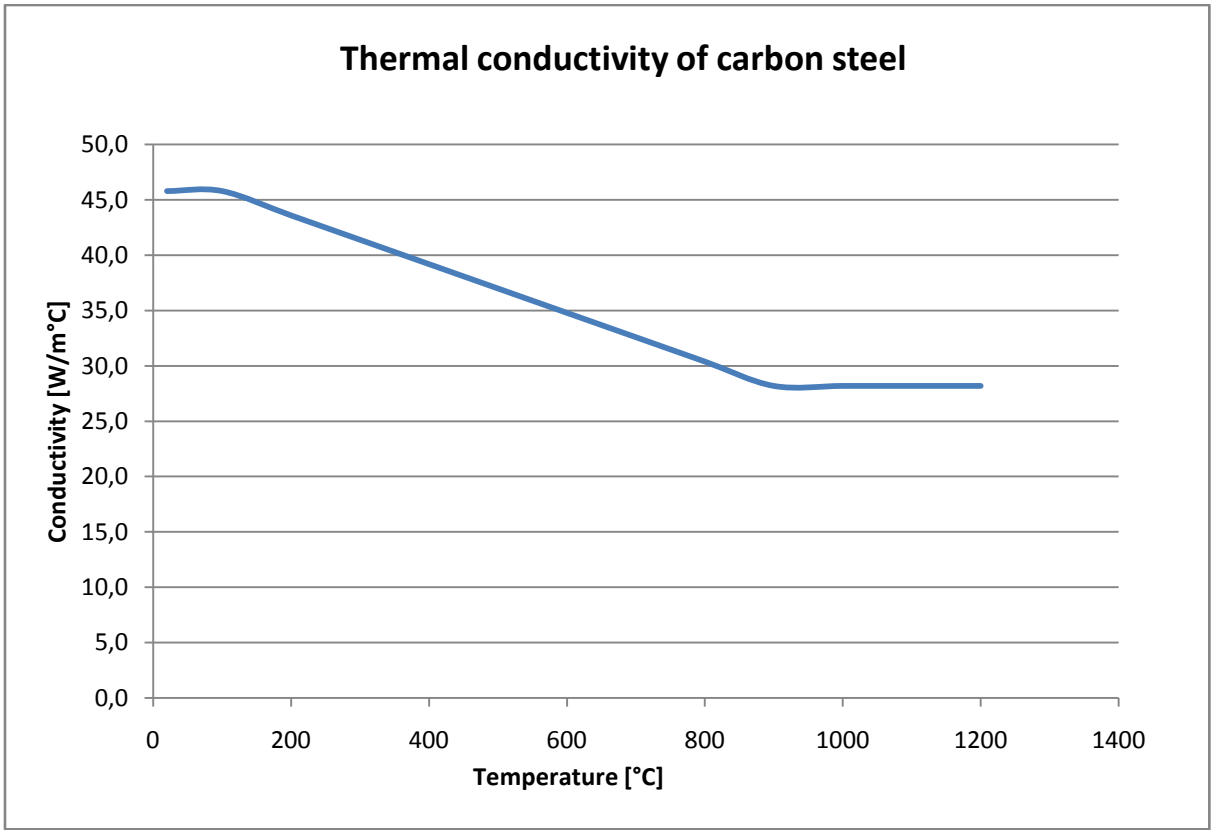

Figure 3 shows the thermal conductivity of carbon steel as a function of temperature (14).

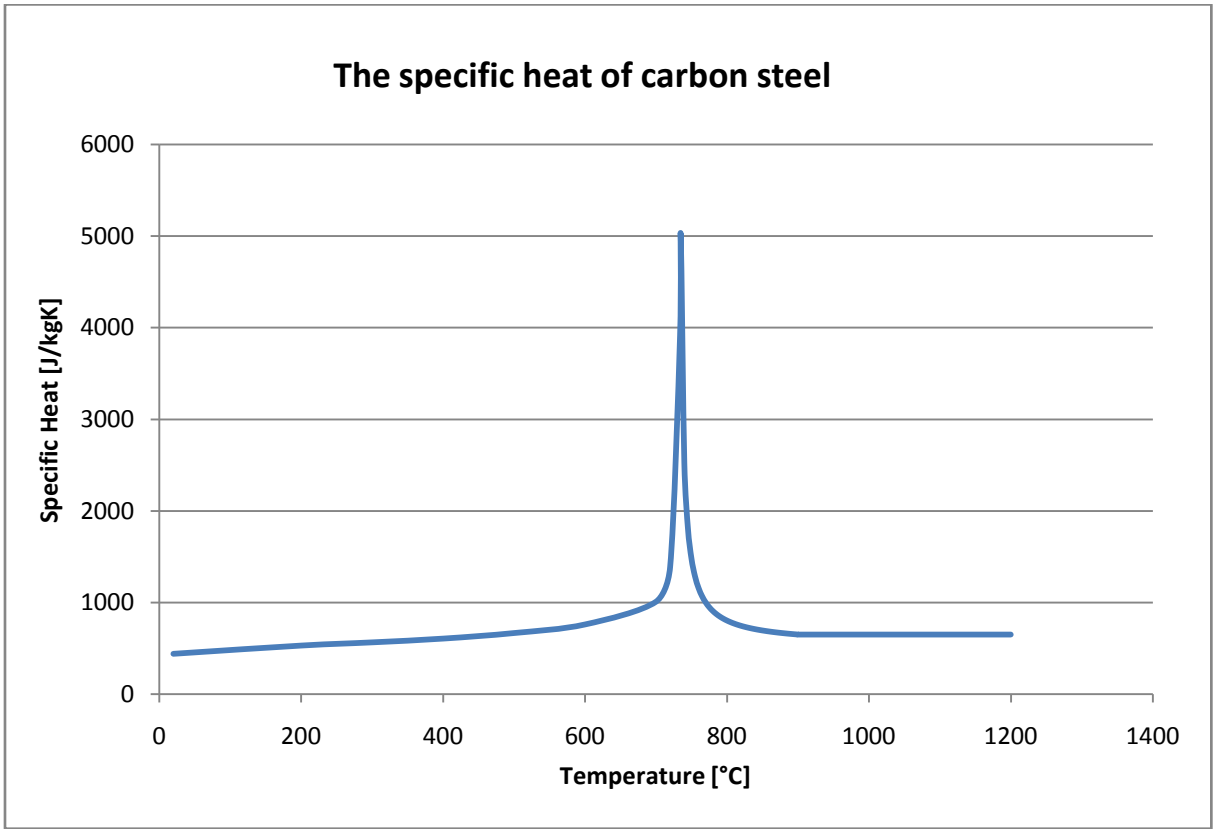

Figure 4 shows the specific heat of carbon steel as a function of temperature (18)

Carbon steel has a density of 7850 kg/m^3 (13) (19).

It is hard to determine the emissivity of steel. In this project emissivities of 0.6 and 0.7 have been used for calculation purposes.

2.2 Passive fire protection materials

This part provides information about passive fire protection materials and how they work. Passive fire protection can be defined as follows (20):

> *"Passive fire protection is the primary measure integrated within the constructional fabric of a building to provide inherent fire safety and protection by responding against flame, heat and smoke to maintain the fundamental requirements of building compartmentation, structural stability, fire separation and safe means of escape"*

Passive fire protection (PFP) materials are materials with low thermal conductivity, which purpose is to cover, and thus protect, other materials. Because of the PFP material's low conductivity, it contributes to slowing down the heat transfer from an eventual fire to the protected material. By using PFP materials in for instance a pipe construction, the structure will therefore get a higher fire resistance and it will be protected against the effects of fire. Also, the amount of fire spread through secondary ignition will be reduced, movement of flame and smoke will be limited, and the danger of fire-induced collapse or structural distortion will be minimized (20).

To illustrate the need for passive fire protection, consider the following example of steel. The solidity of steel is reduced to about 60 % of its values at ambient temperatures when the steel is heated to about 500 °C. When heated to about 800 °C the steels solidity decreases further to about 10 % of its normal values (19).

The most widely used product systems for offshore installation (North Sea) today are Chartek, Firetex, Mandolite, Pyrocrete, Fendolite, Flammastic and fire retardant paint. The thickness of the coating varies from 5 to 30 mm and is normally reinforced with galvanized netting, carbon or glass fibre (21).

2.2.1 Dead material

Dead materials are in this report defined as passive fire protection materials that maintains their physical dimensions when exposed to heat.

There are several different types of dead materials. Many of them are based on having a low conductivity. One such example is calcium silicate boards, which are made up from an inert material and protect only through its insulating properties. Some materials also have the strength of having a high specific heat capacity in addition to a low conductivity. One example of this is gypsum boards. This material contains water, which enhances its insulation abilities because water requires heat to be released and evaporate. The temperature on the exposed side of the gypsum board will increase continuously until about 100 °C is reached, at which time there will be a delay while the water of crystallization is driven off. As the heating continues, the 100 °C temperature plateau will progress slowly

through the board, until the entire board has been converted to a powdery form. Any residual strength depends on glass fibre reinforcing to hold the board together. Gypsum board is an example of an endothermic material (19).

Another PFP material that is very common is mineral wool. This is an isolation material made from minerals like sand, stone, or glass. An example of this type is Rockwool which is made up from rock and is most commonly used as PFP on load bearing steel constructions and also on concrete constructions (22). The density and specific heat capacity for mineral wools may be assumed as constants (23).

PFP materials with a high thermal inertia, which is the product of conductivity, density and specific heat, will have good isolation qualities. When exposed to the same heat source, the surface of materials with low thermal inertia (e.g. polystyrene foam) will heat more rapidly than materials with higher thermal inertia leading to much more rapid ignition. These types of materials will therefore require much energy to get heated and consequently, an increase of temperature in the protected material will be delayed (19).

Ceramic isolation

In this project, the dead isolation materials Kaowool and Firemaster has been tested. Both these two materials are ceramic fibre materials that keep its form and thickness during heat exposure. They are both workable and there are no special equipment needed for application (7) (9).

Kaowool boards are obtained by vacuum forming process. They contain small amount of organic binder to improve the cold handling strength and this burns out on first firing at approximately 200-300 °C. Kaowool has the advantage of being rigid and therefore self-supporting. It has a low conductivity, good abrasion resistance and low heat storage. It can be used to protect iron, steel, ceramics, furnace buildings and others. The type of Kaowool that has been used in the testing furnace is of the type 1400. That is, it is made to withstand 1400 °C (9). Kaowool 1400 has been used both for the purpose of isolating the walls inside the furnace and for testing the isolation's conductivity up against the simulation programme Brilliant. A figure of the conductivity of Kaowool is shown in Figure 2, part 2.1.1.

Firemaster 607^{TM} Blanket is a blanket built up from AES (Alcaline Earth Silicate) fibres. It is non-combustible and does not contain any binders, thus there is no risk of smoke or toxic gas emission or loss of strength during a fire due to binder burn out. The blanket is flexible and are used for bulkhead and deck fire protection in accommodation and process modules, vessel and pipe fire protection as well as structural steel protection to name a few. This product has previously passed a 4 hour hydrocarbon fire test and a one hour jet fire test (7). The material has been used in this project for testing the isolation's conductivity up against the simulation programme Brilliant.

2.2.2 Intumescing materials

Intumescing materials are a form of passive fire protection. These materials may be water based, solvent based or epoxy based. An intumescing material is stable at ambient temperatures and looks like a normal coating. When exposed to fire a chemical reaction takes place and the material starts to expand. How much it expands vary with different materials and it can expand to many times its original thickness. The expansion provides an insulating foam-like coating or char which protects the substrate. A result of the increase of volume, the density of the material decreases. Intumescing materials may be designed for a certain fire exposure. Usually intumescent coatings are designed to perform under severe conditions and to maintain the steel integrity between one and three hours when the temperature of the surroundings is in excess of 1100 °C (1) (8) (24) (25).

2.2.2.1 Thin film intumescent coating

The first intumescent coating was made in 1938 and it has been used actively since 1950 (24).

Intumescing coatings are thin paint films that react upon heat exposure. The coatings form an expanded multicellular layer when heated. This layer acts as a thermal barrier that effectively protects the substrate against rapid increases in temperature. The expansion process is caused by the interaction of three active components (26):

1. Carbon supplier: Char forming polymers or polyols, pentaerythritol
2. Acid source: Normally ammonium polyphosphate or a mineral acid
3. Expanding (blowing) agent: E.g. melamine

These components are bound in a solvent or waterborne polymeric binder. Also, other components are added to improve paint properties, such as easy application and fast drying.

When the coating is exposed to heat, the heat begins to soften the polymeric binder. The acid source breaks down to yield a mineral acid. Furthermore, dehydration of the carbonisation of the polyols begins to take place with help from the acid source. Through the resulting decomposition of the expanding agent, gas is produced, and the coating starts to swell and produce the insulating multicellular protective layer. This protective char limits both the heat transfer from the heat source to the substrate and the mass transfer from the substrate to the heat source, resulting in conservation of the underlying material. In an ideal situation the intumescent can expand some 100 times its original thickness. The final stage of the process involves solidification of the foamed char (8) (27) (25).

Several coats of paint may have to be applied to obtain the necessary thickness. Intumescent paints have the advantage that they allow the structural steel members to be seen directly, without any other cover than the paint (19).

Mathematical description

Despite numerous methods and results there has still not been developed a complete model of combustion of intumescent polymer systems (24). However, here is a short mathematical description of what happens:

Assuming that the total heat absorbed by the polymer from the flame goes to heating, destruction and gasification, the mass burning rate can be expressed as (24):

$$\dot{m} = \frac{\rho_{fl}}{C_p(T_s - T_0) + Q_l}$$

$\dot{m}$ = mass burning rate
ρ_{fl} = density of the heat flux from the flame
C_p = effective thermal capacity of the polymer
T_s = surface temperature
T_0 = initial temperature
Q_l = heat expended on gasification of the polymer

The mass burning rate is a basic parameter of steady combustion of polymers.

The combustion process can be divided into several stages; heating to the decomposition temperature, pyrolysis, ignition and formation of a char on the polymer surface. When the char has been created, the combustion rate decreases. The polymer then extinguishes or the combustion rate stabilizes. When the combustion is steady, the mass rate can be written as follows (24):

$$\dot{m} = \frac{h(T_{flame} - T_{s1}) + \sigma\varepsilon T_{flame}^4 - \sigma\varepsilon_{s1} T_{s1}^4}{C\left[c_c(T_{s1} - T_{s2}) + q_{gas}\right] + c_{pol}(T_{s2} - T_0) + q_{trans} + G\left[c_g(T_{s1} - T_{s2})\right]}$$

h = heat transfer coefficient
T_{flame} = flame temperature
T_{s1} = surface temperature of the char
T_{s2} = surface temperature of the polymer
c_c, c_{pol}, c_g = average thermal capacities of the char, the polymer and the gas
T_0 = initial temperature
σ = Stefan – Boltzmanns constant
$\varepsilon, \varepsilon_{s1}$ = the degrees of blackness of the flame and the char surface
C = portion of the polymer that are converted into char
G = portion of the gasous combustion products (C + G = 1)
q_{gas} = heat release due to chemical reactions of char gasification
q_{trans} = heat release due to chemical reactions of polymer transformations

It is important to notice that the practical value of the given formula is questionable because of the large number of parameters that can only be obtained from experiments and that can vary during combustion (24).

There are many different types of intumescent coatings. They appear as water-borne range and solvent-borne range with a protection of 30, 60, 90 or 120 minutes (8). However, many intumescent paints are not suitable for external use because of unknown durability. All intumescent paints are proprietary products, and many are under continual development (19). Thin film intumescent coatings are designed for traditional buildings and therefore cellulosic fire (normal fire exposures) (1) (8). Figure 5 in part 2.2.2.2 shows a typical time - temperature curve for both cellulosic fires and hydrocarbon fires.

2.2.2.2 Epoxy intumescent systems

Epoxies first appeared in 1942 when epoxy resins were discovered. Epoxies rapidly earned a reputation of having excellent durability and having high chemical and corrosion resistance (6). In the late 80's the offshore oil and gas exploration and production industry almost totally displaced their use of passive fire protection materials from cement based products to use epoxy based products. The primary reason for this change was that correctly formulated epoxy intumescent materials were proven to be weatherable and durable for a lifetime of over 30 years (28).

Epoxies are normally thicker than thin film intumescent coatings. They are yet characterized as thin coatings, because they are between 5-25 mm thick. Epoxies are also more mechanically durable than thin film intumescent coatings, both in ambient conditions and during fire exposure. Epoxies can withstand hydrocarbon fires and jet fires for a certain time (1). There are significant differences between epoxy intumescent materials.

Epoxies, like thin film coatings, work by forming a thick char when exposed to fire or high temperatures. This char slows down the heat transfer through the material. The swelling process is similar to the one described for thin film intumescent coatings in part 2.2.2.1.

It is important to notice that the intumescent will perform differently in different fires. The quantity of heat and rate of delivery will affect the rate of combustion of the intumescent. It will also affect the level of gas liberation and hence degree and speed of intumescence. For instance, a wood or paper fire burns more slowly with a lower peak temperature than a hydrocarbon fire. Figure 5 shows a typical time-temperature curve for both hydrocarbon fires and for cellulosic fires. As seen on this figure, the hydrocarbon fire is much more severe than the cellulosic fire. After only 10 minutes, the hydrocarbon fire has reached 1000 °C, while the cellulosic fire is about 680 °C. The intumescence depends on the nature of the fire exposure, like heat exposure, rate of heating, temperature level, and duration of the fire. It also depends on the type, shape and geometry of the substrate (1) (28).

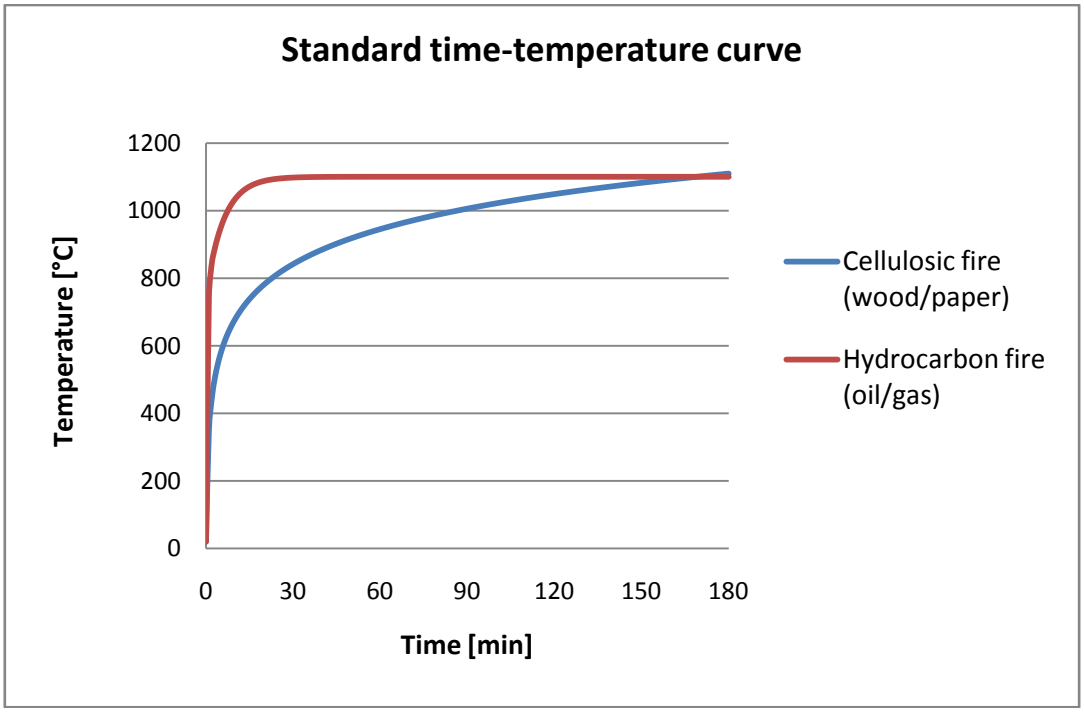

Figure 5 shows a typical time-temperature curve for hydrocarbon fires and cellulosic fires (19) (29).

A figure of how the intumescing process work is shown in Figure 6. As seen in this figure, the char starts to form early, and the longer the material gets exposed to heat the more char develops. Between the unreacted material and the char we have something called the reaction zone. It is here the mastics starts to intumesce because of the heat that has penetrated through the outside layer. In stage 4, when the whole material has reacted, it still forms an efficient heat retardation mechanism (28).

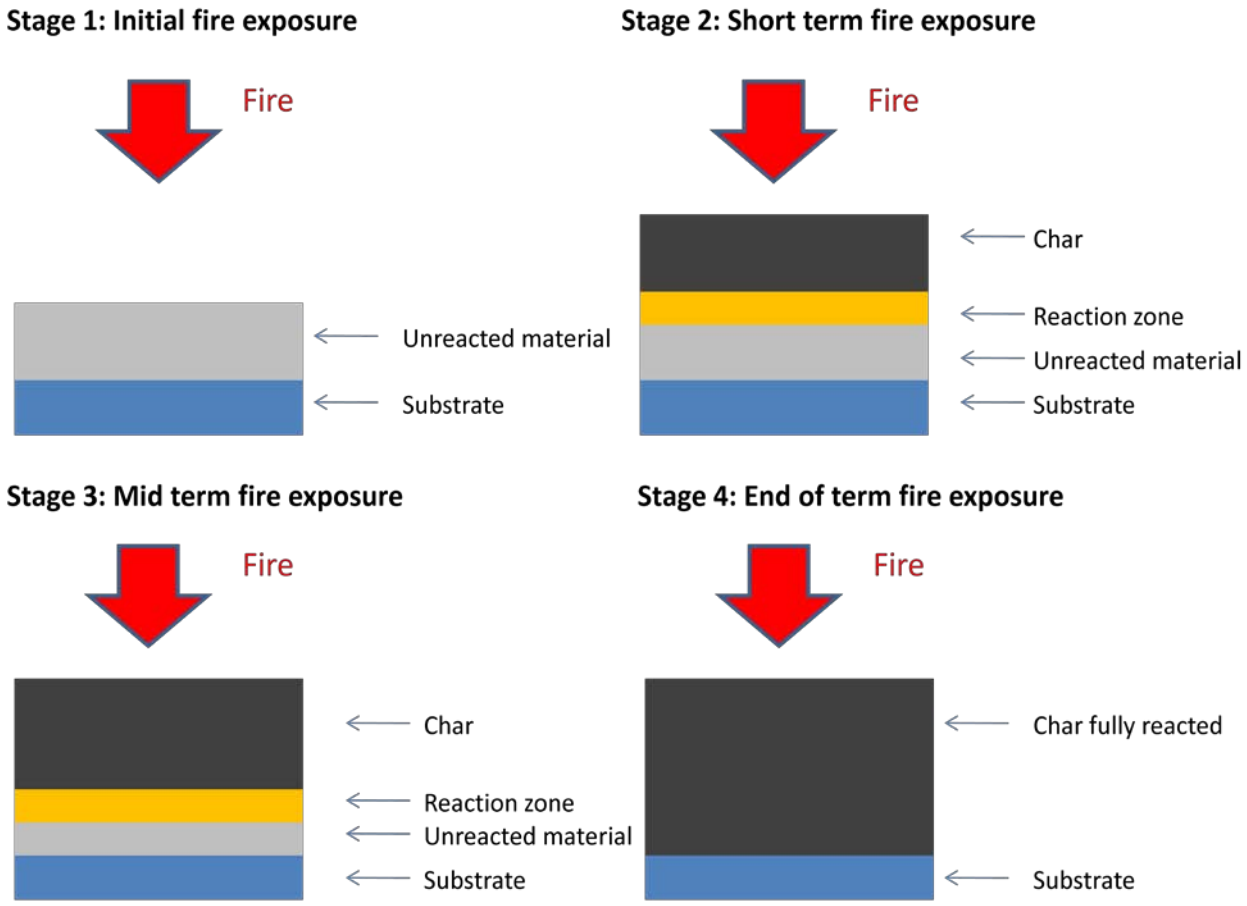

Figure 6 shows how epoxy intumescents work (28)

Study of the efficiency of different intumescent formulations

Jimenez, Duquesne and Bourbigot have performed tests to investigate the efficiency of different intumescent formulations designed to protect steel in case of hydrocarbon fire (27). Four different epoxy resin based formulations were chosen and compared to a virgin steel plate. The test samples were introduced to a furnace that burned 0.3 kg/s of propane at a heat flux of 200-250 KW/m^2 at a distance of 1 m. All the different samples had five thermocouples attached on the unexposed side of the steel plate. The plates were mounted vertically in the furnace and burnt until the thermocouples reached 400 °C. The results from this test are shown in Figure 7. The different formulations tested were:

- A thermoset epoxy resin alone, notation B in the figure.
- Thermoset epoxy resin mixed with Ammonium Polyphosphate (APP) derivative, notation C.
- Thermoset epoxy resin mixed with boric acid (mineral acid), notation D.
- Thermoset epoxy resin mixed with both APP derivative and boric acid, notation E.

A virgin steel plate was also tested for comparison. This has the notation A in Figure 7.

The steel plate covered with the thermoset epoxy resin alone had a temperature gradient that looked quite similar to the one with the virgin steel plate. This means that the thermoset resin did not provide any protective effect. The test where APP was added was a lot better. This ingredient can be used as both an acid source and as a blowing agent. It took 11.3 minutes compared to 5 minutes for the uncoated steel before failure (which occurs when the steel plate reaches 400 °C on the unexposed side). A disadvantage in this scenario was that the char fell off the steel plate before the end of the experiment. This may be seen by the change of slope at 610 °C in Figure 7.

When boric acid was added, the test results were even better. The failure happened after 18.2 min. Development of intumescence was observed, but also in this test, the char fell off. This happened at 400 °C.

The test where both APP and boric acid were used shows the best result. The failure happened after 29.5 minutes and the char adhered to the plate. The swelling started at about 300 °C (27).

The fact that the char fell off is a serious issue. When it comes off it is not protecting the specific construction anymore, and the protection is therefore not useful. Possible reasons for the char to come off may be loss of adherence of the coating on the plate or loss of cohesion of the char combined with the effect of gravity, since the tests were carried out vertically. This test has shown that the adhesion of the coating is weak when phosphorous species are not added in the formulation (27).

Outside this specific test, the char can also be destroyed when subjected to external perturbations such as explosion (e.g. Jet fire) or wind turbulence (27).

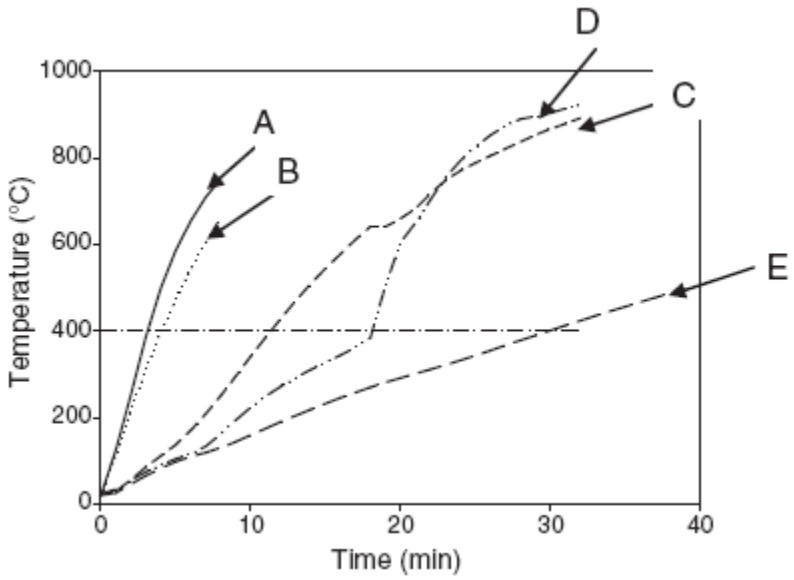

Figure 7 shows results from an experiment made of M. Jimenez, S. Duquesne and S. Bourbigot. It shows the evolution of temperature as a function of time on the back side of a steel plate of different intumescent coatings (27).

ProTek

ProTek is a PFP material of the epoxy type. ProTek is developed by the company Solent Composite Systems (SCS). There are several different types of ProTek with different ingredients, but the main structure is the same. It is very rigorous and it is designed to withstand a two hour jet fire at 0.3 kg/sec gas release. ProTek can therefore be used both onshore and offshore for both topsides and subsea applications. The manufacturer claim that the product has zero corrosion risk and that it is maintenance free for at least 30 years (11).

Different types of ProTek have been tested in this project and these experiments are described later in this report. All of these different types of ProTek contain various compounds of carbon, hydrogen and oxygen. These kinds of compounds can produce toxic gases like CO_x and the carcinogen benzene (30) (31).

A schematic of the structure of ProTek is shown in Figure 8. There are two insulating cores inside the structure that are based on phenolic and ceramic. This core is protected by an epoxy based reinforcement skin that can withstand high blast pressure. The outer protective gel coat on the hazard side is there to provide long term weather resistance. The external ablative layer provides jet fire resistance and the insulation core reduces heat transfer (11).

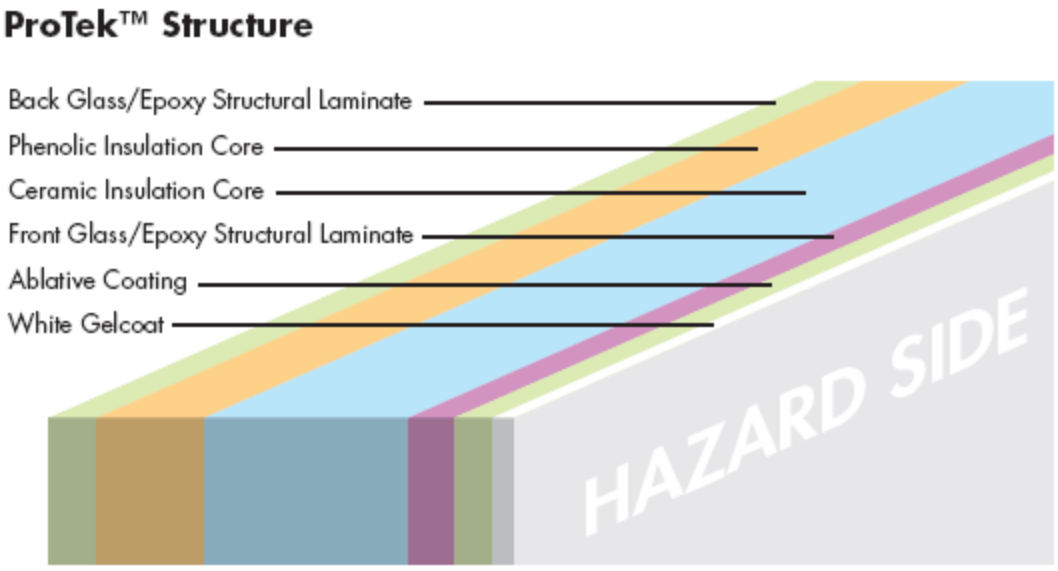

Figure 8 shows the different layers that ProTek is made up from (11)

Chartek 7

Chartek 7 is a high performance epoxy intumescent fire protection coating system. The product may be the most commonly used. Normally it is reinforced with International Protective Coatings' HK-1 carbon fibre mesh. The product consists of epoxy resin and triphenyl phosphate. It is a high build, solvent free, two-pack material providing durability and combined corrosion and fire protection. The product is suitable to protect steel

(structural, divisional and vessels), aluminium and others from hydrocarbon, pool and jet fires. Chartek 7 has been certified to withstand a two hour jet fire. All applications of Chartek 7 shall strictly conform to procedures laid down in the International Coatings Chartek 7 Application Manual (5).

If the product catches fire it will produce a dense black smoke. As a consequence of this, decomposition products such as carbon monoxide, carbon dioxide, oxides of nitrogen and smoke may be produced which may be hazardous to health. The product may also produce hazardous decomposition products when exposed to high temperatures (32).

Benarx F Epoxy roll

Benarx is a range of insulation products for various industrial purposes, including above-ground and underground piping, vessels, structures, and tank foundations. The products are solid epoxy compounds developed by Beerenberg Corp. AS (33).

Benarx F Flexi Roll XP is fastened with acid-proof straps when used around piping. The product is made from hardened epoxy material, called PittChar and reinforced with carbon cloth from Chartek. Benarx F Flexi Roll XP withstands both jet-fire and gas explosion (3).

Benarx F Epoxy roll has been tested in this project and these experiments are later described in this report.

2.3 Measuring the conductivity of passive fire protection materials

This part will describe some of the most common tests used today for measuring the conductivity of passive fire protection materials. Certification of the performance of passive fire protection materials is normally based on laboratory scale standardized fire tests.

This part will also discuss uncertainties in heat release rate experiments for the purpose of showing the size of error that may be expected when working on comparable experiments.

A wide variety of experimental techniques exist for measuring the thermal conductivity of materials at elevated temperatures. Some are specified by the American Society for Testing and Materials (ASTM). High temperature guarded hot plate (ASTM C177), heat flow meter apparatus (ASTM C518), laser flash diffusivity methods (ASTM E1461), transient line/hot wire (ASTM C1113) and plane source methods exists today (34) (35).

Measuring thermal conductivity with transient or steady state techniques

Two types of methods exist to measure the thermal conductivity of a sample. That is steady-state and non-steady-state methods. In steady state techniques a sample of unknown conductivity is placed between two samples of known conductivity. A constant temperature difference is established across the test sample. There is a constant boundary temperature on each side of the specimen. Measurements are taken after the sample has attained equilibrium.

When using transient techniques, property measurements are made with dynamic temperature fields over the test samples. The advantage of this method is that it can be performed more quickly, since there is no need to wait for a steady-state situation. Both measurement techniques provide a temperature gradient and a response in the material to that gradient. The techniques differ otherwise in choice of sample size, testing time, range and methodologies of measurement (1).

High temperature guarded hot plate (ASTM C177)

The objective of this method is to measure conductivity by establishing a steady state condition through flat, homogenous specimen(s) when their surfaces are in contact with solid, parallel boundaries held at constant temperatures. The test covers a wide variety of apparatus constructions, test conditions, and operating conditions. There is no upper limit defined for the magnitude of specimen conductance, but for practical reasons it should be less than 16 W/m^2K. The constant plate temperatures, the thickness of the sample and the heat input to the hot plate are used to calculate the thermal conductivity (36).

Heat flow meter apparatus (ASTM C518)

This test method covers the measurement of steady state thermal transmission through flat slab specimens using a heat flow meter apparatus. The apparatus establishes steady state one-dimensional heat flux through the test specimen which is placed between two parallel plates at constant, but different temperatures. Fourier's law of heat conduction is used to calculate the thermal conductivity. This is a secondary method of measurement, because specimens of known thermal transmission properties must be used to calibrate the apparatus first. The apparatus can be used at ambient temperatures from 10 to 40 °C with thicknesses up to approximately 250 mm, and with plate temperatures from -195 °C to 540 °C at 25 mm thickness (37).

Laser flash diffusivity methods (ASTM E1461)

The flash method is used to measure values of thermal diffusivity, α, by introducing energy pulses using laser techniques. It can measure a wide range of solid materials. The thermal conductivity is then measured according to the relationship:

$$k = \alpha \cdot C_p \cdot \rho$$

This method can be considered as absolute, since no reference standards are required. This is a transient method which can measure diffusivities between the ranges of 10^{-7} to 10^{-3} m^2/s, from about 75 to 2800 K (38).

Transient line/hot wire (ASTM C1113)

This test is another variation of a transient, indirect method. It covers the determination of thermal conductivity of non-carbonaceous, dielectric refractoriness, like refractory brick and

powdered materials. The test is only applicable to refractoriness with k-value less than 15 W/mK. Heat flow from the hot wire is in both directions of the sample. The k-value measured is a combination of the k-values for the width and thickness of the sample. This is because a wide range of temperatures are measured over the sample on both sides, so that several k-values can be determined (39).

Slug calorimeter

This method was developed at the Building and Fire Research Laboratory, National Institute of Standards and Technology (NIST) in 2004, but is not a standard test procedure. Its aim is to evaluate the thermal performance of fire resistive materials (FRMs). Key components of the system include the use of a 'sandwich' specimen to provide an adiabatic boundary condition at its central axis. A schematic and a photo of the slug calorimeter are shown in Figure 9. The 'sandwich' consists of a square central stainless-steel plate (slug) surrounded on two sides by the FRM to be tested. The other four (thin) sides of the steel plate (and FRM specimens) are insulated using a low thermal conductivity fumed silica board. Two metal plates provide a frame for placing the entire sandwich specimen slightly in compression. An electrically heated box furnace is placed at the centre, below the configuration. Multiple heating/cooling cycles gets performed in order to provide information on the influence of reactions and convective transport on the computed effective thermal conductivity values. Knowing the heat capacities and densities of the steel slug and the FRM, an effective thermal conductivity for the FRM can be estimated. The effective thermal conductivity of the FRM will be influenced by its true thermal conductivity and by any endothermic or exothermic reactions or phase changes occurring within the FRM (40).

Tests have also been carried out on 5-6 different intumescent PFP materials. The retaining plate is then produced as an open frame allowing the PFP material to react and expand (1).

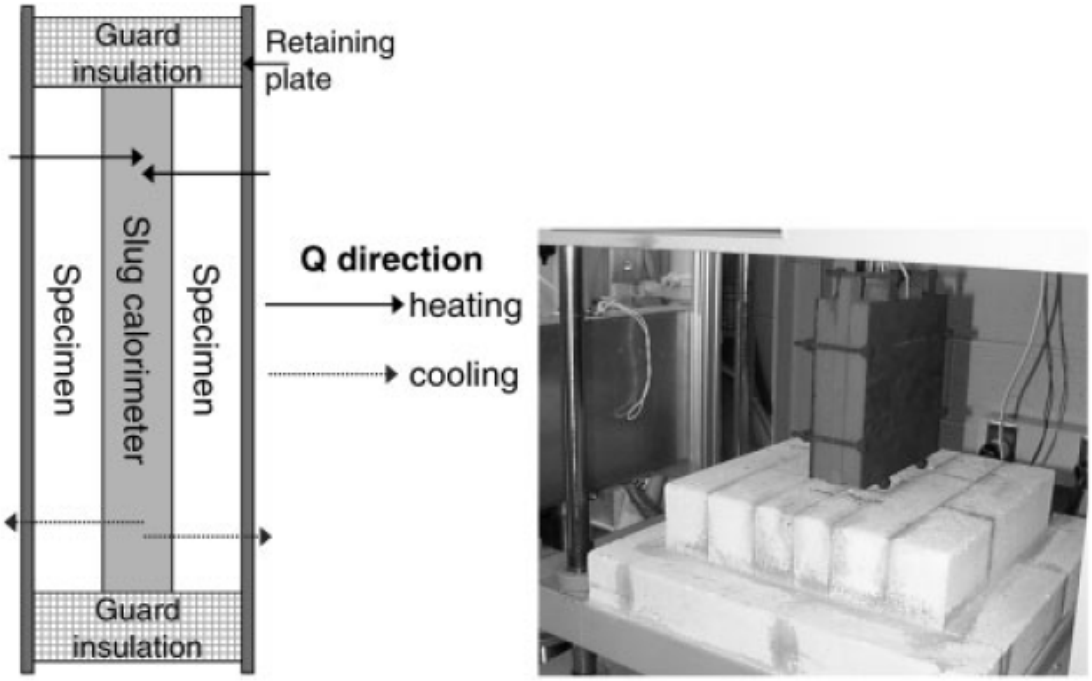

Figure 9 shows a schematic and a photo of the slug calorimeter test set-up. Left: Schematic of a cross section through the middle of the basic slug calorimeter set-up. Right: Photo of a completed sandwich specimen of the fumed-silica insulation board mounted and ready for testing in the furnace (40).

Cone calorimeter

The Cone Calorimeter test is not implemented in Norwegian rules for fire classification, but the test follows the procedure given in international standard ISO 5660-1:1993(E). The test is the most advanced method for assessing materials' reaction to fire. Figure 10 shows a schematic of the Cone Calorimeter. The test gives a possibility to evaluate ignitability, combustibility, smoke production and production of toxic gases. The heating source is a conical heater that can radiate within the range 0-100 kW/m^2. When the specimen gets heated, volatile gases are ignited by an electric spark igniter (41). The specimen can for instance be a steel plate covered with PFP. The specimen is mounted on a load cell which records the mass loss rate of the specimen during combustion. The specimens are of the size 10 x 10 cm with a thickness of maximum 50 mm (41).

The Cone Calorimeter is mainly used for testing time to ignition of a material, its heat release rate and smoke production (41).

It is possible to check the conductivity fairly good by mounting a thermocouple on the unexposed side of the steel plate, as well as on the surface of the PFP material. By knowing the heat input it is then possible to measure the thermal conductivity. There are a lot of uncertainties by using this method, especially when measuring the temperature on the exposed side of the PFP material. Since intumescing PFP materials intumesce and burn, it is nearly impossible to measure the surface temperature. This method is therefore not normally used and has only been tried out to get an idea of the conductivity.

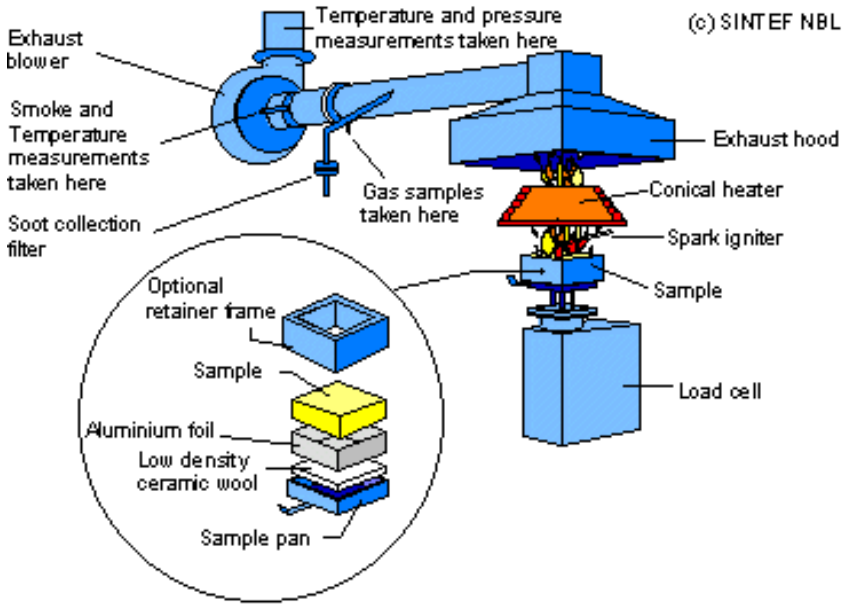

Figure 10 shows a schematic of a Cone Calorimeter (41)

Uncertainties in heat release rate experiments

Several analyses have been performed on uncertainties in the heat release rate calculation for the cone calorimeter test (42). For instance, a study of this uncertainty is presented by Enright and Fleischmann in (43). Their conclusion was that relative uncertainties from ± 5 % to ± 10 % were obtainable at heat release rates larger than approximately 50 kW/m^2. Zhao and Dembsey also performed an analysis on the measurement uncertainty for calorimetry apparatuses, and they concluded that relative heat release rate (HRR) uncertainties decrease as HRR increases (44).

For HRR measurements typical for room fire experiments, the relative uncertainties vary from ± 5 % to ± 11 % (42) (45).

2.4 Temperature reading by means of thermocouples

This part will describe how thermocouples work and it will highlight different precautions for their use.

2.4.1 How thermocouples work

The technology behind how thermocouples work was discovered already in 1821 when a German physicist named Thomas Seebeck found out that the junction between two metals generates a voltage which is a function of temperature. Any two wires of different materials can be used as a thermocouple if they are connected as shown in Figure 11. The Chromel-Alumel connection is what is called the “junction”. For the thermocouple to be able to measure a temperature, it is dependent on that the temperature measured in the junction is different from the reference temperature as shown in Figure 11. When this happens, a low level DC (Direct Current) voltage, called E, will be available at the +/- terminals. The

thermoelectric voltage that is produced depends on which metals that are used and on the temperature relationship between the junctions. If the temperature measured in the two junctions is similar, the voltages produced at each junction will cancel each other out and no current will flow in the circuit. This means that a thermocouple can only measure temperature difference between two junctions. The measuring junction is the one exposed to measure temperature. The reference junction is kept at a known temperature. The reference is then always the terminal temperature. A laboratory thermocouple consists of only a single, measuring, junction where the reference is always the terminal temperature (46) (47).

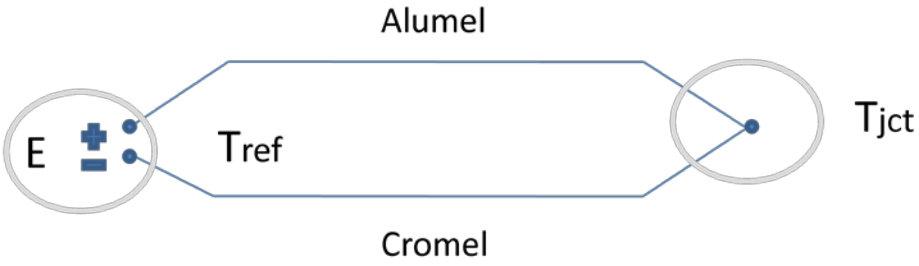

Figure 11 shows a schematic of a simple thermocouple (47)

Thermocouples of the type K are the most common ones. They use Chromel – Alumel alloys to generate voltage. Chromel is an alloy that consists of approximately 90 % nickel and 10 % chromium, while alumel is an alloy consisting of approximately 95 % nickel, 2 % aluminium and 1 % silicon. The alumel wire is magnetic. Thermocouples of type K can be used in the range -200 °C up to 1100 °C (46) (47).

In this project, only thermocouples of type K have been used. This type is known as a 'general purpose' thermocouple. Some of the thermocouples used have been of the capsule kind as shown in Figure 12. These types are more suitable for corrosive media although the thermal response is slower. Some of these thermocouples are insulated by compressed mineral oxide powder. This is enclosed in a seamless, drawn metal sheath, usually stainless steel (46).

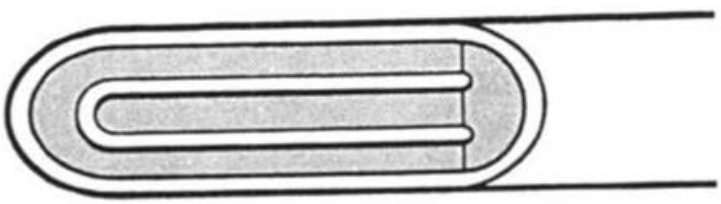

Figure 12 shows an insulated junction (46)

2.4.2 Precautions and considerations for using thermocouples

There are a lot consider when using thermocouples. To make them as accurate as possible it is essential that it has been used properly. Most measurement problems and errors with thermocouples are due to lack of understanding of how thermocouples work (48).

Common problems are listed below (48):

- Connection problems:

  This type of problem can happen if an increase of length is needed. It is then important to remember to use an extension of the same type as the thermocouple. E.g. type K for type K thermocouples. If another type is used, a new junction will arise.

- Lead resistance:

  Thermocouples are made of thin wire to minimise thermal shunting and to improve response time. This can cause the thermocouple to have a high resistance which can make it sensitive to noise. An idea if a long cable is needed is to keep the thermocouple lead short and use a thermocouple extension wire, which is much thicker and has a lower resistance, to run between the thermocouple and measuring instrument.

- Decalibration:

  This is when the distinctive character of the thermocouple changes unintentionally. This can be caused by diffusion of atmospheric particles into the metal at the extremes of operating temperature. It can also be caused by impurities and chemicals from the insulation into the thermocouple wire. It can be a good idea to check the specifications of the probe insulation before using it at high temperatures.

- Noise:

  The output from a thermocouple is a small volt signal, so it is prone to electrical noise pick up. If the noise are the same on both wires it is usually rejected by the measuring instrument. The longer cables the more noise interference can be expected. Generally, thermocouples in electrical contact with the protection tube can easily suffer interference from external voltages through voltage pick-up.

- Thermal Shunting:

  Thermal conductance can cause inaccuracies in the temperature measurement. Heat energy may travel up the thermocouple wire and dissipate to the atmosphere; this can participate in cooling the surface temperature that is measured. This is especially a risk if temperature differences are large, for instance if the wire is 1 °C and the measured surface keeps 1000 °C. To avoid this, as much as possible of the thermocouple wire should be exposed to heat. When using for instance shielded thermocouples, which measure temperature at the end of the tip (somewhere within the outer 1 mm), at least 3-4 cm of the thermocouple should be exposed to the heat, to make the measuring more accurate.

When measuring surface temperature, there are three main problems to consider (47):

- Deciding what needs to be known about the surface temperature; like what is the maximum temperature and what is the average surface temperature.
- Choosing a representative location to measure it.
- Getting the thermocouple in good thermal contact at the chosen location.

When choosing a representative location it is important to consider where it is most likely to be warmest and if there is any point where there will be more cooling than other places. It is also important to remember that a capsule thermocouple measure temperature around the whole tip and not only where it is in contact with the surface. That is, the thermocouple can be exposed to radiation on the side that is not in contact with the surface. An idea is to make a trace in the surface just as big as that the thermocouple can be placed in it sideways. The trace must be so deep that the surface of the thermocouple will be at the same level as the surface you want to measure temperature on. When this is done, the temperature you measure will be the surface temperature. If the thermocouple is placed onto the surface without the trace, most likely a higher or lower temperature will be measured as this will be affect by the air temperature.

In this project some thermocouples isolated with ceramic have been used. The wires are movable and the most common area of application is on surfaces. The wires may be mounted onto a surface like steel as long as it is not conducting power. It is also possible to measure air temperature with this type of thermocouple. The wires are then twisted together so that they have good contact with each other. The first point where they are in contact is where the temperature gets measured. A disadvantage of this thermocouple is that the ceramic isolation burns off quite easily. If that happens, the wires might be in contact with each other before being in contact with the desired spot where the temperature is supposed to be measured. This way, the thermocouple will measure a different temperature than intended.

Another important issue to consider when using thermocouples is the accuracy and the temperature range of the specific type of thermocouple. Table 3 shows an overview of these parameters for a selection of common thermocouples (46) (49):

Thermocouple Type	Temperature range	Accuracy (Std. limits of error)
Type K Chromel-Alumel	-200 °C up to 1100 °C	Greater of 2.2 °C or 0.75 %,
Type J Iron-Constantan	-200 °C up to 750 °C	Greater of 2.2 °C or 0.75 %
Type E Chromel-Constantan	-200 °C up to 900 °C	Greater of 2.2 °C or 0.5 %
Type T Copper-Constantan	-200 °C up to 350 °C	Greater of 2.2 °C or 0.75 %

Table 3 shows temperature range and accuracies for some common thermocouples (46) (49)

The response time for a thermocouple is also something that needs to be considered. The response time is dependent on the thermocouple dimension, construction, tip configuration and the nature of the medium in which the sensor is located. If the thermocouple is to measure temperature on a medium with high thermal capacity and heat transfer is rapid, the effective response time will be practically the same as for the thermocouple itself (the intrinsic response time). However, if the thermal properties of the medium are poor, e.g. in still air, the response time can be 100 times greater (46).

2.5 Software

This part contains general information about the software used to do numerical simulations in this project.

2.5.1 CFD Programmes

CFD stands for Computational Fluid Dynamics and is basically a computational technology that makes it possible to study the dynamics of fluids that flow. The equations that manage the motion of a fluid are called the Navier-Stokes equation, which are based on the principles of conservation of mass, momentum and energy. Computers are used to perform the millions of calculations required to simulate the interaction of fluids and gases (50) (51).

2.5.2 Using thermal properties in CFD simulations

It is important that the thermal properties defined in the numerical simulation programme are correct. This way, the simulation data becomes as similar as possible to how the process would have become in real world. The purpose of a fire engineering simulation is to predict the thermal response and the structural response of for example a fire isolated steel structure. Most thermal response simulators are based on finite elements that rely on a constant geometry mesh. This means that when simulating intumescing materials, the swelling process where the thickness of the material increases will not be included in the model. The real behaviour of the material has to be approximated by other means. This is because the swelling process and its mechanisms are complex and rather difficult to describe mathematically. Normally, a thin film of intumescing material is modelled as a constant layer and the effect of expansion is taken into consideration when deriving a temperature dependent effective thermal conductivity. The conductivity function must therefore take into account the phase change from a solid material to a porous char and the increased thickness (1).

2.5.3 CFD code Brilliant

Brilliant is an object code, based on Computational Fluid Dynamics (CFD) technology developed by Petrell AS. This programme can be used for numerical simulations of flow and heat transport, including chemical reactions and solid materials. Brilliant is used to analyse physical phenomena and their consequences. There are many different available models in Brilliant, like flow model, including laminar and turbulent compressible and incompressible flow. There is also a dispersion model, radiation model, fire model and a pressure model to name a few. Each model is a connection of equations that together will simulate a physical

phenomenon (4). The various models are own objects with specific properties. At the same time, a model can build on another model. An example of this is when there is gas dispersion that builds on a model for turbulent flow. If the two models have common equations, these will be solved at the same time. It is also possible to use the same model in many areas, but with different properties in the different areas (52). In this project, Brilliant's flow model and conduction model have been used. The simulation runtimes have been around 24 hours per simulation, depending on the number of seconds to be simulated.

Brilliant has a built-in library for thermodynamic properties of fluids and a database for solid materials (4).

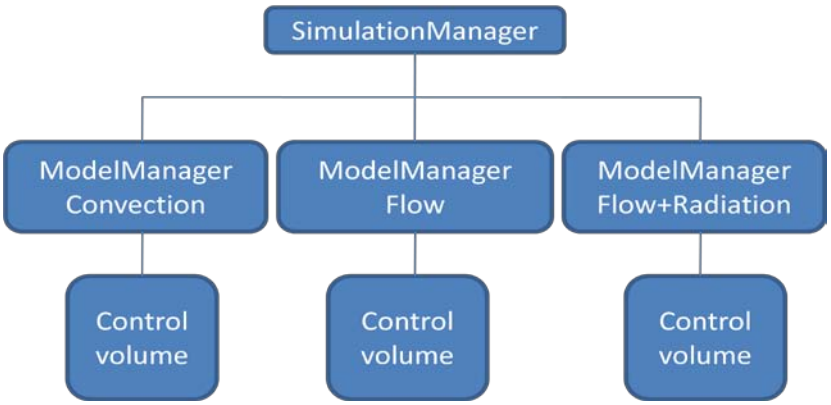

Figure 13: Programme structure for Brilliant (52)

How Brilliant is organized is shown in Figure 13. This figure shows the use of three models, but there is no limit on how many models there can be. Each model administrates a number of control volumes. There are no limits on how many numbers of control volumes there are either and the different models can manage different number of control volumes. The control volumes communicate with each other independent of which model they are employed by (52).

2.5.4 GL View

GL View is a visualizing programme that can for instance read files and show results from the CFD code Brilliant. It was originally developed by Sintef, but it has been further developed through the company Ceetron ASA. GL View utilizes the graphic standard OpenGL for a three-dimensional graphic. This programme visualizes calculated data within structural mechanics and fluid dynamics. The programme can deal with very large data amount (53). An example of how the test furnace looks like in GL View is showed in Figure 14.

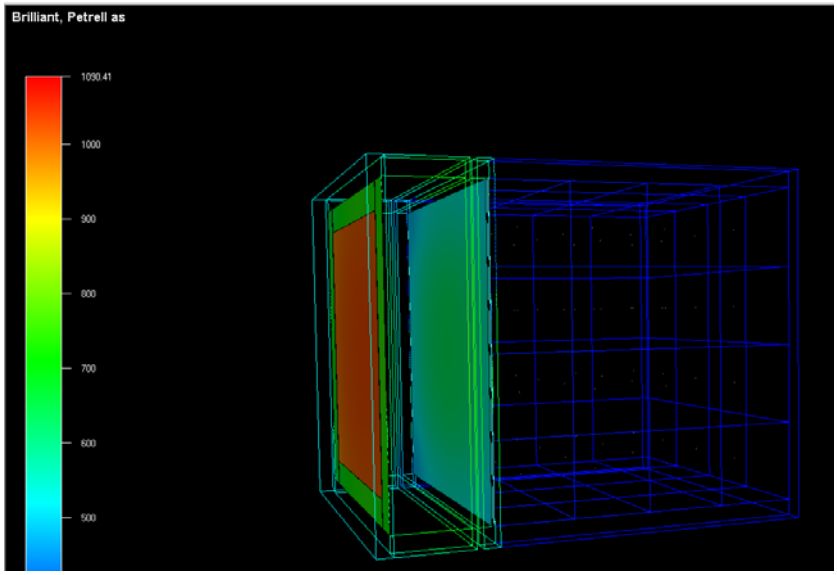

Figure 14 shows an example of how the testing furnace can look like in the programme GL View

3 Methodology

This chapter will describe the method used for finding the thermal conductivity of intumescing materials. This includes a description of the testing furnace; information about the numerical simulation programme used and the test procedure for the experiments.

3.1 Test method

The test method includes both physical experiments and numerical simulations. Data obtained from experiments with intumescing PFP materials will be used as input to the simulation software. The results from the experiments will then be compared with the simulated values. When the data is comparable, the correct thermal conductivity has been found. This procedure is presented as a flow diagram shown in Figure 15.

The total test procedure is roughly described as follows (1):

- The PFP material is mounted to the steel plate
- The steel plate is placed in the testing furnace
- The testing furnace with the PFP material is exposed to heat from radiation foils, while temperatures and the power used is registered with time
- The history of power used is put into a numerical simulation model where the geometry is modelled and the system is simulated for the time period of the experiment
- The thermal conductivity coefficient is modified until the temperature history is reproduced
- The thermal conductivity for the PFP material is then described as function of temperature referring to a constant density and specific heat capacity.

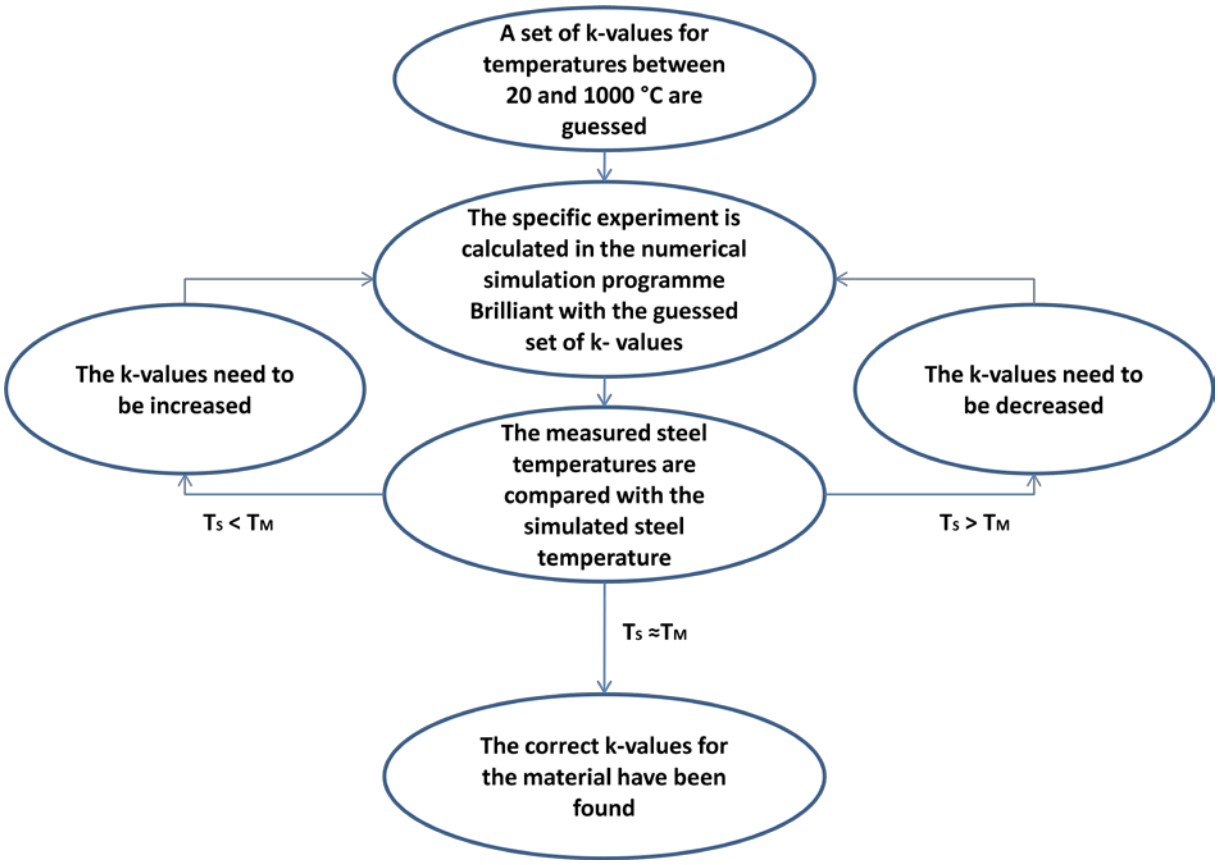

Figure 15 shows a flow diagram for finding the thermal conductivity of intumescing materials. T_s equals the simulated steel temperature, while T_m equals the measured steel temperature.

3.2 Testing furnace

During 2007/08, Sintef NBL AS and Petrell AS built a testing furnace for the purpose of doing experiments with passive fire protection of the type dead and intumescing materials. The goal of the experiments was to gather data that would make it possible to find the conductivity of PFP materials for elevated temperatures with the help of numerical simulation software. The same testing furnace with some adjustments has been used in this project, with the same objectives. This part will describe the testing furnace's construction and functionality. It also includes power calibration and temperature calibration.

3.2.1 Description

The testing equipment is composed of a control panel with a regulator, a thyristor, a transformer and a testing furnace. The equipment is shown in Picture 1. All the test equipment is placed inside a tent at the Norwegian Fire Resource Centre. The testing furnace is built up of 10 cm thick lightweight concrete. The concrete is coated on the inside with 2.5 cm ceramic isolation of the type Kaowool 1400. There is also a thin steel plate covering the ceramic isolation both in the ceiling and the bottom of the furnace. The furnace was built this way in order to make the system close to adiabatic. The inner dimensions in the furnace are 450 x 450 x 150 mm. The sample material will be placed 150 mm from the radiation panel in front of the carbon steel plate.

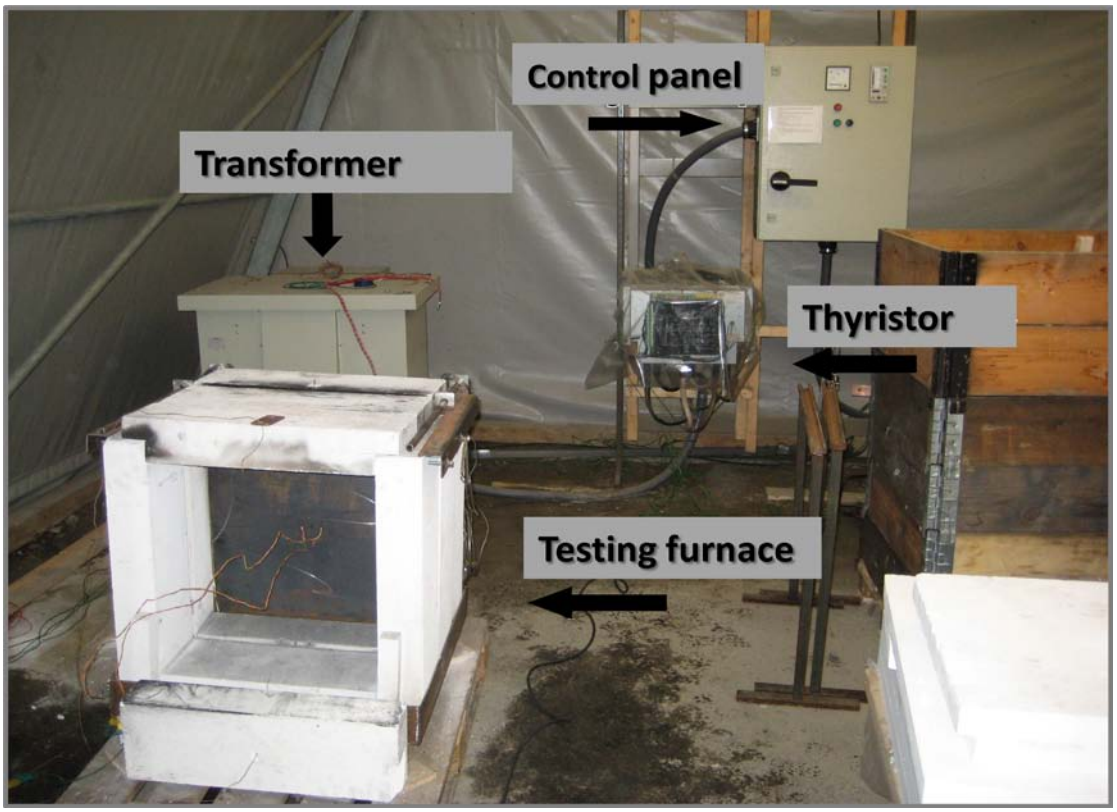

Picture 1 shows the equipment used in the experiments

The radiation panel consists of three vertical foils measuring 145 mm wide, 440 mm long and 0.05 mm thick. The foils are mounted to a copper plate both on top and on the bottom in the testing furnace which again is connected to power between the three different phases in the flow supply. It is important that the foils are tightly fastened to the copper plates in order to keep the foils steady during experiments. The foils will be in motion when exposed to heat, and they will become slightly deformed. They will for instance bend a bit and become a bit larger in the longitudinal direction. Picture 2 shows new radiation foils installed in the furnace. The foils are of the type Knufoil, which is stainless steel that consists of nickel and chrome. It is not recommended by the manufacturer to heat the foil to more than 1200 °C (10). Picture 3 shows the radiation foils when the power supply is on. Picture 4 shows the furnace from where the power cables are connected to the copper plates.

Picture 2 shows how the testing furnace looks like inside without any test specimen. Three vertical foils are shown in this picture that function as the radiation panel.

Picture 3 shows the radiation foils when the power supply is switched on.

Picture 4 shows the furnace from behind where the power cables are connected to the copper plates

In front of the steel plate, there is an air-gap around the whole furnace of 1 cm thickness. This is to allow exhaust gases from isolation materials escape and to avoid build up of pressure in the oven.

For the testing furnace to be useful, it is necessary to know the power input. For this reason, the best option is to use electricity as the heating source. This is because it is easier to know the power and the heat will be spread out more evenly than with for example fire as heating source.

Inside the control panel there is an electric isolation. This is a treatment facility for thermocouples that are in contact with current. Its function is to eliminate radiation and other disruptions from the thermocouples' signals, in order to get the most correct temperature into the logging system. This is only necessary for the thermocouples that are in direct contact with live equipment.

The control panel also contains the power switch for the system. The settings for each experiment are also made here. The input power can either be defined by the foil temperature or the percentage of power output. Both of these inputs can be controlled manually.

3.2.2 Power

The power consist of a 400 Volt three-face power supply, a thyristor controlled by a regulator and a 400/48 Volt transformer. The equipment is dimensioned for a continuous power of 150 kW and a peak power of 300 kW (2).

Adjustments of the power can be made from the control panel with a regulator that controls the thyristor. The thyristor regulates the power strength and therefore the power by clipping the sinus curves and only letting parts of it through, depending on how much power is required (2).

The power used in the experiments has almost been up to 25 kW. Since the radiation foils have an area of 0.44 m x (0.145 x 3) m = 0.19 m^2, the added power will be of the size 25/0.19≈130 kW per m^2. The power supply has the capacity to give the apparatus up to 150/0.19≈790 kW/m^2. The limiting factor in the apparatus is the radiation foils ability to transfer energy without losing its shape or starting to burn off.

To get a better understanding of how much energy the radiation foils actually gives out, an overview of the power of different types of heat sources are given in Table 4 (54).

Table 4: An overview of typical powers from fires

Heat source	Power
Candle light	100 W
Electric radiator	1000 W
Wood-burning stove	10 kW
Fire in a garbage bin	100 kW
Full flash-over in house	10 MW
Fire in a truck	100 MW

3.2.3 Power calibration

The power is registered by a volt signal from the control panel into the IMP 5000. This has a sampling frequency of one per second. The voltage on this signal represents the power sent to the furnace from the control panel. The volt signal needs to be converted to power. To make this conversion correct, it is necessary to calibrate the power measurement. To do this, the power needs to be compared with logging data from the real power sent from the thyristor. The thyristor regulates the power strength and adjusts how much power that is to be let through to the transformer. These adjustments correspond to several thousand adjustments per second. A second logging system that has a larger sampling frequency was therefore needed to get logging data of the power after the thyristor had adjusted it. By using this apparatus, the power signal could only be registered for a few seconds at the time, because of the huge data amounts that needed to be handled. The maximum sapling frequency for this apparatus was used, with a frequency of 9600 Hz distributed to the different channels. A total of 9600 data per second was therefore registered. The signal would despite of the short logging period be very accurate since it samples so often. Both the volt signal from the control panel and the power signal registered after the thyristor has adjusted it are registered at the same time with two different logging systems. The volt signal is then compared to the power signal (2).

There have been installed three measuring transformers between the transformer and the furnace. The reason for this is to be able to calibrate the power. The transformers are connected to the power logging system, which logs the current. Three cables are also connected to three of the bolts which are mounted to the copper plates in the furnace where the power goes in. There is one cable on phase U, one on phase V and one on phase W. These cables are then connected to the power logging system, which logs the voltages. Together there are six channels connected to the power logging system. Each of these has a frequency of 1600 Hz. A sketch of how everything is connected is shown in Appendix C (55).

To calibrate the power, a few seconds on each output from the control panel was registered. This was at 0 %, 10 %, 20 %, 30 %, 40 %, 50 %, 60 %, and 70 %. This was done twice to see if there was any difference. An average of the data from these two tests has been used to get the calibration data.

The results from the calibration tests showed that the current from phase V only had half the power of phases U and W. In order to find whether the phase actually was half the power or if was wrong at the induction reading, it was decided to check the foil temperatures when the situation in the furnace was stable. The control panel was therefore set to 40 % for a couple of minutes. The foil temperatures were very much alike, which indicated that the power was the same in all the three phases, and that the error could be in the measuring transformer. Moving the measuring transformer from phase V to phase W resulted in phase W showing half the power and channel V showing full power. It was concluded that the error was in the measuring transformer, and that all phases had the same power. The data from the affected phase will therefore be multiplied by two.

The volt signal from the second test where 10 % output was used is shown in Figure 16. The volt signal from the second test with 60 % output is also shown in Figure 17. As seen on these two figures, the distribution of the voltage is much more evenly spread out at 60 % output than 10 % output. An analysis of the distribution has been done for the other percentages as well, and it seems like the voltage is only unevenly spread out when the control panel is set to 10 %. As a consequence the foil temperatures may become different when the powers are low, and the heat radiation may become uneven.

In Figure 17, it is also possible to see the characteristic sinus curve that the power logging system is based on. The logging of the voltage has been over a resistance of 7.8 kOhm, while the logging of the current signal has been over a resistance of 10 Ohm.

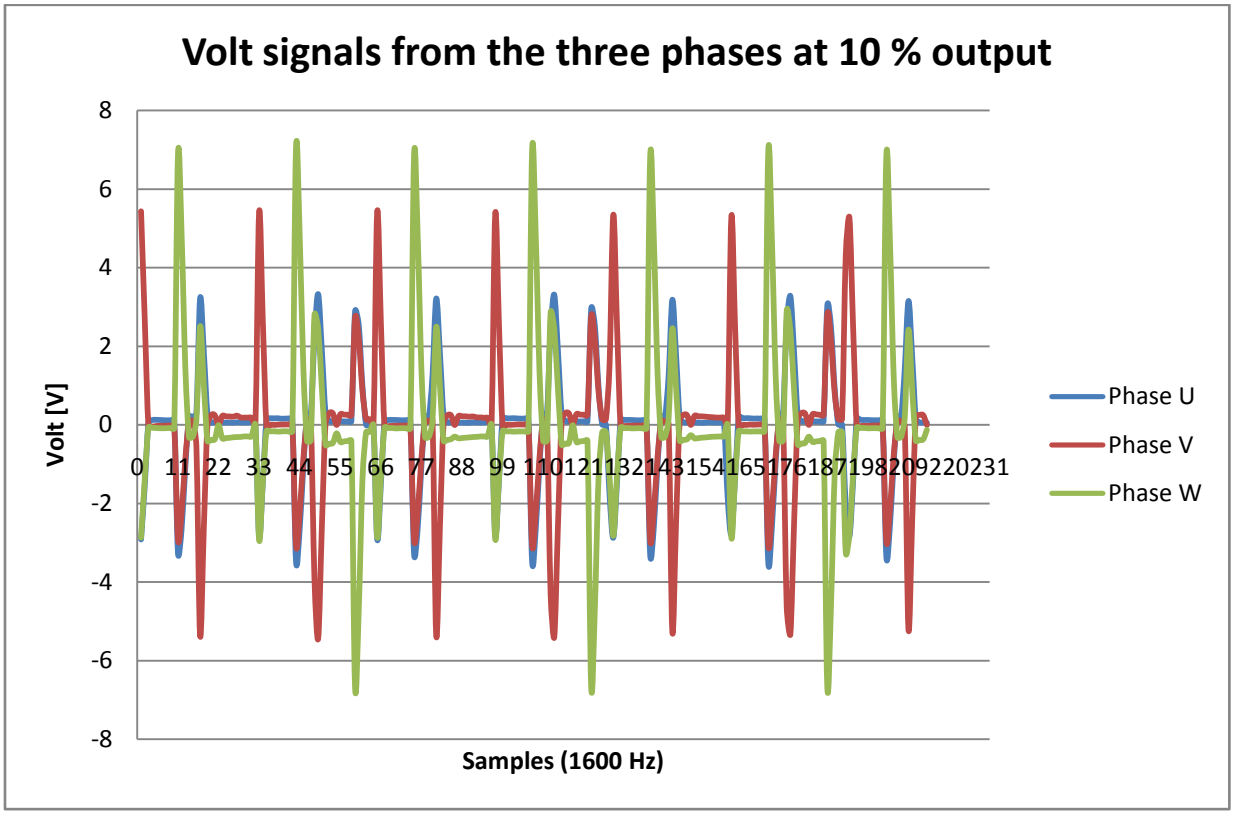

Figure 16 shows the volt signal from the three phases at 10 % output when calibrating the power.

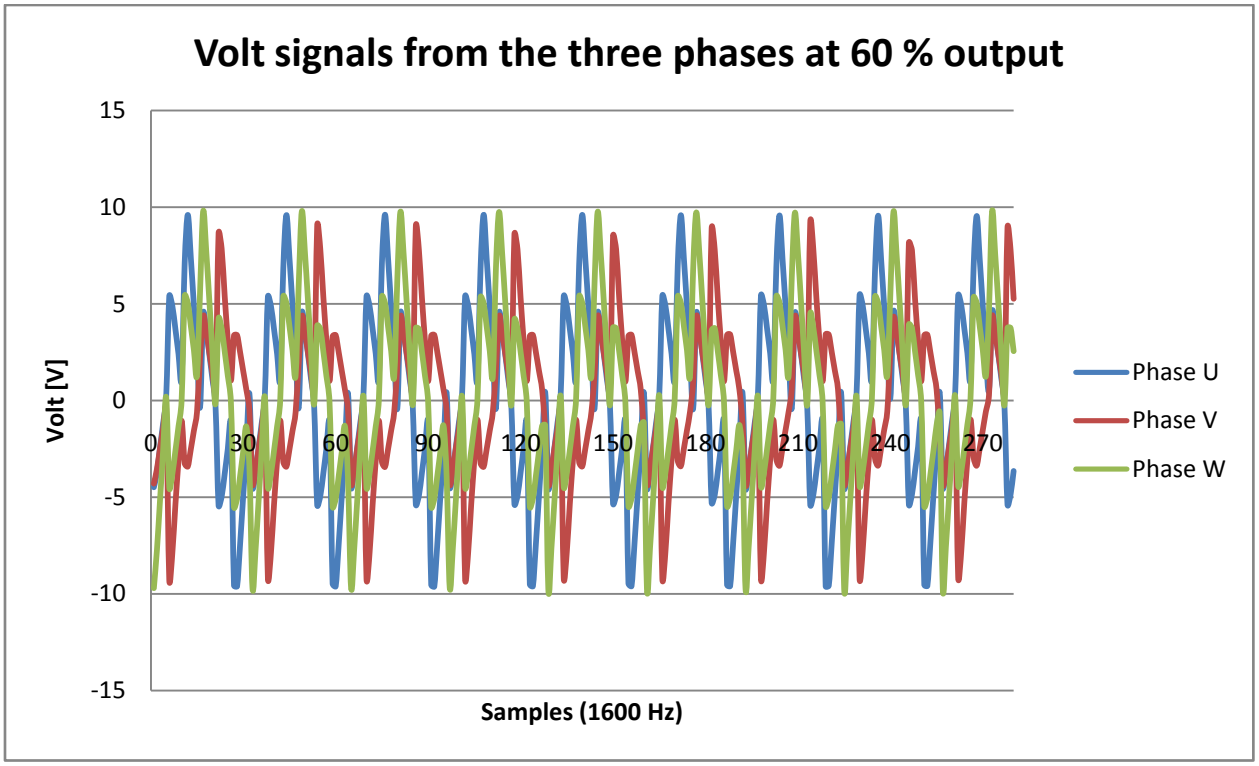

Figure 17 shows the volt signal from the three phases at 60 % output when calibrating the power

Method of calculating the power (55):

$$P_{tot} = P_{(U-V)} + P_{(V-W)} + P_{(W-U)}$$

$$E.g.:$$
$$P_{(U-V)} = U_{(U-V)} \cdot I_{(U-V)}$$
$$U_{(U-V)} = U_{(U)} - U_{(V)}$$
$$I_{(U-V)} = \frac{(I_{(U)} + I_{(V)} - I_{(W)})}{2}$$

Where,

P = the instantaneous power, measured in watts

I = the current through the component, measured in amperes

U = the potential difference (or voltage drop) across the component, measured in volts.

Formulas for calculating P_{total} (55):

$$U_{(U)} = \text{Volt signal} \cdot 7.8kOhm$$
$$U_{(V)} = \text{Volt signal} \cdot 7.8kOhm$$
$$U_{(W)} = \text{Volt signal} \cdot 7.8kOhm$$

$$I_{(U)} = \text{Current signal}/10kOhm$$
$$I_{(V)} = \text{Current signal}/10kOhm$$
$$I_{(W)} = \text{Current signal}/10kOhm$$

$$P_{(U-V)} = ABS((U_{(U)} - U_{(V)}) \cdot ((I_{(U)} + I_{(V)} - I_{(W)} / 2) \cdot (1/1600)$$
$$P_{(V-W)} = ABS((U_{(V)} - U_{(W)}) \cdot ((I_{(V)} + I_{(W)} - I_{(U)} / 2) \cdot (1/1600)$$
$$P_{(U-W)} = ABS((U_{(U)} - U_{(W)}) \cdot ((I_{(U)} + I_{(W)} - I_{(V)} / 2) \cdot (1/1600)$$

$$P_{total} = P_{(U-V)} + P_{(V-W)} + P_{(U-W)}$$

$P_{electricity}$ is set to be equal to the sum of P_{total} after one second. There is therefore one value for $P_{electricity}$ for each percent output. These values are multiplied with 2/3, because the power is only calculated on two phases, which means 2/3 of total power (55). The average value of $P_{electricity}$ from each output was then calculated. Data from each output has been registered twice, except on the outputs 60 % and 70 %. These were only done once. The average value of P_{volt} was also calculated. The ratio between $P_{electricity}$ and P_{volt} was then found by using this equation (55):

$$P_{\text{electricity average}}^{0.6} / P_{\text{volt average}}$$

To find the equation for the best adjustment, this equation was used (55):

$$P_{\text{volt adjutment}} = \text{Average ratio} \cdot \text{P}_{\text{volt average}}^{(1/0.6)}$$

The equation used to find the power from the volt signal is then:

$$4.961427 \cdot \text{volt signal}^{1.67}$$

Where 4.961427 is the average ratio of $P_{electricity}$ and P_{volt}, and 1.67 is 1/0.6, where 0.6 is the best adjustment. A graph of the power as a function of the output is shown in Figure 18. More detailed data on the power calibration is shown in Appendix E.

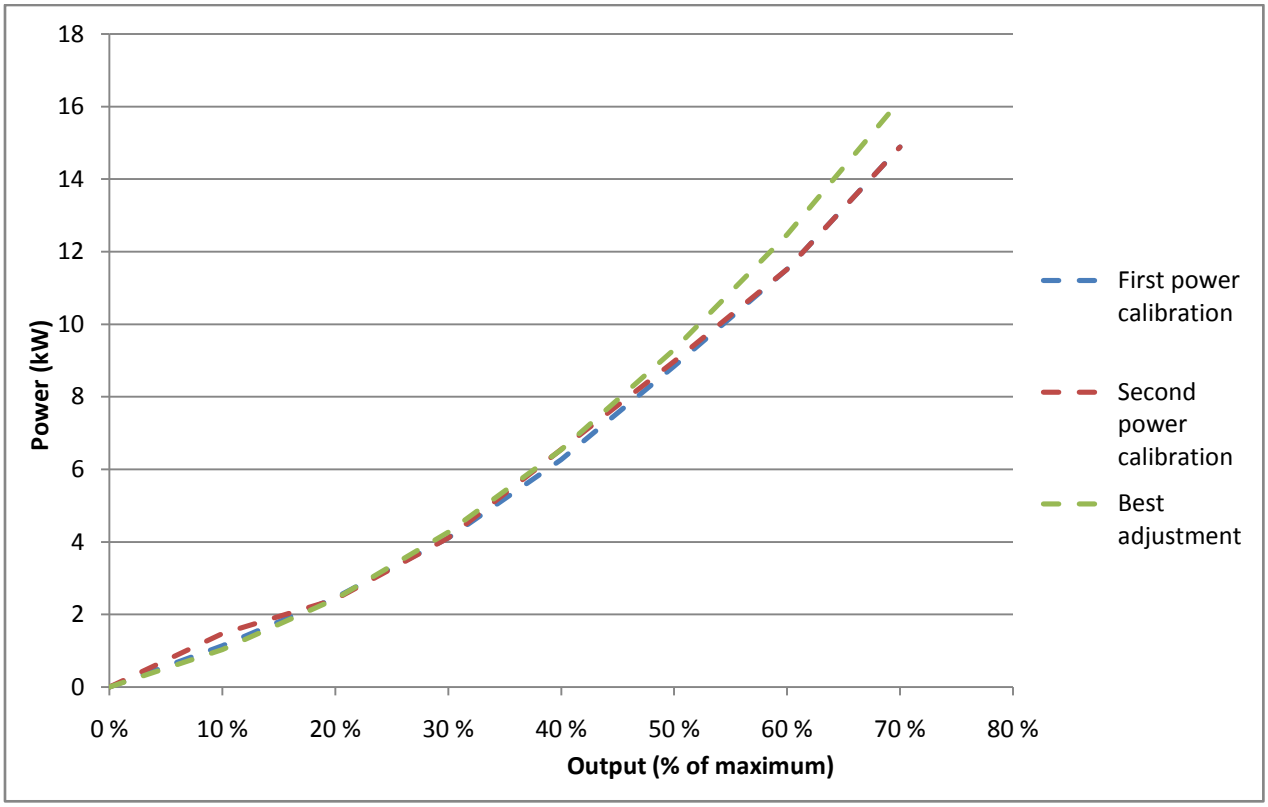

Figure 18 shows the power as a function of the output from power calibration

A sketch of the different phases is shown in Figure 19 (55).

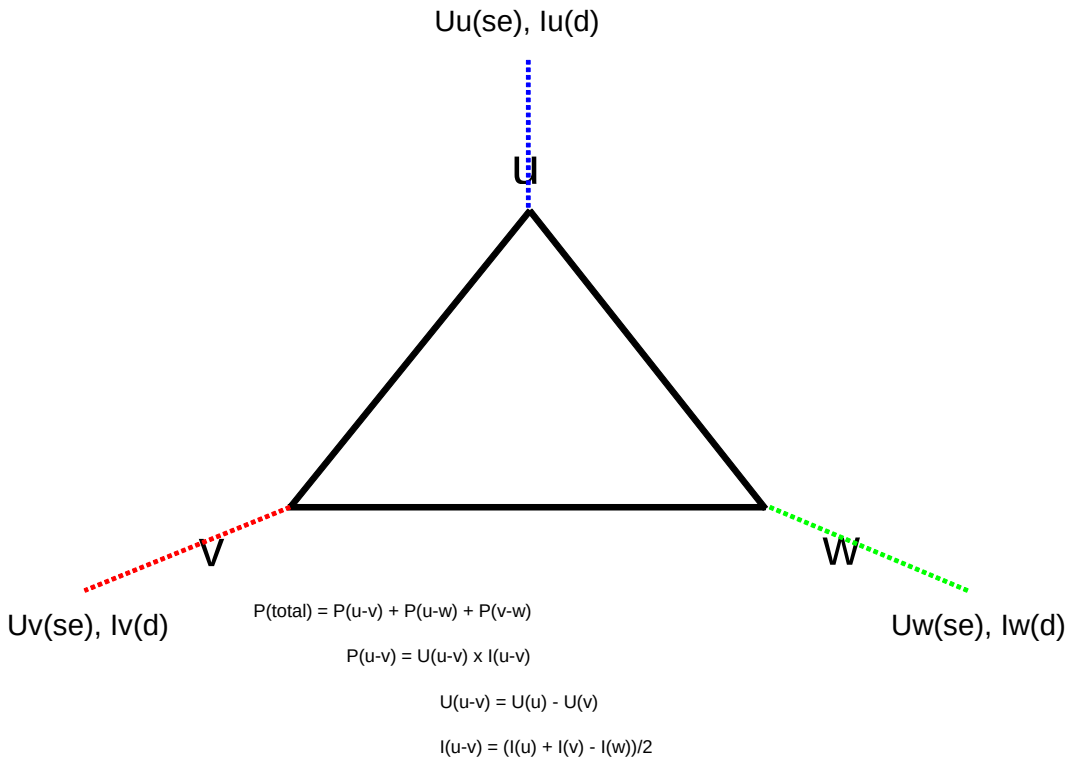

Figure 19 shows a sketch of the different phases in the power supply (55)

3.2.4 Measuring temperature

This part will describe how temperatures were measured in the furnace. Measuring the foil temperature seemed to be quite difficult and several methods were tested. All these methods are described in this part.

3.2.4.1 Overview

The surface temperature on the three foils that function as a radiation panel has been measured by a thermocouple of type K. A more detailed explanation of how this has been done is described in part 3.2.4.2. One of these temperatures is controlled by the control panel. The temperature is set and the amount of input power is decided by the control panel.

Heat transport through the steel plate is measured by two 1 mm thick thermocouples of type K, which are welded onto the steel plate. The thermocouples are placed in the centre of both exposed and unexposed side of the steel plate. These thermocouples consist of two open conductors that measure temperature when they are in contact either with each other or with a material that conducts power, like the steel plate. In this case both of the conductors have contact with the steel plate at different points. It is very important that the two open conductors are not in contact with each other at other places than where the temperature is supposed to be measured. This can happen if for example the isolation surrounding the conductors burn off and the conductors touch each other before touching the steel plate.

On the front of the furnace there are two thermocouples. One of these is placed on top of the furnace and the other one is on the bottom. The purpose of these thermocouples is to measure the convection on the unexposed side of the steel plate. These two temperatures are logged directly and not through the electric isolation in the control panel. This is because there is no power related to these two thermocouples. The temperature on the bottom is used as T_{air} in the numerical simulation programme Brilliant. This is the ambient temperature in the room.

Three shielded type K thermocouples were used for measuring temperatures at different spots on one of the copper plates that hold the radiation foils in place. This is further explained in part 3.2.7.

From the transformer to the radiation panel there is an electric conductor. In one of the previous reports on this work it was discussed whether the heating that was measured on the electric conductors was because of ohmic resistance in the conductors, or if it was because of conduction from the radiation panel (2). To investigate this, four thermocouples were mounted on the electric conductor at four different spots, respectively 3 cm, 20 cm, 25 cm and 78 cm from the back of the test furnace. The temperature expansion was recorded for 15 minutes. The results from this experiment showed that the electric conductor was considerably heated 3 cm from the furnace, but almost nothing at 78 cm from the furnace.

This meant that the heating source was not ohmic resistance, but conduction from the radiation panel (2).

3.2.4.2 Measuring the foil temperatures

Measuring the foil temperatures has proven to be a challenging task. The foils are very thin and become fragile after exposure to heat. They also move during the experiments, and conduct power. This part will describe the different methods to measure the foil temperatures that have been tested.

3.2.4.2.1 Measuring the foil temperatures in experiment 171008, 271008 and 051108

In the first experiments (171008, 271008 and 051108) the thermocouples on the foils were measuring the temperatures on the back of the foil, on the same side as the wall isolation. The surface temperature on the three foils in the radiation panel was measured by a 0.5 mm thick thermocouple of type K. The thermocouples were placed in the middle of each foil so that the thermocouples' tips, that measure the temperature, were in contact with the foil. To make this work, the thermocouples were "sewed" onto the foils. Each thermocouple was pulled through a foil from the backside and back through the foil at a different spot. Only 1-2 millimetres of the thermocouple were sticking out on the back. There it was squeezed together with the foil to measure the foils surface temperature.

The mentioned experiments showed significant variations in the measured foil temperatures. This was due to the fact that the thermocouples had not been in contact with the foils during parts of the experiments. It is essential that the thermocouples are in good contact with the foils to obtain correct measurements, and therefore the method of measuring this temperature had to be further developed.

3.2.4.2.2 Measuring the foil temperatures in experiment 111108 and 141108

Three new ways of measuring the surface temperature on the foils were tested. The first solution tested involved fastening each thermocouple to a tiny steel plate that was screwed onto the foil. This was tested without any test specimens in the furnace, so that it would be possible to see the foils while they were heated. It was visible that the foils' surfaces were warmer around the tiny steel plates than at the rest of the foils because of the foils' colours. This method was therefore abandoned.

The second test involved using a thermocouple with open conductors. One of the conductors was fastened between the copper plate and foil at the top and the other one was fastened between the copper and the foil at the bottom. This type of thermocouple measures an average temperature through the whole foil. The foil conducts power, so in between the two open conductors, it would measure the temperature. This method resulted in a measured temperature of about 220 °C while control measurements showed 600 °C. A reason for this deviation could be that the isolation around the conductors burnt off and the thermocouples actually measured a temperature outside the foil, at the point where the

conductors met. The isolation can only withstand about 300 °C. The use of thermocouples with open conductors was therefore abandoned.

Another method applying shielded thermocouples was tested. Instead of “sewing” the thermocouples by pulling them through the foils twice, it was tested whether three “stitches” would help keeping the foils more stable. Using this method implied that thermocouple’s tip would be on the foil surface pointing towards the test specimen. The tip was squeezed together with the foil so that there would be good contact between them. This is shown in Picture 5.

This method was based on the assumption that it did not matter which side of the foils the thermocouples’ tips were mounted on. It was however brought forward that if the problem with bad contact between the thermocouple and the foil should reappear, it would have greater consequences if the thermocouples were on the side pointing towards the test specimen. On this side there is 15 cm from the foils to the test specimen, whereas on the back there is only 1 cm of air separating the foil from the wall isolation. If the thermocouple moves only 0.01 mm from the foil, it will be cooled down by convection. This effect is stronger on the front than on the back of the foil, due to stronger temperature gradients. Therefore, the thermocouples should be located on the back of the foil, but in a different way than before.

Picture 5 shows a close up of how the foil surface temperature was measured in experiment 111108 and 141108

Before any new ways of measuring the foil temperature were tested, a test on the conformity of the foil temperatures was performed. This was needed in order to verify whether inaccuracies and variations were caused by the measuring methods or by the foils themselves. The top cover and the steel plate were removed from the furnace, and a new thermocouple was manually pressed against the front of each foil. This resulted in equal measurements for all foils. This meant that the electric conductors from the transformer were distributing the power evenly to the six copper parts, which again leads the power to the three foils.

3.2.4.2.3 The foil temperature measurement in all experiments from 181108 to 041208.

In the experiments from 171008 to 141108 thermocouples with a diameter of 0.5 mm were used. Because these thermocouples broke very easily, they were replaced with thermocouples of 1.5 mm. These were twisted into springs, and placed between the back wall of the furnace and the foils. The intension of the spring was to keep the tip of the thermocouple pressed against the foil during movements in the foil itself. This is shown in Picture 6. This method resulted in quite stable temperature measurements, but variations in the input power still existed.

Picture 6 shows how the surface temperatures on the foils were measured in the experiments 181108 to 041208.

3.2.4.2.4 Measuring the foil temperature on independent foil bits from experiment 041208 and onwards

Three new independent foil bits of the same type as the radiation foils, and measuring 3 x 3 cm were placed against the isolation behind the radiation foils. One foil bit was placed behind each of the three radiation foils. The distance from the foil bits and the radiation foils was then about 1 cm. Since there no electricity was connected to these independent foil bits, it was possible to weld a thermocouple with open conductors to them. This made the temperature measurement a lot more stable than if the thermocouple was placed against the foil. Because of the distance between the radiation foil and the foil bit, it had to be taken into consideration that the temperature measured on the foil bits would become slightly lower than the surface temperature on the radiation foils. The first experiments where the foil bits were used, the temperatures on the radiation foils were also measured to assess the temperature differences between the two. For all experiments on intumescing materials, the measurement of the temperature on the radiation foils was abandoned. Picture 7 shows one of the foil bits installed in the furnace.

Picture 7 shows one of the installed foil bits placed against the isolation as a small square on the left side. The thermocouple, designed as a spring, measuring the surface temperature on the radiation foil can be seen above the foil bit.

3.2.5 Temperature calibration

There are twelve thermocouples all together. Seven of these go through the electric isolation in the control panel. Four of the thermocouples are directly plugged into the IMP 5000 and comes out in degree Celsius. The remaining thermocouple is the one that is controlled by the control panel. This thermocouple was calibrated when the control panel was installed. The signal from the control panel comes out as the power input to the system in the IMP 5000. All the other thermocouples need to be calibrated. This is to make sure that the temperatures that are measured are tolerably correct. All of them will have their own adjustment constant, because of different lengths on the cables and transfer contacts that can disturb the signal.

To calibrate the temperatures, a Promac DHT 740 calibrator, was used. The volt signal from 20 °C, 500 °C and 1000 °C was recorded from each thermocouple. It was then calculated a value for A and B using linear regression. The values from this calibration are listed underneath. The linear graph is shown in Figure 20. The calculation and the different values for the A and B constants, for every thermocouple, are shown in Appendix D.

Calibration data

Channel	Description	Temperature [°C]	Volt signal [V]
2	foil middle	20	0,739
3	foil left	20	0,737
4	steel exposed	20	0,745
5	steed unexposed	20	0,741
8	copper T2	20	0,734
9	copper T1	20	0,742
10	copper inside	20	0,72
2	foil middle	500	2,253
3	foil left	500	2,253
4	steel exposed	500	2,257
5	steed unexposed	500	2,253
8	copper T2	500	2,248
9	copper T1	500	2,256
10	copper inside	500	2,336
2	foil middle	1000	3,829
3	foil left	1000	3,829
4	steel exposed	1000	3,83
5	steed unexposed	1000	3,826
8	copper T2	1000	3,822
9	copper T1	1000	3,831
10	copper inside	1000	3,8072

Linear regression:

Volt signal = A*temp + B

A	B
0,00315083	**0,67920779**

Temp = a * volt signal + b

a	B
317,301578	**- 215,393871**

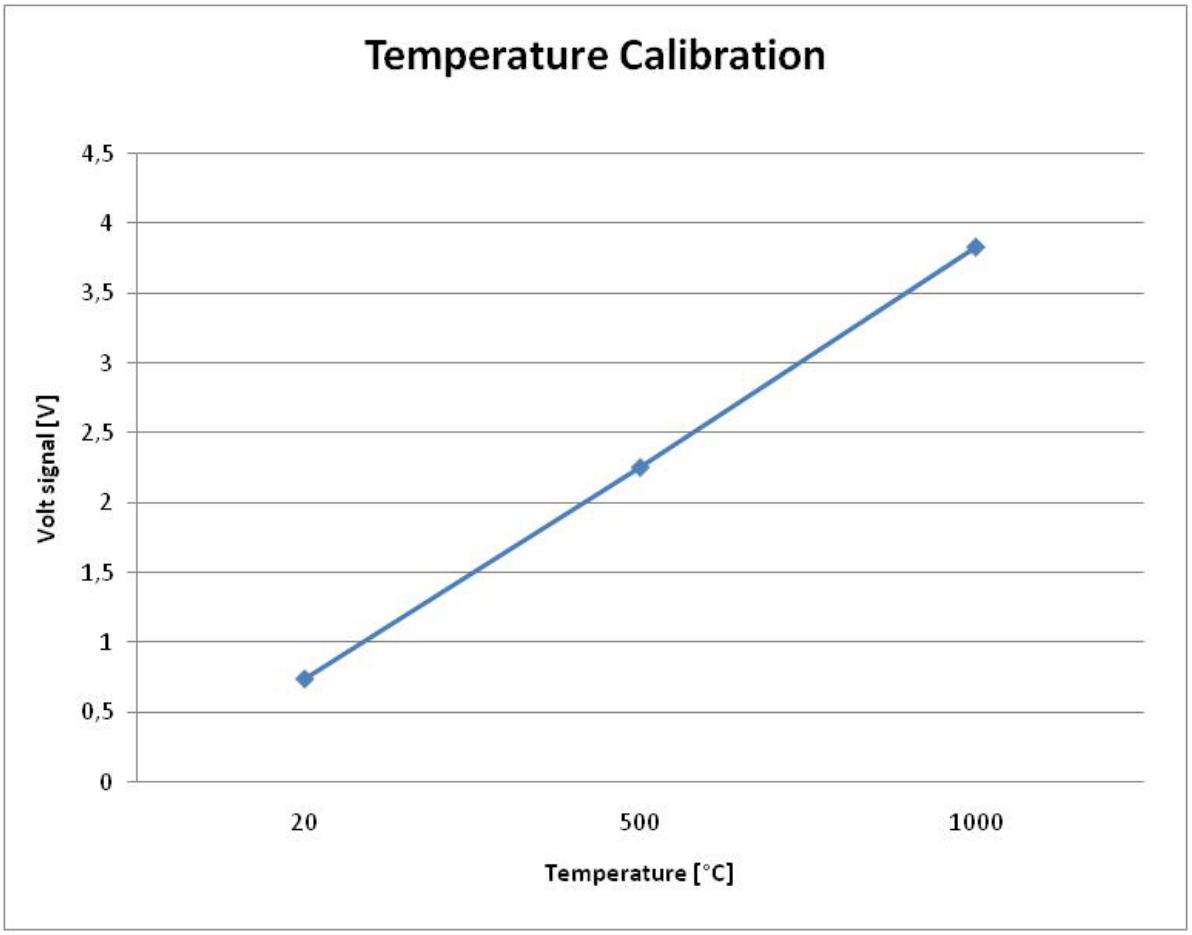

Figure 20 shows the temperature calibrated as a function of the volt signal.

3.2.6 Heat balance in the testing furnace

During an experiment, steady state is reached after a few minutes. The exact time length depends on what sort of isolation there is installed to protect the steel plate. When steady state is reached, the same amount of heat inserted to the furnace will be the same amount that is going out of the furnace. That is:

Input power = Heat loss in form of radiation, convection and transmission.

$$\dot{q}_{power} = \dot{q}_r + \dot{q}_c + \dot{q}_t [W]$$

$\dot{q}_r = \varepsilon \cdot \sigma \cdot T_f^4 \cdot A\ [W]$, where ε is the foils emissivity, σ is Stefan Boltzmann's constant and T_f is the surface temperature of the foil.

$\dot{q}_c = h \cdot \Delta T \cdot A[W]$ In this case $h = 10 W/m^2 \cdot K$ is assumed as a proper value (2).

$$\dot{q}_t = -k \cdot \frac{dT}{dx} \cdot A[W]$$

The energy from the radiation foils will mostly be given by radiation, some will be given by convection and a small amount will be given by conduction through the copper plates.

A detailed figure of the furnace and its components seen as a cross-section from the side is shown in Figure 21. The same figure is shown over again in Figure 22 where the heat balance in the furnace is shown.

From the air gap on top of the furnace there will flow heated air which will be compensated by cooler air from the air gap on the underside. This heat loss will be modelled in the numerical simulation. The circulation happens by natural convection because warm air expands and rises. The velocity of this flow is controlled by the width of the air gap and the foils temperature.

The copper plates that hold the foils in place conducts heat which will result in heat loss through the copper plates and out to the power cables. How this heat loss has been calculated is explained in part 3.2.7. The amount of heat loss through the copper plates depends on the temperature. The higher temperature there is in the furnace, the more heat loss there is.

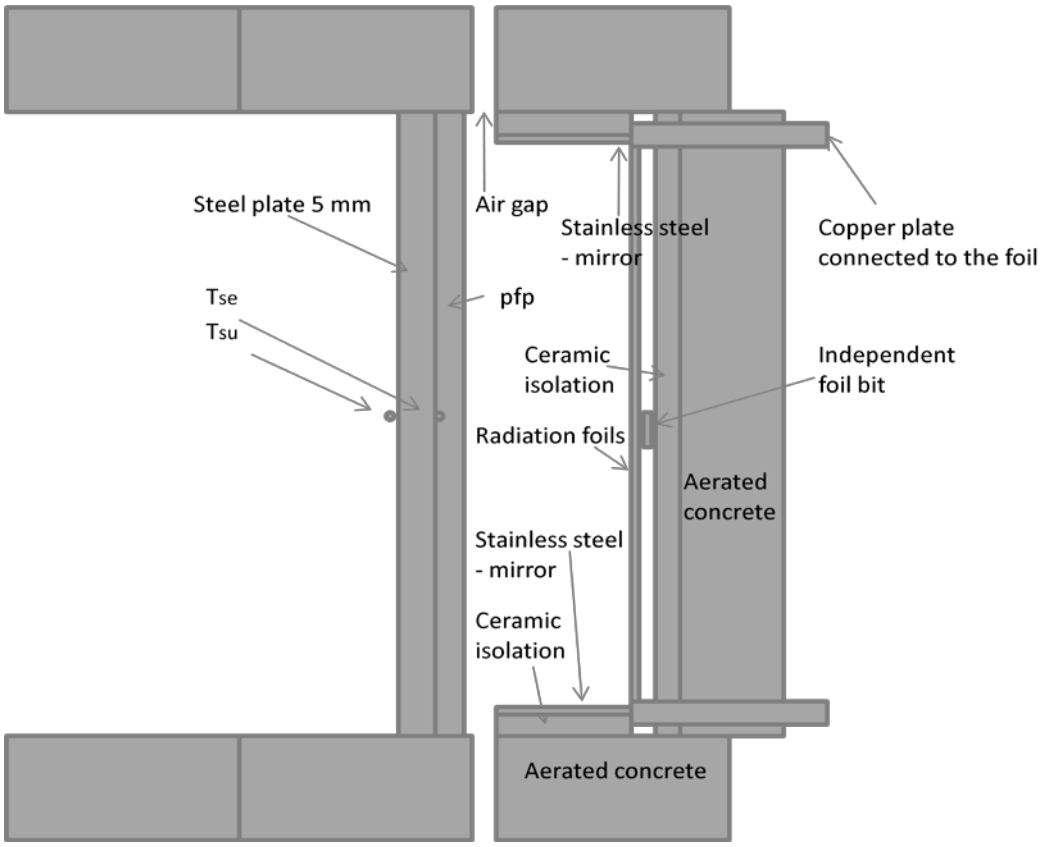

Figure 21 shows a detailed sketch of the furnace with all its components

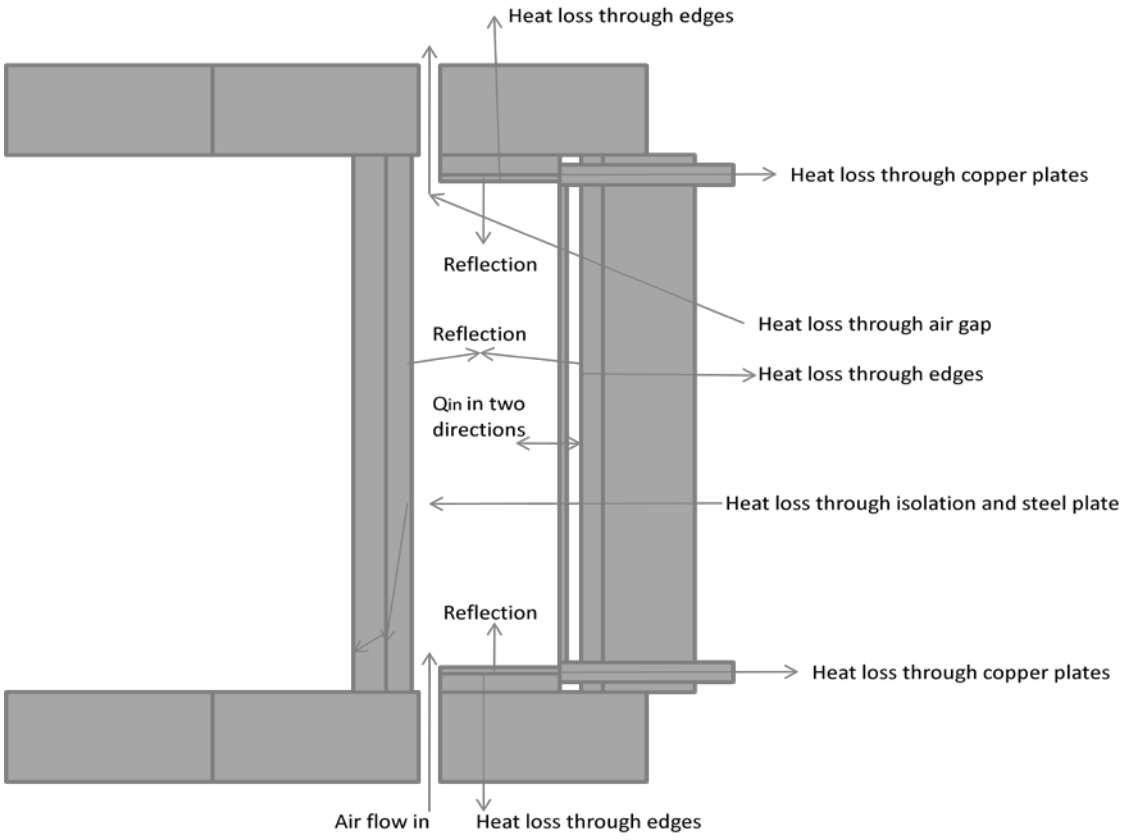

Figure 22 shows a sketch of the furnace including heat balance

3.2.7 Calculation of the heat loss to the copper plates

The power input to the system goes through six different copper plates. These copper plates get heated during an experiment. This requires energy that will be referred to as heat loss for heating. Heat loss through the copper plates will also occur as they conduct heat.

In all the experiments from 171008 to 191108, the energy required for heating the copper plates and keeping them heated was included in the calculations of heat loss. The copper plates were divided into two parts when calculated; one top part (with notation 'copper inside') and one length part (with notation 'copper outside'). The 'inside' part is the part inside the furnace, while the 'outside' part represents both the copper on the outside and the copper inside the isolation and the lightweight concrete. The equations used to calculate these heat losses are:

$$P_{Heating,inside} = \Delta T_{inside} \cdot C_{p_{copper}} \cdot V_{copper-plate,inside} \cdot \rho_{copper} \cdot 6[J]$$

Where $\Delta T_{inside} = T_{inside,n+1} - T_{inside,n}$

$$P_{Heating,outside} = ((T_{inside,n+1} + T_{outside,n+1})/2) - ((T_{inside,n} + T_{outside,n})/2) \cdot C_{p_{copper}} \cdot V_{copper-plate,outside} \cdot \rho_{copper} \cdot 6[J]$$

The equations are multiplied with six because of the six copper parts. The equation for heating the 'copper outside' calculates the average temperature between T_{inside} and $T_{outside}$. This gives an estimate of the temperature in the middle of the outside part. A sketch of where the thermocouples were placed on the copper plates is shown as red dots in Figure 23. The thermocouples were shielded ones of type K with a thickness of 1.5 mm.

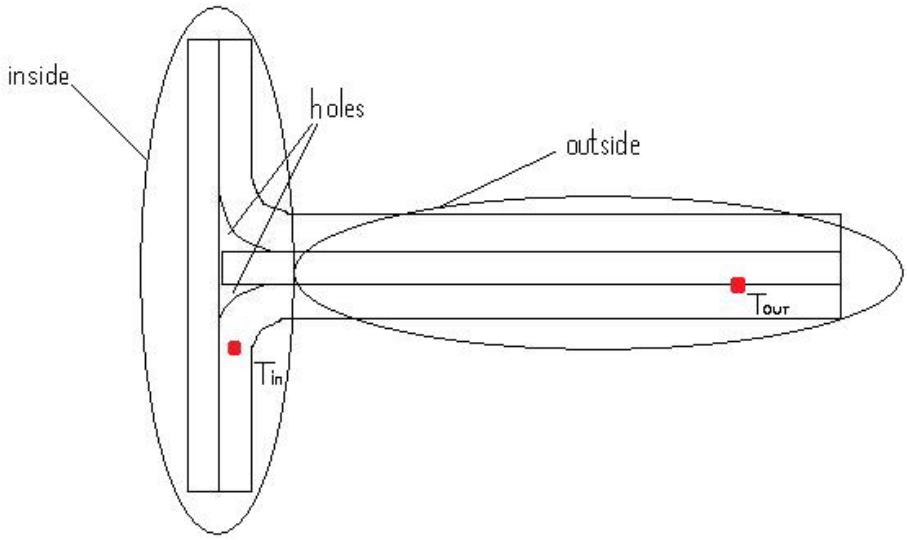

Figure 23 shows a sketch of a copper plate. The red dots show where the thermocouples were placed in the experiments from 171008 to 191108.

The dimensions of the two copper parts:

	Length [cm]	Width [cm]	Height [cm]	Cross-sectional area [m^2]	Volume [m^3]
Copper inside	14,5	1	2	0.0002	2.8*10^-5
Copper outside	19	1,5	2	0.0003	5.7*10^-5

In the calculation of the volume of each part, 0.5 cm on the length of the inside part and 1 cm on the length on the outside part where withdrawn. This was because of two holes between the outside and inside part. These holes are shown in Figure 23.

After subtracting the calculated heat losses from the total input power, the delivered powers became quite turbulent. This occurred due to delays in the logging system. An average heat loss over ten seconds was therefore calculated. This would make the delivered power curves more fluent.

In experiments from 171008 to 191108, the heat loss due to conduction through the copper plates was not included in the calculations. This was later added as a part of the heat loss. By including both energy lost for heating the copper plates and heat conduction through them, the total amount of heat loss would become more accurate. The experiments from 211108 and onward include both these heat losses.

To calculate the thermal conductance through the copper plates it was necessary to measure the temperature on the copper in a different way than before. To make the calculation most accurate, one thermocouple was placed on the copper on the edge where the isolation starts, denoted T_1, while another one was placed in between the isolation and the lightweight concrete, denoted T_2. The isolation is 2.5 cm thick, which means that there would be 2.5 cm between the two thermocouples. A sketch of where the thermocouples were placed is shown in Figure 24. Picture 8 and Picture 9 show one of the copper plates with the three thermocouples installed.

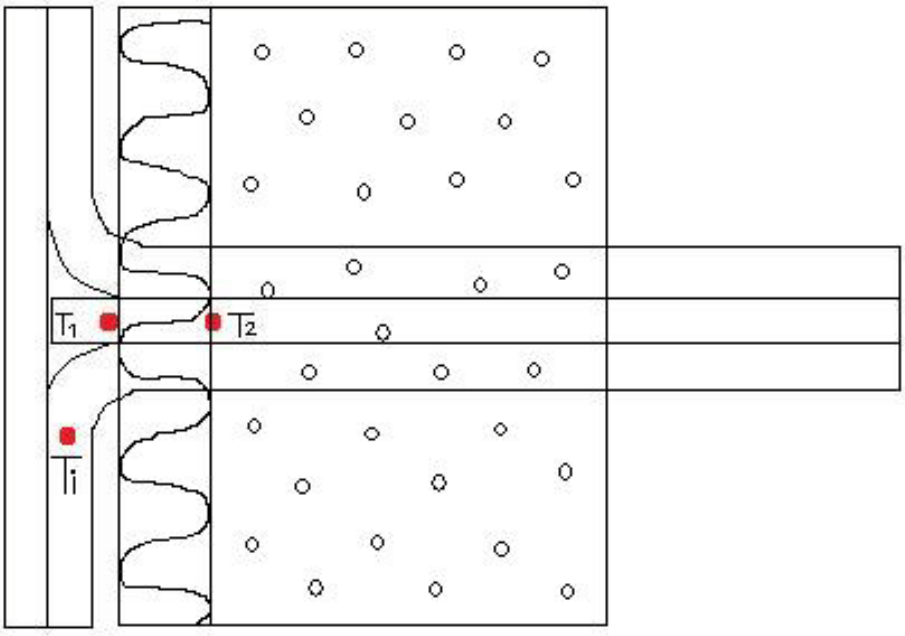

Figure 24 shows a sketch of a copper plate showing where the thermocouples were placed from experiment 211108 and onwards

Picture 8 to the left shows one of the copper plates with all the thermocouples in place.

Picture 9 to the right shows one of the copper plates with the three thermocouples in place. The isolation between thermocouple T1 and T2 is also in place.

The heat loss calculation for heating 'copper inside' would be the same as earlier. For calculations of the energy required for heating 'copper outside', the temperature recorded from the thermocouple denoted T_1 in the sketch in Figure 24 was used. This heat loss was calculated for the first bit of the copper length. This means the part from where the inside and the outside divide to where the lightweight concrete starts, approximately a distance of 3 cm. The equation used is as follows:

$$P_{Heating,outside} = \Delta T_{outside} \cdot C_{p_{copper}} \cdot V_{copper-plate,outside} \cdot \rho_{copper} \cdot 6[J]$$

Where $\Delta T_{outside} = T_{outside,n+1} - T_{outside,n}$

All the equations used for calculating heat loss to the copper plates have been calculated for every second of each experiment. Each value is therefore $\frac{P}{\sec} = \dot{q}[W]$

The thermal conductance through the six copper plates is calculated as follows:

$$\dot{q} = \frac{k \cdot \Delta T \cdot A \cdot 6}{\Delta x}[W]$$

Where $\Delta T = T_2 - T_1$

$\Delta x = 0.02m$

$k = 387W / m \cdot K$

$A = (0.015 \cdot 0.02)m = 0.0003m^2$

The delivered power equals:

$$\dot{q}_{delivered} = \dot{q}_{total} - \dot{q}_{heating,inside} - \dot{q}_{heating,outside} - \dot{q}_{conduction}$$

3.2.8 Application of the test specimens

The dead materials that were tested were mounted onto the steel plate by use of four metal pins. The pins could be pressed through the isolation and fit through holes that were drilled in the metal plate. Eight metal clips were used to lock the pins in place, one for each end of every pin.

Since Kaowool boards are quite hard and stiff, there were some areas where the Kaowool and the steel plate were not completely in contact. In these areas, the heat would first transport through the Kaowool isolation, then flow through a small air gap before reaching the steel plate. This can be a source of failure in the experiments, since heat transports differently through solids than through air.

Firemaster is a softer material than Kaowool, and was therefore easy to press onto the steel plate. However, one needs to be careful, as pressing the material too hard could result in a change of density. Even though the material was easily applied onto the steel plate, there was still a good chance that the isolation was not completely in contact with the steel plate.

When applying the intumescing materials to the steel plate, the same procedure as for dead materials was used. However, the intumescing materials were hard plates, and therefore required drilling of the necessary holes. Picture 10 shows the test specimen ProTek B3 (an intumescing material) installed in the furnace ready for testing. Picture 11 shows ProTek B3 fastened to the steel plate after being tested.

Picture 10 shows ProTek B3 (an intumescing material) ready to be tested inside the furnace.

Picture 11 shows ProTek B3 (an intumescing material) fastened to a steel plate after being exposed to heat for about an hour

3.2.9 Logging system

The logger used to get data from the experiments was an IMP 5000. IMP stands for Isolated Measurement Pod and can among others give precise measurements of dc voltage and temperature direct from thermocouples, which is what it was used for in this thesis. IMP 5000 is a data module containing signal conditioning, 16 bit ADC (Analogue-to-digital-converter) and communications to host computer (56). In the start-up phase, some of the thermocouple connections didn't function as intended. The IMP 5000 did not receive any signal from them. These connections were replaced. Picture 12 shows the IMP 5000.

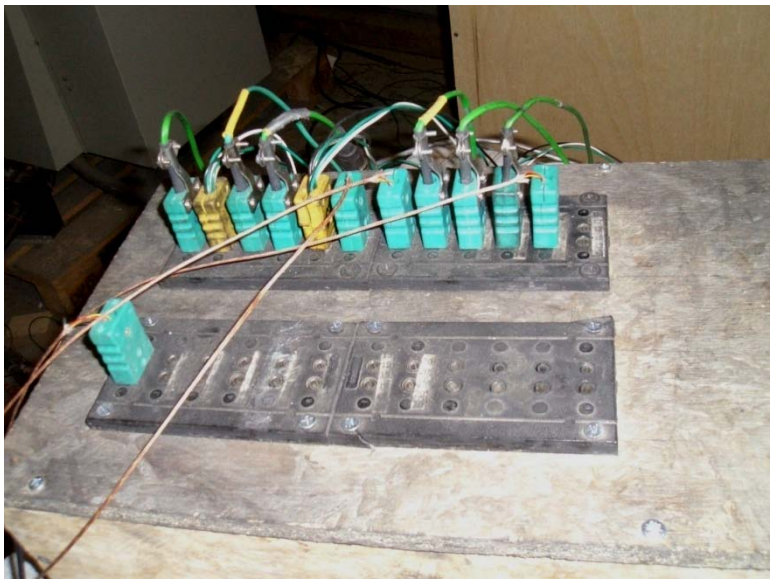

Picture 12 shows the IMP 5000 with thermocouples connected in it

3.2.10 Instructions for using the power supply connected to the testing furnace

Before testing

- Check that the main-power-switch on the control panel is set in the «0»-position.
- The fuse connected to the control panel is the one in distribution locker A in drawer called “Byggstrøm”. Insert the fuse in the fuse terminal box and put the drawer in place.
- Check that the testing furnace with all its thermocouples and connections are intact.
- Set the main-power-switch in position «1» (on).
- Adjust the PID-controller[1] (57).

During a test

- Start logging from the programme «DataQ» on the computer
- Start the oven by pressing the green button on the control panel
- Adjust the power input slowly to desired level

After testing

- Turn off the power supply by pressing the red button on the control panel
- Set the main-switch-power to position «0»

[1] PID-controller is a regulator with three parameters that decides the effect. These parameters are the proportional, the integral and the derivative values. By summing these three terms, the output and the PID controller is defined.

- Stop logging from the programme «DataQ»
- Remove the fuses in the “Byggstrøm” drawer, and put them on top of the distribution locker.

3.2.11 Step by step procedure of how the experiments are carried out

1. Clean out soot from the furnace if necessary
2. Check that all the thermocouples are in place and that the power supply is connected properly.
3. Make sure that all the foils are intact.
4. Insert the steel plate (with or without isolation attached to it). Make sure that the thickness of the isolation is measured before attaching it to the steel plate. This should be measured by a slide caliper. Each specimen should also be weighed before testing.
5. Plug in the thermocouples connected to the steel plate.
6. Fit on the top cover on the furnace. Make sure that the air gap is intact.
7. Follow the instructions described in 3.2.10.
8. During each test, pay attention to the temperatures registered and make sure that the control panel is switched off if one of the foils burn off. This is noticeable by a sudden drop on the foil temperatures.
9. After each test, the furnace should be cooled down before subsequent tests are performed.
10. If an intumescing material has been tested, the thickness of the material should be measured by means of a slide caliper.

3.3 Numerical simulation method

The CFD code Brilliant has been used to perform all the numerical simulations. This part will describe the simulation model used for finding the thermal conductivity of intumescing materials. Firstly, the setup of the numerical simulations will be described. This gives a description of how the furnace is reproduced in software. Subsequently, the various input data to the simulation are described.

3.3.1 Numerical simulation setup

An algorithm has been written for this project that describes the furnace as a physical model with the correct physical dimensions and properties of the materials that are in it. Details have been included in the model to the extent that they are necessary to make the model representative (1).

The physical processes that take place in the furnace, such as radiation, convection and conduction are described in control volumes. Brilliant calculates heat conduction through all surfaces and radiation from all surfaces. It also calculates heat convection in all areas with air. The calculation model is limited by specific boundary conditions. These conditions are fixed for all dimensions. For the x dimension, air is set to move at a velocity of 0.1 m/s from

both directions at the boundary. In the z dimension (the top boundary), pressure is set to be constant above the furnace, but air may flow through. In the y dimension no boundary has been specified, which means that the system is adiabatic with no flow.

Figure 25 shows the simulated furnace from above, taken from an example simulation. The edges are not shown on this figure, which is why the air gap is marked. The area between the radiation panel and the steel plate shows control volumes that are specified as air. The left hand side shows the colour/temperature scale. These temperatures are shown in Kelvin. As seen in Figure 25, the air inside the furnace is mostly green. This colour represents a temperature of approximately 700-800 K, while the yellow/orange foil represents a temperature of approximately 1000 K. Figure 26 shows the radiation panel with colours. It is noticeable that the isolation on the upper part gets warmer than the isolation on the lower part. This happens by natural convection because warm air rises. The red colour on the foils shows that they radiate heat very evenly with a temperature of approximately 1100 K.

Figure 27 shows the radiation panel on the left hand side and the steel plate covered with isolation on the right hand side. It is possible to see that the steel plate is turquoise on the unexposed side, which represents a temperature of approximately 600 K. Figure 28 shows the same foils and the isolated steel plate from the opposite direction. The colours on the isolation indicate a temperature of about 900-1000 K.

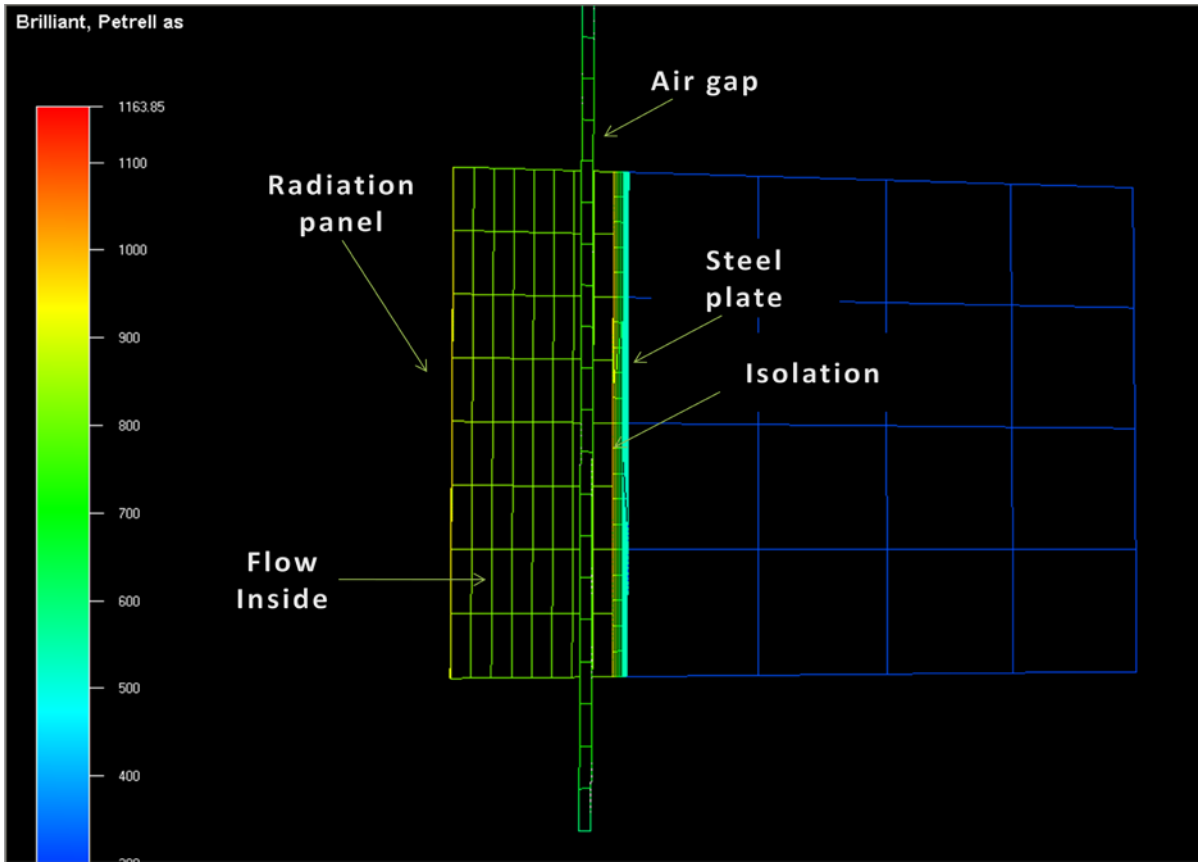

Figure 25 shows the testing furnace from above in GL View

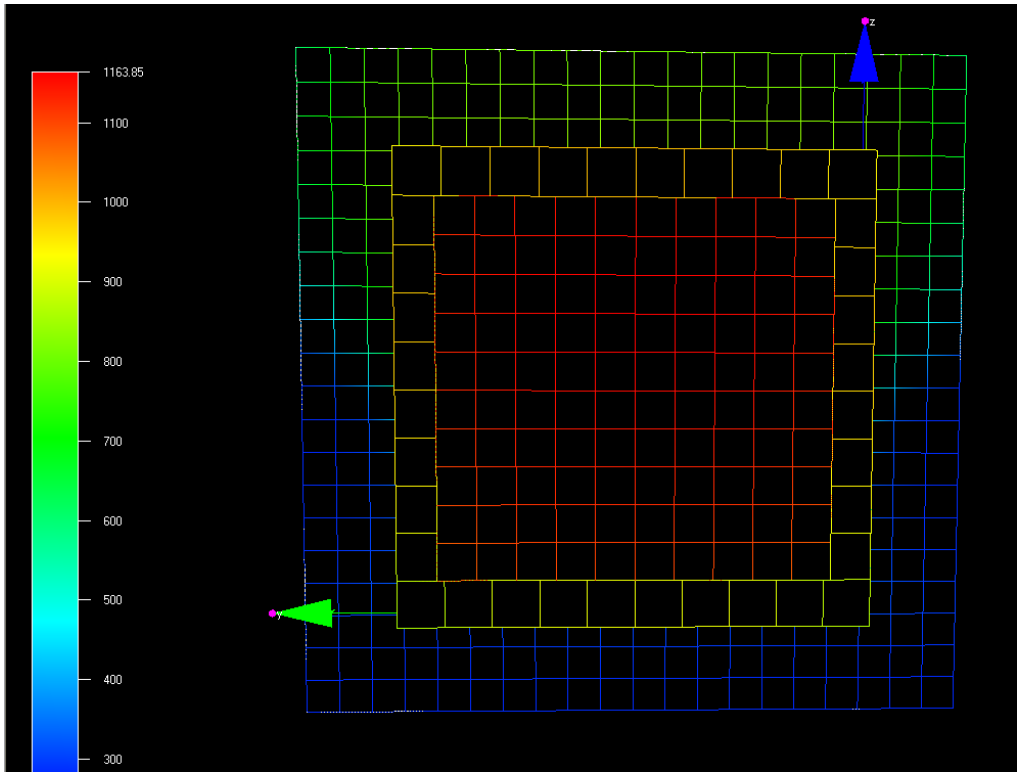

Figure 26 shows the radiation panel with isolation around. It also shows the colours that represents different temperatures.

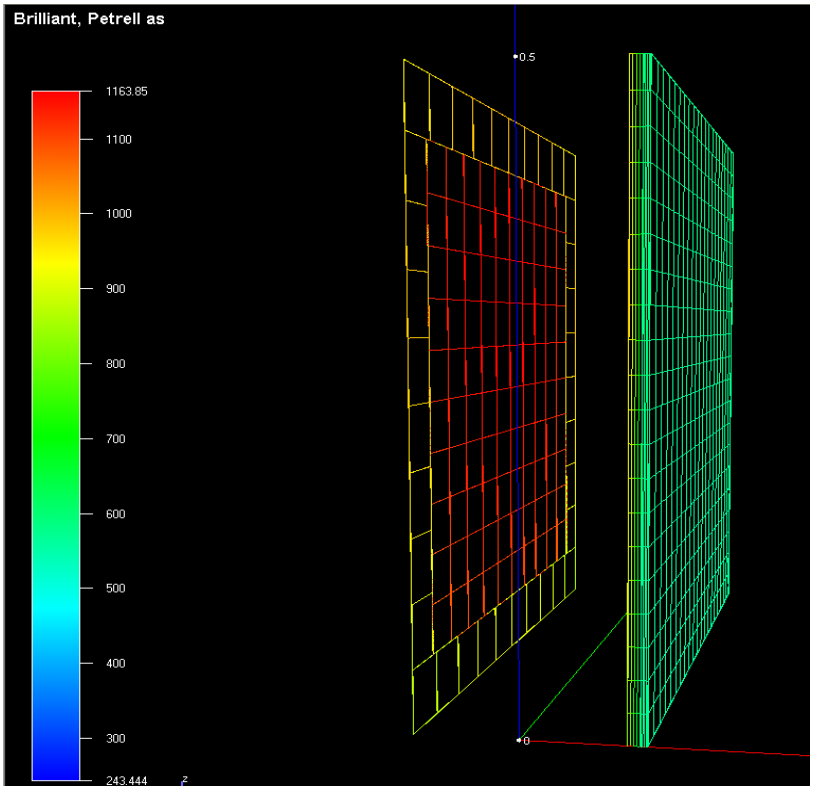

Figure 27 shows the radiation panel on the left hand side and the steel plate on the right hand side in the testing furnace. The colours represent the temperatures.

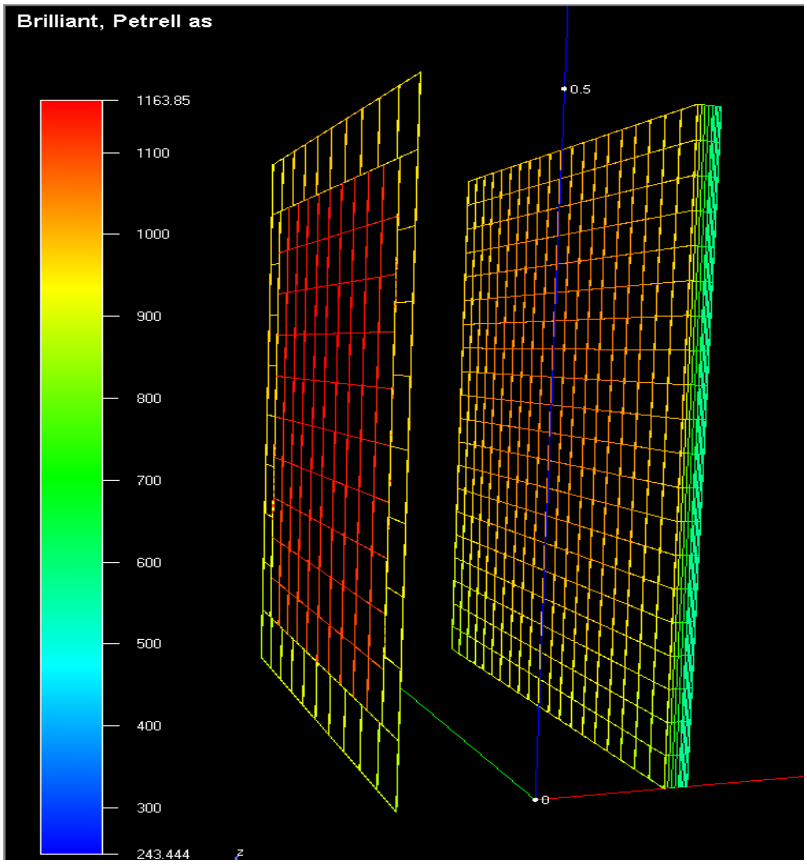

Figure 28 shows the radiation panel on the left hand side and the isolation that protects the steel plate on the right hand side in the testing furnace. The colours represent the temperatures.

3.3.2 Input data

The initial specification of the input data used in the numerical simulations has been prepared by Petrell AS. Throughout the project, improvements in the simulations have lead to changes and more input data is added.

In addition to the furnace setup described in the previous part, Brilliant takes as input several variables specific to each trial, coded in a syntax which is specific to the programme. The parameters that are depending on each test setup are:

- Simulation time
- Initial temperatures
- Delivered power
- Isolation material when applicable

Simulation time

The simulation time defines how many seconds the numerical simulation should cover. This parameter is defined in the admin file. It is the duration of each specific experiment that decides the length of the numerical simulation. In experiments without isolation on the steel plate, most experiments lasted for about 15-20 minutes. Experiments using dead material as

isolation lasted for about 50 min and the ones using intumescing materials as isolation lasted for about 60-70 min.

Initial temperatures

The initial temperatures are defined in the scenario file. Four different initial temperatures are defined here. These are T_{air}, T_{steel}, $T_{isolation}$ and T_{foil}. T_{air} is the initial surrounding temperature, T_{steel} is the initial temperature on the steel plate on the unexposed side, $T_{isolation}$ is the initial temperature on the isolation's exposed side or the steel temperature if no isolation is installed and T_{foil} is the initial temperature on the foils.

Delivered power

The delivered power is defined in the scenario file. The delivered power is specific for each experiment. The values have been calculated in Excel spread sheet and equal the total power from the control panel less the heat loss to the copper plates. See part 3.2.7 for further details on the calculation of the heat loss to the copper plates.

Isolation material

The isolation material is defined in the geometry file when applicable. In the experiments without isolation, this line was annotated. That signifies that the steel plate was defined instead. In the geometry file, the specific material and its thickness was defined. The specifications on the specific isolation material were put into the programme's database. These specifications include the materials density, specific heat capacity and the conductivity at different temperatures.

Other parameters that have been modified in the numerical calculation are defined below:

- Emissivities
- Dimensions of the furnace and materials
- Radiation
- Radiation beams
- Radiation frequency
- Control volume
- Time step

Emissivity

The emissivities of the foils, the steel plate and the isolation and the edges inside the furnace have been defined in the scenario file. The emissivity on the radiation foils is an important parameter when calculating heat radiation from the foils. The emissivity controls the amount of heat released and therefore the foil temperatures. This will again influence the temperatures in the rest of the system as well. An emissivity of 0.7 and 0.8 has been used on the foils in the numerical simulations.

The emissivity of the steel plate also influences the foil temperatures as well as the temperature on the steel plate. A value of 0.6 and 0.7 has been used.

The edges consist of a 2.5 cm layer of Kaowool. The emissivity has been changed a bit forth and back from 0.3 to 1. This emissivity was in the first simulations set to 0.3 and changed after a while. When emissivities were changed and to what are specified in Appendix A.2. The final emissivities chosen for the components radiation foil, steel plate and the edges in the furnace are shown in Table 5. These parameters have been used when simulating experiments from 051208_02 and onwards.

Part	Emissivity [-]
Radiation foil	0.7
Steel plate	0.7
Isolation edges	1

Table 5 shows the final emissivities chosen for the components in the furnace from simulation of experiment 051208_02 and onwards

Dimensions of the furnace and materials

All dimensions and materials of the furnace have been defined in the geometry file. What has been changed in the simulations along the way is the thickness of the isolation/concrete surrounding the furnace. The size of the air gap has also been changed a few times. At first the furnace was defined with a 2.5 cm thick Foamglas isolation surrounding the furnace. The 10 cm thick Siporex which made up the oven itself was therefore not included in the simulation. At first the total thickness was changed from 2.5 cm to 12.5 cm of Foamglas isolation. Later the edges were split up into two parts, representing both Kaowool isolation and Siporex, with the correct dimensions. Before this was done, different thicknesses was tried out mainly because of problems running Brilliant.

Radiation

The radiation is defined in the files 'RomFlow.brl' and 'FlowInnvendig.brl'. The radiation was first activated in the numerical simulation 211108_03b. In all subsequent simulations the radiation has been activated. Radiation was first deactivated by mistake. However, when comparing simulations with and without activating the radiation, the difference is less significant with a temperature difference of only a couple of degrees. This was tested in experiment 211108_03 and the results are shown in table 9 in part 6.2.

Radiation beams

The properties of radiation beams are defined in the files 'RomFlow.brl' and 'FlowInnvendig.brl'. Here it is possible to define azimuth and polar. Azimuth, which is number of radiation points from a control volume towards another control volume in the same plane, was changed from 8 to 12. Polar, the number of radiation points from a control volume towards another control volume not in the same plane, was changed from 6 to 12.

This was done because the numerical simulation would most likely become more accurate by having more radiation beams. This change resulted in significant increases in numerical simulation runtimes, without yielding any effect on the results. It also resulted in problems running Brilliant. It was therefore reset to the initial values. The simulations in which these parameters were changed are listed in the Appendix A.2 Overview of numerical simulations.

Radiation frequency

The radiation frequency is defined in the files 'RomFlow.brl' and 'FlowInnvendig.brl'. The value sets the denominator in the fraction of time steps where radiation calculations should be included. A radiation frequency of 5, for instance, means that radiation is included in 1 of 5 time steps. In an attempt to speed up the numerical simulations, this value was changed from the default setting of 1 to 5. The numerical simulation seemed to crash more often after this change, so it was reset to 1.

Control volumes

The number of control volumes is defined in the geometry file. Increasing the number of control volumes leads to more calculations, but also makes the numerical simulations more correct. Also, problems in running Brilliant have lead to trials of different control volume setups. The control volumes were first changed in simulation 051208_02e. Different numbers of control volumes have been run for the edges in the furnace as well as for the air gap, radiation foils and for the air volumes inside the furnace. See definitions in chapter 1 for further explanation of control volumes.

Time step

The time step is defined in the admin file. The number defines the time interval of the integration process. In general, smaller the time step, the more accurate the numerical simulation will be. Small time steps involve more calculations and longer runtimes. If this time step is too high, Brilliant can run into numerical instability.

Time steps can for instance be defined as follows: 0.02 50 0.05 200 0.1. This would mean that for the first 50 seconds, the time step is 0.02 seconds and then for the next 200 seconds the time step is 0.05. For the remainder of the simulation the time step is 0.1 second. It can be useful to have a small time step in the beginning of the simulation since this is the most critical point to achieve stability.

4 Experiments

This chapter will describe the experiments that have been performed. It will also describe significant improvements to the test apparatus, improvements necessary to achieve repeatability. Some results are also discussed, as they point to problems in the experiments, and provide the background for changes made to subsequent experiments. Results are described and discussed in chapters 0 and 6 respectively.

An overview of all the experiments that have been performed is listed in Appendix A.1, and an overview of all the numerical simulations are listed in Appendix A.2.

Table 6 shown at the next page gives a summary of the experiments that were simulated in Brilliant. All the temperatures and the powers were taken at the end of each experiment, when most temperatures were stabilized. Deviations in percent have been calculated between measured and simulated foil temperatures, as well as between measured and simulated steel temperatures. Deviations were not calculated for the experiments where the measured temperature on one of the independent foil bits was controlled by the control panel. This temperature should theoretically become lower than the foil temperature calculated by numerical simulation, as this temperature was calculated directly on the radiation foil. The different ways of measuring the foil temperatures are pointed out in Table 6 in forms of chapter numberings. These numberings refers to the specific part in the report where the relevant measuring method has been described.

Reference code	Test specimen	Foil temp. set at the control panel [°C]	Power output [W]	Measured temp. middle foil [°C] (foil bit r)	Sim. temp. foil [°C]	Deviation between foil temp. [%]	Measured steel temp. [°C]	Sim. steel temp. [°C]	Deviation between steel temp. [%]	Method for measuring foil temp.
171008_01	Steel plate	600	2950	639	598	-6.9	333	365	8.8	3.2.4.2.1
271008_01	Steel plate	600	2360	598	520	-15	324	280	-15.7	3.2.4.2.1
271008_02	Steel plate	800	4900	766	756	-1.3	532	500	-6.4	3.2.4.2.1
271008_03	Steel plate	1000	8660	995	930	-7	725	690	-5.1	3.2.4.2.1
051108_01	Steel plate	600	3660	609	652	6.6	403	400	-0.8	3.2.4.2.1
051108_04	Steel plate	800	7670	820	900	8.8	619	625	0.9	3.2.4.2.1
111108_01	Steel plate	600	3350	620	622	0.3	351	373	5.9	3.2.4.2.2
111108_02	Steel plate	800	6950	813	866	6.1	564	600	6	3.2.4.2.2
141108_01	Steel plate	600	4200	628	683	8.1	393	420	6.4	3.2.4.2.2
141108_02	Steel plate	800	8250	833	920	9.5	611	656	6.9	3.2.4.2.2
141108_05	Steel plate	1000	12500	1018	1100	7.5	809	815	0.7	3.2.4.2.2
181108_01	Steel plate	600	3340	618	630	1.9	379	399	5	3.2.4.2.3
191108_01	Steel plate	600	3720	619	665	6.9	418	424	1.4	3.2.4.2.3
191108_03	Steel plate	800	6600	813	858	5.2	606	600	-1	3.2.4.2.3
191108_05	Steel plate	1000	11100	1009	1038	2.8	799	739	-8.1	3.2.4.2.3
211108_02	Steel plate	800	7130	804	832	3.4	605	574	-5.4	3.2.4.2.3
211108_03	Steel plate	1000	11000	1012	1028	1.6	800	738	-8.4	3.2.4.2.3
261108_02	Steel plate	600	3065	590	520	-13.5	255	293	13	3.2.4.2.3
261108_04	Steel plate	800	6300	808	802	-0.7	494	549	10	3.2.4.2.3
051208_02	Steel plate	500	3820	494	587	-	334	342	2.3	3.2.4.2.4
081208_03	Steel plate	750	7420	763	817	-	538	564	4.6	3.2.4.2.4
111208_01	Steel plate	900	11600	914	966	-	661	688	3.9	3.2.4.2.4
230109	Kaowool_1400	900	6200	920	872	-	296	303	2.3	3.2.4.2.4
270109_02	Firemaster607	900	5940	910	875	-	303	321	5.6	3.2.4.2.4
050309	ProTek B3	900	2350	892	879	-	294	303	3	3.2.4.2.4
060309_01	ProTek A3	900	1950	891	897	-	256	269	4.8	3.2.4.2.4
060309_02	ProTek A4	900	1900	894	930	-	253	239	-5.9	3.2.4.2.4
170409	ProTek A1	900	1750	912	907	-	281	275	-2.2	3.2.4.2.4

Table 6 shows a summary of the experiments that were simulated in the numerical simulation programme Brilliant. The measured and simulated values from each experiment/simulation are presented in the table. The values are sampled from the end of each experiment.

4.1 Adjusting the testing furnace

This part will describe the adjustments to the testing furnace that were necessary to make it function as intended. One important goal has been to make all experiments reproducible. This part will describe initial experiments and corresponding numerical simulations, as well as any problems or inaccuracies discovered in them, and the measures taken to overcome them. All of these experiments were with a steel plate without isolation. Three different temperatures on the radiation foils were tested. These temperatures were 600 °C, 800 °C and 1000 °C. Later when new foil bits were installed in the furnace, temperatures of 500 °C, 750 °C and 900°C were used.

4.1.1 Experiments using the temperature on the radiation foils to control the input power

First start-up

The test apparatus was unused for about a year. The first time the thyristor was turned on in this project it gave an immediate hardware failure. The condenser was broken and had to be changed. The condenser had probably been exposed to too low temperature during the winter. To prevent that this would happen again, a wooden box was built around it and a 60 Watt light bulb was installed inside the box to keep it from freezing.

Experiment – 171008_01. Foils heated to 600 °C – logging every 5 sec

This experiment was performed after the power calibration (see part 3.2.3). During the work with the power calibration, the thermocouples were tested and some were replaced.

All the temperatures from this experiment that were recorded are shown in Figure 39 in Appendix B.1. The steel temperatures are following each other nicely and there are on average about two degrees between exposed and unexposed side. After 1080 seconds the temperatures were close to stable. At the end of the experiment the steel temperature was about 350 °C.

The foil temperatures are very similar to each other, but they are a bit high. They are both around 640 °C. The way the foil temperatures have been measured is described in 3.2.4.2.1.

Both the power curve and the delivered power are shown in Figure 47, in Appendix B.1. The power goes straight up to 6415 Watts and then it drops down to 2953 Watts over a period of 1170 seconds. The reason why the power is so high in the beginning is that the foil needs more power to get heated. When both the foil and the oven is warm, there will be less heat loss to the environment around the foil and the foil needs less power for keeping a temperature of 600 °C. As the steel plate gets heated, it will take part in keeping the oven warm because some radiation is returned to the foils. As seen on the graph, the copper temperature inside the oven rises quite quickly, which indicates that much energy is used to heat the copper early in the experiment.

When reviewing the results it became clear that the IMP 5000 had only logged every 5 seconds. This was due to an input mistake as the logging should have occurred every second.

This experiment was simulated in Brilliant. It was simulated with the same parameters that were already specified in the programme by Petrell AS. Only the delivered power and the time step were changed. The results from the numerical simulation are shown in Figure 40, Appendix B.1. The delivered power is set to be the logged power, given by the IMP 5000, less the energy required to heat the copper plates. The simulated foil temperatures lie at about 600 °C. It has a few jumps on the way. This is because the delivered power curve has the same jumps. This again is because the measured copper temperature has been a bit unstable, especially between 137 °C to 140 °C. These inaccuracies are probably due to the logging taking place every 5 seconds instead of every second, which would have given smoother measurements.

The IMP 5000 was programmed to record every second.

Experiment – 271008_01. Foils heated to 600 °C – logging every second

The measured foil temperatures in this experiment are similar to each other. One foil temperature shows 600 °C while the other one shows around 620 °C. There is about one degree difference on the exposed and unexposed side of the steel plate. Measured and simulated temperature graphs are shown in Figure 41, Appendix B.1.

Simulation of the experiment in Brilliant gave foil temperatures about 100 °C lower than expected.

The power curve is shown in Figure 47 and the delivered power is shown in Figure 48, Appendix B.1.

It was noticed that the furnace was programmed to be 2.5 cm thick with isolation. It has a 2.5 cm thick isolation, but it is also surrounded by a 10 cm thick layer of lightweight concrete. This was changed in the programme, so that the total thickness of the furnace was 12.5 cm and not 2.5 cm. The reason why the simulated foil temperature was hundred degrees below what it should be could have been because the simulation programme had calculated too much heat loss through the walls. The same experiment was therefore simulated over again with a correct wall thickness to see if this would have a positive effect on the foil temperature. These results are shown in Figure 42 , Appendix B.1. The new simulated foil temperature was a bit higher than earlier, but not enough to make up for the difference. This temperature has the notation ‘Foil sim 2’ in the figure. The simulated steel temperatures are a bit lower than measured. These temperatures have the notation ‘Steel exposed sim 2’ and ‘Steel unexposed sim 2’ in the same figure.

Experiment – 271008_02. Foils heated to 800 °C

The foil temperatures from this experiment differ about 50 °C from each other, but they were both close to 800 °C. The temperatures are shown in Figure 43, Appendix B.1. The simulated foil temperatures go up to 800 °C, but then they fall down to about 750 °C. These results are shown in the same figure as the measured values. The measured steel temperatures lie a bit above the simulated ones, but they follow each other nicely.

In order to see whether or not a change in the emissivity on the edges in the furnace could correct this inaccuracy in the foil and steel temperatures, the simulation was repeated with the emissivity reduced from 0.7 to 0.3. This however showed to have little effect on the results. The resulting foil temperatures showed little change, and simulated steel temperatures were a bit lower than earlier.

The power curve from this experiment is shown in Figure 50, Appendix B.1.

Experiment – 271008_03. Foils heated to 1000 °C

Figure 44, Appendix B.1 shows how both foil temperatures were close to 1000 °C in this experiment. The figure also shows that one foil has been exposed to interference during the trial, but only temporarily. The simulated foil temperature is very similar to the experimental ones.

The simulated steel temperatures are slightly lower than the measured ones, but they follow each other nicely. The measured steel temperature stabilized at approximately 735 °C while the simulated value is about 705 °C. Because the simulated steel temperature is lower than the measured one, an adjustment of the simulated emissivity of the steel plate from 0.6 to 0.7 was tried. This showed to have no positive effect on the temperature of the steel plate.

The power curve from this experiment is shown in Figure 45, Appendix B.1. The power is stable just above 8 kW.

Experiment – 051108_01. Foils heated to 600 °C – repetition of 271008_01

Because there were significant deviations between simulated and measured values of experiment 271008_01, the experiment was repeated. This time one of the measured foil temperatures was very low, while the other one was very accurate and stayed around 610 °C. The thermocouple on the right hand side had a poor connection with the foil. That is why this temperature was lower and was exposed to more turbulence. All the temperatures from this experiment are shown in Figure 46, Appendix B.1.

The simulated values for the foil temperature are very high in the beginning, over 700 °C, but it stabilizes at around 650 °C.

Both measured and simulated steel temperatures stabilize at about 400 °C.

The power curve from this experiment is shown in Figure 47 and the delivered power is shown in Figure 48, both in Appendix B.1.

The calculated heat losses through the copper plates have values that vary a lot. In fact, these values show variations in all experiments, and cause fluctuations in the simulated foil temperatures. It was therefore decided that an average heat loss through the copper plates should be calculated. Average heat losses over periods of ten seconds were calculated. This is the case for every simulation from this point. The total energy loss in the system will still be the same.

In order to increase the precision of the simulations, the initial temperature in the furnace has been added in the simulation programme. This temperature had not been defined earlier.

Experiment – 051108_04. Foils heated to 800 °C – repetition of 271008_02

This experiment was performed three times. The first one ended with foil breakage. The temperatures were very unstable and in the middle of the experiment one of the foils burnt off. The experiment was done over again after the foil was changed, but the foil temperatures were still very unstable. So was the input power. All the results from these two experiments were rejected. A possible reason for the failures is poor contact between the thermocouples and the foils, which may have caused difficulties for the control panel in deciding the correct temperature. Because of this it would send out wrong amounts of power. It was decided to change which of the foils that should be controlled by the control panel. Until this point the foil on the left hand side had been controlled by it, now the foil on the right hand side should be controlled by the control panel instead. When that was done, the foil temperature became more stable and the power curve became “normal”. These results are shown in Figure 49, Appendix B.1.

One of the foil temperatures is stable around 820 °C, while the other one lies a bit higher at around 855 °C. The last-mentioned is exposed to some disruption after about 200 seconds that lasts for about 20 seconds. The temperature rises up to 950 °C.

The simulated foil temperatures are around 100 °C higher than measured.

Both measured and simulated steel temperatures are stabilising at approximately 600 °C.

Both the delivered power and the power curve are shown in Figure 50, Appendix B.1.

Summary of the power curves from experiment 171008, 271008 and 051108

The power curves in Figure 47 and Figure 48 in Appendix B.1, showing the 600 °C trials, show that the power varies significantly. This is also reflected in the simulations. The power curve from 271008_01 is the lowest one and in this simulation the foil temperature was about 100 °C lower than measured. The experiment from 171008_01 is the one where the simulated

foil temperatures are the most similar to the measured temperatures. The power curve that belongs to this experiment is therefore assumed to be good. The power curve from 051108_01 is the highest one. The simulated foil temperature is here from 50-100 °C higher than the measured one.

From experiments where the foils have been heated up to 800 °C, the power curves are also different from each other. From experiment 271008_02, the power curve shows lower values than 051108_04 does. In 271008_02 the simulated foil temperature shows about 50 °C less than the measured temperatures do. From 051108_04 the simulated foil temperature is about 100 °C higher than the experimental ones.

At this point, only one experiment with 1000 °C has been carried out. This trial showed a good correspondence between the measured temperatures and the simulated temperatures.

A new way of measuring the foil temperature will be tried out next. This method is further explained in part 3.2.4.2.2.

Experiment – 111108_00. Foils heated to 600 °C – an example of foil breakage

In this experiment one of the foils burnt off after about 540 seconds. The temperature graph is shown in Figure 51.

Experiment – 111108_01. Foils heated to 600 °C - new way of measuring the foil temperatures

The results from this experiment are shown in Figure 52 in Appendix B.1. The measured foil temperatures lay around 620-635 °C, whereas the simulated foil temperature lay around 600-610 °C. The simulated foil temperature slowly rises after about 10 minutes. The power curve is shown in Figure 57, Appendix B.1.

The simulated steel temperatures haven't stabilized yet after 18 minutes and it seems like it is going to stabilise at a higher temperature than the measured steel temperatures. The steel temperatures are however very similar the first ten minutes.

Experiment – 111108_02. Foils heated to 800 °C

Since the simulation of the experiment 051108_02 showed such high values for the foil temperature, this experiment was repeated to see if the power would be just as high this time. The temperatures are shown in Figure 53, Appendix B.1. The temperature on the foil in the middle show around 810 °C, which is very similar to the foil temperature that is controlled by the control panel. The left foil temperature shows higher values. These are around 840 °C and are also exposed to some disturbance. The simulated foil temperatures have a slowly rising curve. It rises from 800 °C to 866 °C over a period of 1035 seconds. The power curve is shown in Figure 58 , Appendix B.1.

Also in this simulation, the steel temperature stabilises at a higher temperature than measured, but it's not more than 40 °C above.

Experiment - 141108_01. Foils heated to 600 °C – verification of 111108_01

It is a requirement that at least two experiments of the same type shall be simulated where the simulations give tolerably similar and correct results. Throughout the experiments, the thermocouples have been fastened to the foils somewhat differently. Therefore the experiments from 111108 were repeated to see if the results would be reproducible.

All the temperature curves from both the experiment and the simulation are shown in Figure 54 in Appendix B.1. As seen on this figure, the simulated foil temperature rises from 650 °C to 690 °C over a period of 1000 seconds. The fact that the temperature rises show that the same problem as in all experiments from 111108 still exists. The simulated values from experiment 141108_01 lie a bit higher than the values in experiment 111108_01.

The simulated steel temperatures are about to stabilize a little bit higher than the measured ones. The power curve is shown in Figure 57, Appendix B.1.

Experiment - 141108_02. Foils heated to 800 °C – verification of 111108_02

This experiment has much of the same problem as 141108_01. The simulated values are too high. The simulated foil temperature is however stable at about 925 °C. That is 125 °C above what the radiation foil that is controlled by the control panel shows. All the temperatures are shown in Figure 55, Appendix B.1.

The power curve from this experiment is shown in Figure 58, Appendix B.1.

Experiment - 141108_05. Foils heated to 1000 °C –verification of 271008

During this experiment the isolation on the thermocouple on the exposed side of the steel plate burnt off. Therefore these measurements were not reliable. Still the measurements made on the unexposed side were unaffected, and could be compared with simulated results.

Both simulated and measured steel temperatures stabilises at about 800 °C. The foil temperatures that were measured are very similar and they both go from being around 1035 °C to being 1020 °C. The control panel shows around 1000 °C, which indicates that the measured temperatures are trustworthy. The simulated foil temperature is too high and lies around 1150-1100 °C. The temperature curves are shown in Figure 56, Appendix B.1.

The power curve is shown in Figure 59, Appendix B.1.

Summary of the power curves from experiment 111108 and 141108

In the experiments where the foils were heated to 600 °C and 800 °C, the power curve from 141108 is significantly higher than in the 111108 experiment. The power curves are shown in Figure 57 and Figure 58 in Appendix B.1. In the 111108 experiments the simulated values were not significantly different from the measured ones, but in the experiments 141108, the simulated foil temperatures were much higher than measured.

In experiment 141108_05 where foils were heated to 1000 °C, the power curve can only be compared with the experiment from 271008_03 where the simulated values was very similar compared to the measured ones. In experiment 141108_05, the simulated values lay much higher, and the power curve was also higher than before. The power curve for 141108_05 is shown in Figure 59 in Appendix B.1.

Another method for measuring foil temperature will be tried out next. This method is further explained in part 3.2.4.2.3.

Experiment - 181108_01. Foils heated to 600 °C – yet another way to measure the foil temperature

The measured temperatures from this experiment and the temperatures from the following simulation are shown in Figure 60, Appendix B.1. The measured temperatures on the exposed and unexposed side of the steel plate show a difference of about 10 °C. The expected value would be about 2 °C difference, which is the simulated value. The reason for this could be that the isolation around the thermocouple had started to burn off and that the thermocouple measured a temperature a bit outside the steel plate. The temperature measured and simulated on the exposed side of the steel plate are very similar.

The measured foil temperatures have a small gap between them of 10 °C. One shows 620 °C and the other one shows 630 °C. The simulated foil temperature lie around 620-630 °C. This is a bit higher than the temperature shown on the control panel, which was 600 °C, but the simulated value should be somewhere in the middle of all the three foils, so this experiment is concluded satisfying.

The power curve for this experiment is shown in Figure 66 in Appendix B.1.

At this point it seems like the new way of measuring the foil temperatures worked out very well, because the results from this experiment has been the best seen so far.

Experiment - 191108_01. Foils heated to 600 °C – verification of 181108

This experiment is the same as 181108_01 in every way, but the results are different. The simulated foil temperatures lay again above the measured ones. This means that the experiments are still not reproducible. The temperatures are shown in Figure 61, Appendix B.1. The simulated foil temperature lay between 640 - 670 °C while the measured foil

temperatures are stable at 620 °C. The steel temperatures are quite similar and it seems like they will stabilise at about the same temperature, just above 400 °C.

The power curve for this experiment is shown in Figure 66 in Appendix B.1.

Experiment - 191108_03. Foils heated to 800 °C

Both the measured foil temperatures are stable at about 820 °C in this experiment. The simulated value is stable at a higher temperature, 850 °C. What is worth noticing is that the control panel showed about 807 °C the first 5 minutes of the experiment. The measured steel temperature stabilises at 600 °C. The simulated steel temperature seems to be stabilising at the same temperature as the measured ones. All the temperatures are shown in Figure 62 in Appendix B.1.

The power curve for this experiment is shown in Figure 67 in Appendix B.1.

Experiment - 191108_05. Foils heated to 1000 °C

One of the measured foil temperatures go from being 1077 °C to being 1026 °C over a period of 1320 seconds. The other measured foil temperature goes from 1034 to 1010 °C over the same time period. The control panel showed a temperature of about 1010 °C the first 5 minutes of the experiment. This can explain why the temperatures are higher in the beginning. The simulated foil temperature lies above both the measured foil temperatures, at about 1070 °C.

A temperature difference between exposed and unexposed side of the steel plate when the temperatures had stabilised were measured to be 22 °C, which is significantly higher than what the simulation promises, that shows a difference of 7 °C. All the temperatures are shown in Figure 63 in Appendix B.1. The measured steel temperature on the exposed side stabilises at 800 °C, and the simulated steel temperature on the exposed side stabilises at about 780 °C.

The power curve is shown in Figure 68 in Appendix B.1.

Since the experiment from 181108 was not reproducible compared to what was recorded in 191108, the fact that the experiment from 181108 was so good, is assumed to be a bit of luck. It seems that most of the experiments have simulated values that lay above the measured values. One hypothesis was that some kind of heat loss in the system had not been taken into account in the simulation inputs. The copper that holds the foil conducts heat, and this heat conduction has not been included in the calculation of heat loss from the copper. The only heat loss that has been included is the energy that is required for heating the copper plates.

It was decided that the copper temperature should be measured at two new places. The reader is referred to chapter 3.2.7 for further details. This way the conduction through the

copper could be calculated and this heat loss plus the heat loss required to heat the six copper plates would be subtracted from the input power. The delivered power entered into the simulation programme should now have lower values than earlier.

Experiment - 211108_02. Foils heated to 800 °C – heat loss through the copper plates included in simulation

The results from this experiment are shown in Figure 64 in Appendix B.1. The measured foil temperatures differed slightly. One of them lay between 816 - 803 °C, while the other one lay at around 850 – 830 °C. The simulated foil temperature was a bit high between 120 – 240 seconds, but later it had the same value as the measured foil temperature that showed the highest values.

The measured steel temperatures stabilises at 600 °C. The simulated steel temperature shows a bit lower values. These stabilises at 570 °C.

The power curve from this experiment is shown in Figure 67 in Appendix B.1.

Experiment - 211108_03. Foils heated to 1000 °C

The results from this experiment are shown in Figure 65 in Appendix B.1. The measured foil temperatures differ a bit from each other. One of them lies between 1015 - 1020 °C, while the other one lies at around 1045 – 1030 °C. After 500 seconds of the experiment, the simulated foil temperatures are very close to the measured foil temperature that shows the lowest values. Before this the simulated foil temperature shows quite high values, around 1050 °C.

The measured steel temperature stabilized at 800 °C. In this experiment only the exposed steel temperature was recorded. The simulated steel temperature stabilises at 740 °C.

Overall, it looks like that there is a time-delay in the measured temperatures. When comparing the measured and simulated foil temperatures, it is seen that the simulated foil temperature rises much quicker than the measured ones. There is about 30 seconds' difference.

The power curve from this experiment is shown in Figure 68 in Appendix B.1.

Summary of the power curves from experiment 181108, 191108 and 211108

In the experiments where the foils were heated to 600 °C, the power curve from 191108_01 is higher than 181108_01. In the latter experiment the simulated foil temperatures were very similar to the measured temperatures. In the experiment 191108_01 however, the simulated foil temperature were about 50 °C above measured foil temperature.

When the foils were heated to 800 °C, the power curve from 211108_02 was a bit higher than the one from 191108_03, but the delivered power curve shows the opposite. There has

been included extra heat loss in the calculations of the delivered power in 211108, so that is the reason why the delivered power in 211108_02 shows lower values than the delivered power from 191108_03. The simulated foil temperature from 191108_03 lay approximately 50 °C higher than the measured values. In the experiment from 211108_02, the simulated foil temperature was very similar to one of the measured foil temperatures.

In the experiments with foil temperatures of 1000 °C, the power curves are very similar. The delivered power curve from 211108_03 is lower than the one from 191108_05, but this is again because the extra heat loss has been included in the calculation of the delivered power. The simulated foil temperature from 191108_05 shows about 80 °C more than the measured foil temperatures do. In the experiment 211108_03, the simulated foil temperature shows values very similar to the measured ones.

Experiment - 261108_01. Foils heated to 600 °C

All the foils were new when this experiment was performed. The isolation in the bottom of the furnace was removed, because the steel plate had become so bent that it actually made the isolation cover the air-gap. By removing the isolation, the air-gap would still be intact.

The resulting power curve in this experiment was very low and so was the steel temperature. It was discussed whether this was due to the new radiation foils. The foil properties might change after being heated and require more power the next time it is heated. If this is the case, the foils would need less power during the first heating. In order to see whether this assumption was correct, it was decided that the experiment should be repeated (261108_02). The experiment was not simulated.

Experiment - 261108_02. Foils heated to 600 °C

This experiment is identical to the previous experiment (261108_01). It resulted in a similarly low power curve and temperatures as it did in 261108_01.

To see whether the removal of the isolation was the reason for the low temperatures, the experiment was repeated with the isolation in place (261108_03).

This experiment was simulated in Brilliant. These results together with the measured results are shown in Figure 69, Appendix B.1. As seen in this figure, the simulated foil temperature lay much lower than the measured ones. There is almost 100 °C difference. The simulated steel temperature is similar to the measured ones the first 10 minutes, but while the measured temperature seems to have reached steady state, the simulated value keeps rising.

The power curve for this experiment is shown in Figure 71, Appendix B.1.

Experiment - 261108_03. Foils heated to 600 °C

This experiment is identical to the two previous experiments (261108_01 and 261108_02), but with the isolation in front of the steel plate in place. Again it resulted in a similarly low power curve and temperatures as in the previous two.

The experiment was therefore not simulated as the numerical simulation results would have become similar.

Experiment - 261108_04. Foils heated to 800 °C

This experiment was primarily done to see if the low power curves from 261108_01, 261108_02 and 261108_03 would recur with higher temperatures.

The power curve was lower than it usually is when the foils are heated to 800 °C. The simulated foil temperatures were quite low compared to the measured ones in the beginning but they kept rising. The simulated steel temperature was above the measured one. The temperature curve for this experiment is shown in Figure 70, Appendix B.1.

The power curve is shown in Figure 72, Appendix B.1.

4.1.2 Experiments using an independent foil bit to control the input power

Experiment – 051208_01. New independent foil bits installed heated to 500 °C

Since results of experiments from 261108 differed quite a lot from previous experiments, it was stated that the chosen method did not work as intended and changes had to be made. Three new foil bits of 3 x 3 cm were installed behind the radiation foils. This method is explained in more detail in part 3.2.4.2.4. The foil bit in the middle was chosen to be controlled by the control panel, while the other two was connected directly in the IMP 5000. Three experiments of the same type were performed to check the reproducibility, and the results from 051208_01 are shown in Figure 73, Appendix B.1. The data from the five first minutes of the experiment was unfortunately not saved. Because of this, it was chosen to simulate one of the other two similar experiments instead, 051208_02.

The power curve from this experiment is shown in Figure 76, Appendix B.1.

The temperature difference between the foils that function as radiation panel and the foil bits behind it are about 100 °C.

The simulated temperature on the radiation foils will no longer be compared to the measured temperature on the radiation foils, because the measured foil temperatures are considered too uncertain. Therefore, the measured and simulated steel temperatures will be compared to check the experiments reproducibility in the numerical simulation.

Experiment – 051208_02. Foil bits heated to 500 °C

This experiment is identical to the one above and was performed to check the reproducibility. Data from this experiment was simulated. These results as well as the measured values are shown in Figure 74. By comparing this experiment with the previous one, 051208_01, it is seen that the temperatures are very similar.

The power curve from this experiment is shown in Figure 76, Appendix B.1.

Experiment – 051208_03. Foil bits heated to 500 °C

This experiment was performed to check the reproducibility of experiment 051208_01 and 051208_02. The results are shown in Figure 75, Appendix B.1. All these three experiments are very similar to each other.

The power curve from this experiment is shown in Figure 76, Appendix B.1.

Experiment – 081208_01. Foil bits heated to 750 °C

This experiment was performed three times to check the reproducibility. The experiments are similar to the ones in 051208 with the only difference that the temperature is set to 750 °C. The results from this experiment are shown in Figure 77, Appendix B.1.

The power curve from this experiment is shown in Figure 80, Appendix B.1.

The temperature difference between the radiation foils and the foil bits are approximately 40 °C.

Experiment – 081208_02. Foil bits heated to 750 °C

This experiment is identical to 081208_01. The results are shown in Figure 78, Appendix B.1.

The power curve from this experiment is shown in Figure 80, Appendix B.1.

Experiment – 081208_03. Foil bits heated to 750 °C

This experiment is identical to 081208_01 and 081208_02 and has been simulated. The results from the simulation and data from the experiment are shown in Figure 79, Appendix B.1. All the three identical experiments have very similar results.

The power curve from this experiment is shown in Figure 80, Appendix B.1.

Experiment – 111208_01. Foil bits heated to 900 °C

This experiment was performed three times to check the reproducibility. The experiments are similar to the ones in 051208 and 081208 with the only difference that the temperature is set to 900 °C. This experiment was simulated. The results from the simulation and the experiment are shown in Figure 81, Appendix B.1.

The temperature difference between the radiation foils and the foil bits are approximately 20 °C.

The power curve from this experiment is shown in Figure 84, Appendix B.1.

Experiment 111208_02. Foil bits heated to 900 °C

This experiment was performed to check the reproducibility of 111208_01. It became very similar. The thermocouple on the copper plate, T1, experienced some bad contact, and it was therefore showing a temperature 30 °C higher than expected. The thermocouple is supposed to stay firmly inside a hole in the copper plate, but it wasn't totally inside the hole. Because of this temperature difference, the calculated heat loss through the copper became larger than what was expected. The total power curve was however comparable to 111208_01. The power curve from this experiment is shown in Figure 84, Appendix B.1.

The resulting temperatures from this experiment are shown in Figure 82, Appendix B.1.

Experiment 111208_03. Foil bits heated to 900 °C

This experiment was performed to check the reproducibility of 111208_01 and 111208_02. It became very similar. The thermocouple, T1, on the copper plate had bad contact like it had in experiment 111208_02. The total power curve was however similar. The power curve is shown in Figure 84, Appendix B.1.

The results from this experiment are shown in Figure 83, Appendix B.1.

4.2 Dead materials

This part will describe the different experiments performed with isolation of the type dead material mounted onto the steel plate. For all experiments with dead materials the radiation panel was adjusted to give an amount of power that would keep the temperature of the independent foil bits at 900 °C. These experiments were run for approximately 45-50 minutes, compared to 15-20 minutes for the experiments without any isolation. This difference in duration is caused by the fact that the experiments with the isolated steel plate reach steady state slower.

A new steel plate was installed before these experiments were performed. The steel plates that were used for testing without isolation had become bent, so that the isolation would not lie completely against the steel plate.

Results are described and discussed in parts 5.2 and 6.4 respectively.

Experiment 230109 with 0.9 cm Kaowool 1400 isolation

The isolation boards come in 2.5 cm thickness. As experienced earlier, when the power was calibrated, the power distribution would become quite unstable below 10 %. See Figure 16. This is not desirable, so a thinner isolation was preferred. To avoid that the input power in

the furnace would go below 10 %, the isolation was divided, and a layer of 0.9 cm was applied. There is enough heat loss in the system to keep the input power fairly high. The power curve is shown in Figure 86. The measured temperatures and the simulated values are shown in Figure 85, Appendix B.2.

In the start-up of this experiment, the control panel did not reduce the power input quickly enough to keep the foil temperature at 900 °C. In just a few seconds it was getting close to 1000 °C. To avoid foil breakage at this point it was necessary to turn down the power manually to reduce the foil temperature. This is why the foil temperatures show a sudden drop around 1000 °C. The drop can also be seen on the corresponding power curve.

The exposed steel temperature rises to almost 300 °C.

Experiment 270109_02 with 1 cm Firemaster607 128 as isolation

In conformity with Kaowool, Firemaster607 also gets delivered with a thickness of 2.5 cm. The isolation was divided and a thickness of 1 cm was used in this experiment.

The measured steel temperature on the exposed side stabilises at 300 °C. The measured temperatures and the simulated values are shown in Figure 87, Appendix B.2.

The power curve is shown in Figure 88, Appendix B.2.

4.3 Intumescing materials

This part will describe the different experiments performed with intumescing materials as isolation mounted onto the steel plate. The radiation panel was adjusted to give a power that would keep the independent foil bits stable at 900 °C. All experiments were run for approximately one hour.

Results are described and discussed in parts 5.3 and 6.5 respectively.

Experiment 170209 with 1 cm ProTek B4 isolation

The isolation caught fire after about 2 minutes when the foils were reaching approximately 600 °C. The isolation material produced a lot of smoke and large flame tongues kept coming out of both the air gap and behind the steel plate on the furnace. The experiment was therefore terminated after only 3 min 47 sec. At this point, the whole tent was full of smoke and there was a risk of destroying the computer and the thyristor.

The solution to the fire and smoke problem was to move the furnace outside the tent. The rest of the experiments with intumescing materials were done outside.

Experiment 050309 with 0.91 cm ProTek B3 isolation

Before this experiment was carried out, the oven was half rebuilt to remove the air gaps that had started to appear around the steel plate. The isolation inside the oven was also replaced.

The isolation started burning after 3 minutes when the foils were about 750 °C. Flame tongues came out around the air gap in all directions. The isolation kept burning for at least 30 minutes. The experiment lasted for 65 minutes. Picture 13, Picture 14 and Picture 15 are all taken from this experiment.

Picture 13 shows the furnace during experiment 050309. Flame tongues are visual around the air gap.

Picture 14 shows the furnace during experiment 050309. Flame tongues are visual around the air gap.

Picture 15 shows the furnace during experiment 050309. No flame tongues are visual, but the specimen still produces a lot of smoke.

This experiment was simulated in Brilliant. At first the delivered power that was registered from the control panel was used as input to the simulation. The simulated values became very low and did not fit the measured values. The reason for this was that the isolation material caught fire during the experiment, and therefore contributed in heating the foils. The power from the control panel was therefore reduced, which lead to the reduction in the simulated values. This causes a problem, as it obscures the actual power delivered to the material. The measured values from this experiment and the simulated values are shown in Figure 89, Appendix B.3.

Because the delivered power did not at this point include the power contribution from the fire in the isolation material, heat release rate data from a cone calorimeter test of the same material was added to the input power (adjusted for area differences) (58). The sum was used as input to a new simulation.

These simulated values were very high. Under the assumption that only the middle of the specimen would release heat for the first couple of minutes, the heat release and power was adjusted, and the simulation was repeated. Still, the simulated steel temperatures were about hundred degrees above measured values.

Since adjusting the delivered power with the heat release data did not give satisfactory results, the power curve from another experiment was used in the simulation. The assumption was that the power curve from the testing of a dead material would show the power necessary for keeping the foils at 900 °C when isolation is protecting the steel plate. The dead materials did not contribute in raising the temperature in the furnace in other ways than isolating, so the delivered power could theoretically be the same as in this experiment with ProTek B3.

The power from the experiment 270109_02 with 1 cm of Firemaster as isolation was put into the simulation programme. Firstly, the k-values from Firemaster were used as a starting point to compare the resulting steel temperatures with the experimental results. Several similar simulations had to be performed in order to find the correct k-value by trial and error. These results are described in part 5.3.

Experiment 060309_01 with 0.91 cm ProTek A3 isolation

When the foil bits had reached a temperature of about 500 °C, the isolation caught fire, and fire tongues were coming out through the openings of the furnace, especially around the air gap. This is shown in Picture 16 and Picture 17. After about 30 minutes no more flames were visible from the outside of the furnace. The experiment was conducted for 68 minutes, at which point the top of the oven was removed. The ‘conlit klæber’, the adhesive used for fastening the Kaowool inside the oven, was burning with a small blue flame.

Picture 16 on the left side shows flames coming out of the air gap during experiment 060309_01

Picture 17 on the right side shows flame tongues coming out of small openings in the furnace during experiment 060309_01

Again, because the isolation caught fire during the experiment, the delivered power was obscured by the heat release from the isolation. The power curve used in Brilliant was therefore the one from experiment 270109_02, the same as the one used in the simulation of 050309. These results are described in part 5.3.

Experiment 060309_02 with 0.6 cm ProTek A4 isolation

The logger started to record first after 9 minutes of the experiment. This specimen did not burn as aggressively as the previous ones, and only a few fire tongues were visible from the outside of the furnace. The experiment ran for 64 minutes. When the top was removed, the isolation behind the foils was burning. This is shown in Picture 18.

The power curve used in Brilliant was the one from experiment 270109_02. These results are described in part 5.3.

Picture 18 shows the furnace from the inside right after experiment 060309_02 was performed. There are still visible flames inside the furnace, both behind the foils and behind the isolation on the edges.

Experiment 170409_02 with 0.94 cm ProTek A1 isolation

Like the other experiments with intumescing materials, this specimen also caught fire. The experiment lasted for 62 minutes. When this experiment was performed, the specimen had already been exposed to heat in the furnace for about 10 minutes. The specimen had therefore already started to swell. See Appendix A.1 for more details.

The power curve used in Brilliant was the one from experiment 270109_02. These results are described in part 5.3.

Experiment 180409_02 with 0.25 cm Benarx F Flexi Roll XP isolation

Benarx F Flexi roll XP was delivered ready mounted onto a 5 mm thick steel plate similar to the steel plates that have been used in earlier experiments. The test specimen itself had a thickness of 0.25 cm, and was fixed to the steel plate with 0.18 cm of glue.

During the experiment the specimen caught fire, and started producing thick black smoke. After about ten minutes, no flames were visible on the outside of the furnace, and the smoke production had nearly stopped.

The experiment had to be terminated because of foil breakage. This happened after about 65 minutes. The steel temperature was not yet stable.

The results from this experiment are described in part 5.3.

5 Results

This chapter will describe the results gained from adjusting the furnace, testing dead PFP materials and from testing intumescing PFP materials.

5.1 Results from adjusting the furnace

After the initial experiments with the furnace, it was clear that the method did not work as intended, as the experiments were not reproducible. It was concluded that this was due to inaccurate measurements of the temperatures on the radiation foils. Therefore, methods including measurements of radiation foil temperatures were abandoned in subsequent experiments.

Three independent foil bits were installed in the furnace, each with thermocouples welded on them. When one of these independent foil bits temperatures were used for controlling the input power, the experiments became reproducible. The measured results were also comparable to simulation results. As shown in Table 7, nor the foil temperatures, the steel temperatures or the powers show deviations exceeding 5 %. This method was concluded satisfactory.

Reference code	Foil temp [°C]	Deviation	Steel temp [°C]	Deviation	Power [W]	Deviation
051208_01	512	1,19 %	338	3,52 %	3857	0,00 %
051208_02	506	0,00 %	328	0,46 %	3889	0,83 %
051208_03	508	0,40 %	326,5	0,00 %	3932	1,94 %
081208_01	762	0,00 %	530	0,00 %	7775	2,84 %
081208_02	767	0,66 %	534	0,75 %	7560	0,00 %
081208_03	763	0,13 %	533	0,57 %	7563	0,04 %
111208_01	916	0,00 %	673	0,00 %	11714	4,57 %
111208_02	918	0,22 %	687	2,08 %	11256	0,48 %
111208_03	931	1,64 %	689	2,38 %	11202	0,00 %

Table 7 shows an overview of the experiments using the temperature measurement on the independent foil bit for controlling the input power. The different values are taken at t=1000 sec (051208), t=1200 sec (081208) and t=1400 sec (111208). Maximum deviations in percent have been calculated for the foil temperatures, the steel temperatures, and powers. The calculations are based on using the experiment with the lowest temperature as base.

5.2 Results from testing dead isolation materials

In experiment and simulation 230109 testing Kaowool 1400 isolation, the simulated values correspond well to the measured values. Before the system reaches steady state, there is a difference between the simulated and measured steel temperatures of about 30-40 °C. See Figure 85, Appendix B.2. However, when steady state has been reached, the simulated steel temperatures are very similar to the measured ones, with differences of only about 6-7 °C. The thermal conductivities given by the manufacturer correspond well to the simulated values. These thermal conductivities are shown in Table 1 in part 2.1.1.

In experiment 270109_02 testing Firemaster607 and the following simulation 270109_02b, the simulated temperatures on the steel plate correspond well with the measured values. See Figure 87, Appendix B.2. The curves follow each other nicely. Towards the end of the simulation the simulated steel temperature were slightly higher than measured, with a difference of approximately 15 °C. The conductivity data received from the manufacturer seems to be correct. These thermal conductivities are shown in Table 1 in part 2.1.1.

The simulated temperature on the radiation foil in both simulation 230109 and 270109_02b show a simulated foil temperature lower than the temperatures recorded on the foil bits. These results have been discussed in part 6.4.

5.3 Results from testing intumescing materials

Since the k-values for the intumescing materials tested are not known, these values had to be guessed and approximated by trial and error.

Different simulations were performed on experiment 050309 using ProTek B3 isolation. Before the best temperature match was found, different k-values had to be tested and a list of them is shown in Appendix G. The different lists of k-values are called ProTek1, ProTek2 and so on. The simulated values, using the k-values in list ProTek5, together with measured values are shown in Figure 90, Appendix B.3. As seen in this figure, the simulated steel temperatures are close to the measured values, so theses k-values seems to be the correct thermal conductivity for this specific test specimen in this case scenario. The k-value as a function of temperature is shown in Figure 29.

The isolation was 0.91 cm thick before testing and 0.97 cm after testing. This means that the isolation had swelled 0.6 mm.

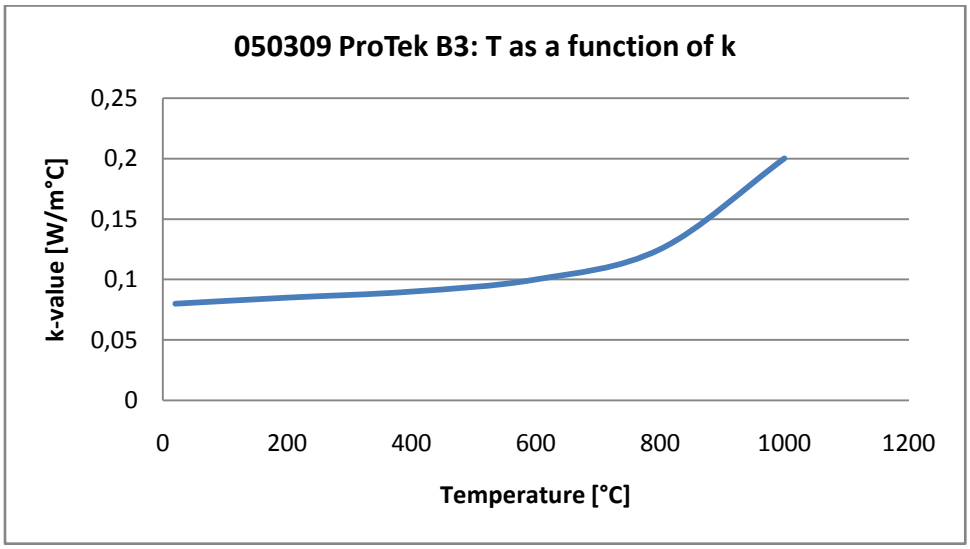

T [°C]	k [W/mK]
20	0.08
200	0.085
400	0.09
600	0.1
800	0.125
1000	0.2

Figure 29 shows the resulting k-values as a function of temperature found from experiment 050309, specimen ProTek B3

Several simulations were performed on experiment 060309_01, testing ProTek A3. A summary of the simulated steel temperatures with the different k-values are gathered in

Figure 91, Appendix B.3. As the figure shows, the simulation with the group of k-values denominated ProTek14 is the simulation where the simulated steel temperatures are most similar to the measured ones. Both simulated temperatures and measured temperatures from this experiment are shown in Figure 92, Appendix B.3. The k-value as a function of temperature is shown in Figure 30.

The simulation with k-values from ProTek13 show an even better result, but this result was obtained by changing the Cp-value. As it was decided to keep this value constant for all ProTek simulations, this result was deemed invalid.

The isolation was 0.91 cm thick before testing and 2.21 cm after. The isolation had swelled 1.3 cm.

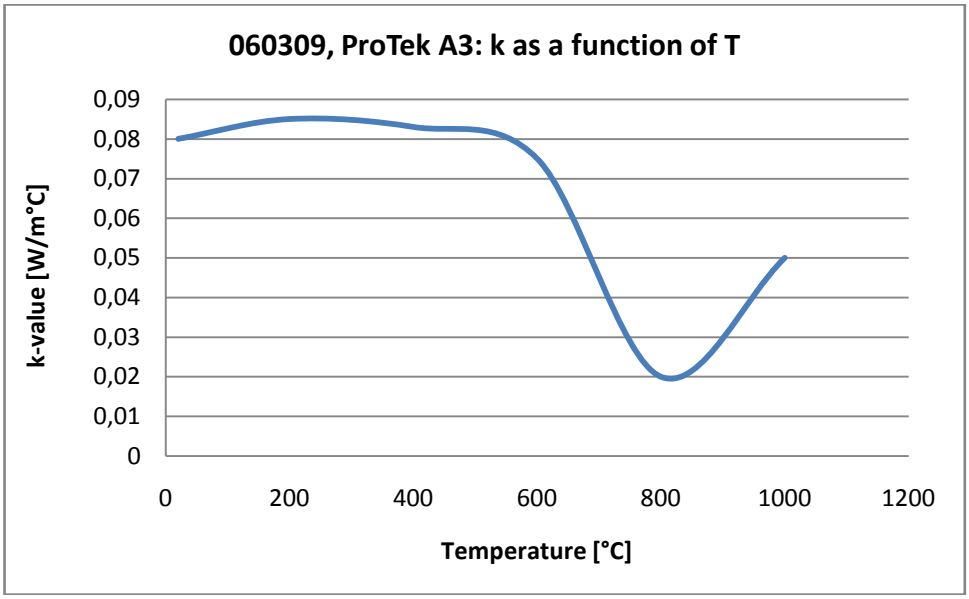

T [°C]	k [W/mK]
20	0.08
200	0.085
400	0.083
600	0.075
800	0.02
1000	0.05

Figure 30 shows the resulting k-values as a function of temperature found from experiment 060309_01, specimen ProTek A3

Two simulations were performed on experiment 060309_02, ProTek A4. The k-values used in these simulations are denoted ProTek15 and ProTek16 in Appendix G. The best fit between simulated and measured values was obtained when using the k-values denoted ProTek16. Both simulated values using ProTek16 and measured values are shown in Figure 93, Appendix B.3. The k-value as a function of temperature is shown in Figure 31.

The isolation was 0.6 cm thick before testing and 1.67 cm after. It had thus swelled 1.07 cm.

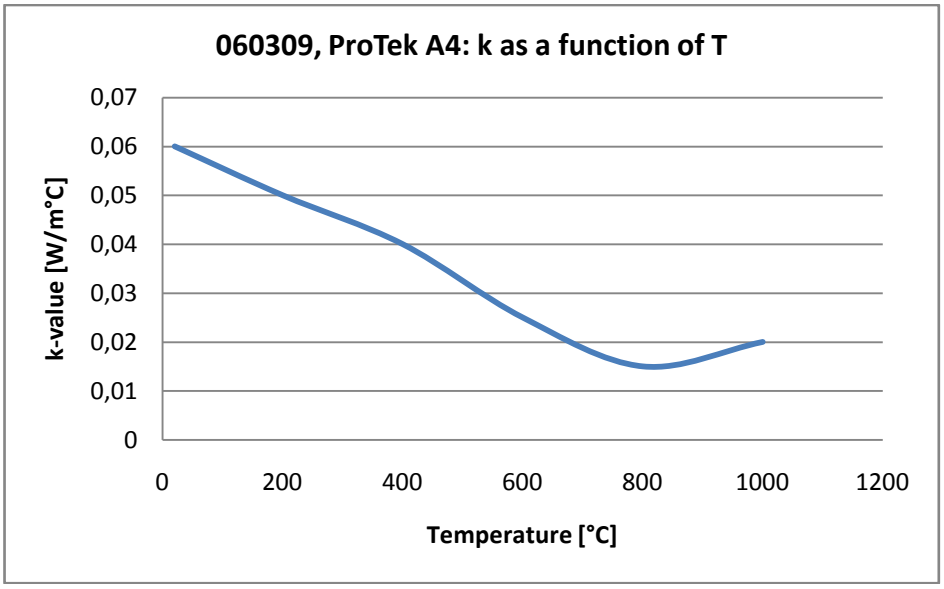

T [°C]	k [W/mK]
20	0.06
200	0.05
400	0.04
600	0.025
800	0.015
1000	0.02

Figure 31 shows the resulting k-values as a function of temperature found from experiment 060309_02, specimen ProTek A4

The experiment 170409_02 testing ProTek A1, was simulated with the k-values denoted ProTek12 described in Appendix G. The measured values and the simulated values are shown in Figure 94, Appendix B.3. As seen in this figure, the measured and simulated steel temperatures are very similar. The assumed k-values for this isolation material suit the experiment. The k-value as a function of temperature is shown in Figure 32.

The isolation was 0.94 cm thick before testing and 1.71 cm thick after testing. It swelled 0.77 cm.

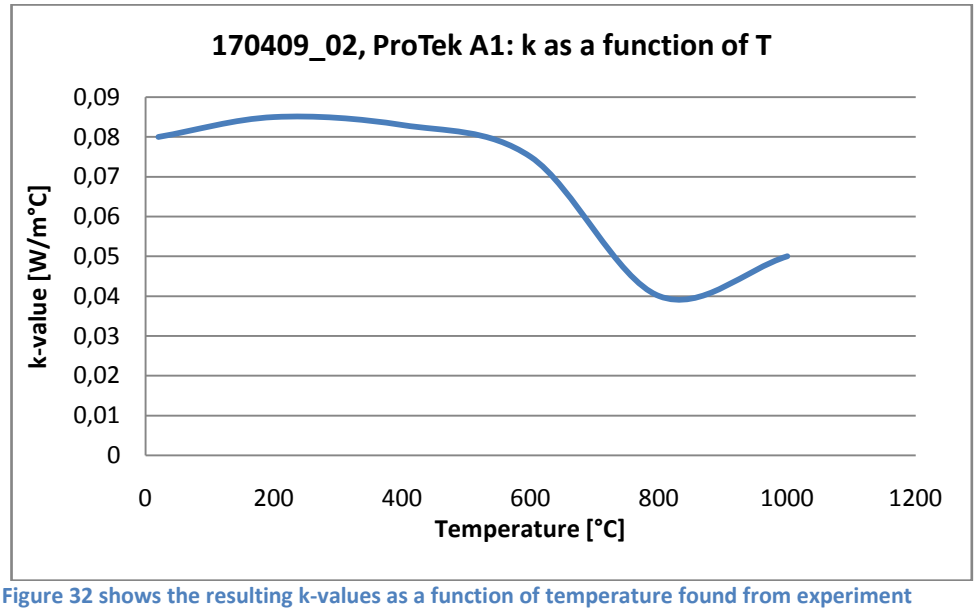

T [°C]	k [W/mK]
20	0.08
200	0.085
400	0.083
600	0.075
800	0.04
1000	0.05

Figure 32 shows the resulting k-values as a function of temperature found from experiment 170409_02, specimen ProTek A1

Experiment 180509_02 testing Benarx F Flexi roll XP was not simulated. The reason for this is discussed in part 6.5. The measured temperatures are shown in Figure 95, while the power curve is shown in Figure 96, both in Appendix B.3. The material swelled 0.875 mm during the experiment.

6 Discussion

This chapter includes discussions about results from the different phases of the work that has been performed. Results from the initial adjustments of the furnace, as well as from the testing of both dead and intumescing materials are treated. The different input data used in the numerical simulation programme Brilliant will be discussed with focus on the thermal conductivity. The chapter also includes a more extensive analysis of the steel plate temperatures, where for example deviances between simulated and measured temperatures are discussed. Finally, the chapter discusses the need for further developments of the test furnace and the method's relevance for use in numerical simulation models.

6.1 Power curves found during adjustment of the furnace

Different trends were seen when trying to make the experiments reproducible and obtain results comparable to those from the belonging numerical simulations. A returning problem was that the input power would differ from experiment to experiment, even though the experiments were similar. A few reasons will be discussed.

A lower measured power curve than expected would result in a numerical simulation where the foil temperature would keep falling. The steel temperatures would as a result become lower than measured. This was the case in experiment 271008_01 and 271008_02.

In some experiments the simulated foil temperatures were a lot higher than the measured ones. A comparison of different power curves entered into the simulations pointed towards that the input power in these simulations was too high. A possible reason why the power inputs were higher in some experiments could be that the foil that controlled the power input was actually warmer than the desired temperature, but that it showed a lower value due to insufficient contact between the thermocouple and the foil. In experiments 051108_01, 051108_04, 141108_05, 191108_03 and 191108_05 the simulated foil temperatures were too high. However, the simulated temperatures on the steel plate were very similar to measured values.

In experiment 111108_01, 111108_02, 141108_01, 141108_02 and 191108_01 the simulated foil temperatures have slightly rising curves, above the measured curves. The simulated steel temperatures from these experiments were also higher than measured, except from experiment 191108_01, which had a simulated steel temperature that matched the measured steel temperature very well. None of the delivered power curves seen from these experiments fell as quickly as previous power curves. They were almost constant. This would lead to more energy in the system than required, and result in rising foil temperatures. It was investigated whether the power could be influenced by the initial temperatures in the furnace or in the environment around it. This suggestion was disregarded, when it was seen that there were no relation between the power inputs and the initial temperatures in the furnace. Whether the differences could be related to the

number of times the foils had been heated, was also investigated. This suggestion was also disregarded, when it didn't seem to make any difference when tested. Another reason for the delivered power to become almost constant could be an underestimation of the heat loss from the system. Also, the measured foil temperatures could be incorrect, which would lead to a higher delivered power than necessary.

When the heat loss through the copper plates was included in the calculations, (experiment 211108_02 and 211108_03), the simulated foil temperature became very similar to the measured foil temperatures. However, the simulated steel temperatures in these two experiments were somewhat lower than measured. Although, when these experiments were repeated, the results became very different. The simulated foil temperature was a lot lower than measured and it had a rising curve.

Because different power curves were seen on the same types of experiments, the accuracy of the volt signal was questioned. The manufacturer claims that the volt signal is accurate (59).

The power calibration could theoretically change over time. Still, three power calibrations have been performed over the past two years, with very similar calibration parameters.

During an experiment the live cables get heated. The electric resistance in cables increase with temperature. This means that when the cables are warm, higher powers are required. Between experiments without covering the steel plate with isolation, the furnace has been cooled down for about 30-60 minutes between experiments. This amount of time may have been insufficient for the cables to cool down to their initial temperature of the first trial. A closer study of which experiment was performed when and what the different initial temperatures were have been performed and the power curves were compared. The results show that this effect was insignificant. E.g. experiment 141108_01 was performed with an initial copper temperature inside the oven of 5 °C and the power curve from this experiment were high. Experiment 181108_01 was performed with an initial copper temperature inside the oven of 150 °C. The power curve from this experiment was much lower than the one from 141108_01.

The resistance in the connection between the foils and the copper plates can differ after a foil change. Even so, experiments with the same foil have given different results. As seen from the experiments 181108_01 and 191108_01, the latter gives a higher power curve than 181108_01. The same foils have been used in both of these experiments.

Based on these findings, the method for measuring the foil temperatures was concluded to be inadequate. Therefore, this approach was abandoned in the early stages of the project.

After the independent foil bits were installed in the furnace and the input power was controlled by one of these, the power curves became similar for experiments of the same type. This result supports the conclusion that the method for measuring the radiation foils

directly was insufficient, and that the reason for all the different power curves were incorrect measuring of the foils that controlled the input power.

6.2 Input data to Brilliant

For the simulated results to be reliable, it is essential that the input data is equally reliable. This part will discuss the precision of the different input data used in the numerical simulation programme Brilliant. Especially C_p-values, k-values, emissivities and dimensions will be discussed.

C_p- and ρ- values as constants and a non-constant k-value

When simulating PFP materials both the specific heat capacity and the density of the materials are treated as constants, even when simulating intumescing materials. How much this means for the simulated results is shown in the transport equation below.

$$\frac{\partial \rho C_p T}{\partial t} - \frac{\partial}{\partial x} k \frac{\partial T}{\partial x} = q$$

If the chosen density and specific heat capacity for a certain material differ from the correct values for the material, this can be compensated for by adjusting the k-value. This will however lead to less reliable k-values.

As seen in the first term of the transport equation, the larger density and specific heat capacity, the more energy is needed for heating the material. Changing these parameters therefore results in a different picture of the period for the simulated temperatures.

The specific heat capacity and the density of some selected materials used in this project are shown in Table 8 (9) (15) (60). These two constants were given by the manufacturers for the dead isolation materials FireMaster607 and Kaowool, and for the lightweight concrete Siporex. For the intumescent PFP material ProTek these values weren't available from the manufacturer. The specific heat capacity for ProTek had to be assumed. Because ProTek consists of 15-40 % glass fibres, the specific heat of glass was assumed to be a suitable value (13) (30).

The ProTek samples were weighed to be approximately 3 kg each. The volume of each ProTek sample was $V = 0.45m \cdot 0.45m \cdot 0.0091m = 0.00184m^3$. This implies a density of approximately 1600 kg/m^3.

Material	C_p [J/kgK]	ρ [kg/m^3]
Siporex	550	535
FireMaster607	1074	128
Kaowool 1400	1130	260
ProTek	840	1600

Table 8 shows specific heat capacity and density of a selection of the materials used in this project (9) (15) (60).

As mentioned earlier in part 2.5.2 the swelling process of intumescing materials will not be simulated. In this swelling process, the thickness of the intumescing material increases, and as a consequence the density of the material decreases. To make the numerical simulation as similar as possible to a real situation, the thermal conductivity takes into account the phase change from a solid char to a porous char and the increased thickness. The effect of expansion is taken into consideration when deriving a temperature dependent effective thermal conductivity for the specific case. Because of this the k-values found for the intumescing materials are not a correct physical parameter.

Appendix G gives a list of all the k-values used when simulating experiments with intumescing materials. In all these experiments the temperature on the foil bits were stabilised at 900 °C. This means that the intumescing materials' surface temperatures were approximately 800 °C. This was seen in the simulated results. The k-value at 800 °C is therefore the most important parameter as this is the one Brilliant uses when the system has stabilised in each simulation. A k-value at 1000 °C has also been set, as the temperature on the isolation can become a bit higher than 800 °C. For most simulations a k-value at 20 °C, 200 °C, 400 °C, 600 °C, 800 °C and 1000 °C has been determined. This should be sufficient since Brilliant interpolates between the temperatures.

Emissivity

The emissivities chosen for the different materials in the furnace have great influence on the simulated results. Especially the emissivity on the radiating foils is an important parameter, because it controls the amount of heat released. This impacts the heat exposure on the other materials in the furnace. By using a high emissivity on the radiation foil, the surface temperature on the foil will decrease. This is seen in simulation 211108_03f (Table 9) where the emissivity on the foil was increased from 0.7 to 0.8. The surface temperature on the foil where the emissivity was 0.8 showed 20 °C less than when the emissivity was 0.7. The steel temperature increased by 1 °C when the emissivity of 0.8 was used.

The emissivity on the steel plate has also an influence on the foil temperatures. In simulation 211108_03c, 1000 °C (Table 9), the emissivity on the steel plate was increased from 0.6 to 0.7. The results showed that when the emissivity was 0.7, the temperature on the foil decreased by almost 25 °C. At the same time, the temperature on the steel plate had decreased by 15 °C. The same trend happened when simulating experiment 081208_03 (750 °C). First the experiment was simulated with an emissivity of 0.6 on the steel plate, and then increased to 0.7. At t=1200 sec, the difference in foil temperature was 22 °C, where the simulation using an emissivity of 0.6 showed the highest values. Also the steel temperatures became higher with an emissivity of 0.6. This temperature difference was 15 °C.

When studying the equation for radiation, it is seen that when the temperature decreases, the emissivity will increase $\dot{q}'' = \varepsilon \cdot \sigma \cdot T^4 \left[W/m^2 \right]$. This shows that the experiences with the changes in emissivity in the numerical simulation programme are credible.

Parameters that affect the results

Six numerical simulations were performed on data collected from experiment 211108_03 (1000 °C) with different parameters. This was done in order to see which parameters that would have big impact on the simulated results. Since the simulated steel temperature in the first simulation was 65 °C lower than measured, it would be interesting to see if any of the new parameters would result in an increased steel temperature to resemble the measured one. A description and a comparison of the numerical simulation results are shown in Table 9. As seen in these results, the simulation that made the steel temperature increase the most was the one that included radiation, had a smaller defined air-gap and included both heat conduction and energy for heating the copper plates as heat loss. However, the resulting steel temperature was still about 60 °C lower than measured.

For these numerical simulations, the dimensions of the air gap were changed in Brilliant. Since the size of the air gap did change during and between some experiments, it was of interest to know how much the size would affect temperatures, especially the foil temperature and the temperature on the steel plate. The steel plate could start to bend during some of the experiments due to high temperatures. After every experiment, the steel plate was removed for cooling. By removing it and putting it back in, the air gap could very easily decrease/increase.

Experiment 211108_03:

Measured values at t = 716 sec Foil middle: 1016.5 °C

Foil right: 1031.9 °C

Steel temperature exposed side: 798 °C

Description of the input parameters when simulating experiment 211108_03	**Calculated foil temperature at t= 716.4 s [°C]**	**Calculated steel temperature exposed side at t=716.4 s [°C]**	**Comments**
Sim 211108_03: **Normal parameters**	1020.6	732.6	
Sim 211108_03b: **Radiation activated**	1023.7	735	Temperatures were hardly affected. Not before the end did the simulated values get higher than earlier (1-3 °C)

Sim 211108_03c: **Radiation activated and the emissivity on the steel plate increased to 0.7 (0.6 before)**	999.7	720.3	Lower values
Sim 211108_03d: **Radiation activated, air-gap reduced from 1 cm to 0.5 cm. More heat loss to the copper included (energy for heating the copper on the long part).**	1025.4	741.7	Generally quite high values
Sim 211108_03e: **Radiation activated, heat loss copper included, air-gap reduced to 0.5 cm, emissivity on the edges sat to 0.5 instead of 0.3. Material on the edge is changed from being Foamglas to Kaowool_1400**	1012.7	723.09	This simulation is just like the one above, only that the material and the emissivity on the edges are changed. The foil temperature has decreased by 12.7 °C and the steel temperature has decreased by 18.61°C.
Sim 211108_03f: **Radiation activated, emissivity on the foil changed from 0.7 to 0.8.**	1003.9	736	The foil temperature is 19.8 °C lower than when the emissivity on the foil was 0.7. The steel temperature is raised by 1 °C.
Sim 211108_03g: **Radiation activated. More control volumes on the foil, changed from 1x10x10 to 1x 20x20. More radiation points: Azimuth is changed from 8 to 12 and Polar is changed from 6 to 12.**	1028.2	738.2	Results are quite similar to the simulation with the regular parameters, but with radiation activated. Steel temperature has been raised by 3.2 °C.

Table 9 shows an overview of numerical simulations done on the same experiment with different parameters.

6.3 Steel plate temperature

As described in part 3.2.4.1, the temperature on the steel plate was measured at one spot on both the exposed and unexposed side. The thermocouples were mounted on in the middle of the steel plate, because it was assumed that this spot would be warmest. A closer study of the temperatures on the steel plate will be described in this part as well as a study of the differences between the temperatures on the steel plate's exposed and unexposed sides. The steel plate temperature's dependency on emissivity will also be emphasized.

6.3.1 Temperatures on the whole steel plate

When simulating the experiments in Brilliant, it is possible to analyse the temperature on the steel plate at different locations. Each side of the steel plate consists of 400 control volumes where it is possible to see the temperatures in each of them. In order to see whether the calculations done by Brilliant on the steel plate temperatures were reasonable, a closer study of the temperatures was done on experiment 111208_01.

Nine different points on each side of the steel plate was collected and studied. Selected points on the exposed and unexposed sides were directly opposite one another, in order to see the temperature difference through the steel plate. The selected points lay as shown in Figure 33. Each of the 3 x 3 points is represented by four coloured squares surrounding the point.

The results from the analysis show that the hottest point is the one in the middle of the steel plate, as expected. All the temperatures are shown in Figure 34. The next hottest point was at the top in the middle. The temperature in the middle on the left and right side comes as the third hottest points. The coolest spots on the steel plate is found on the lower left and right side, which was also expected since heat naturally moves upwards.

This study showed that the different temperatures calculated in Brilliant were reasonable.

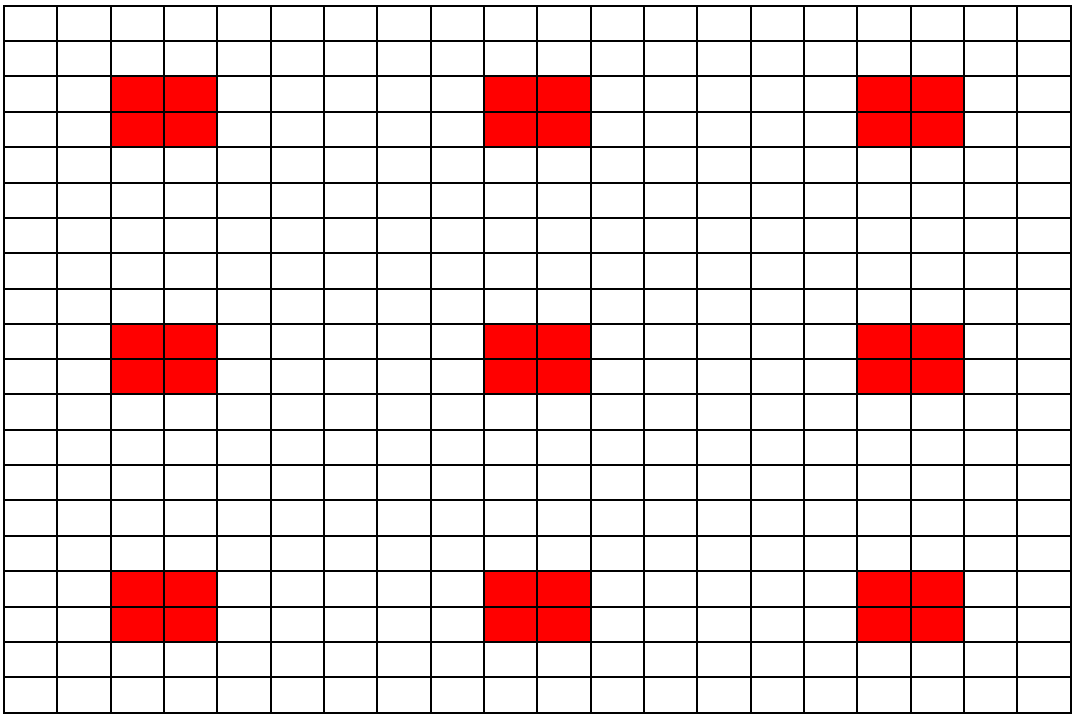

Figure 33 represents the steel plate with control volumes as it is seen in Brilliant. The red squares surrounds the points selected for further study of the temperatures.

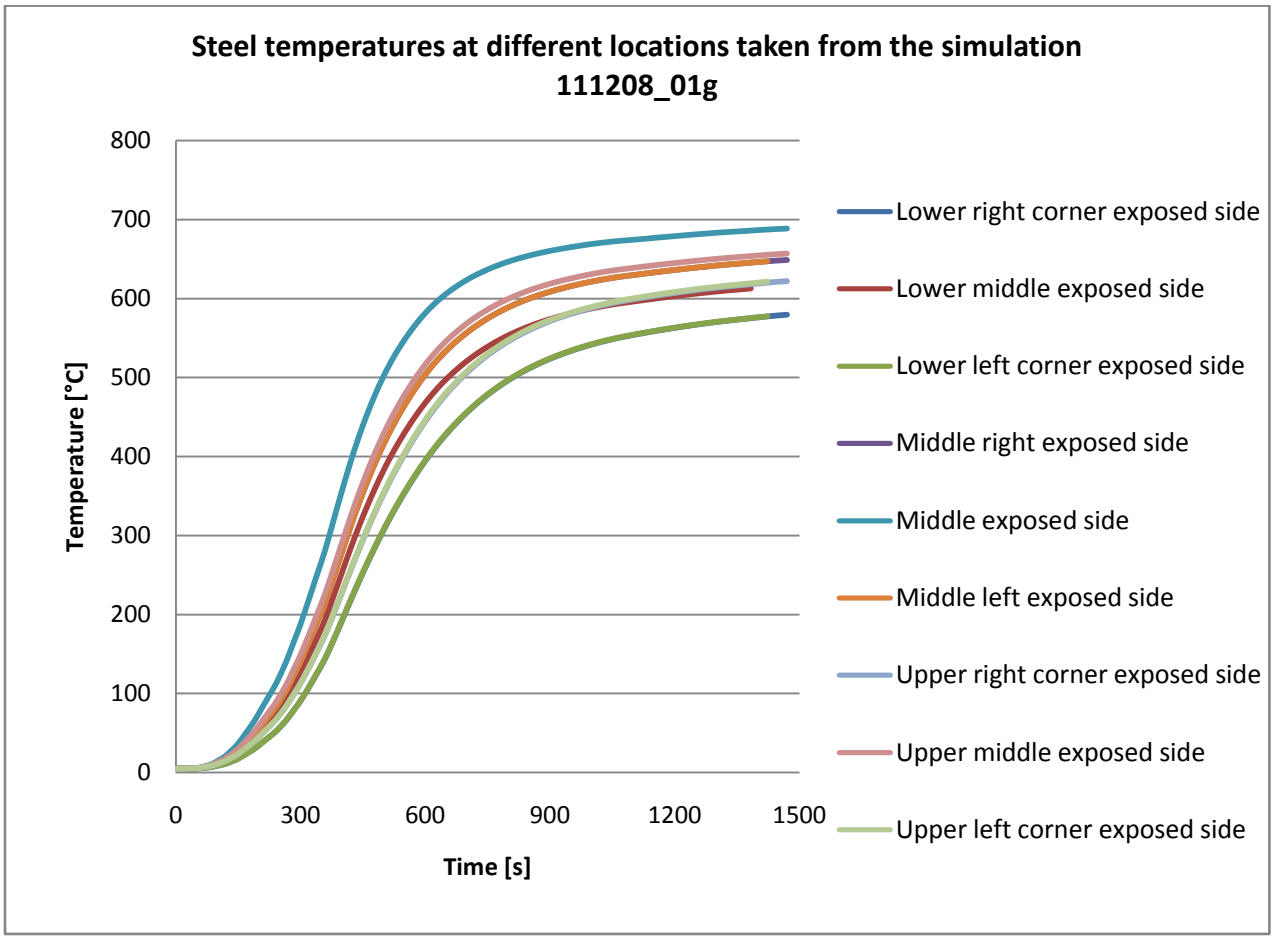

Figure 34 shows steel temperatures at different locations taken from the numerical simulation 111208_01g

6.3.2 Analysis of the temperature difference between the steel plate's exposed and unexposed side

This part will analyse the difference in temperature between the steel plate's exposed and unexposed sides. A comparison of the measured and simulated temperature difference from experiment 111208_01 shows a deviation between the two results. The temperature difference has therefore been calculated manually, in order to see which result is the most reliable. The calculation is based on the measured temperature on the radiation foil together with the measured temperature on the exposed side of the steel plate.

Measured temperatures taken at t = 1200 seconds of experiment 111208_01 are shown in Table 10. At this point steady state has been reached, and temperatures are stable. The numerically calculated temperatures from the corresponding simulation, taken at t = 1200 seconds, is shown in Table 11.

Part	Temperature [°C]
Foil middle	931
Foil left	932
Steel exposed side	669
Steel unexposed side	655

Table 10 shows measured temperatures on the foils and the steel plate at t = 1200 seconds in experiment 111208_01

The total power registered at t = 1200 seconds is 11767 W.

Part	Temperature [°C]
Steel exposed side	679.23
Steel unexposed side	674.45

Table 11 shows simulated temperatures on the steel plate taken from simulation 111208_01g. The values are at t=1200 seconds.

As seen on these two tables, the measured temperature difference between the exposed and unexposed side of the steel plate was (669-655) °C = 14 °C, while the simulated temperature difference was (679.23-674.45) °C=4.78 °C. There is thus a difference of 9.22 °C between the two results.

Before the temperature on the unexposed side of the steel plate can be calculated manually, the amount of power reaching the steel plate must be calculated. This includes the equation for calculating the total radiation emitted from the foils together with how much radiation the steel plate absorbs subtracting the amount of radiation reflected from the steel plate. In order to calculate the radiant intensity at a point distant from the radiator, a configuration factor must be used. Considering the two surfaces, radiation foil and steel plate, the configuration factor between the two becomes (14):

$$F_{1-2} = \frac{D^2}{4 \cdot R^2 + D^2} = \frac{(0.44m)^2}{4 \cdot (0.15m)^2 + (0.44m)^2} = \underline{0.68}$$

D = diameter on the radiation foils

R = distance from radiation foil to steel plate

The total radiation emitted from the foils at t=1200 sec is:

$$\begin{aligned}\dot{q}_r &= \varepsilon_f \cdot \sigma \cdot T_f{}^4 \cdot F_{1-2} \\ &= 0.7 \cdot 5.669 \cdot 10^{-8} \, {}^{W}\!/_{m^2 \cdot K^4} \cdot (932+273)K^4 \cdot 0.68 \\ &= 56893W\end{aligned}$$

Amount of heat absorbed by the steel plate less the amount of radiation reflected from the steel plate.

$$\begin{aligned}\dot{\mathrm{q}}_{\mathrm{net}} &= \dot{q}_r \cdot a_s - \varepsilon_{\mathrm{s}} \cdot \sigma \cdot \mathrm{T_s}^4 \\ &= 56893W \cdot 0.7 - 0.7 \cdot 5.699 \cdot 10^{-8} \, {}^{\mathrm{W}}\!/_{\mathrm{m}^2 \cdot \mathrm{K}^4} \cdot (669+273)\mathrm{K}^4 \\ &= \underline{8578\mathrm{W}}\end{aligned}$$

a_s = absorption, steel plate

The correct coefficient of thermal conductivity of steel at 669 °C is found by this equation:

$$\begin{aligned}k_{steel} &= -0.022 \cdot T + 48 \\ &= -0.022 \cdot 669°C + 48 \\ &= \underline{33.28 \, {}^{W}\!/_{m \cdot K}}\end{aligned}$$

The temperature on the steel plate's unexposed side becomes:

$$T_{un\exp} - T_{\exp} = \dot{q}_{delivered,steelplate} \cdot \frac{\Delta \mathrm{x}}{-\mathrm{k} \cdot \mathrm{A}} = 8578W \cdot \frac{0.005m}{-33.28 \, {}^{\mathrm{W}}\!/_{\mathrm{m} \cdot \mathrm{K}} \cdot (0.45 \cdot 0.45)\mathrm{m}^2} + 669°\mathrm{C}$$

$$T_{un\exp} = \underline{662.5°\mathrm{C}}$$

This calculation implies a temperature difference of 6.5 °C between the exposed and the unexposed side of the steel plate. This difference is closest to the one calculated by Brilliant, which was 4.78 °C. Compared to the measured difference of 14 °C, the simulated values seem to be the most reliable in this case.

The full simulated temperature difference profile (taken from the middle of the steel plate in simulation 111208_01g) is shown in Figure 35. The figure shows a significant increase in temperature difference between exposed and unexposed side of the steel plate when the

temperature on the exposed side rises. This is reasonable, as Fourier's law states that ΔT rises with increasing supplied heat (q). The equation is explained in more detail in part 2.1.1.

Figure 36 shows a schematic of the steel plate from the programme GL View at approximately 1450 seconds of the numerical simulation (111208_01g). The left side of the figure shows a colour scale, representing temperatures in Kelvin. The figure indicates that the steel plate (represented in yellow /green) keeps a temperature of about 950 K = 677 °C, which can be verified by the temperatures in Figure 34. A careful look at Figure 36 also reveals that the upper and the middle part of the steel plate is warmer than the lower part.

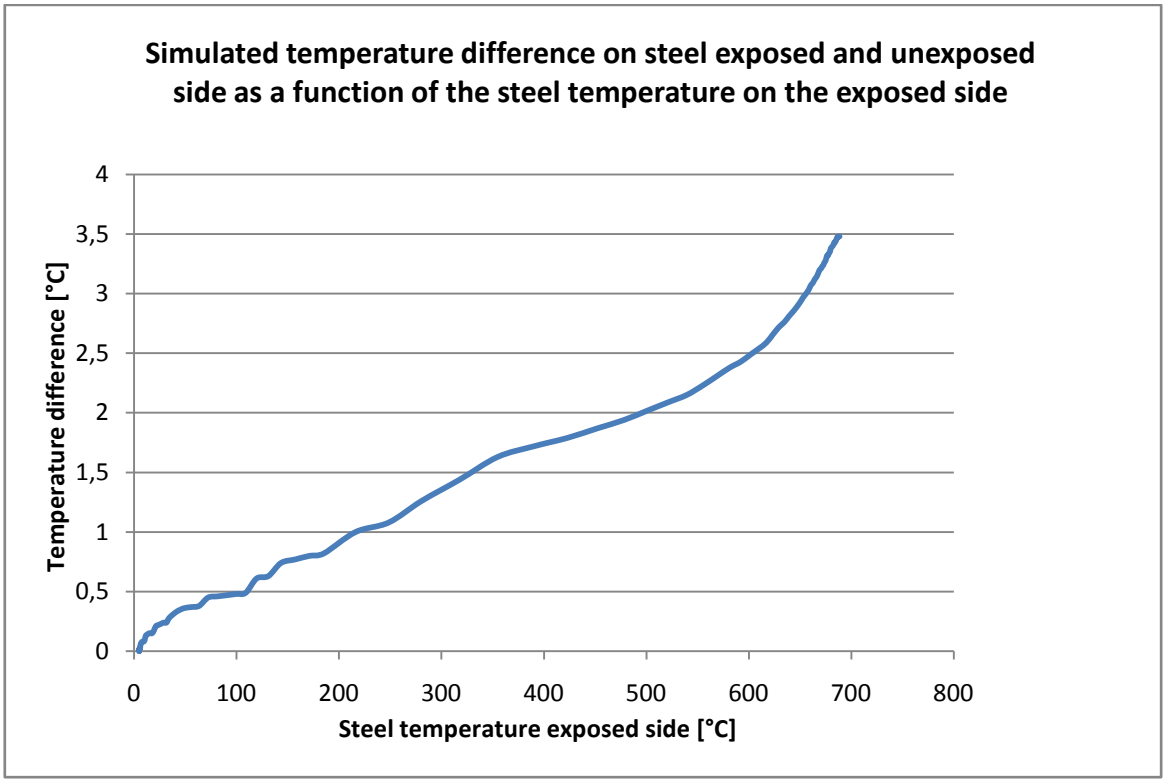

Figure 35 shows how the simulated temperature difference on the steel plate changes with temperature

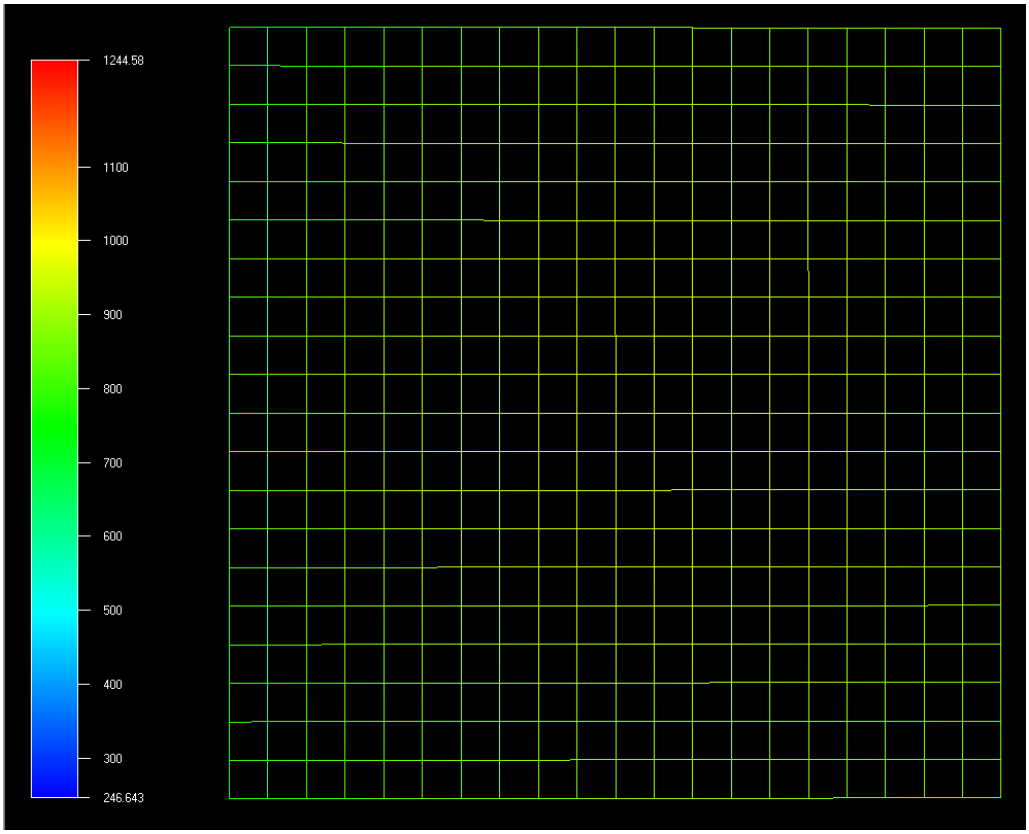

Figure 36 shows the simulated steel plate schematized in GL View. The colour scale on the left side shows which colour represents which temperature in Kelvin. A careful look also reveals that the upper and the middle part of the steel plate is warmer than the lower part.

Values gathered from experiment and simulation 230109 with 0.9 cm Kaowool 1400 isolation also showed deviation between the measured and simulated temperature differences between the exposed and unexposed side of the steel plate. The measured difference was about 13 °C, which seems to be a bit high, while the simulated temperature difference was around 0-0.49 °C, which seems to be too low. A manual calculation was performed in order to assess which of the two results is the most reliable. The calculation is based on the simulated temperature on the isolation's exposed side together with the simulated temperature on the steel plate's unexposed side.

Measured values taken from experiment 230109 at t=2400 seconds in the experiment.

Part	Temperature [°C]
Steel exposed side	292
Steel unexposed side	279

Simulated values taken from simulation 230109 at t=2400 seconds in the simulation.

Part	Temperature [°C]
Steel exposed side	296.71
Steel unexposed side	296.23
Kaowool exposed side	786.4

Calculations of the amount of power going through the Kaowool isolation and the steel plate are shown below. A calculation of the temperature on the steel plate's exposed side is also shown. A sketch of the isolation and the steel plate is shown in Figure 37.

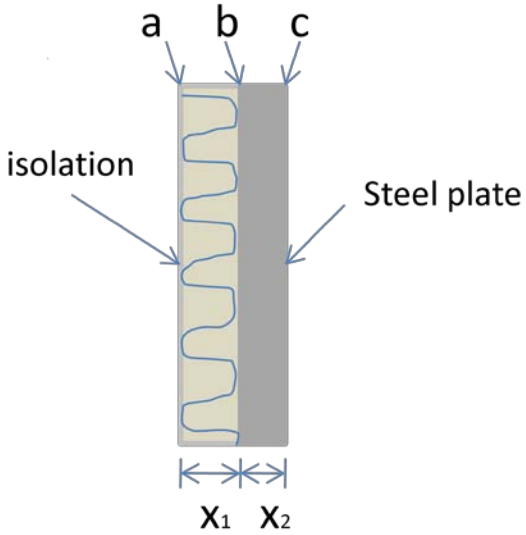

Figure 37 shows a sketch of the isolation and the steel plate in the furnace. The notation a, b and c represent the temperature on the isolation surface, the temperature on the steel plate's exposed side and the temperature on the steel plate's unexposed side respectively.

$$\dot{q} = -k_1 \cdot A \cdot \frac{(T_b - T_a)}{\Delta x_1} \Rightarrow T_b = \frac{-\dot{q}}{k_1 \cdot A} \cdot \Delta x_1 + T_a$$

$$\dot{q} = -k_2 \cdot A \cdot \frac{(T_c - T_b)}{\Delta x_2} \Rightarrow T_c = \frac{-\dot{q}}{k_2 \cdot A} \cdot \Delta x_2 + T_b$$

$$T_c = \frac{-\dot{q}}{-k_2 \cdot A} \cdot \Delta x_2 + \frac{-\dot{q}}{-k_1 \cdot A} \cdot \Delta x_1 + T_a$$

$$\dot{q} = \frac{(T_a - T_c)}{\frac{\Delta x_1}{k_1 \cdot A} + \frac{\Delta x_2}{k_2 \cdot A}}$$

$$\dot{q}'' = \frac{(T_a - T_c)}{\frac{\Delta x_1}{k_1} + \frac{\Delta x_2}{k_2}} = \frac{(786.4 - 296.23)°C}{\frac{0.009m}{0.1 W/m \cdot K} + \frac{0.005m}{41.4 W/m \cdot K}} = 5439 W/m^2$$

$$\dot{q} = \dot{q}'' \cdot A = 5439 W/m^2 \cdot 0.2m^2 = \underline{1088W}$$

$$T_b = \frac{-\dot{q}}{k_1 \cdot A} \cdot \Delta x_1 + T_a = \frac{-1088W}{0.1 W/m \cdot K \cdot 0.2m^2} \cdot 0.009m + 786.4°C = \underline{296.8°C}$$

The temperature difference became (296.8-296.23) °C = 0.57 °C, which is only a little bit higher value than simulated. This low temperature difference is most likely to be correct, because of the low input power. The less power into a system, the lower temperature difference will appear on the steel plate and opposite.

As a conclusion, the simulated temperature difference on the exposed and unexposed side of the steel plate is the most reliable.

6.3.3 The steel plate's dependency on the isolation thickness on the edges in the furnace

When simulating different thicknesses of isolation on the edges in the furnace, it was noticed that the temperature on the steel plate increased when the thickness of the edges decreased. This runs contrary to expectations, as the steel temperature is expected to decrease when the isolation thickness in the furnace decreases. When the thickness on the edges is reduced, there should presumably be more heat loss through the walls, resulting in lower temperatures inside the furnace.

An example of this is shown in Figure 38. This figure shows the measured results from experiment 111208_01 together with two numerical simulations, with the only difference between them being the thickness of the edges. The thicknesses are 7.5 cm (sim 2) and 12.5 cm (sim 3) respectively. As the figure shows, the steel plate is the warmest for the numerical simulation with edges of 7.5 cm. Why this happens is not known. The values found when the

edges are adjusted to the same as the actual furnace, which is 12.5 cm, are presumed to be correct.

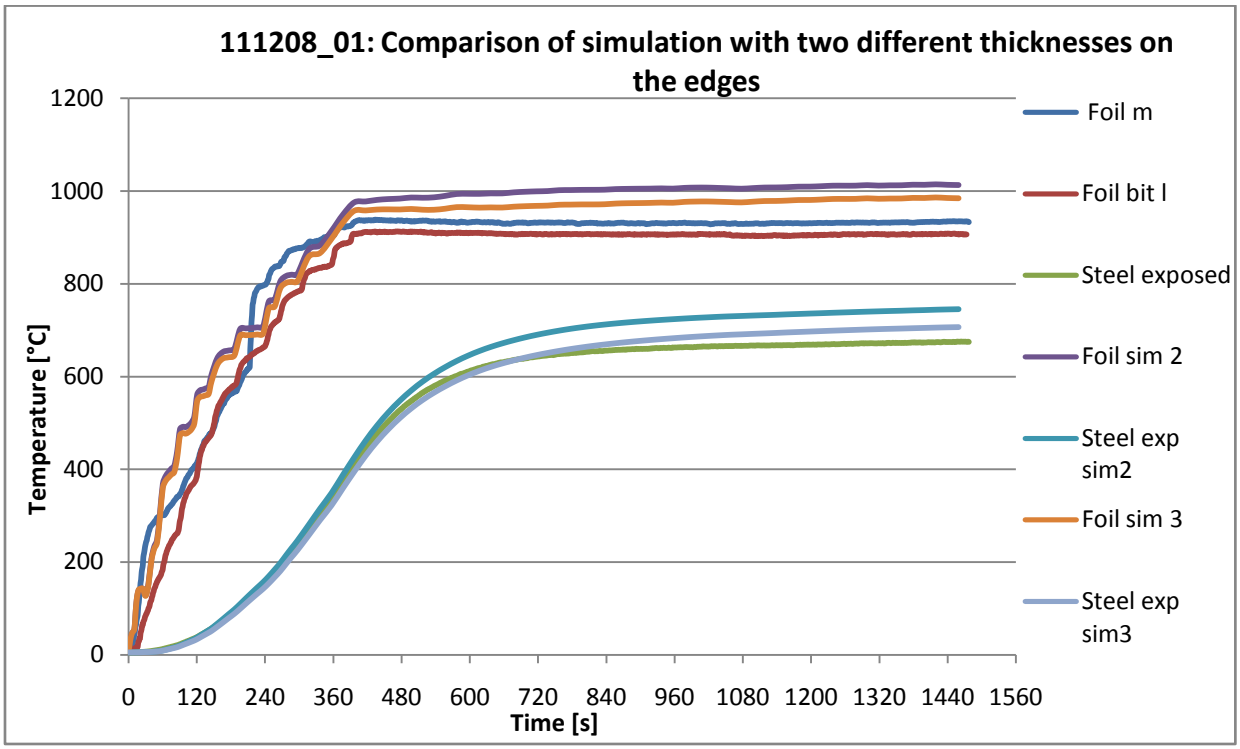

Figure 38 shows foil and steel temperatures from experiment 111208_01. Two different numerical simulations have been performed on this experiment where the only difference is the thickness of edges in the furnace. 'Sim 2' has the smallest thickness on the edges, while 'sim 3' has the largest.

6.4 Discussion about results from testing of dead materials

By running experiments and subsequent numerical simulations on dead materials, the method for finding the thermal conductivity could be tested. The thermal conductivities of the test specimens were given by the manufacturers, and were therefore known. It was of great interest to see if the simulations would reproduce the experiments, with the given thermal conductivity. If the simulations fit the experiment, this would indicate that the method for finding the thermal conductivity would function as intended.

Two experiments with corresponding numerical simulations were performed and evaluated for dead materials, which were Kaowool 1400 and Firemaster607 respectively. In the simulations of these two experiments (230109 and 270109_02b), the simulated foil temperatures showed lower values than what was measured on the foil bits. Theoretically, the simulated foil temperature should be somewhat higher than the temperature on the foil bits. The simulation gathers the temperatures from the actual radiation foil, whereas in the experiments, the foil bits where temperature measurements are taken are placed behind the radiation foils. However, because the simulated temperature on the steel plate fit the measured values well, it is assumed that the power input in the numerical simulation is sufficient, even though the simulated temperature on the foil is a bit low.

6.5 Discussion about results from testing of intumescing materials

In all the numerical simulations on intumescing materials, the input power has been the same, taken from experiment 270109_02. Because of this, the simulated foil temperatures will have the same conditions. They do however not have the same temperatures in the different simulations. This is because of the different k-values used. The lower the k-value in the simulation, the less heat loss there will be through the isolation and the steel plate, and the higher the temperature in the furnace. For example, when comparing simulation 050309h and 060309_02b it is seen that the simulated foil temperature in 060309_02b is higher than in 050309h. The k-values decided for 060309_02b, denoted PT16 have lower values than PT15 which are simulated in 050309h.

Another issue with using an input power that does not belong to the specific experiment is that special occurrences will not appear in the simulation. Such an occurrence could be for example a sudden jump in the input power. This will however be seen on the measured temperatures. The initial phase is different for each experiment. From the moment the control panel is switched on, it can take between 2-4 minutes until the foil bits have reached 900 °C. A specific recipe for the initial phase could have been developed, so that every specimen in every experiment would be heated with the same speed. Even though this has not been done, it does not seem to have affected the simulation results. As can be seen on the temperature curves from the experiments with intumescing materials, the temperature on the steel plate does not start to increase during the first 2-4 minutes. The preset power input is presumed to give an adequate representation of the situation.

During the experiments with intumescing materials there has been quite a lot of foil breakages due to foils burning off. These breakages can sometimes be hard to notice. In earlier experiments, when measuring the temperature directly on the radiation foil, it was very easy to determine a foil breakage, because the measured temperature on the foil that burnt off would decrease rapidly. When the foil temperature is not measured directly on a breaking foil, but on the foil bit behind it, the temperature on the foil bit will decrease. The input power will then quickly rise, pushing the temperatures back up to the required level. This also results in higher strain on the remaining foils, increasing the risk of another foil breakage. One solution to this problem could be to resume the direct measuring of foil temperatures, for the purpose of early detection of foil breakages.

When performing experiment 170409, the control panel shut down because of too high temperatures on the foils. The control panel was programmed to shut down if the temperature on the foil bit exceeded 1050 °C in all the experiments done with intumescing materials. The experiment was started over again when the steel temperature had cooled down to 76 °C. The specimen had started to swell, though this did not seem to cause any problems when simulating this specific case.

The independent foil bit in the furnace on the right side stopped functioning after experiment 060309_02, as the thermocouple that was welded onto the foil bit loosened. This was not improved for later experiments, because of lack of suitable equipment.

The independent foil bit behind the centremost radiation foil is the one that is controlled by the control panel. This foil bit's temperature will naturally become slightly higher than the other two foil bits, as it is exposed to radiation from the radiation foils on both sides. This is while the other two foil bits only will be exposed to the radiation from the foil in front and on one side. Empirically, the temperature on the foil bit in the middle is around 20 °C higher than the other two.

As seen on the k-value graphs in part 5.3, the k-values differ quite a lot between the experiments with all ProTek specimens. The measured steel temperatures are however not that different. A closer study of the k-values used in each of the four experiments has been done and a comparison was made. Experimental and simulated values are shown in Table 12.

Specimen	Thickness before exposure [cm]	Swelling [cm]	Thickness after exposure [cm]	k-value at 800 °C [W/mK]	Steel temp. measured at t=2880 s [°C]	Steel temp. simulated at t=2880 s [°C]	Isolation temp. at exposed side simulated at t=2880 s [°C]
ProTek B3	0.91	0.06	0.97	0.125	292	301	791
ProTek A3	0.91	1.3	2.21	0.02	255	268	825
ProTek A4	0.6	1.07	1.67	0.015	250	237	862
ProTek A1	0.94	0.77	1.71	0.04	280	273	830

Table 12 shows a comparison of the four different experiments done on the intumescing material ProTek together with simulated results and the k-value used.

As the table shows, the lower the k-value, the higher the temperature becomes on the isolation's exposed side. This is to be expected and shows consistency in the results.

ProTek A4 resulted in the lowest steel plate temperature of the four specimens. The simulation of this experiment also required the lowest k-value.

ProTek B3 resulted in the highest steel temperature, and the simulation also required the highest k-value.

The difference in measured temperatures on the steel plate between ProTek A3 and ProTek A4 is only 5 °C. Even so, the k-values differ. The simulated results of ProTek A3 show a steel temperature of 13 °C above measured, while the simulated results from ProTek A4 show a steel temperature of 13 °C below measured. It is possible that k-values between 0.02 and 0.015 W/mK would suit the measured values better for both specimens.

The measurements in experiment 060309_02, where ProTek A4 is tested, are not very good. Within the first 30 minutes of the experiment, the measured and simulated steel temperatures do not fit very well. At t=960 seconds, the measured steel temperature stops rising for a few seconds before it continues to increase. The measured values are therefore not deemed to be reliable.

As only one experiment has been performed on each of the above mentioned products, more experiments should be carried out in order to verify the results.

The experiment 180509_02 testing Benarx F Flexi roll XP was not simulated. Preferably another equal experiment should be performed first to verify the measured results. However, four experiments were performed with this material, where three of these attempts ended with foil breakage early in the experiment. The other experiment (180509_02) also ended with foil breakage, but this was first after 65 minutes. All the foil breakages occurring during testing this specific material are probably caused by the gases that the specimen produces. These gases may contain corrosive components that will contribute to faster oxidation of the metallic foils.

A second reason why the experiment was not simulated was that the C_p-value for this specimen was unknown. None of the C_p-values for the ingredients of the specimen was known either, so it would be difficult to assume a value.

The shape of the temperature curve on the steel plate in experiment 180509_02 (Figure 95, Appendix B.3) differs from earlier experiments with two sudden changes in its temperature gradient. The first change can be seen 200 seconds into the experiments, while the other change happens at 2300 seconds. These changes are most likely caused by a change in the swelling process.

The power in the same experiment increases, instead of decreasing like the power in the other experiments. A reason for this rising power curve could be that the test specimen's heat contribution decreased more and more.

The measurements of all the test specimens' swelling were performed on the edges of the specimens. This is because the slide caliper used for these measurements is not large enough for measuring the thickness on the middle of the specimens. The thicknesses in the middle of the specimens are usually somewhat thicker than on the edges.

6.6 Proposals for further development of the furnace

Some challenges still remain regarding the dependability of the method. A recurring problem is that the radiation foils burn off under high temperatures, rendering the experiment in progress useless. Therefore, there is a need for a method that allows a higher heat flow without increasing the temperature on the radiation foils.

Since the intumescing materials start burning at a certain temperature and the heat from the flames and the gases produced may result in even more fragile foils, it should be considered whether the radiation foils may be placed at a longer distance from the test specimen.

A higher heat flux is also desired so that a k-value for temperatures up to 1100 °C may be found. This is due to the standard time-temperature curve for hydrocarbon fires that reaches 1100 °C. PFP materials are often tested within a standard fire test condition.

6.7 The method's relevance for use in numerical simulation models

The thermal properties data gained from this method are likely to be useful in future numerical simulations. When using the data in simulations, it is however very important that the test conditions used to derive the data are considered. For instance, in this case, the experimental data were obtained during the first heating of the PFP products. When exposed to heat, intumescing materials go through a phase change and endothermic/exothermic reactions. These are very important for the fire protective capability of the products. Phase changes and endothermic/exothermic reactions are normally irreversible processes, which are not reproducible in subsequent heating (1).

Active intumescing PFP materials will react upon fire dependent on (1):

- Heat exposure
- Size and shape of the substrate
- Partition protection or structural protection
- Mechanical impact from fire (e.g. erosion in jet fire)
- PFP thickness vs. substrate thickness
- PFP thickness vs. duration of heat exposure

All these parameters need to be considered before entering the thermal properties into a numerical simulation model. The mechanical properties are very important because cracking, shrinking and adhesion of the PFP material will not be known without testing the product. It is common to overestimate the fire protecting ability of a material when the mechanical properties are unknown. Mechanical properties will only be available through physical tests (1).

As a standard hydrocarbon fire reaches 1100 °C (29), it would be of interest to see how the intumescing materials would act in higher temperatures than 900 °C, which is the highest temperature tested in this thesis. Because the radiation foils in the furnace are rapidly worn

down when exposed to high temperatures, and start to burn off, testing with higher temperatures has been found difficult. The foils can be heated to 1050 °C without burning off, but empirically only for a limited period of time. As all experiments with intumescing materials last for about an hour, foil breakages are very likely to occur, rendering the data useless. Further development of the furnace is required before tests can be performed under higher temperatures.

In this thesis, k-values have been found for intumescing materials for temperatures lower than 800 °C. These values may be applied in numerical simulations within the same temperature range.

7 Conclusion

The prototype furnace developed by Sintef NBL AS and Petrell AS, did not give reproducible results at the start of this work. It was concluded that this was due to inaccurate measurements of the temperatures on the radiation foils. The furnace was further developed and three independent bits of foil were installed, each with thermocouples welded onto them. One of these independent foil bits temperatures were used for controlling the input power. This made experiments reproducible. The measured results were also comparable to simulated results. The method is therefore concluded to be satisfactory for the purpose of the analysis in this thesis.

One of the objectives of this project has been to make the method easy and relatively quick in use. Some issues still remain. Because of several foil breakages, it would be advantageous if the same heat flow could be achieved at lower temperatures on the radiation foils. It should also be considered whether the radiation foils may be placed at a longer distance from the test specimen in order to make them last longer.

The thermal conductivities given by the manufacturer for the dead materials Kaowool 1400 and Firemaster607 corresponded well with the simulated values.

The method has been used to find the thermal conductivity at elevated temperatures for four different test specimens. The k-values found for these specimens were for temperatures from 20 °C to 800 °C. These values may be applied in simulations within the same temperature range. However, a higher heat flux is desired so that a k-value for temperatures up to 1100 °C may be found.

This work demonstrates the many challenges related to numerical simulations and physical experiments. The number of experiments that have been performed without reproducibility indicates how sensitive test apparatus can be and how difficult it is to achieve good measured results. Even when the result is known, calculating it by means of numerical simulations is difficult. This is a paradox, especially when considering the number of calculations that have been performed without verification.

8 Bibliography

1. **Berge, Geir and Danielsen, Ulf.** *Thermal properties of passive fire protection materials.* Trondheim : Sintef NBL as and Petrell as. Project proposal.

2. **Bjørn Egil Rossebø, Arve E. Fredriksen, Geir Berge.** *Simuleringsmodell for å beregne termiske egenskaper til passive brannbeskyttende materialer.* Trondheim : SINTEF NBL as, 2008.

3. **Beerenberg Corp. AS.** Benarx F Piping Insulation System Flexi Roll XP. [Online] [Cited: 19 May 2009.] http://www.benarx.com/products/benarx-f-flexi-roll-xp.

4. **Petrell AS.** Brilliant. [Online] [Cited: 17 November 2008.] www.brilliant-cfd.com.

5. **International Protective Coatings.** *Product datasheet Chartek 7.* [Online] [Cited: 20 April 2009.] www.international-pc.com/MPYAPCPCProductDatasheets/2045+P+eng+A4.pdf.

6. **Intumescents Associates Group.** Epoxy technology. [Online] [Cited: 16 November 2008.] http://www.intumescentassociatesgroup.com/epoxytech.htm.

7. **Morgan Thermal Ceramics.** *Firemaster 607 TM Blanket.* [Online] [Cited: 09 February 2009.] http://www.hbas.no/pdf/Firemaster%20607%20produkt%20informasjon.pdf.

8. **Nullifire.** Intumescent coating. [Online] [Cited: 16 November 2008.] www.nullifire.com/intumescent_coating/index.htm.

9. **Morgan Thermal Ceramics.** *Kaowool TM Board Product Information.* [Online] 31 October 2008. http://www.thermalceramics.com/pdfs-uploaded/datasheets/europe/5-7-22E.pdf.

10. **Knight Strip Metals.** Knufoil. [Online] [Cited: 10 November 2008.] www.knight-group.co.uk/stainless-steel/knufoil-user-manual.pdf.

11. **Solent Composite Systems.** ProTek Passive Fire & Blast Restraint System. [Online] [Cited: 20 February 2009.] www.solentcomposites.com/downloads/ProTek.pdf.

12. **Mills, A.F.** *Heat and mass transfer.* USA : The Richard Irwin series in heat transfer, 1995.

13. **Drysdale, Dougal.** *An introduction to Fire Dynamics.* Edinburgh, UK : John Wiley & Sons, 2002.

14. **Hagen, Bjarne Christian.** *Grunnleggende brannteknikk.* Haugesund : s.n., 2004.

15. **Morgan Thermal Ceramics.** Properties of Firemaster found on the product case. 2008.

16. **Markestad, Asbjørn and Maage, Magne.** *Bygningsmateriallære, volume two.* Trondheim : Tapir A/S, 1978.

17. **Electro Optical Industries.** An Emissivity Primer. [Online] [Cited: 14 December 2008.] http://www.electro-optical.com/bb_rad/emissivity/emisivty.htm.

18. **University of Manchester.** One stop Shop in Fire Engineering. [Online] [Cited: 28 01 2009.] http://www.mace.manchester.ac.uk/project/research/structures/strucfire/materiallnFire/Steel/HotRolledCarbonSteel/thermalProperties.htm.

19. **Buchanan, Andrew H.** *Structural Design for Fire Safety.* Chichester : John Wiley & Sons, Ltd., 2001. p. 176.

20. **Passive Fire Protection Federation.** PFPF Definition. [Online] [Cited: 15 November 2008.] http://pfpf.org/pfpf_definition.htm.

21. **D&F Group.** Passive Fire Protection. [Online] [Cited: 15 November 2008.] http://www.dfgroup.no/category.php?categoryID=64.

22. **Rockwool A/S.** Rockwool guiden. [Online] [Cited: 20 February 2009.] http://guiden.rockwool.no/produkter/passiv-brannsikring/conlit-300.

23. *Post-Flashover Fires in light and heavy Timber Construction Compartments.* **Hakkarainen, Tuula.** 2002, Journal of Fire Sciences.

24. *Mathematical description of combustion of intumescent polymer systems.* **Reshetnikov, I.S., Antonov, A.V. and Khalturinskii, N.A.** 6, Moscow : Springer New York, November 1997, Combustion, Explosion and Shock Waves, Vol. 33. ISSN 1573-8345.

25. **International Protective Coatings.** Epoxy Intumescent Fire Protection Materials - Are they all the same? [Online] 2005. [Cited: 16 November 2008.] http://www.chartek.com/productdata/marketing_notes/MN006_Epoxy%20Intumescent%20Fire%20Protection%20Materials_Rev1.pdf.

26. *Intumescent paints: fire protective coatings for metallic substrates.* **Duquesne, S., et al.** Bruat-la-Buissière : Elsevier B.V., 2003, Surface and coatings Technology, Vols. 180-181.

27. *Characterization of the performance of an intumescent fire protective coating.* **Jimenez, M., Duquesne, S. and Bourbigot, S.** Villeneuve d'Ascq : Elsevier, 2006, Science Direct.

28. **International Protective Coatings.** Chartek Fireproofing - Fire Exposure Case Studies. [Online] [Cited: 16 November 2008.] http://www.chartek.com/productdata/marketing_notes/MN008_Fire%20Exposure%20Case%20Studies.pdf.

29. **Promat.** *Fire curves.* [Online] [Cited: 16 November 2008.] www.promat-tunnel.com/en/hydrocarbon-hcm-hc-rabt-rws.aspx.

30. **Pride Chess AS.** *ProTek Fire Panels HMS Datablad.* Sandnes : Solent Composite Systems, 2005.

31. **Steen-Hansen, Anne Elise (Department manager at Sintef NBL AS).** *Conversation.* Trondheim, 2009.

32. **International Protective Coatings.** Safety Data Sheet Chartek 7. [Online] 19 December 2007. [Cited: 20 April 2009.] http://datasheets.international-coatings.com/msds/302120_GBR_ENG.pdf.

33. **D&F Group AS.** Material Data Sheet. [Online] Benarx, 27 August 2008. [Cited: 19 May 2009.] http://www.benarx.com/products/benarx-f-flexi-roll-xp/Benarx%20F%20epoxy%20roll.pdf.

34. *Towards A Methodology for the Characterization of Fire Resistive Materials with Respect to Thermal Performance Models.* **Bentz, Dale P., Prasad, Kuldeep R. and Yang, Jiann C.** Gaithersburg : National Institute of Standards and technology (NIST), 2004, Journal of Fire and Materials.

35. **ASTM International.** About ASTM International. [Online] [Cited: 14 December 2008.] www.astm.org/about/aboutASTM.html.

36. —. *ASTM C177 - 04.* [Online] [Cited: 25 February 2009.] www.astm.org/Standards/C177.htm.

37. —. *ATM C518 -04.* [Online] [Cited: 25 February 2009.] www.astm.org/Standards/C518.htm.

38. —. *ASTM E1461 - 07.* [Online] [Cited: 25 February 2009 .] www.astm.org/Standards/E1461.htm.

39. —. *ASTM C1113.* [Online] [Cited: 25 February 2009.] www.astm.org/Standards/C1113.htm.

40. *A slug calorimeter for evaluating the thermal performance of fire resistive materials.* **Bentz, D.P, et al.** U.S.A. : John Wiley & Sons, Ltd., 2005.

41. **SINTEF NBL AS.** ISO 5660-1:1993: The Cone Calorimeter Test. [Online] 28 April 2005. [Cited: 24 February 2009.] http://www.sintef.com/Home/Building-and-Infrastructure/SINTEF-NBL-as/Key-projects-and-topics/Fire-testing-of-railway-seats/ISO-5660-11993-THE-CONE-CALORIMETER-TEST/.

42. *Precision of Heat Release Rate Measurement Results.* **Lukošius, A. and Vekteris, V.** 3, Vilnius : s.n., 2003, MEASUREMENT SCIENCE REVIEW, Vol. 3.

43. *Uncertainty of Heat Release rate Calculation of the ISO 5660-1 Cone Calorimeter Standard Test Method.* **Enright, Patrick A. and Fleischmann, Charles M.** 2, s.l. : Fire Technology, 1999, Vol. 35.

44. *Measurement uncertainty analysis for calorimetry apparatuses.* **Zhao, Lei and Dembsey, Nicholas A.** 1-26, Worcester : Fire and Materials, 2008, Vol. 32.

45. *Uncertainty analysis of energy release rate measurement for room fires.* **Yeager, Raymond W.** 4, s.l. : Journal of fire Sciences, 1986, Vol. 4.

46. **UKL Technical Services.** *The Temperature Handbook.* West Sussex : Labfacility Ltd, 2004.

47. **Moffat, Dr. Robert J.** Electronics Cooling: Notes on using thermocouples. [Online] Stanford University, January 1997. [Cited: 26 February 2009.] www.electronics-cooling.com/articles/1997/jan/jan97_01.php 26.feb09.

48. **pico Technology.** Thermocouple Application Note. [Online] [Cited: 6 October 2008.] www.picotech.com/applications/thermocouple.html.

49. **Omega.** Thermocouples - An introduction. [Online] [Cited: 8 October 2008.] www.omega.com/thermocouples.html.

50. **FEAInformation.** *CFD.* [Online] [Cited: 28 October 2008.] www.computationalfluiddynamics.com.

51. **Fluent Inc.** *What is CFD.* [Online] [Cited: 28 October 2008.] www.fluent.com/solutions/whatcfd.htm.

52. **Berge, Geir and Brandt, Øyvin.** *Analyse av brannlast.* Trondheim : Norges branntekniske laboratorium as, 2003. NBL A04108.

53. **Ceetron AS.** *GL View Inova.* [Online] [Cited: 28 October 2008.] http://www.ceetron.com/en/glview_inova1.aspx.

54. **Steen-Hansen, Anne.** *Branntekniske krav.* Trondheim : SINTEF NBL as, 2009.

55. **Rossebø, Bjørn Egil.** Excel file: Power calibration. Trondheim : s.n., January 2008.

56. **Solartron Mobrey Limited.** IMP 3595 & 5000 Series. [Online] February 2001. [Cited: 12 November 2008.] www.ivesequipment.com/customer/iveqco/principals/solartron/datasheets/ip9001.pdf .

57. **Araki, M.** *PID Control.* Kyoto University. Kyoto : Encyclopedia of Life Support Systems (EOLSS).

58. **Rossebø, Bjørn Egil.** Excel-file: ISO 5660 Cone calorimeter test of ProTek (35 kW/m2). Trondheim : s.n., 18 February 2008.

59. **Brungot, Andreas.** *Conversation about the accuracy of the volt signal from the control panel.* Trondheim, 21 November 2008.

60. **Norsk Porebetong A/S v/Vegard Karlsen.** *Thermal properties Siporex.* January 2009.

Appendix A – Overview of experiments and numerical simulations

A.1 Overview of physical experiments

This table gives an overview of all the experiments done throughout this project. Each experiment has an own reference code. A comment has been made for the specific experiment when changes were made and if something unexpected occurred.

Reference	Test specimen	Temperature	Comments
290908	Empty box	10 % output	Testing the functionality of the thermocouples. Installed new radiation foils. Changed isolation on the edges in the furnace. One of thermocouples didn't function. Made a new connection.
011008	Empty box	10 % output	Thyrsitor broke. One of the foils burnt off.
131008	Carbon steel plate 5 mm	10 % output	Changed one foil. Incorrect data from foil left side and steel exposed side.
141008	Carbon steel plate 5 mm	10 % output	Collecting data for power calibration. Testing the power logging system
151008	Carbon steel plate 5 mm	0-70 % output	Collecting data for power calibration
171008_01	Carbon steel plate 5 mm	1-50 % output	Collecting data for power calibration
171008_02	Carbon steel plate 5 mm	40 % output	Checking the logging system
171008_03	Carbon steel plate 5 mm	40 % output	Checking the measuring transformer
171008_04	Carbon steel plate 5 mm	600 °C	The IMP 5000 registered signals every 5 seconds.
271008_01	Carbon steel plate 5 mm	600 °C	The IMP 5000 registered signals every second.
271008_02	Carbon steel plate 5 mm	800 °C	One of the thermocouples that measured the foil temperature jumped off during the experiment. The thermocouple that was intact during the experiment will be used for comparison of the simulated temperatures.
271008_03	Carbon steel plate 5 mm	1000 °C	
051108_01	Carbon steel plate 5 mm	600 °C	Calculation of an average heat loss to the copper plates.
051108_02	Carbon steel plate 5 mm	800 °C	Foil breakage.
051108_03	Carbon steel plate	800 °C	One new foil. Very unstable foil

	5 mm		temperatures. Rejected results.
051108_04	Carbon steel plate 5 mm	800 °C	The foil temperature that is connected to the control panel was changed from left hand side to the foil on the right hand side, seen from the back of the oven.
101108_01	Carbon steel plate 5 mm	800 °C	No volt signal received from one of the thermocouples. Rejected results.
101108_02	Carbon steel plate 5 mm	1000 °C	Foil breakage after 5 min
101108_03	Carbon steel plate 5 mm	600 °C	All the foils were new. Tested different ways for measuring the foil temperatures. Foil breakage.
111108_00	Carbon steel plate 5 mm	600 °C	One new foil. Foil breakage
111108_01	Carbon steel plate 5 mm	600 °C	All the foils were new. New way to measure the foil temperatures
111108_02	Carbon steel plate 5 mm	800 °C	Some disruption recorded from one of the foil temperatures
111108_03	Carbon steel plate 5 mm	600 °C	Testing different ways of measuring the foil temperatures.
111108_04	Carbon steel plate 5 mm	600 °C	Computer crash. All data lost.
111108_05	Carbon steel plate 5 mm	1000 °C	Incorrect volt signals received from one of the thermocouples connected to the foils. Test terminated.
141108_01	Carbon steel plate 5 mm	600 °C	
141108_02	Carbon steel plate 5 mm	800 °C	
141108_03	Carbon steel plate 5 mm	1000 °C	Foil breakage
141108_04	Carbon steel plate 5 mm	1000 °C	All the foils were new. Quite large differences in the foil temperatures.
141108_05	Carbon steel plate 5 mm	1000 °C	Incorrect volt signals on the steel plates exposed side. The values gained from the unexposed side of the steel plate may be used for comparison of the simulations. Foil breakage in the end of the experiment.
181108_00	Carbon steel plate 5 mm	600-1000 °C	All the foils were new. Testing the foil temperatures by holding an enclosed thermocouple onto the foils by hand.
181108_01	Carbon steel plate 5 mm	600 °C	New way of measuring the foil temperatures
191108_01	Carbon steel plate 5 mm	600 °C	

191108_02	Carbon steel plate 5 mm	800 °C	Significant temperature difference between the steel plates' exposed and unexposed side registered. The isolation around the conductors burnt off, which lead to measuring a temperature outside the steel plate. Rejected results.
191108_03	Carbon steel plate 5 mm	800 °C	
191108_04	Carbon steel plate 5 mm	1000 °C	Significant temperature difference between the steel plates' exposed and unexposed side registered. Rejected results.
191108_05	Carbon steel plate 5 mm	1000 °C	Significant temperature difference between the steel plates' exposed and unexposed side registered.
191108_06	Kaowool_1400 2.5 mm	600 °C	Ran experiment for about 30 min. Very low power curve. Rejected results.
211108_01	Carbon steel plate 5 mm	600 °C	A new hole in one of the copper plates for a thermocouple to be placed in was made. Results rejected, because the distance between TC (thermocouple) 1 and TC2 were too long.
211108_02	Carbon steel plate 5 mm	800 °C	A third hole in the copper plate was made. Heat loss through the copper may now be calculated. Distance between TC1 and TC2 was 2.5 cm. Logging only the volt signals from the copper plates.
211108_03	Carbon steel plate 5 mm	1000°C	The volt signal from the unexposed side of the steel plate was not registered. Foil breakage in the end of the experiment, but the registered data may be used.
261108_01	Carbon steel plate 5 mm	600 °C	All the foils were new. The isolation in the bottom close to the steel plate was removed, because it partly covered the air gap. Gained very low power curves and low steel temperatures.
261108_02	Carbon steel plate 5 mm	600 °C	Low power curves and low steel temperatures.
261108_03	Carbon steel plate 5 mm	600 °C	The isolation in the bottom close to the steel plate was put back in (see 261108_01) to see if the steel temperatures would rise. No positive effect.
261108_04	Carbon steel plate 5 mm	800 °C	Quite low power curve and also quite low values on the steel plate.
021208_01	Carbon steel plate 5 mm	800 °C	Ran through this experiment to see if the resulting power curve gained in the

			previous experiment would still be the case. The power curve became a bit higher. The temperatures on the steel plate became low. At the first the temperatures on the steel plates exposed and unexposed side were very similar to each other, and then the temperature on the unexposed side became higher than the one on the exposed side.
021208_02	Carbon steel plate 5 mm	800 °C	The thermocouples on the steel plate were logged directly into the IMP5000 to see if there was any difference compared to logging this temperature through the electric isolation. The results became similar. The thermocouples were again connected through the electric isolation.
041208_01	Carbon steel plate 5 mm	600 °C	Installed three new independent foil bits on the back of the radiation panel. The temperatures on these were directly logged in the IMP5000. One of the thermocouples on the copper plate had bad contact.
041208_02	Carbon steel plate 5 mm	800 °C	Two of the thermocouples on the copper plate jumped off during the experiment. The unexposed side of the steel plate shows a larger temperature value than the exposed side.
051208_01	Carbon steel plate 5 mm	500 °C	The foil bit on the back of the radiation panel is controlled by the control panel. Logging of the data started 5 minutes in the experiment. Changed the thermocouple on the exposed side of the steel plate. The unexposed side still showed a higher temperature than the exposed side.
051208_02	Carbon steel plate 5 mm	500 °C	The independent foil bit is controlled by the control panel. The unexposed side of the steel plate shows higher temperatures than exposed side.
051208_03	Carbon steel plate 5 mm	500 °C	The unexposed side of the steel plate shows higher temperatures than exposed side.
051208_04	Carbon steel plate 5 mm	500 °C	The furnace was not cooled down. Testing the steel plate temperatures by using a second steel plate with other

			thermocouples. This resulted in 'normal' temperatures on the steel plate. One of the thermocouples on the copper plate jumped off.
081208_01	Carbon steel plate 5 mm	750 °C	Both thermocouples on the steel plate were changed. The exposed side showed higher values than unexposed.
081208_02	Carbon steel plate 5 mm	750 °C	Verification of 081208_02a
081208_03	Carbon steel plate 5 mm	750 °C	Verification of 081208_02a and 081208_02b
081208_04	Carbon steel plate 5 mm	950 °C	Foil breakage.
111208_01	Carbon steel plate 5 mm	900 °C	All foils were new. Used 7 minutes to reach desired temperature on the independent foil bit.
111208_02	Carbon steel plate 5 mm	900 °C	Verification of 111208_01. The thermocouple that represents T1 on the copper had bad contact. It shows about 30 °C less than expected.
111208_03	Carbon steel plate 5 mm	900 °C	Verification of 111208_01 and 111208_02. The thermocouple that represents T1 on the copper had contact. It shows about 30 °C lower than expected.
230109	Kaowool_1400 9 mm	900 °C	New steel plate. Ran the experiment for 50 min
270109_01	Firemaster607_128 12 mm	900 °C	Thermocouple on steel exposed side loosened during the experiment. Experiment completed, but results rejected.
270109_02	Firemaster607_128 10 mm	900 °C	Ran the experiment for about 45 min
170209	ProTek B4 9mm	900 °C	The experiment had to be terminated after 3 min 47 sec because the isolation started to burn. The experiment was performed inside a tent and large flame tongues kept sticking out of the furnace towards the tent canvas. The isolation produced a lot of black smoke.
050309	ProTek B3 9.1 mm	900 °C	The oven was rebuilt before this experiment was carried out. New foils were installed. Thermocouple T1 inside on the copper was replaced. The experiment lasted for 65 min. The material swelled 0.6 mm.
060309_01	ProTek A3 9.1 mm	900 °C	The experiment lasted for 68 min.

			ProTek swelled 13 mm.
060309_02	ProTek A4 6 mm	900 °C	Experiment lasted for 64 min. ProTek swelled 10.7 mm
160309	Carbon steel plate 5 mm	900 °C	Testing whether using a sooted isolation on the edges compared to a new isolation would make a difference on the input power. Foil breakage after 2 minutes. Rejected results.
170409_01	ProTek A1 9.4 mm	900 °C	New radiation foils were installed. The experiment lasted for 10 min. The temperature on the foils exceeded the limiting temperature of 1050 °C and the power was automatically turned off.
170409_02	ProTek A1 9.4 mm	900 °C	The experiment lasted for 62 min. The material swelled 7.7 mm. The specimen had already been heated one time (170409_01). The specimen was cooled down to 75 °C before this test was performed.
180509_01	Benarx F Flexi Roll XP 2.5 mm	900 °C	The foils burnt off after 8 minutes. Experiment terminated.
180509_02	Benarx F Flexi Roll XP 2.5 mm	900 °C	All the foils were new. Two of the foils burnt off after 65 minutes. The results may be used.
190509	Benarx F Flexi Roll XP 2.5 mm	900 °C	All the foils were new. One of the foils burnt off after 7 minutes. Experiment terminated.
290509	Benarx F Flexi Roll XP 2.5 mm	800 °C	The foil that burnt off in the previous experiment was replaced. One of the foils burnt off after 12 minutes. Experiment terminated.

A.2 Overview of numerical simulations

All the numerical simulations have been performed with a specific setup. Throughout the project errors and inaccuracies in the simulations has lead to changes and additions in the input data. These changes are explained in the comments column.

Reference	Test specimen	Temperature	Comments
171008_01	Carbon steel plate 5 mm	600 °C	All initial temperatures were set to 20 °C. (19 and 20 °C from earlier simulations (2)).
271008_01	Carbon steel plate 5 mm	600 °C	Time step 0.05
271008_01b	Carbon steel plate 5 mm	600 °C	Sat the wall thickness to be 12.5 cm and not 2.5 cm as was already defined from earlier simulations. This is the case for the rest of the simulations as well until something else has been specified.
271008_02	Carbon steel plate 5 mm	800 °C	2.5 cm wall thickness. Time step 0.05.
271008_02b	Carbon steel plate 5 mm	800 °C	
271008_02c	Carbon steel plate 5 mm	800 °C	Changed the emissivity on the edges to be 0.7 instead of 0.3. This is only the case for this specific simulation.
271008_03	Carbon steel plate 5 mm	1000 °C	2.5 cm wall thickness.
271008_03b	Carbon steel plate 5 mm	1000 °C	
271008_03c	Carbon steel plate 5 mm	1000 °C	Changed the emissivity on the steel plate from 0.6 to 0.7.
051108_01	Carbon steel plate 5 mm	600 °C	
051108_01b	Carbon steel plate 5 mm	600 °C	Used the input power, less the average heat loss for power input to the simulation.
051108_04	Carbon steel plate 5 mm	800 °C	
051108_04b	Carbon steel plate 5 mm	800 °C	Used the input power, less the average heat loss for power input to the simulation. Added a new parameter called T_{air} that will represent the surrounding initial temperature.
111108_01	Carbon steel plate 5 mm	600 °C	
111108_02	Carbon steel plate 5 mm	800 °C	
141108_01	Carbon steel plate	600 °C	

	5 mm		
141108_02	Carbon steel plate 5 mm	800 °C	
141108_04	Carbon steel plate 5 mm	1000 °C	
141108_05	Carbon steel plate 5 mm	1000 °C	
181108_01	Carbon steel plate 5 mm	600 °C	
191108_01	Carbon steel plate 5 mm	600 °C	
191108_03	Carbon steel plate 5 mm	800 °C	
191108_05	Carbon steel plate 5 mm	1000 °C	
191108_05b	Carbon steel plate 5 mm	1000 °C	Included heat loss through the copper. The 'old' measuring points were used.
211108_01	Carbon steel plate 5 mm	600 °C	
211108_02	Carbon steel plate 5 mm	800 °C	
211108_03	Carbon steel plate 5 mm	1000 °C	Heat loss through conduction included in the simulations from this point and onwards. Ordinary parameters.
211108_03b	Carbon steel plate 5 mm	1000 °C	Sat the radiation as 'true'. This count for the rest of the simulations as well where nothing else has been specified.
211108_03c	Carbon steel plate 5 mm	1000 °C	Changed the emissivity on the steel plate from 0.6 to 0.7
211108_03d	Carbon steel plate 5 mm	1000 °C	Changed the air-gap from 1 cm to 0.5 cm. More heat loss to the copper plates included (energy for heating 2.5 cm on the long part of the copper plate). This heat loss counts for the rest of the simulations as well where nothing else has been specified.
211108_03e	Carbon steel plate 5 mm	1000 °C	The emissivity on the edges is changed from 0.3 to 0.5. The material on the edges is changed from Foamglas to Kaowool 1400. Air-gap set to 0.5 cm.
211108_03f	Carbon steel plate 5 mm	1000 °C	Changed the emissivity on the foils from 0.7 to 0.8.
211108_03g	Carbon steel plate 5 mm	1000 °C	Doubled the number of control volumes on the foils. Added more radiation spots. Changed Azimuth from 8 to 12 and Polar from 6 to 12.
261108_01	Carbon steel plate	600 °C	Same parameters as in 211108_03g

	5 mm		
261108_02	Carbon steel plate 5 mm	1000 °C	Same parameters as in 211108_03g
051208_02	Carbon steel plate 5 mm	500 °C	
051208_02b	Carbon steel plate 5 mm	500 °C	Emissivity on the steel plate changed from 0.6 to 0.7. Radiation frequency changed from 1 to 5.
051208_02c	Carbon steel plate 5 mm	500 °C	ε_s (emissivity steel plate) = 0.7 ε_e(emissivity edges) = 1 Lx (wall thickness) = 0.075
051208_02d	Carbon steel plate 5 mm	500 °C	ε_s=0.7 ε_e=1 Lx=0.125
051208_02e	Carbon steel plate 5 mm	500 °C	ε_s=0.7 ε_e=1 Lx=0.125 Control volumes on the edges changed from 10x10x1, 10x1x10, 1x10x10 to 10x10x6, 10x6x10, 6x10x10. Inserted new specifications on the material on the edges, called AB_M.
051208_02f	Carbon steel plate 5 mm	500 °C	Radiation frequency changed back from 5 to 1. Control volumes air gap changed from 1x40x40 to 1x20x20. Flow inside the furnace is changed from $FlowInnvendig.brl to $RomFlow.brl Control volumes inside the furnace changed from 10x10x10 to 5x10x10. Materials on the edges are the same as in the experiment; Kaowool and Siporex. Control volumes on edges: 4x4x4, 4x4x4, 4x4x4
081208_03	Carbon steel plate 5 mm	750 °C	
081208_03b	Carbon steel plate 5 mm	750 °C	Emissivity on the steel plate sat to be 0.7 instead of 0.6. Radiation frequency changed from 1 to 5.
081208_03c	Carbon steel plate 5 mm	750 °C	ε_s=0.7 ε_e=1 Lx=0.125
081208_03d	Carbon steel plate 5 mm	750 °C	ε_s=0.7 ε_e=1 Lx=0.025

			Control volumes on the air gap changed back to 1x40x40.
081208_03e	Carbon steel plate 5 mm	750 °C	ε_s=0.7 ε_e=1 Lx=0.125 Control volumes on the edges: 10x10x4, 10x4x10, 4x10x10. Density 0.5. Inserted new specifications on the material on the edges, called AB_M.
081208_03f	Carbon steel plate 5 mm	750 °C	ε_s=0.7 ε_e=1 Lx=0.125 Changed geometry on the edges. Divided them into two with two different materials, Kaowool as insulation and Siporex as the light-weight concrete. Control volumes on edges: 10x10x4, 10x4x10, 4x10x10. Simulation crashed after 30 sec.
081208_03g	Carbon steel plate 5 mm	750 °C	Radiation frequency changed back from 5 to 1. Control volumes air gap changed from 1 40 40 to 1 20 20. Flow inside the furnace is changed from $FlowInnvendig.brl to $RomFlow.brl Control volumes inside the furnace changed from 10x10x10 to 5x10x10. Materials on the edges are the same as in the experiment; Kaowool and Siporex. Control volumes on edges: 4 4 4, 4 4 4, 4 4 4.
111208_01	Carbon steel plate 5 mm	900 °C	
111208_01b	Carbon steel plate 5 mm	900 °C	ε_s=0.7 R. f. = 5
111208_01c	Carbon steel plate 5 mm	900 °C	Calculated a new power curve based on the temperature measured on one of the foil bits. Used these values in the simulation. ε_s=0.7 R. f. = 5 This resulted in very low temperatures. This power curve will not be used in future simulations.
111208_01d	Carbon steel plate	900 °C	ε_s=0.7

	5 mm		ε_e=1 Lx=0.075
111208_01e	Carbon steel plate 5 mm	900 °C	ε_s=0.7 ε_e=1 Lx=0.125
111208_01f	Carbon steel plate 5 mm	900 °C	ε_s=0.7 ε_e=1 Lx=0.125 Control volumes on the air gap changed back to 1x40x40. Inserted new specifications on the material on the edges, called AB_M.
111208_01g	Carbon steel plate 5 mm	900 °C	ε_s=0.7 ε_e=1 Lx=0.125 Density 0.5 Radiation frequency changed back from 5 to 1. Control volumes air gap changed from 1x40x40 to 1x20x20. Flow inside the furnace is changed from $FlowInnvendig.brl to $RomFlow.brl Control volumes inside the furnace changed from 10x10x10 to 5x10x10. Materials on the edges are the same as in the experiment; Kaowool and Siporex. Control volumes on edges: 4 4 4, 4 4 4, 4 4 4.
230109	Kaowool_1400 9 mm	900 °C	
270109_02	Firemaster607_128 10 mm	900 °C	
270109_02b	Firemaster607_128 10 mm	900 °C	Inserted a modified power curve
050309	ProTek 9.1 mm	900 °C	Power curve from this experiment. k-values PT1
050309b	ProTek 9.1 mm	900 °C	Estimated a heat release from ProTek and added this amount of power to the current power curve. The estimation was based on the power curve found in experiment 111208_01. k-values PT1
050309c	ProTek 9.1 mm	900 °C	Added heat release from the isolation material. These data were found from a cone calorimeter test done earlier by Sintef NBL. This heat release was added to the delivered power. k-values PT1

050309d	ProTek 9.1 mm	900 °C	Same power as in 050309c. k-values PT2
050309e	ProTek 9.1 mm	900 °C	Same power as in 050309c. k-values PT3
050309f	ProTek 9.1 mm	900 °C	Added the same heat release as in 050309c, but with a reduction in the area of where the heat release occurred in the beginning of the experiment. This would reduce the amount of heat released in the first minutes of the simulation. k-values PT2
050309g	ProTek 9.1 mm	900 °C	The same power as in 050309f. k-values PT3
050309h	ProTek 9.1 mm	900 °C	Used the power curve from experiment 270109_02, which is an experiment using Firemaster isolation. The k-values used in this simulation is the same as for Firemaster.
050309g	ProTek 9.1 mm	900 °C	Same power as 050309f (Firemaster). k-values PT4
050309h	ProTek 9.1 mm	900 °C	Same power as 050309f (Firemaster). k-values PT5
060309_01	ProTek A3 9.1 mm	900 °C	Power taken from experiment 270109_02 (Firemaster). k-values PT6
060309_01b	ProTek A3 9.1 mm	900 °C	Power taken from experiment 270109_02 (Firemaster). k-values PT7
060309_01c	ProTek A3 9.1 mm	900 °C	Power taken from experiment 270109_02 (Firemaster). k-values PT8
060309_01d	ProTek A3 9.1 mm	900 °C	Power taken from experiment 270109_02 (Firemaster). k-values PT9
060309_01e	ProTek A3 9.1 mm	900 °C	Power taken from experiment 270109_02 (Firemaster). k-values PT10
060309_01f	ProTek A3 9.1 mm	900 °C	Power taken from experiment 270109_02 (Firemaster). k-values PT11
060309_01g	ProTek A3 9.1 mm	900 °C	Power taken from experiment 270109_02 (Firemaster). k-values PT12
060309_01h	ProTek A3 9.1 mm	900 °C	Power taken from experiment 270109_02 (Firemaster). k-values PT13
060309_01i	ProTek A3 9.1 mm	900 °C	Power taken from experiment 270109_02 (Firemaster). k-values PT14
060309_02	ProTek A4 6 mm	900 °C	Power taken from experiment 270109_02 (Firemaster). k-values PT15
060309_02b	ProTek A4 6 mm	900 °C	Power taken from experiment 270109_02 (Firemaster). k-values PT16
170409_02	ProTek A1 9.4 mm	900 °C	Power taken from experiment 270109_02 (Firemaster). k-values PT12

Appendix B – Temperature and power graphs from experiments

B.1 Adjusting the furnace

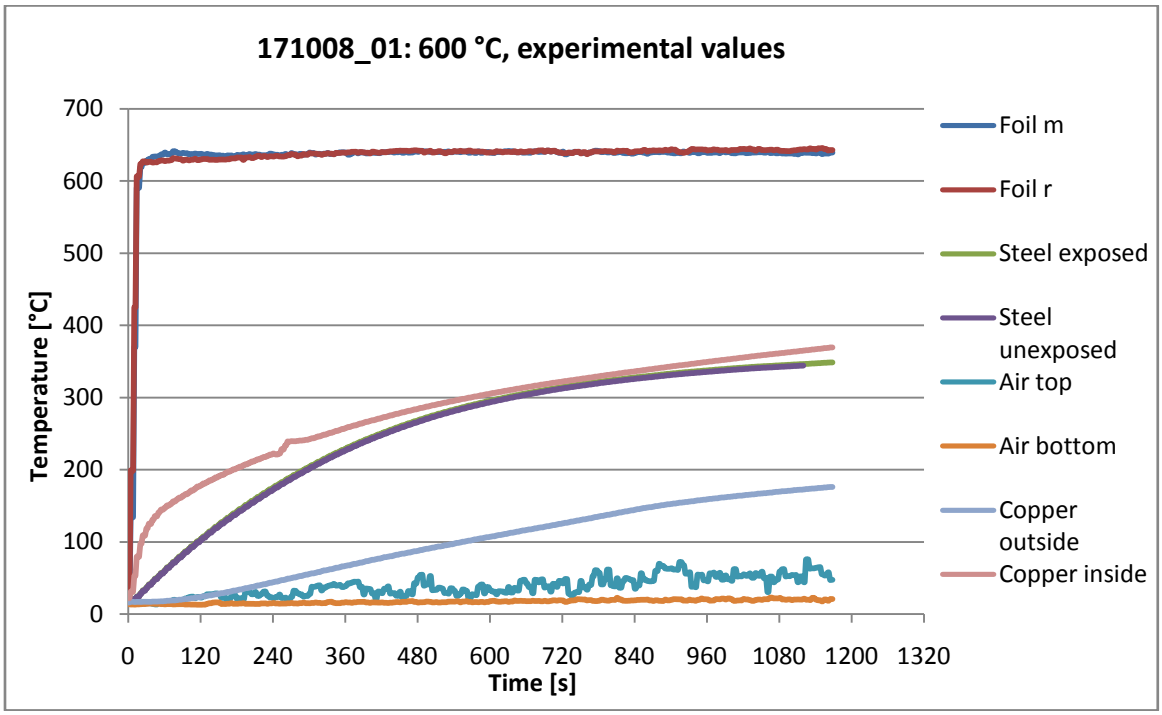

Figure 39 shows temperatures from 171008_01

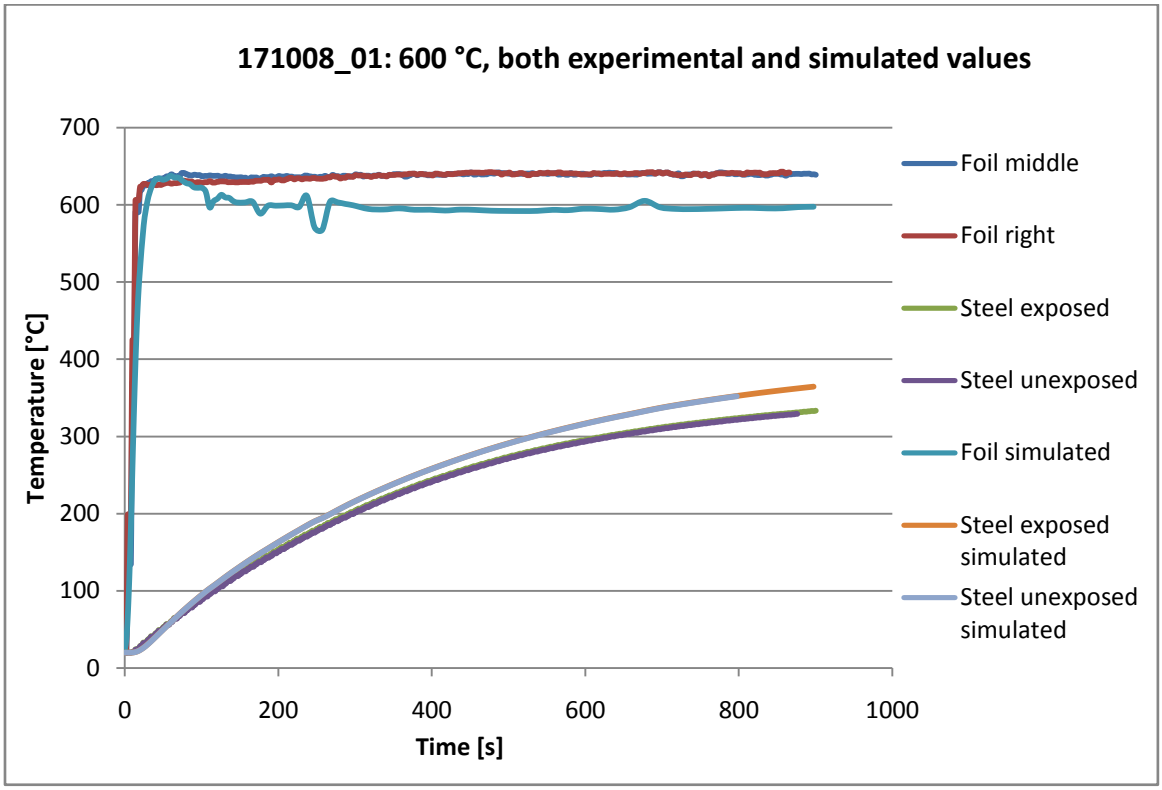

Figure 40 shows both experimental and simulated values from 171008_01

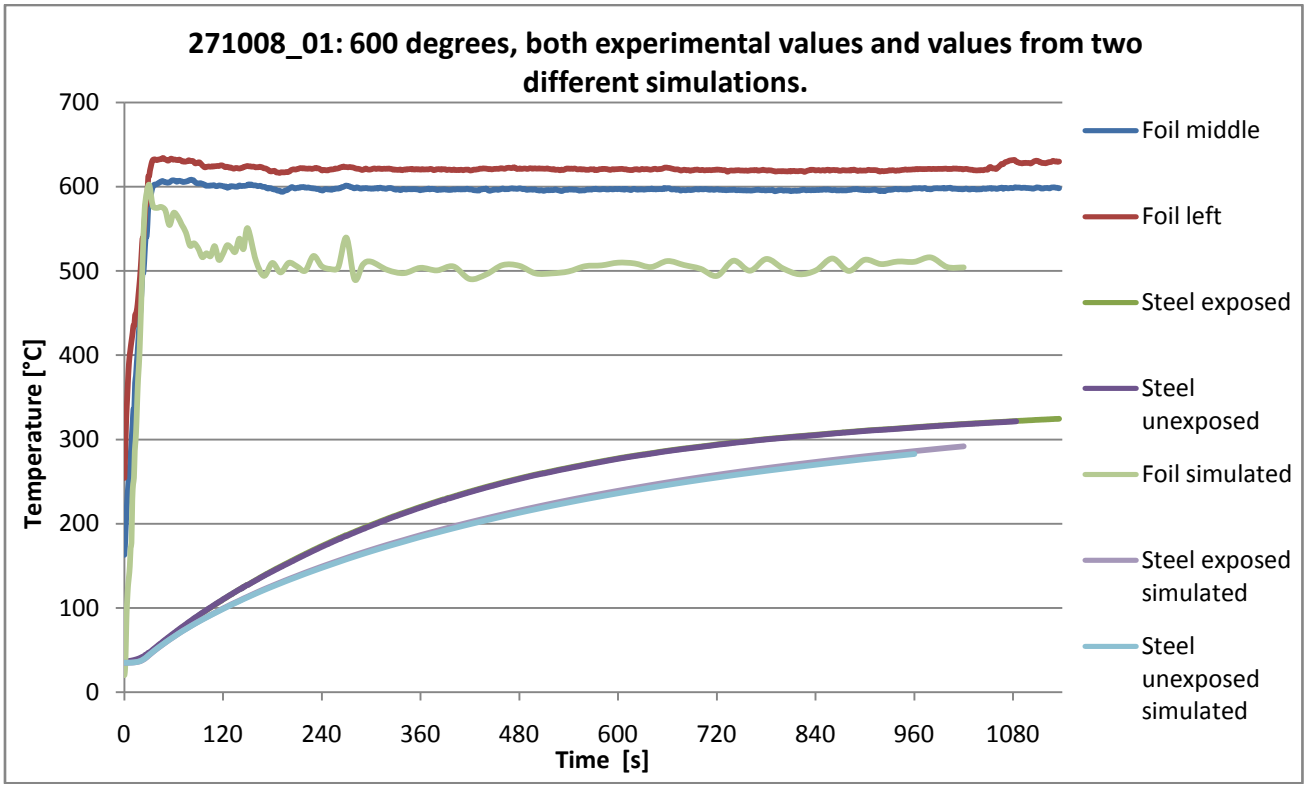

Figure 41 shows both experimental and simulated values from 271008_01

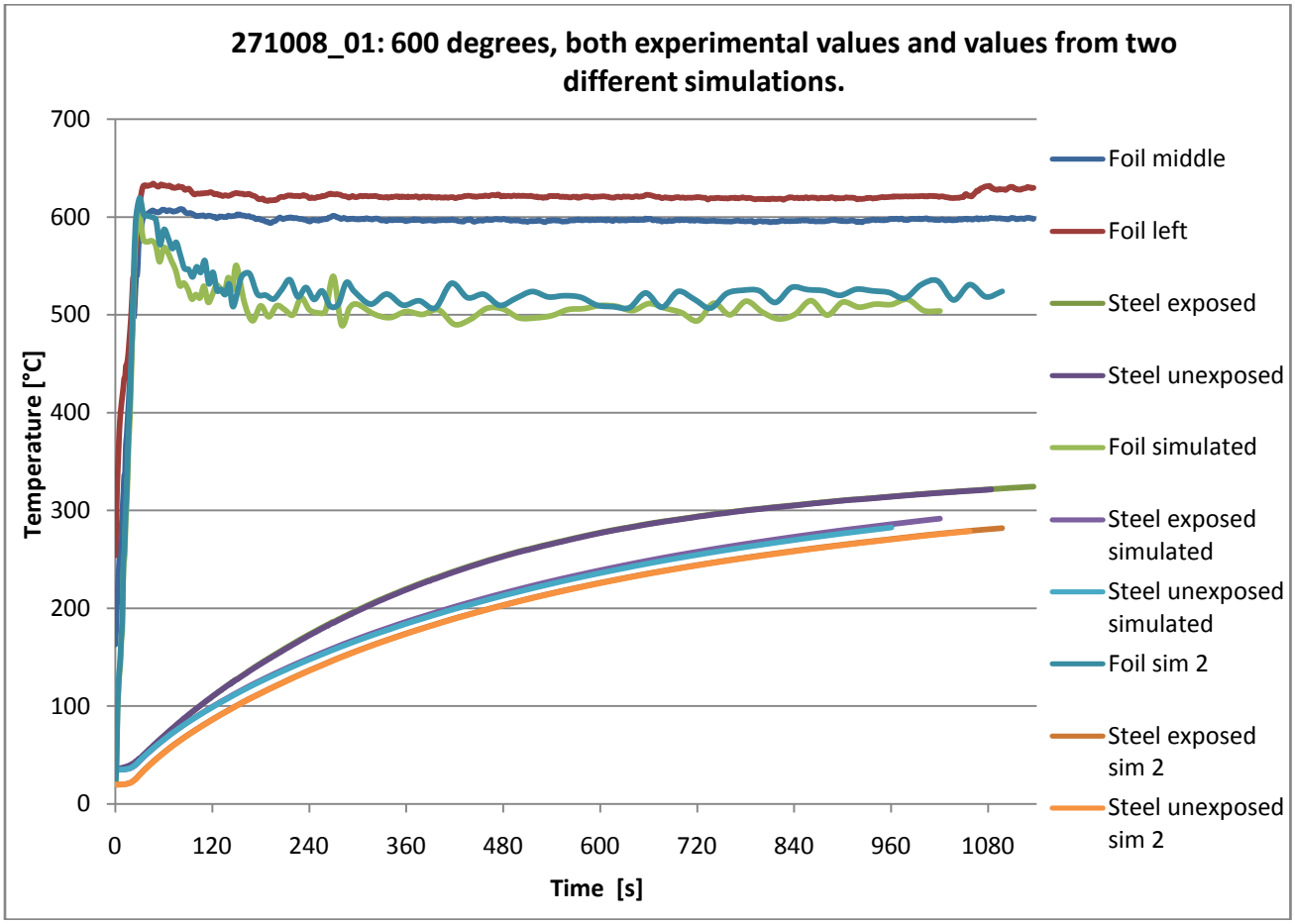

Figure 42 shows a comparison of temperatures from two different simulations from 271008_01

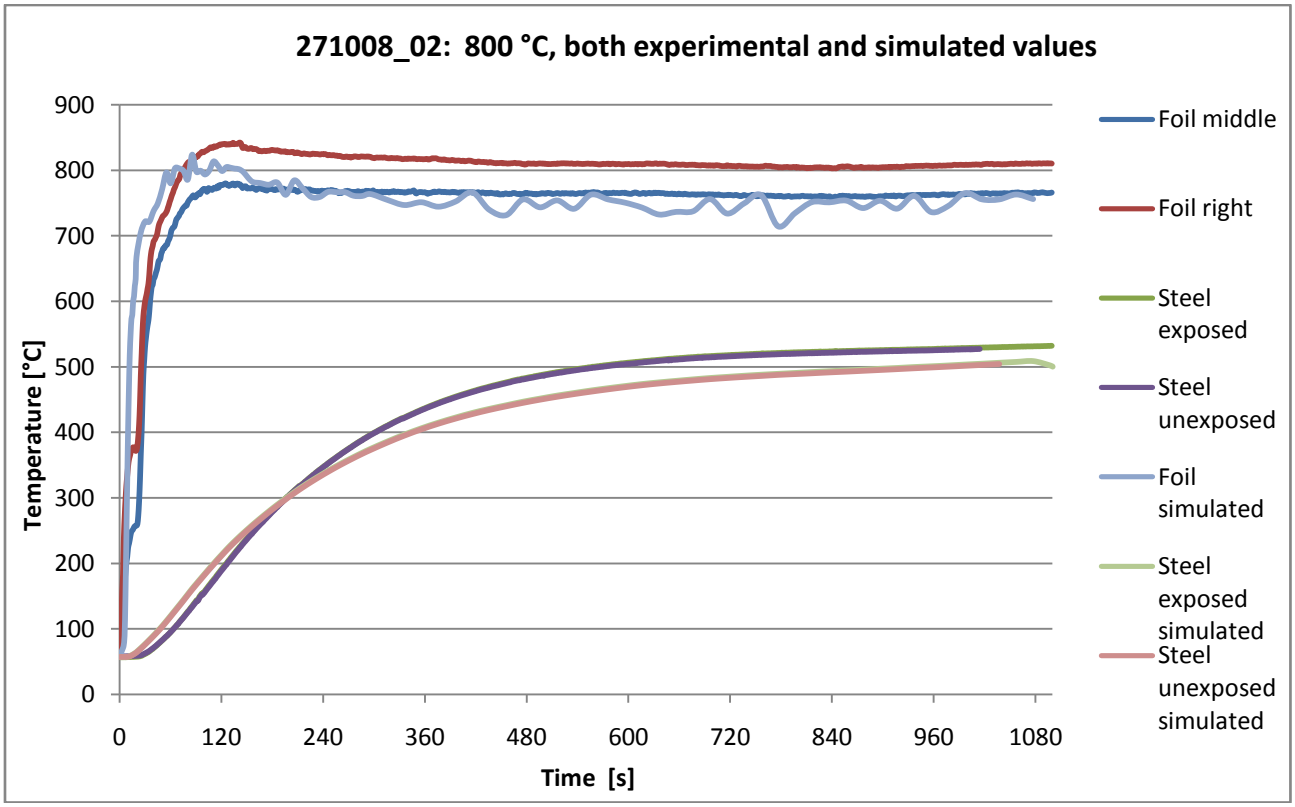

Figure 43 shows both experimental and simulated values from 271008_02.

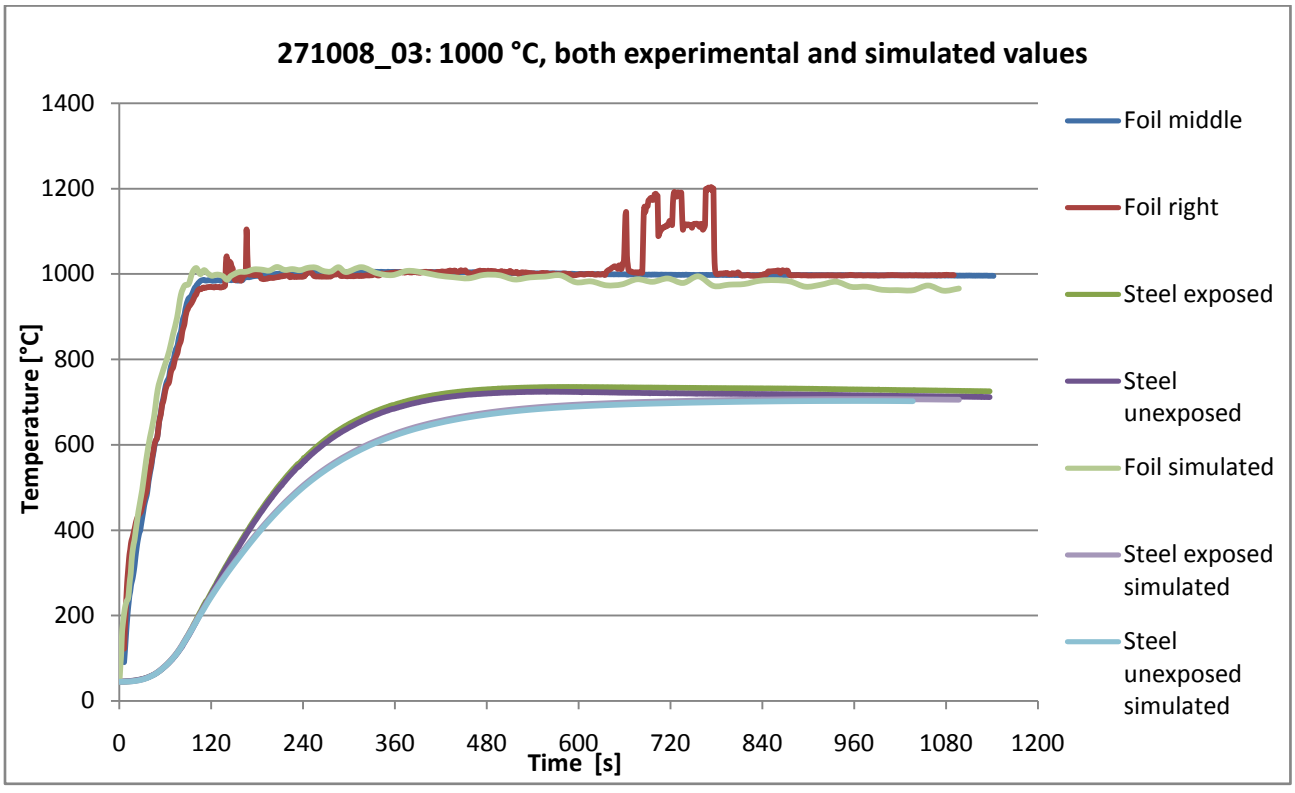

Figure 44 shows both experimental and simulated temperatures from 271008_03

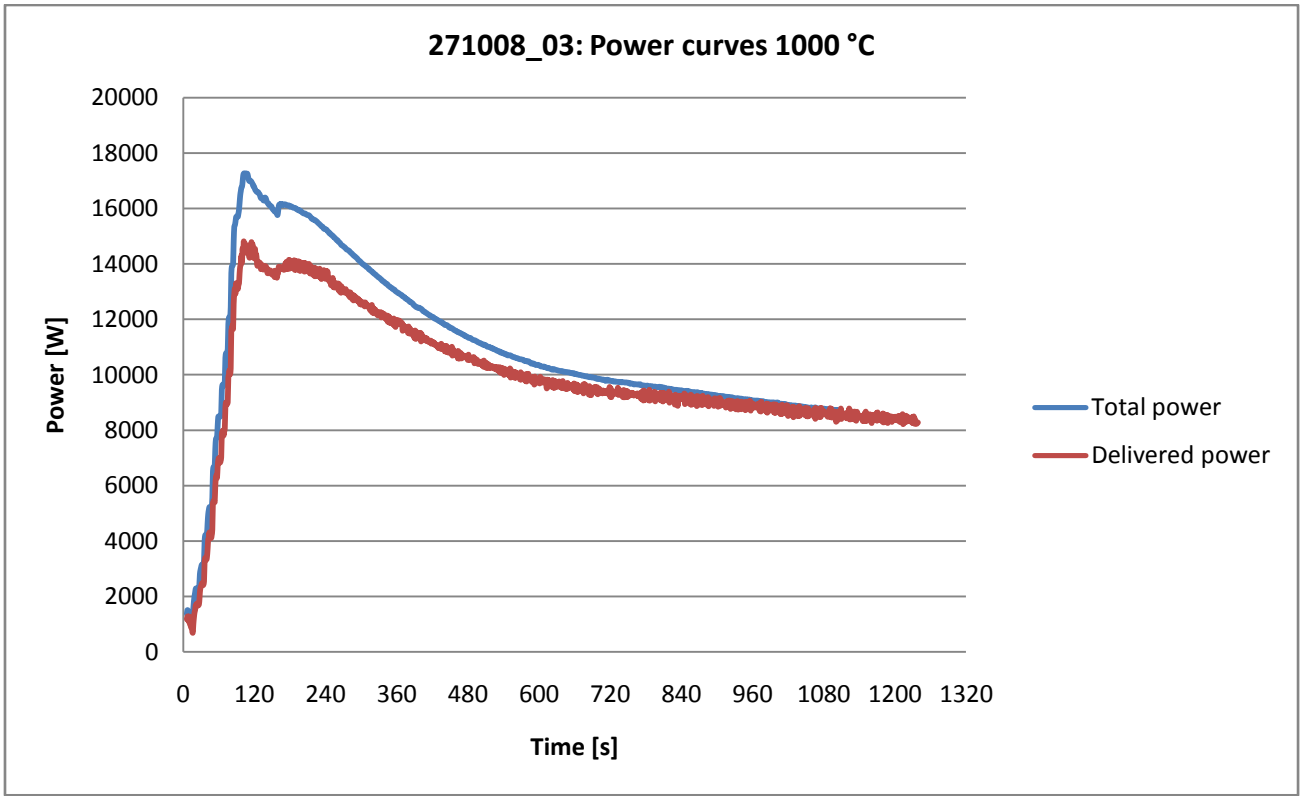

Figure 45 shows both the power and the delivered power curve from 271008_03

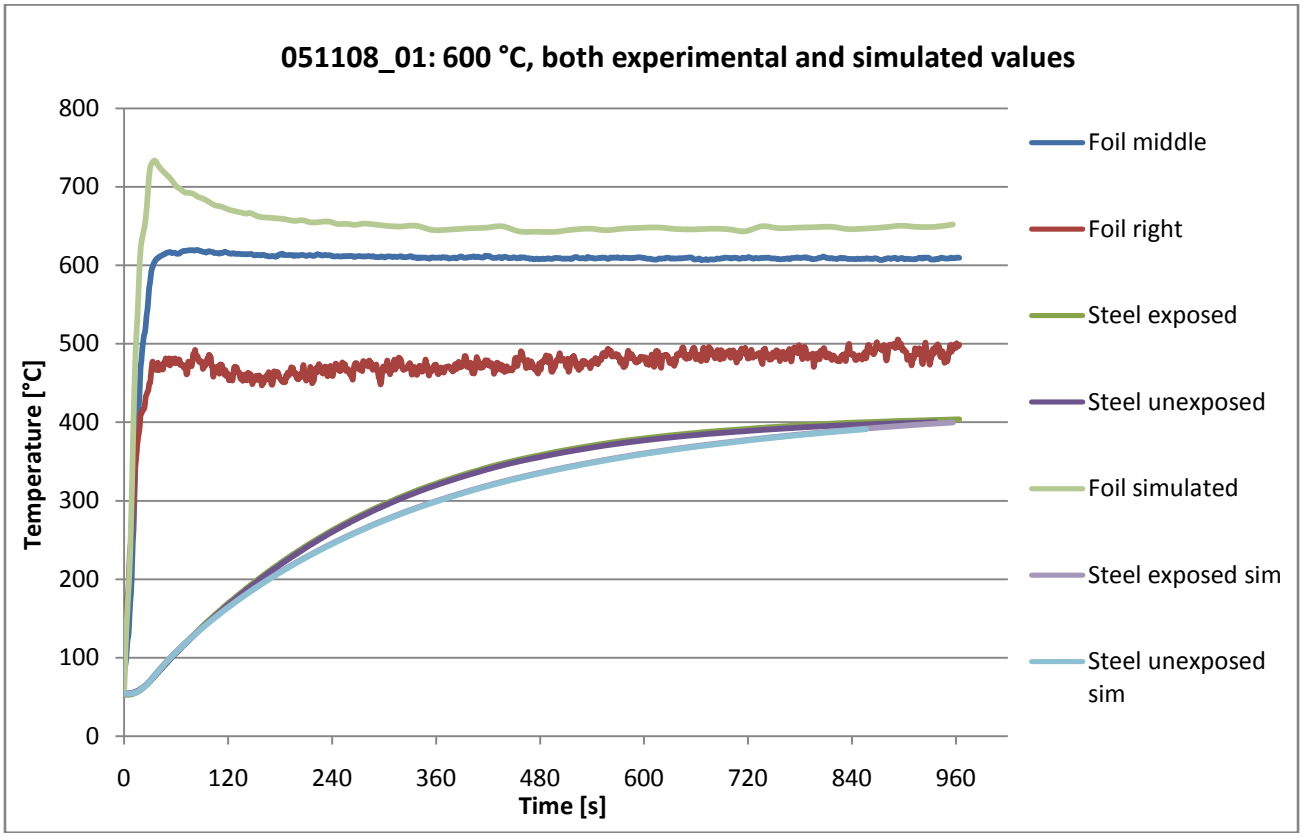

Figure 46 shows both experimental and simulated values from 051108_01

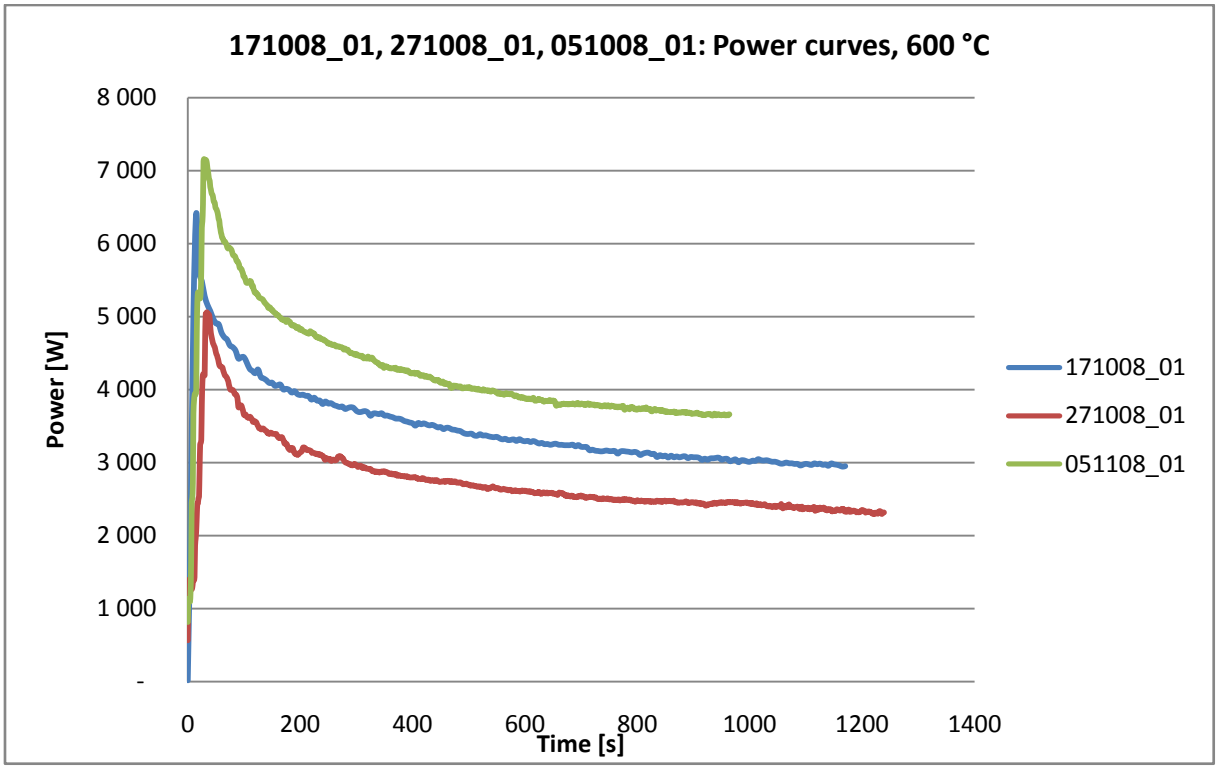

Figure 47 shows the powers from the experiments 171008_01, 271008_01 and 051108_01.

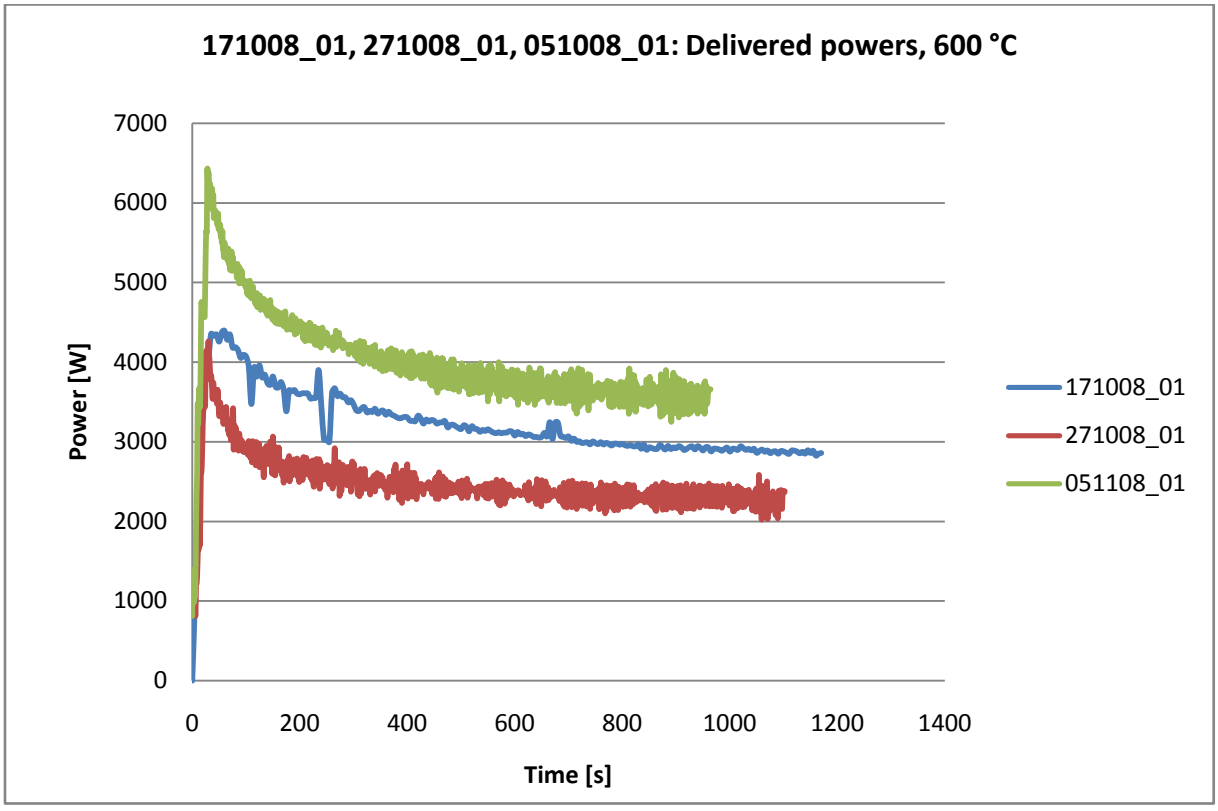

Figure 48 shows the delivered powers from experiment 171008_01, 271008_01 and 051108_01

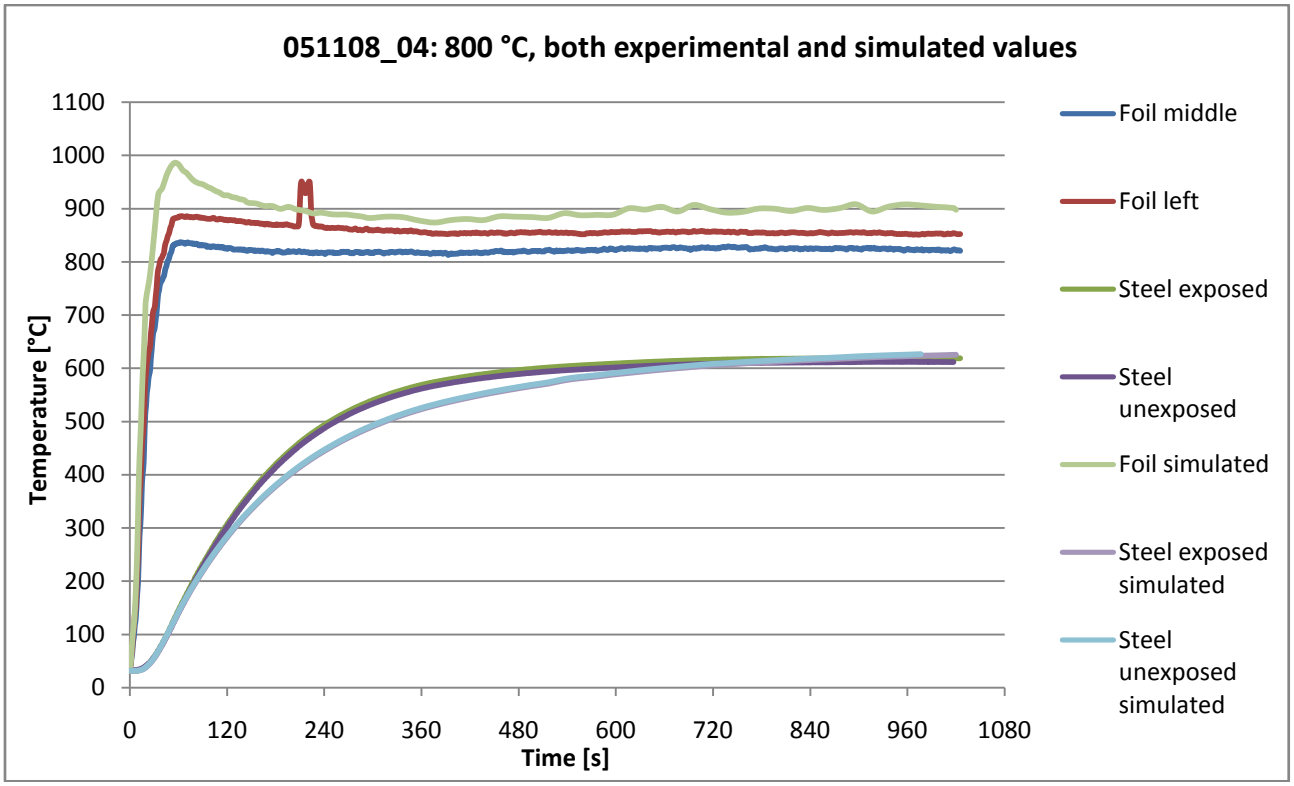

Figure 49 shows both experimental and simulated values from 051108_04.

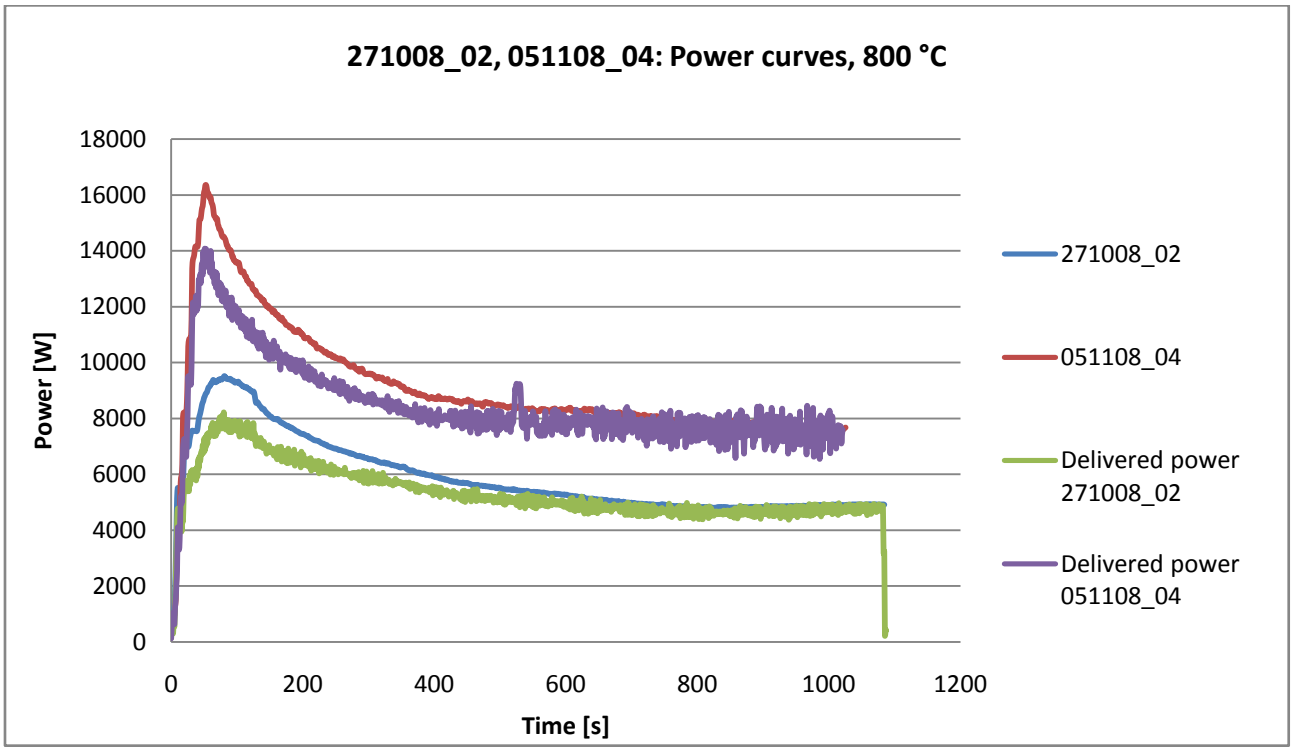

Figure 50 shows both the delivered powers and the power curves from the experiments 271008_02 and 051108_04.

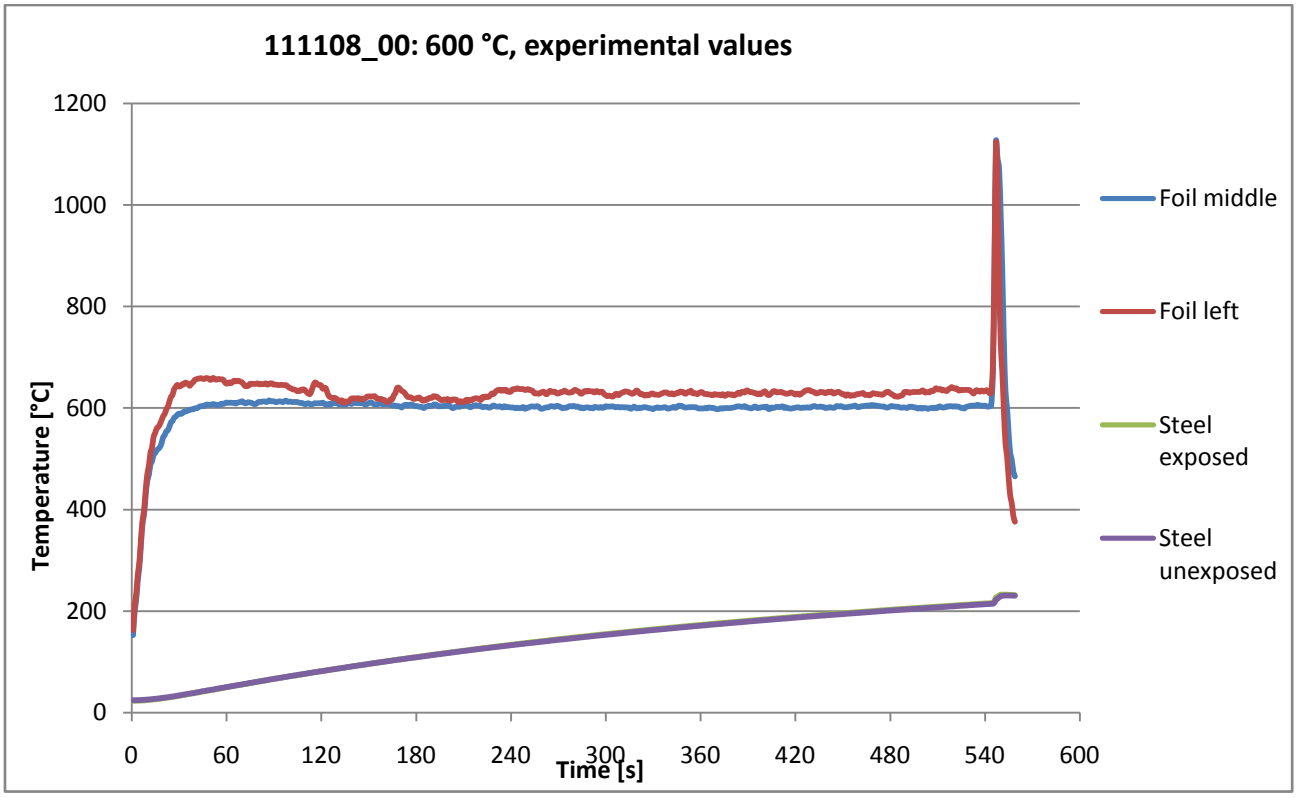

Figure 51 shows temperatures from 111108_00. This is an example of how the temperature curve looks like when the foil breaks.

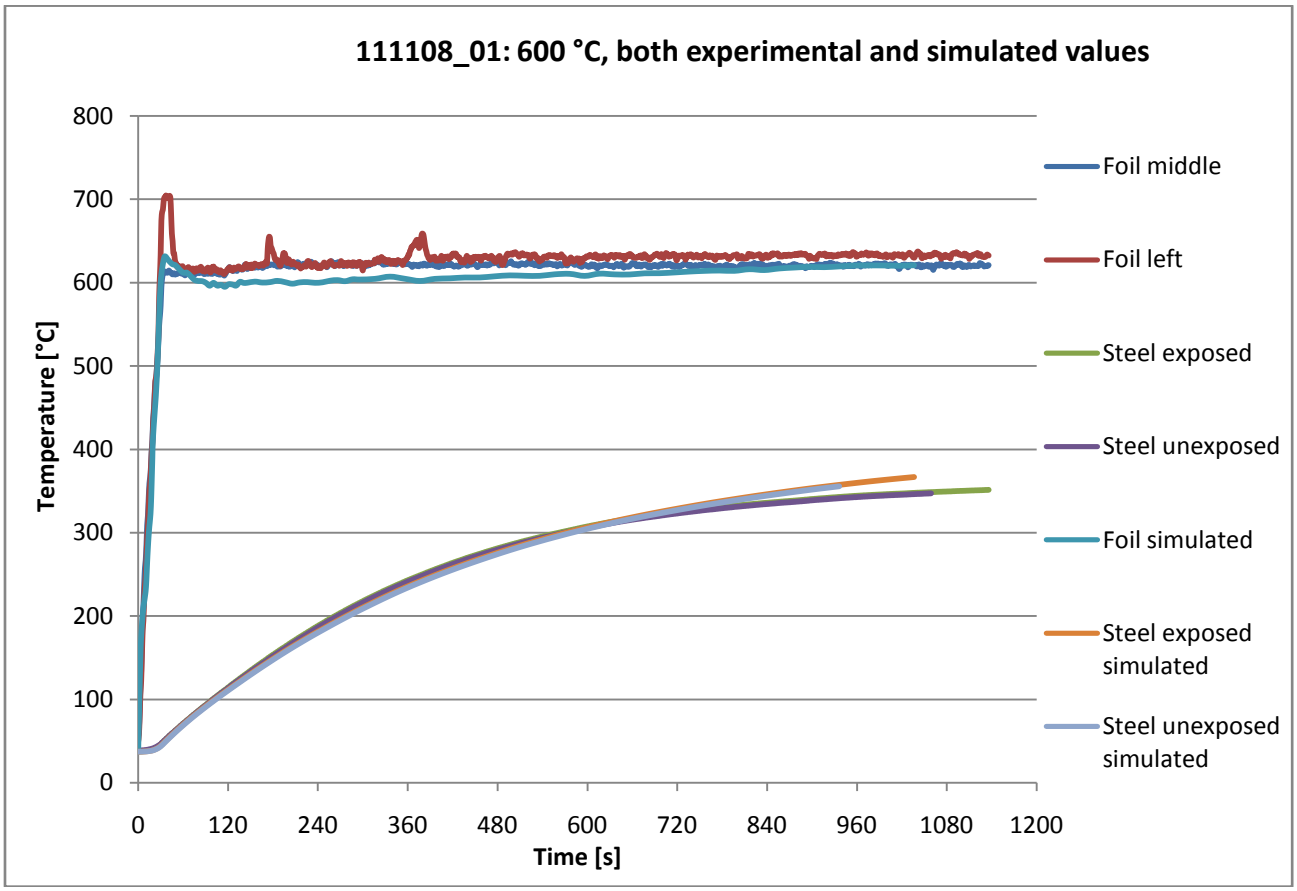

Figure 52 shows both experimental and simulated values from 111108_01

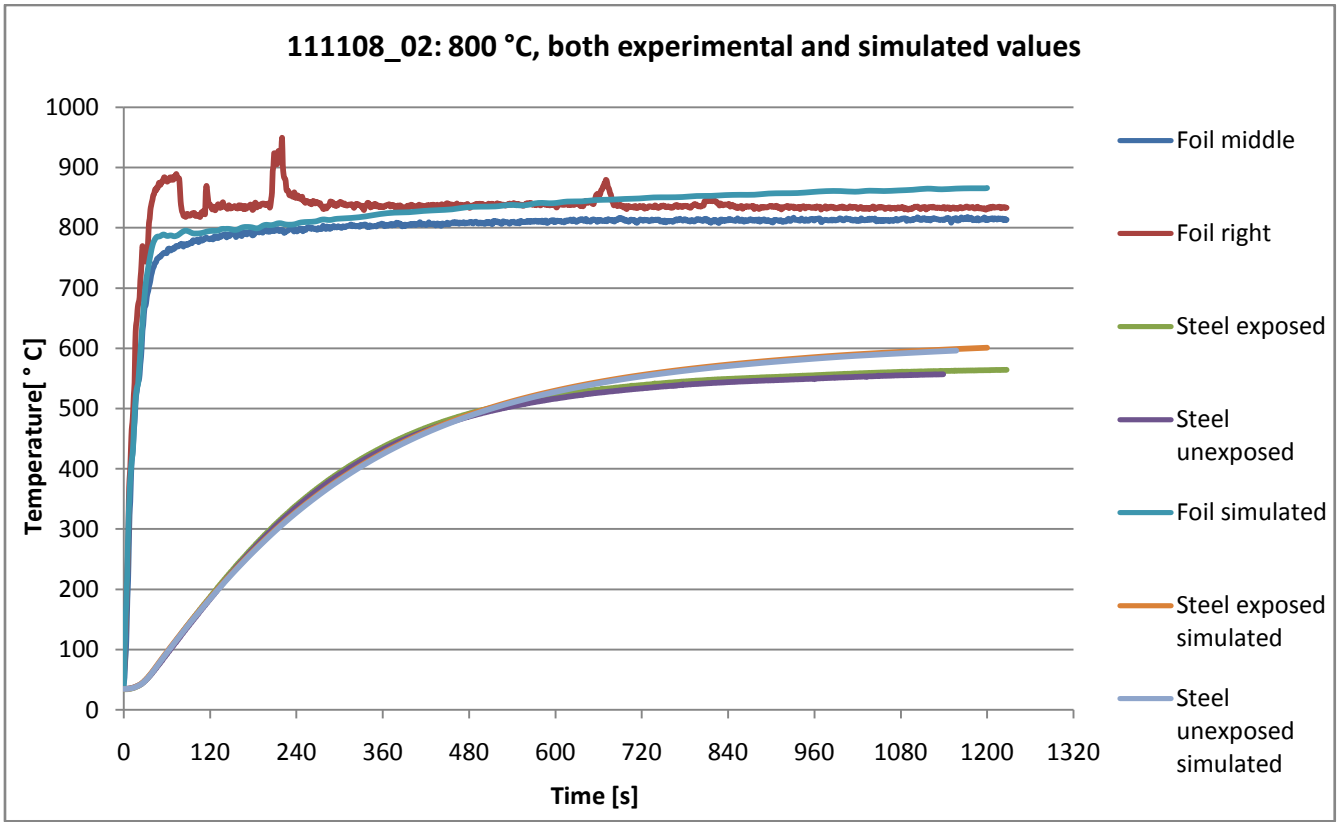

Figure 53 shows both experimental and simulated values from 111108_02

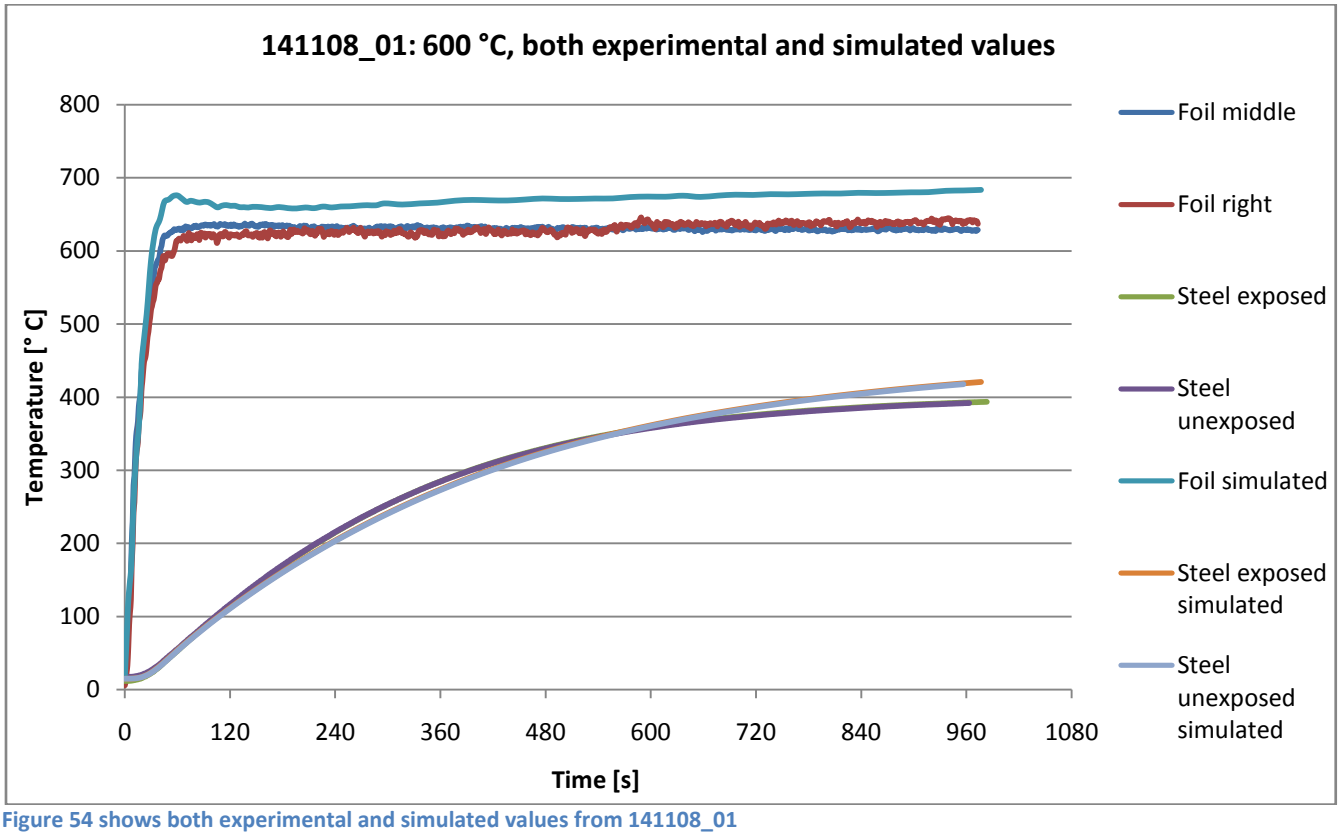

Figure 54 shows both experimental and simulated values from 141108_01

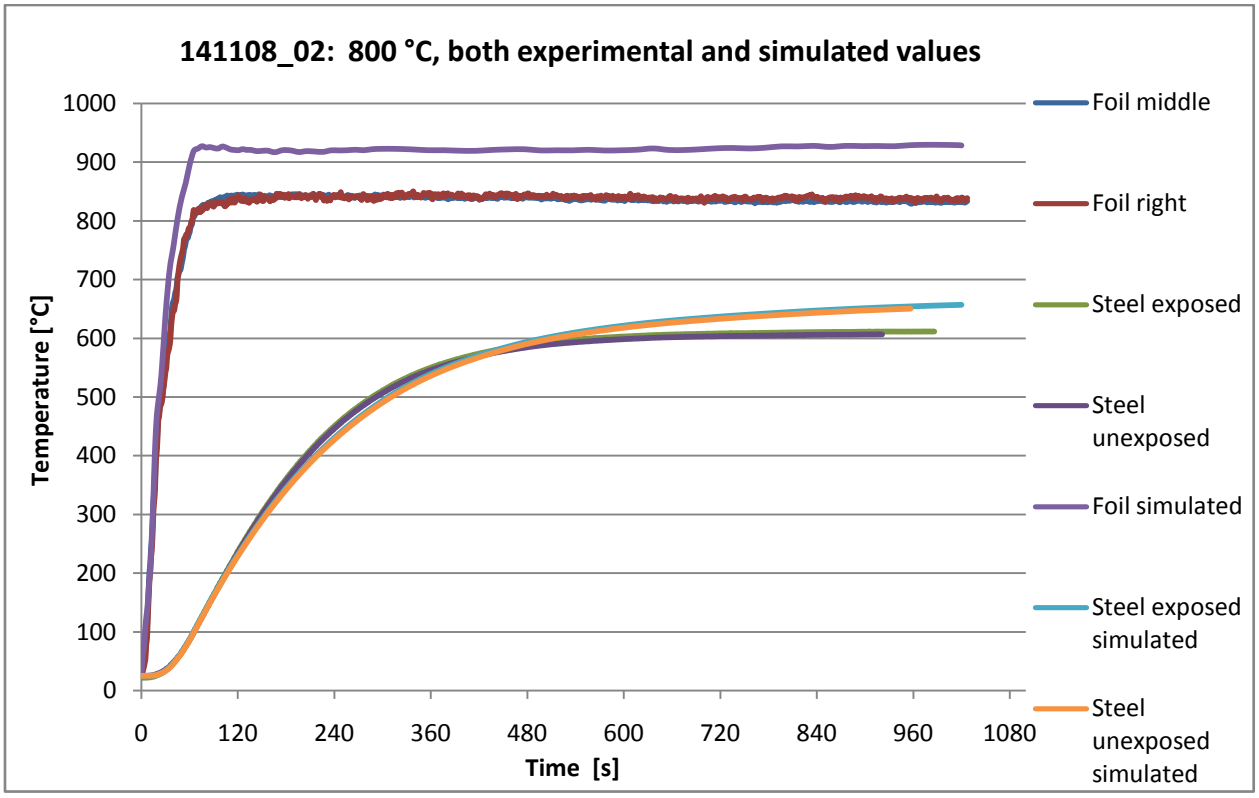

Figure 55 shows both experimental and simulated values from 141108_02

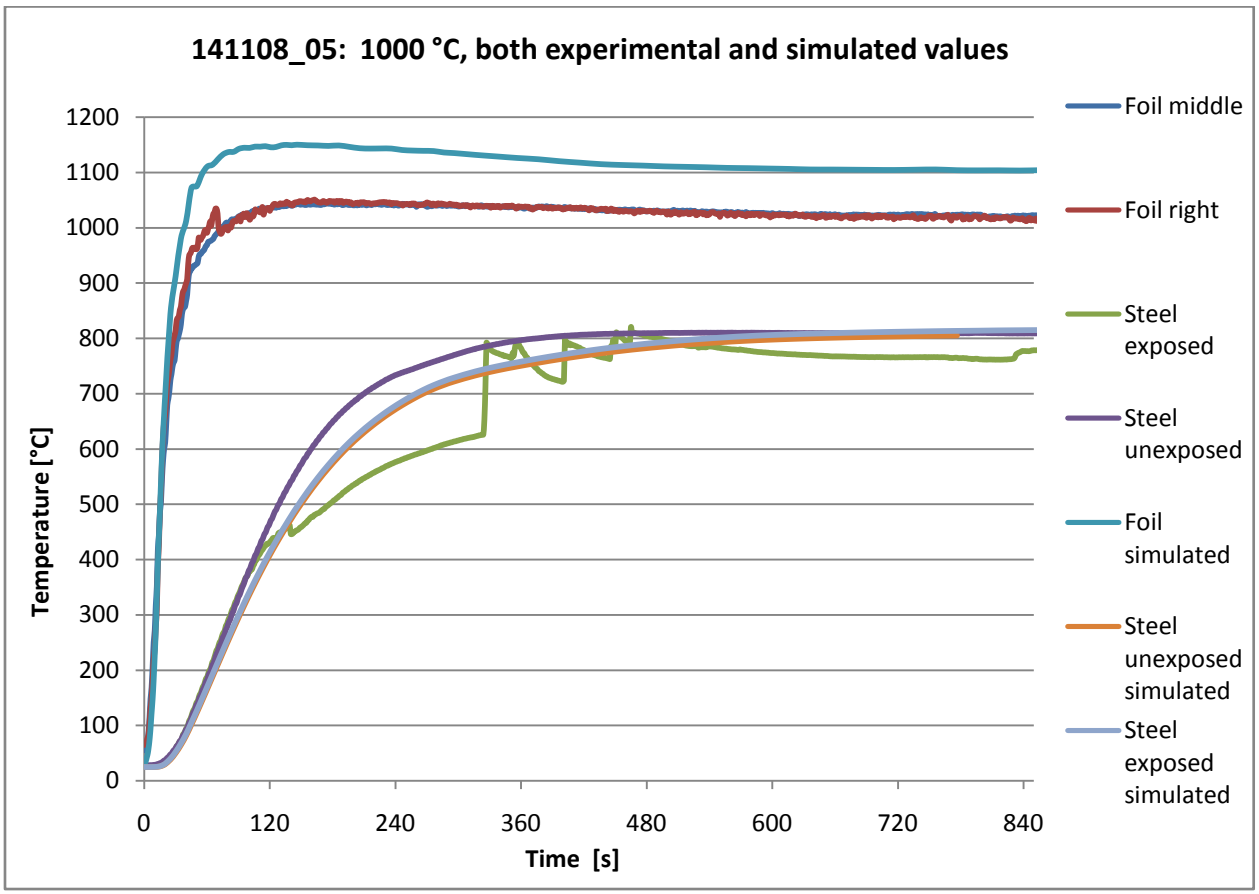

Figure 56 shows both experimental and simulated values from 141108_05

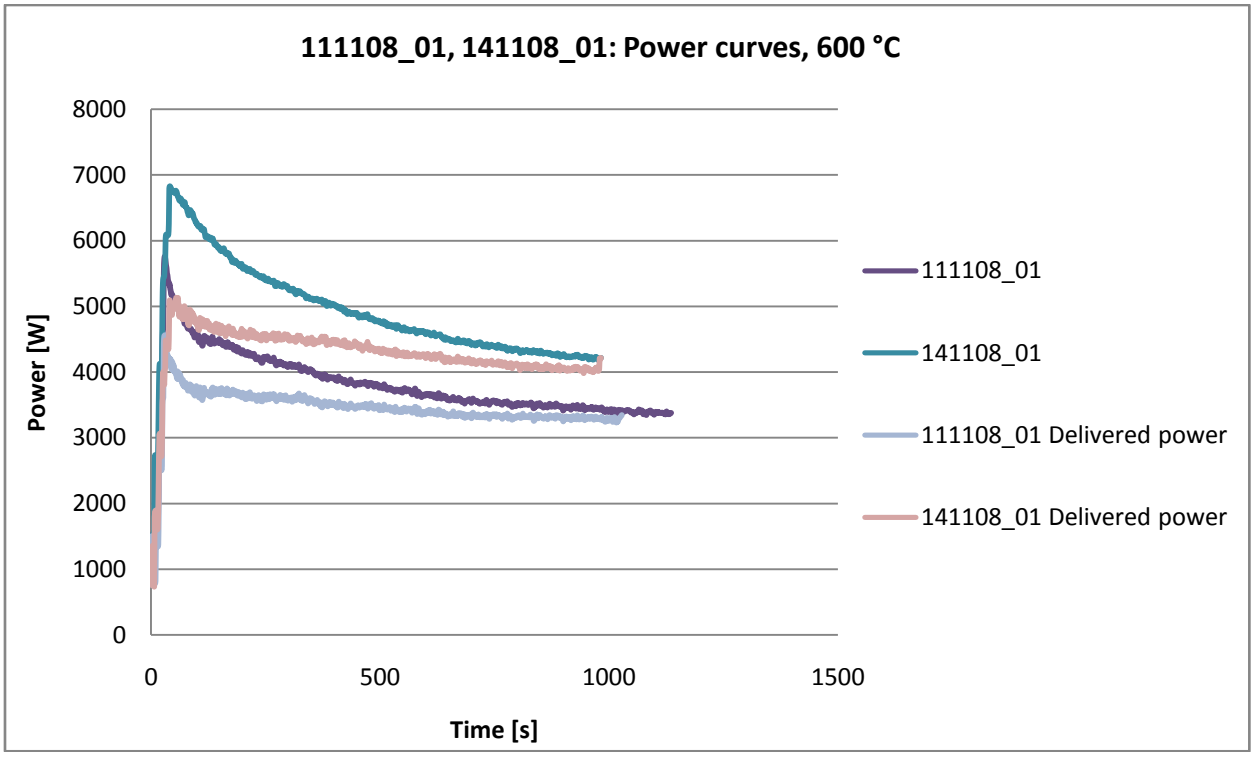

Figure 57 shows both the power and the delivered power curve from the experiments 111108_01 and 141108_01

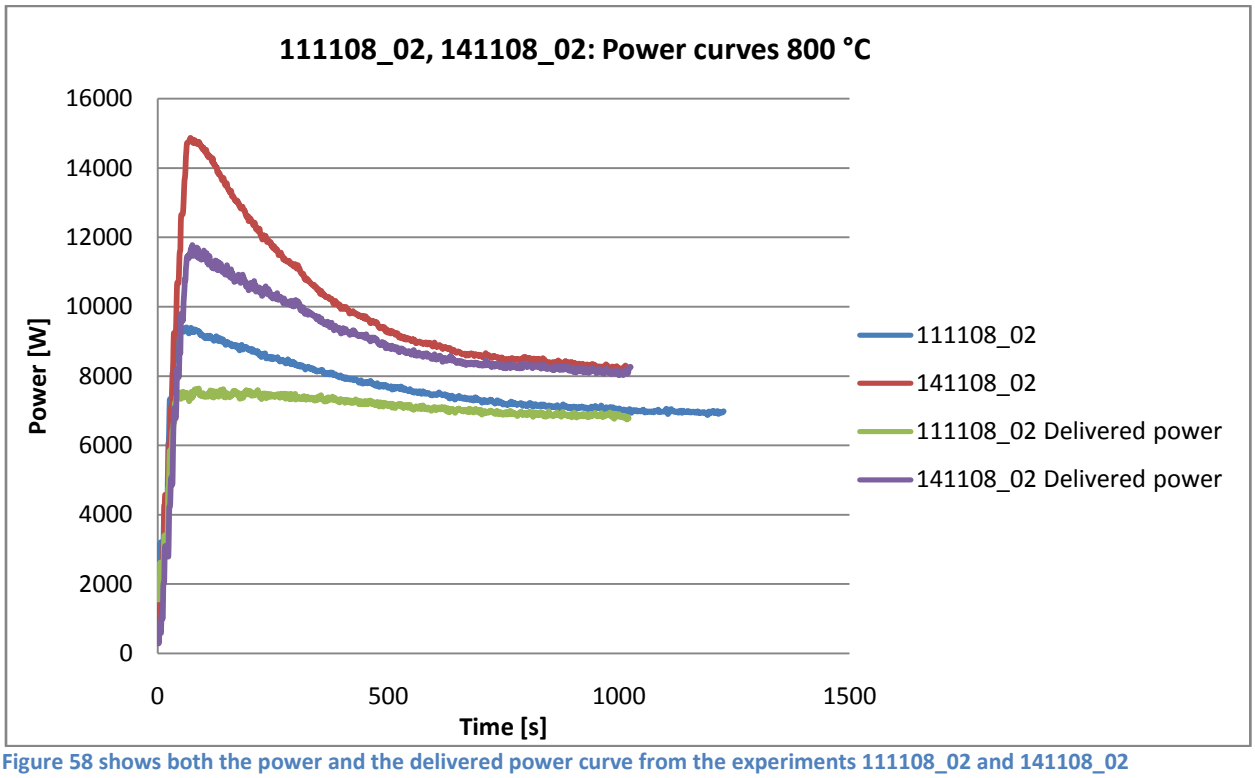

Figure 58 shows both the power and the delivered power curve from the experiments 111108_02 and 141108_02

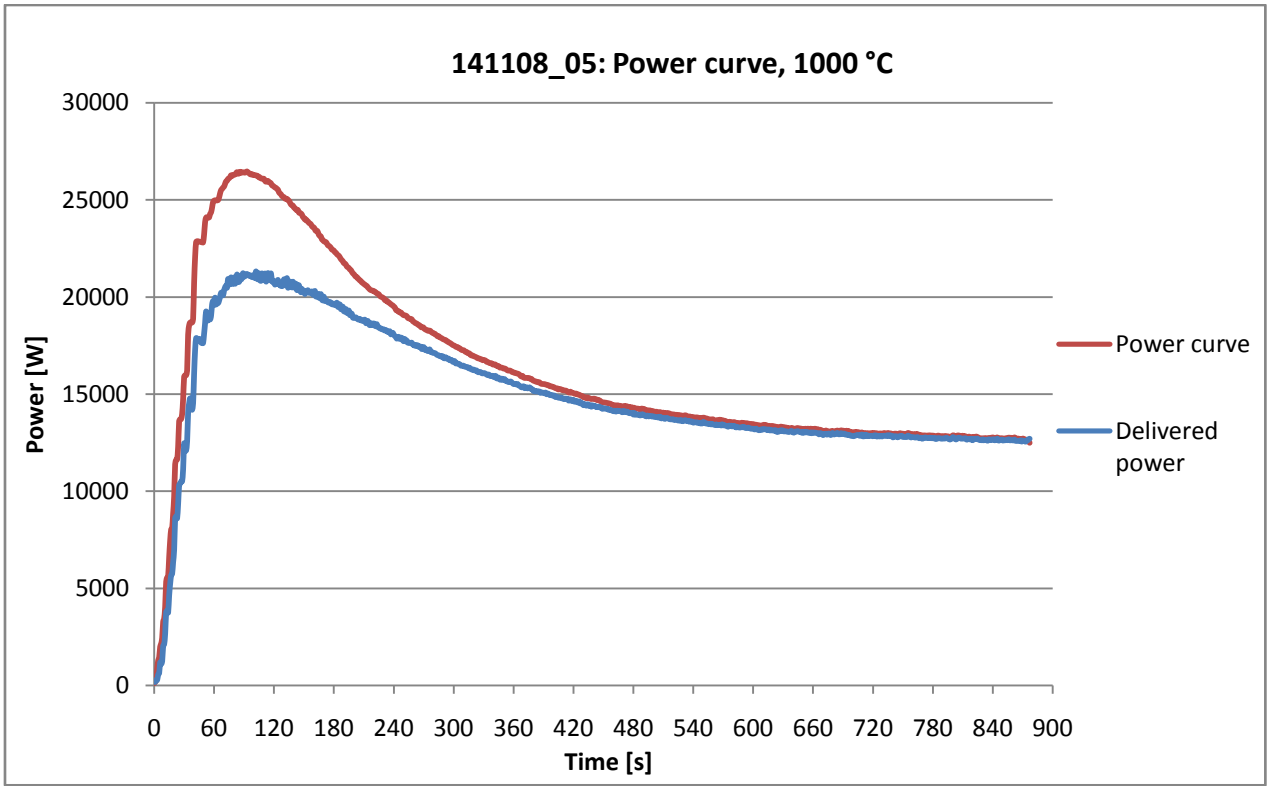

Figure 59 shows both the power and the delivered power from 141108_05

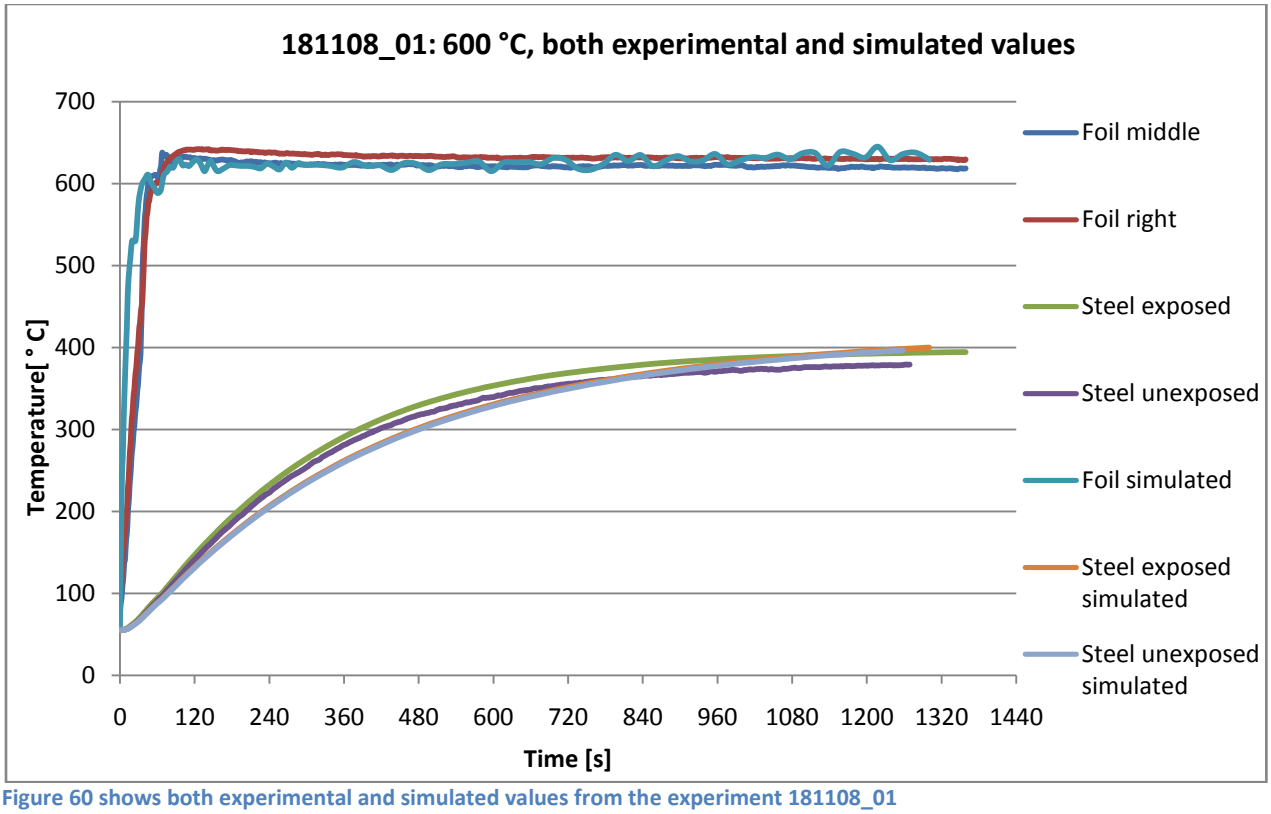

Figure 60 shows both experimental and simulated values from the experiment 181108_01

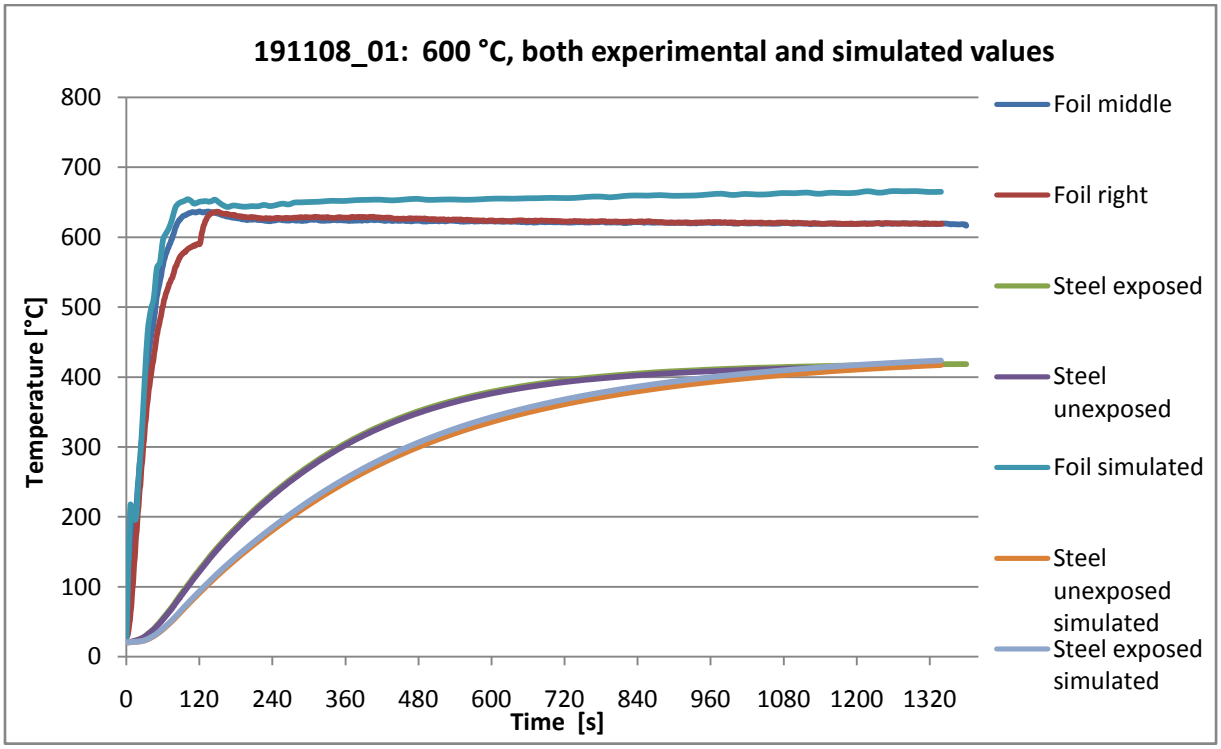

Figure 61 shows both experimental and simulated values from the experiment 191108_01

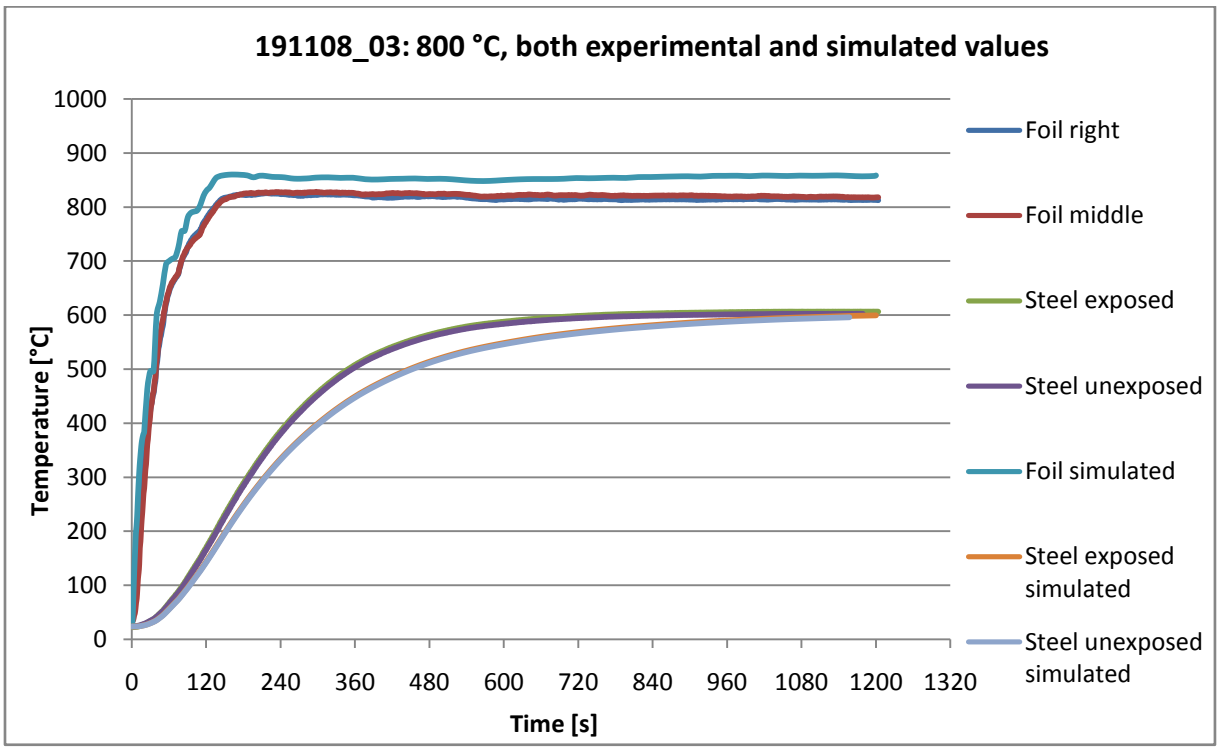

Figure 62 shows both experimental and simulated values from the experiment 191108_03

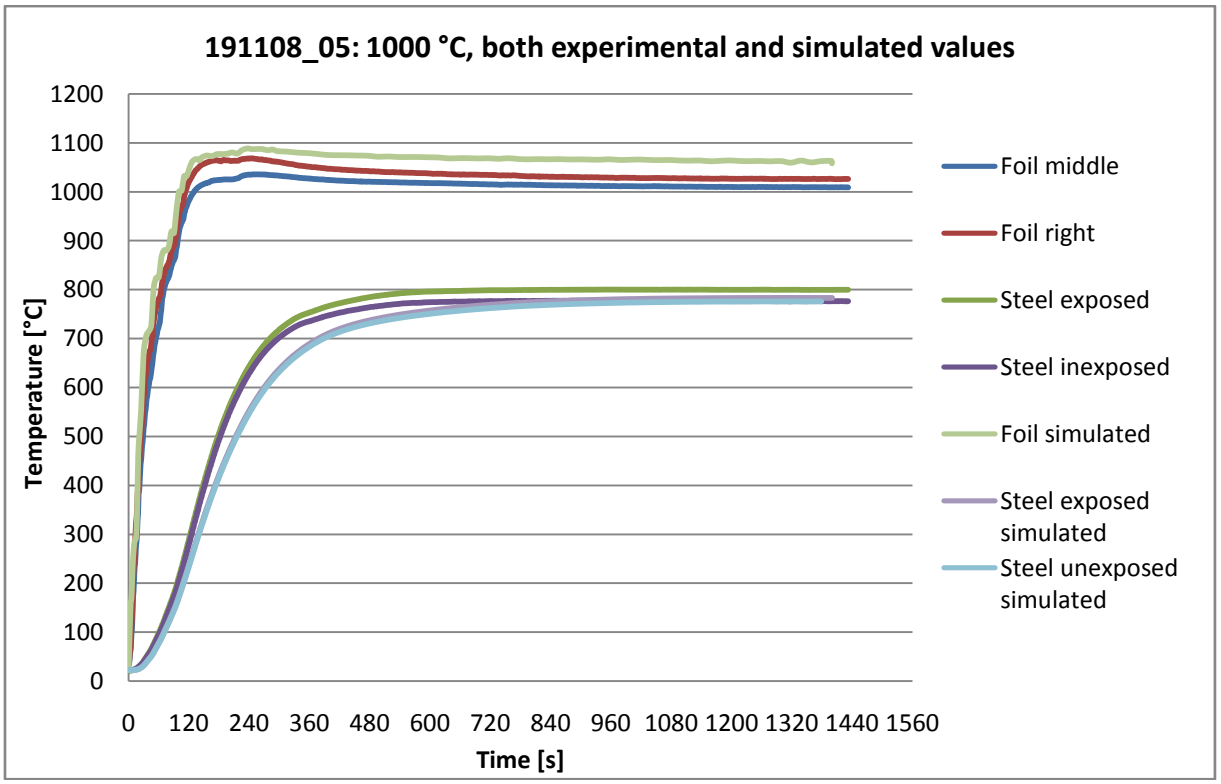

Figure 63 show both experimental and simulated values from the experiment 191108_05

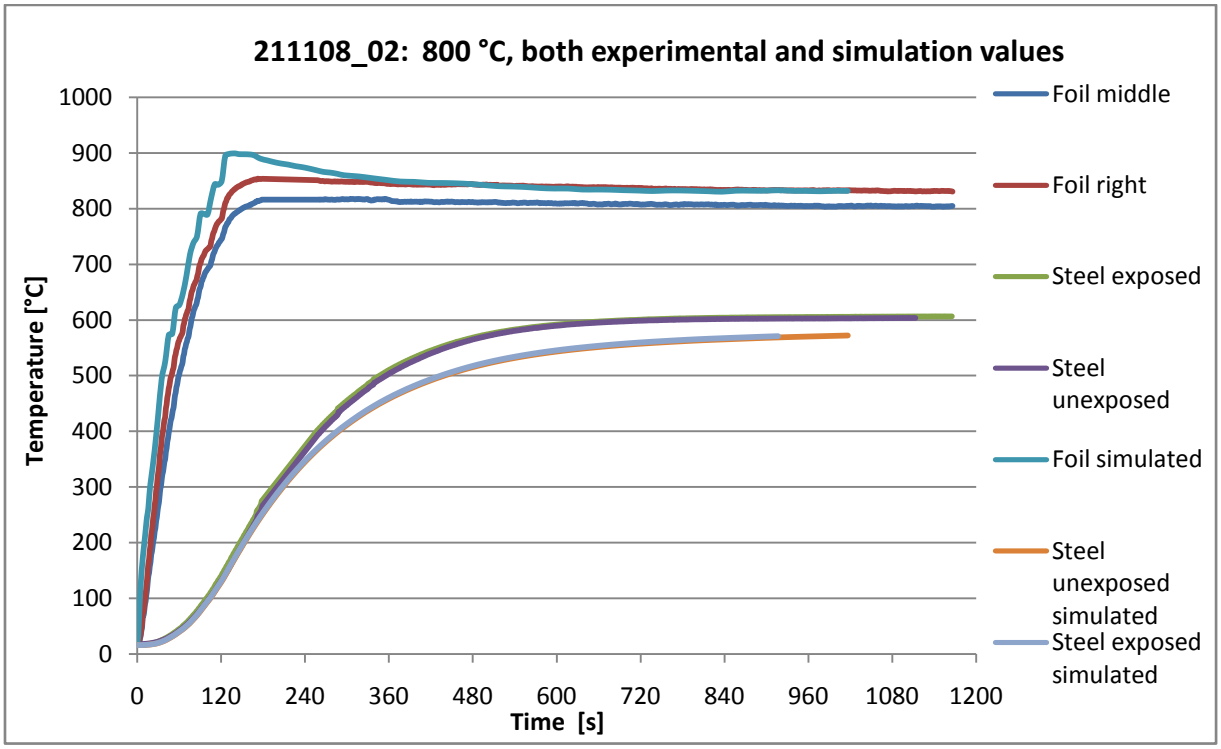

Figure 64 shows both experimental and simulated values from 211108_02

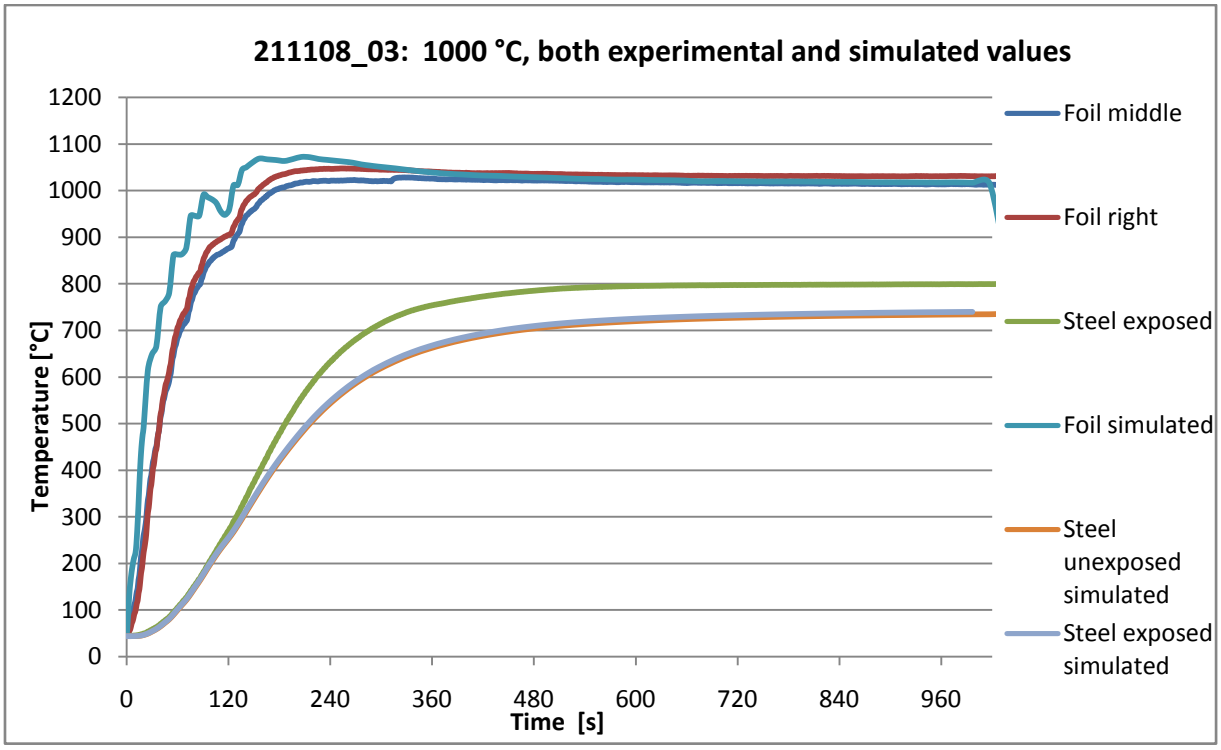

Figure 65 shows both experimental and simulated values from 211108_03

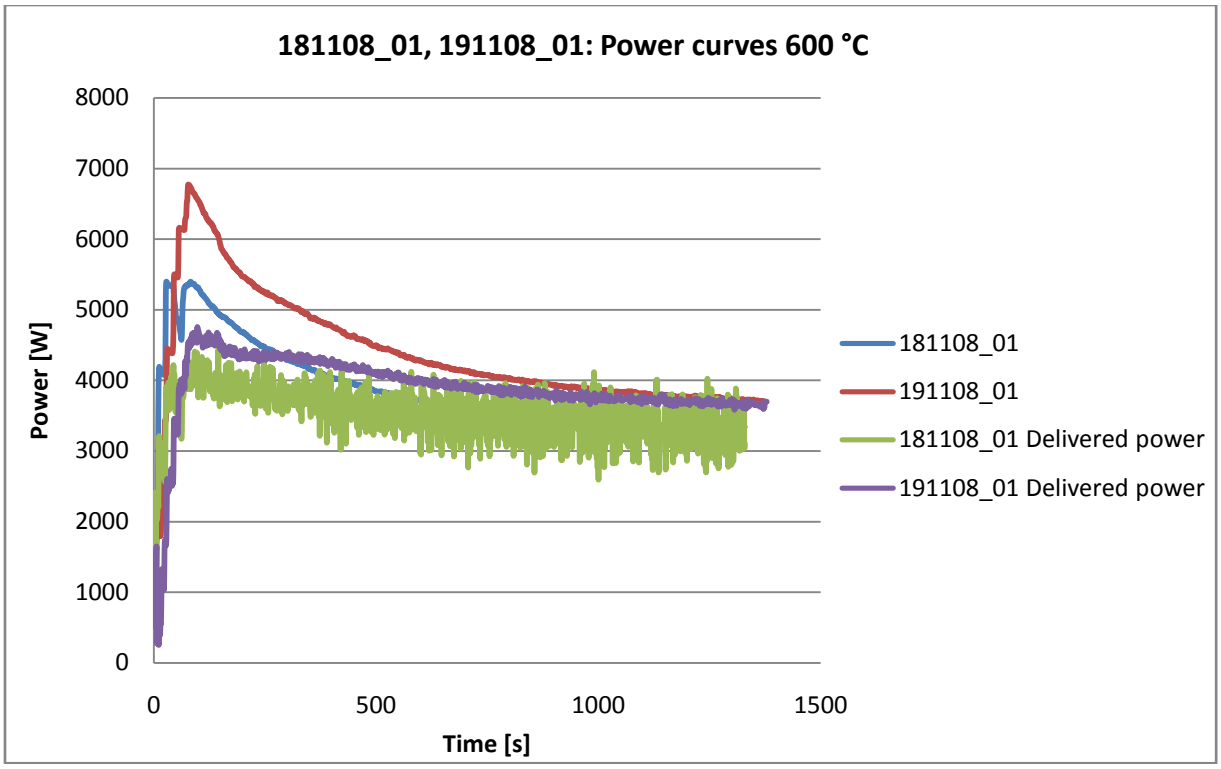

Figure 66 shows the power curves from 181108_01 and 191108_01

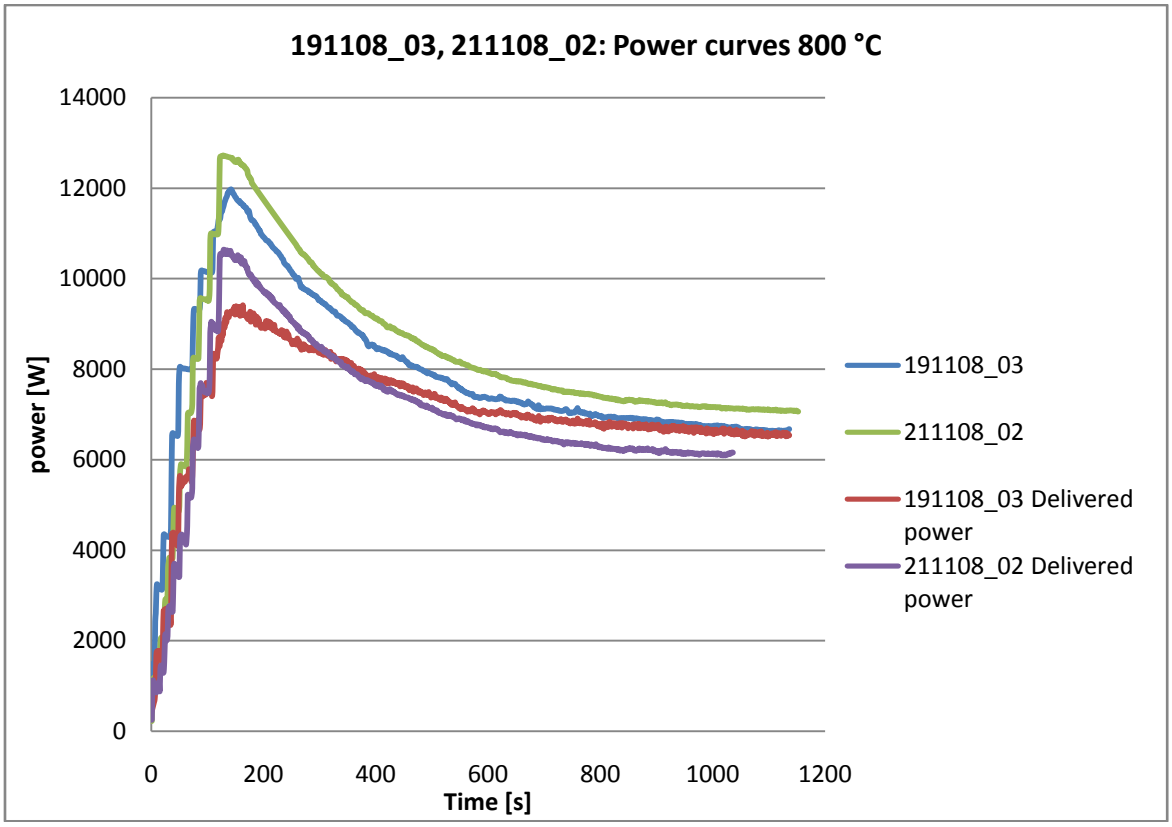

Figure 67 shows the power curves from 191108_03 and 211108_02

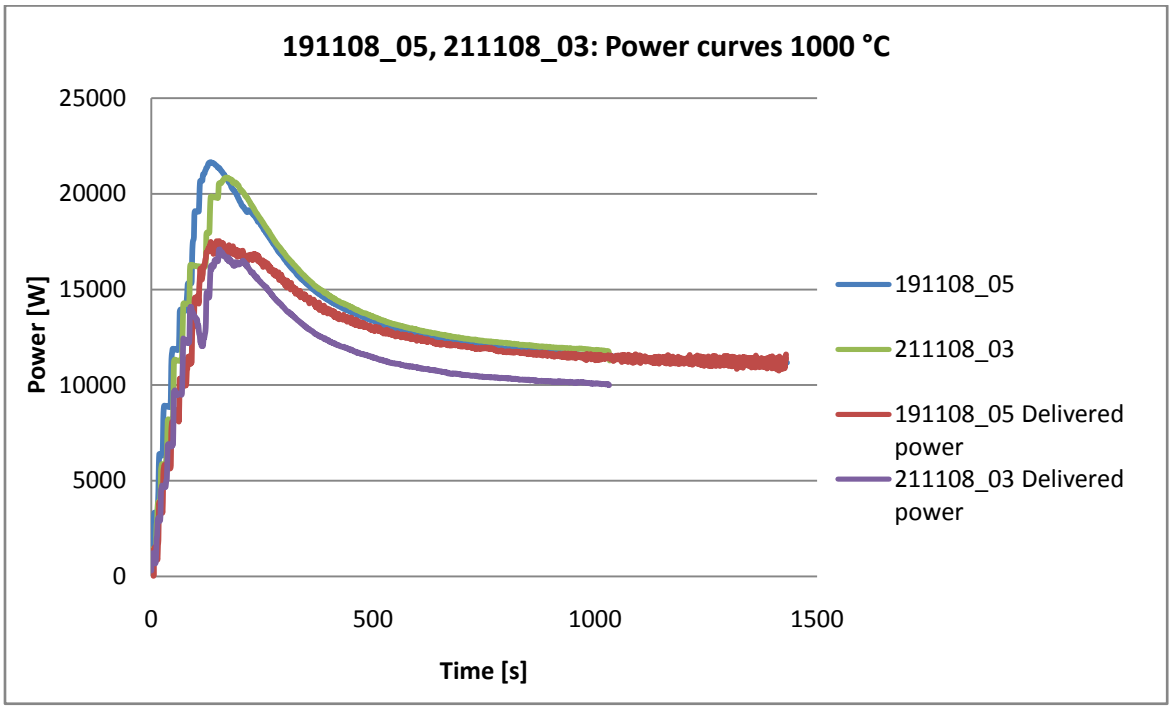

Figure 68 shows the power curves from 191108_05 and 211108_03

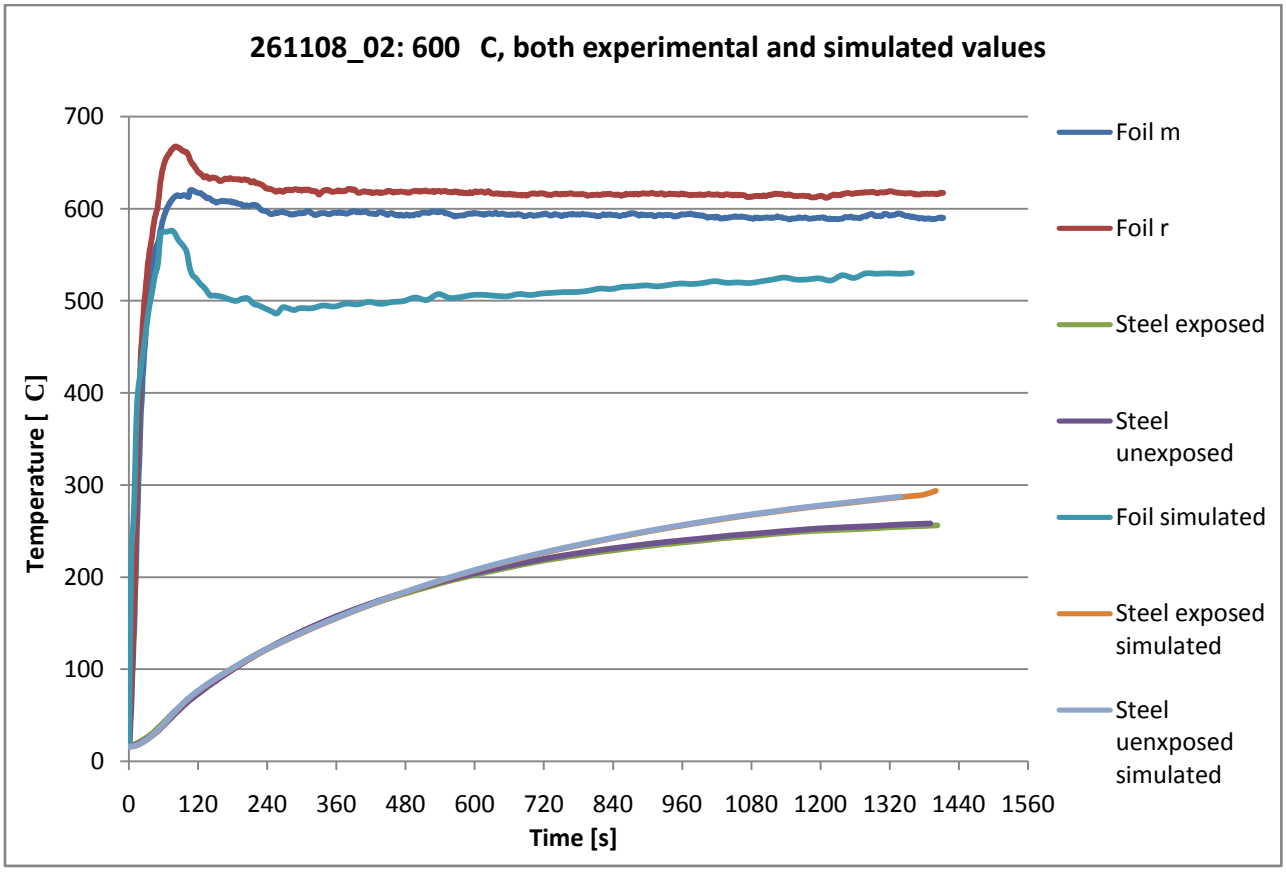

Figure 69 shows both experimental and simulated values from the experiment 261108_02

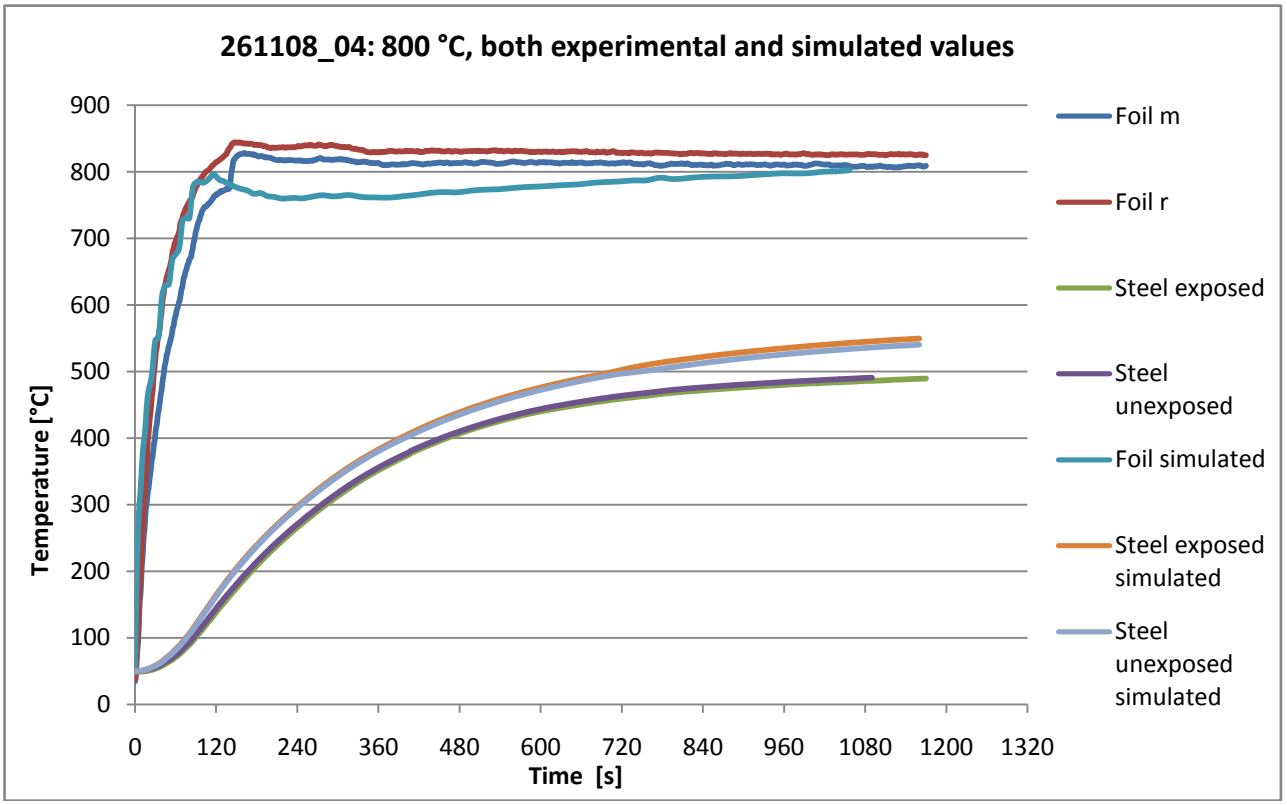

Figure 70 shows both experimental and simulated values from the experiment 261108_04

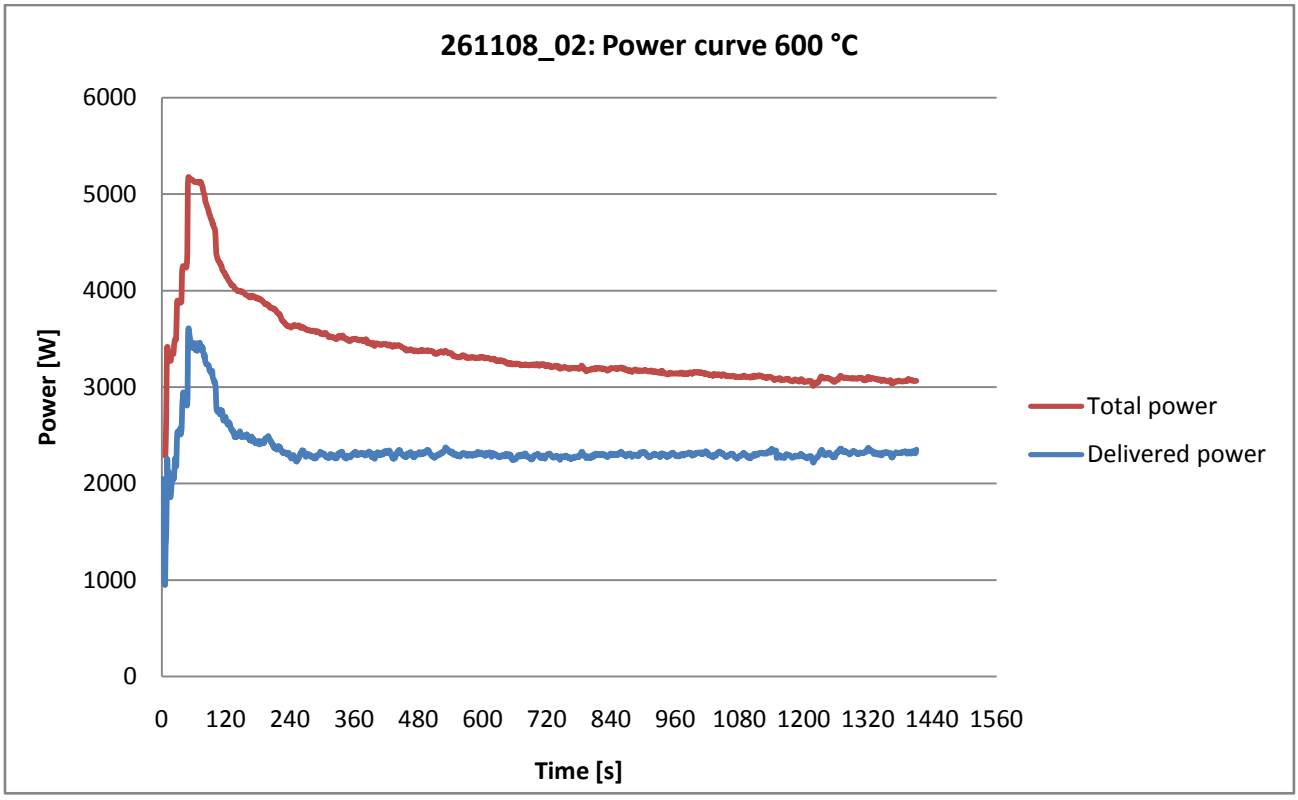

Figure 71 shows the power curve from 261108_02

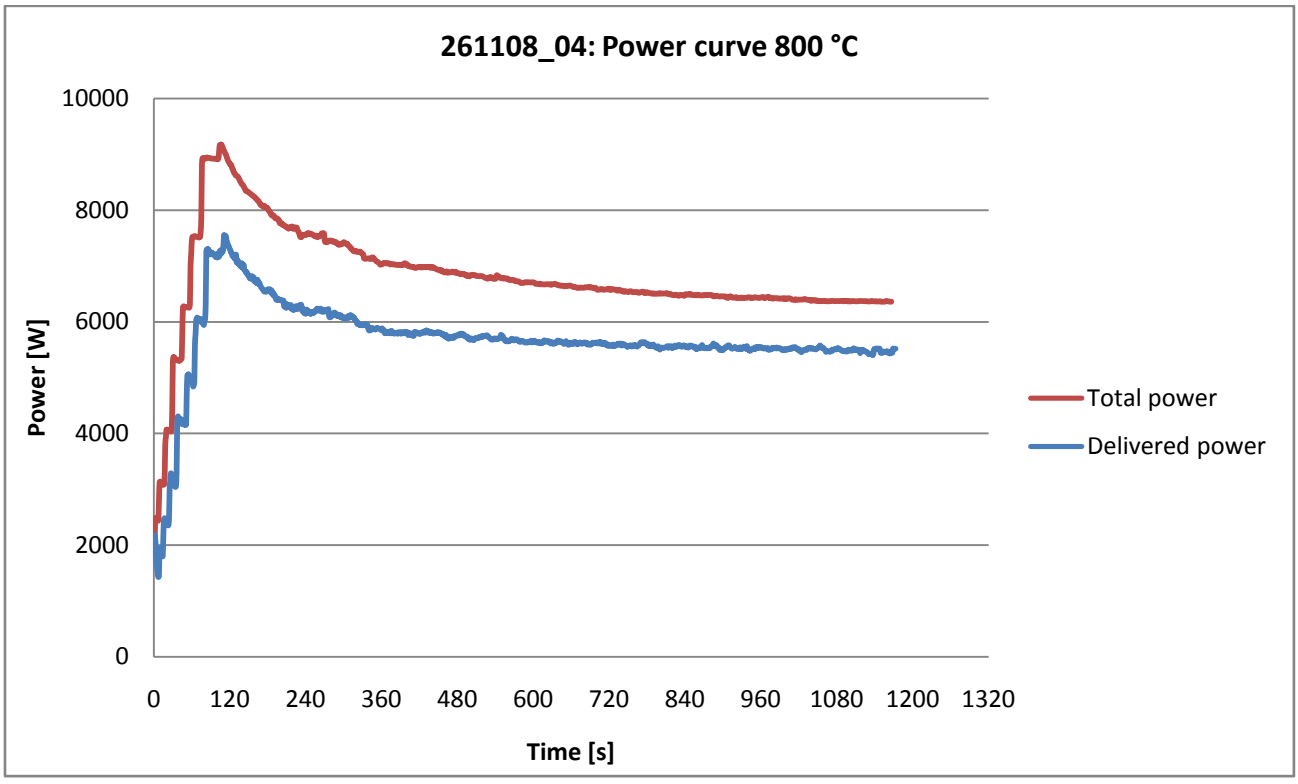

Figure 72 shows the power curve from 261108_04

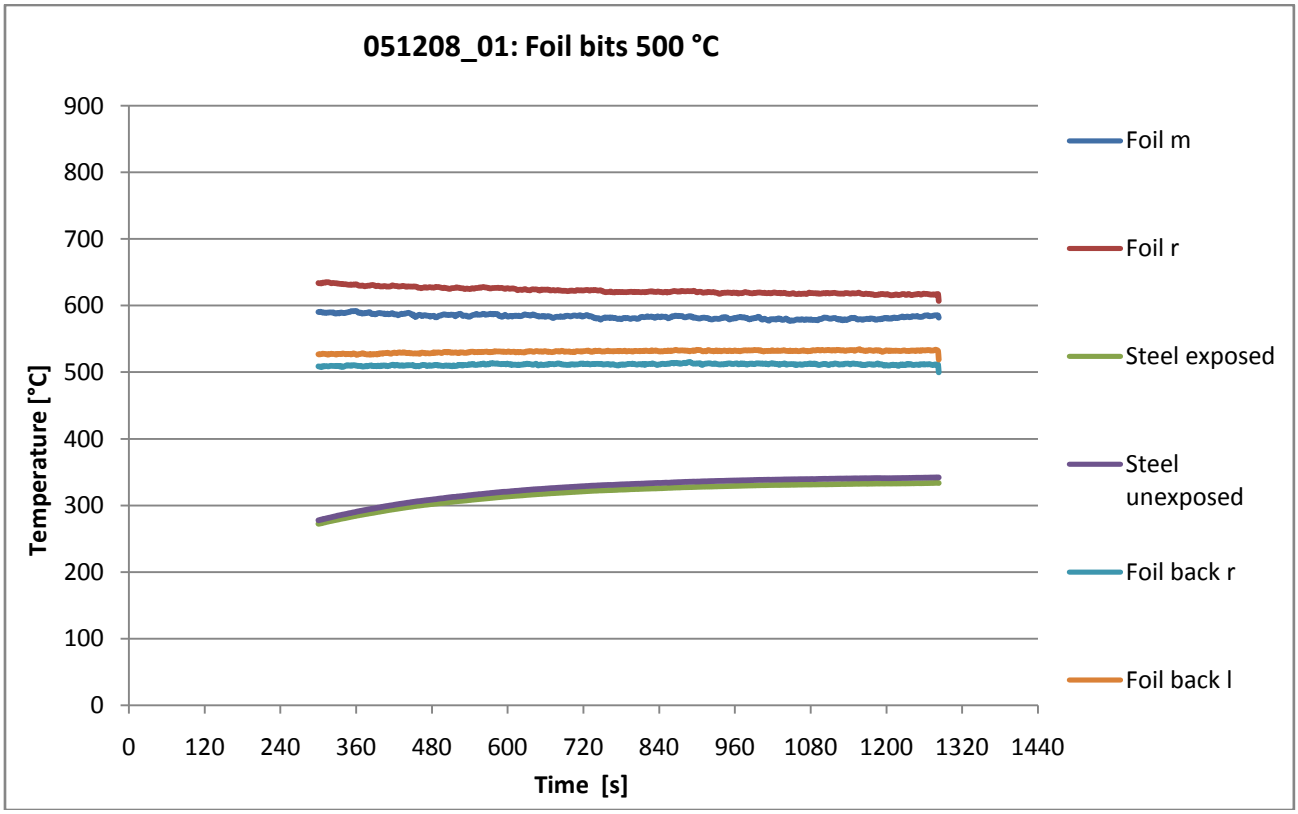

Figure 73 shows experimental values from 051208_01

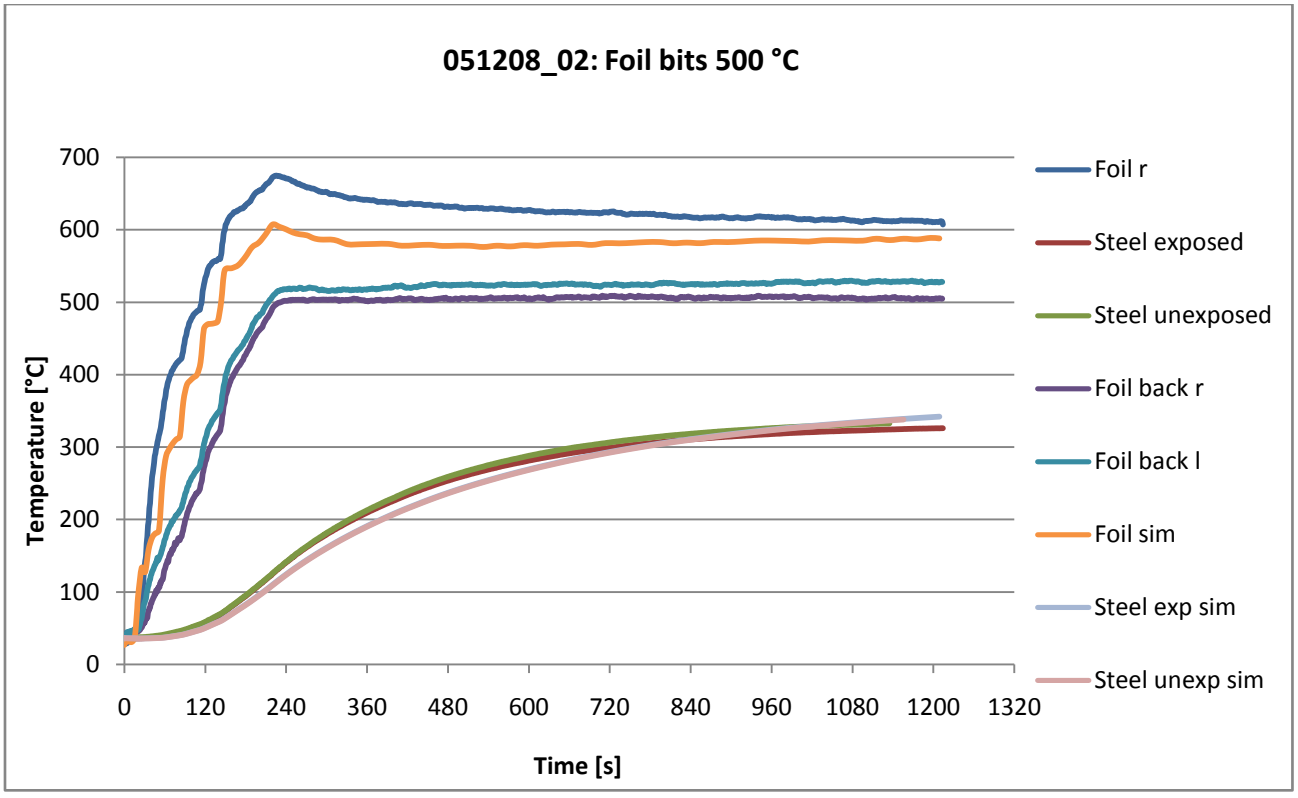

Figure 74 shows experimental and simulated values from 051208_02

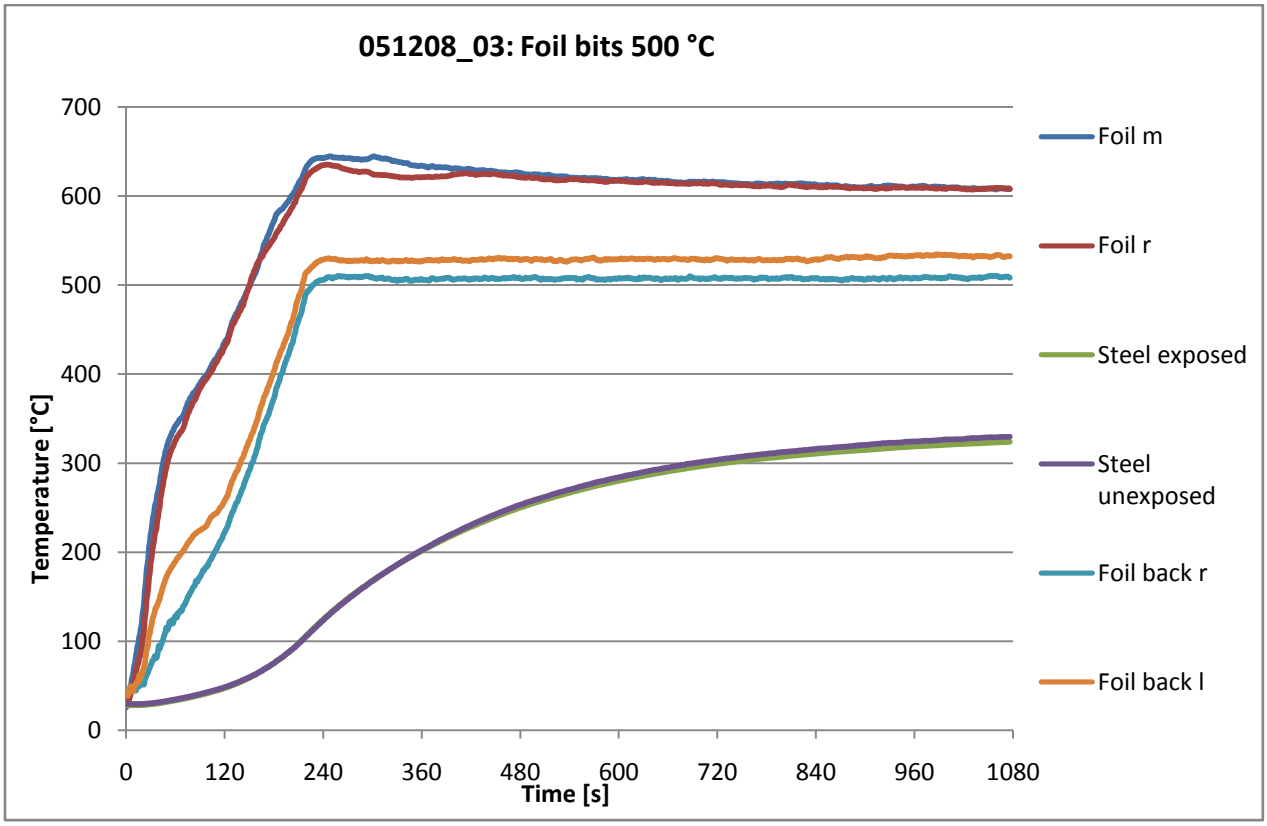

Figure 75 shows experimental data from 051208_03

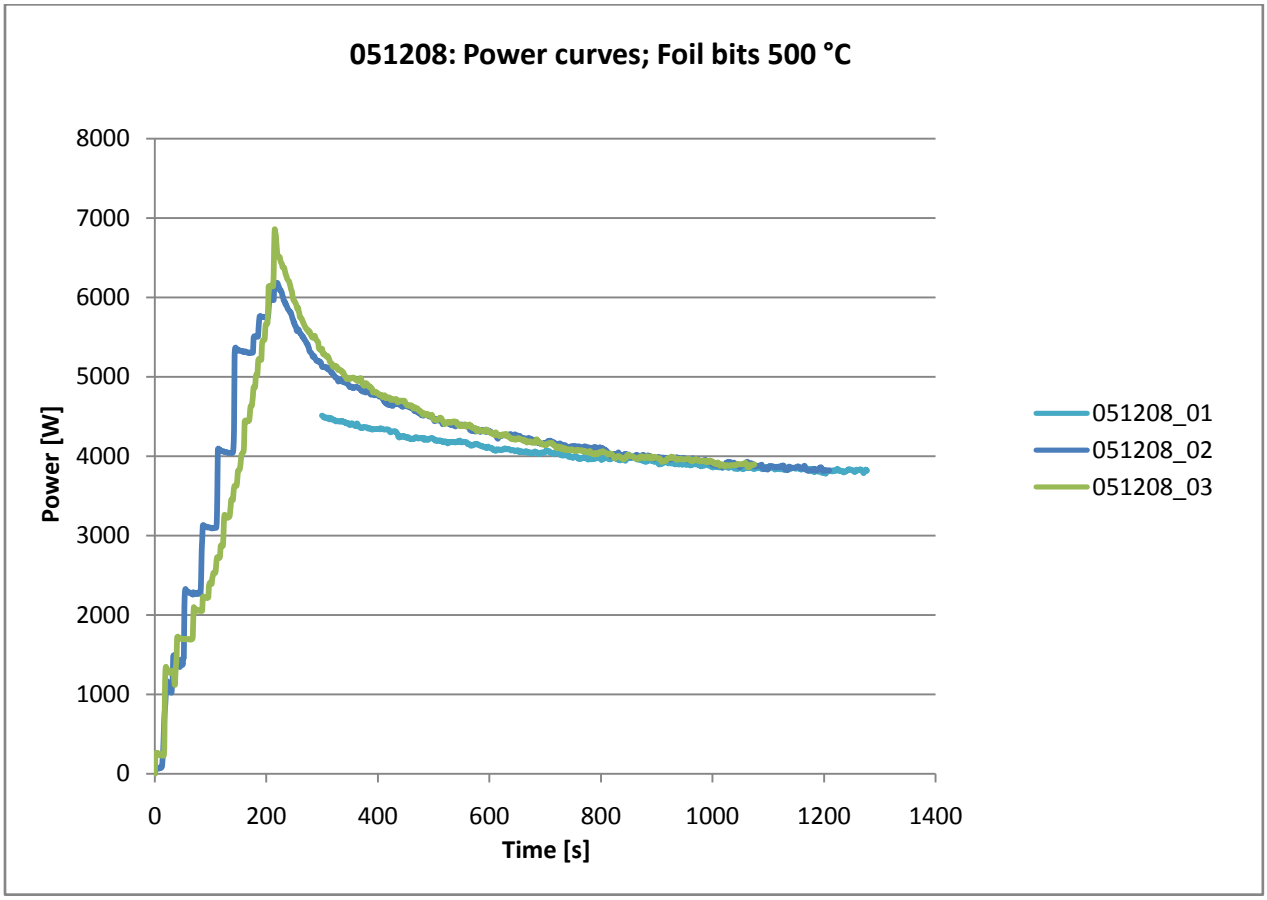

Figure 76 shows the total power curve from 051208_01, 051208_02 and 051208_03

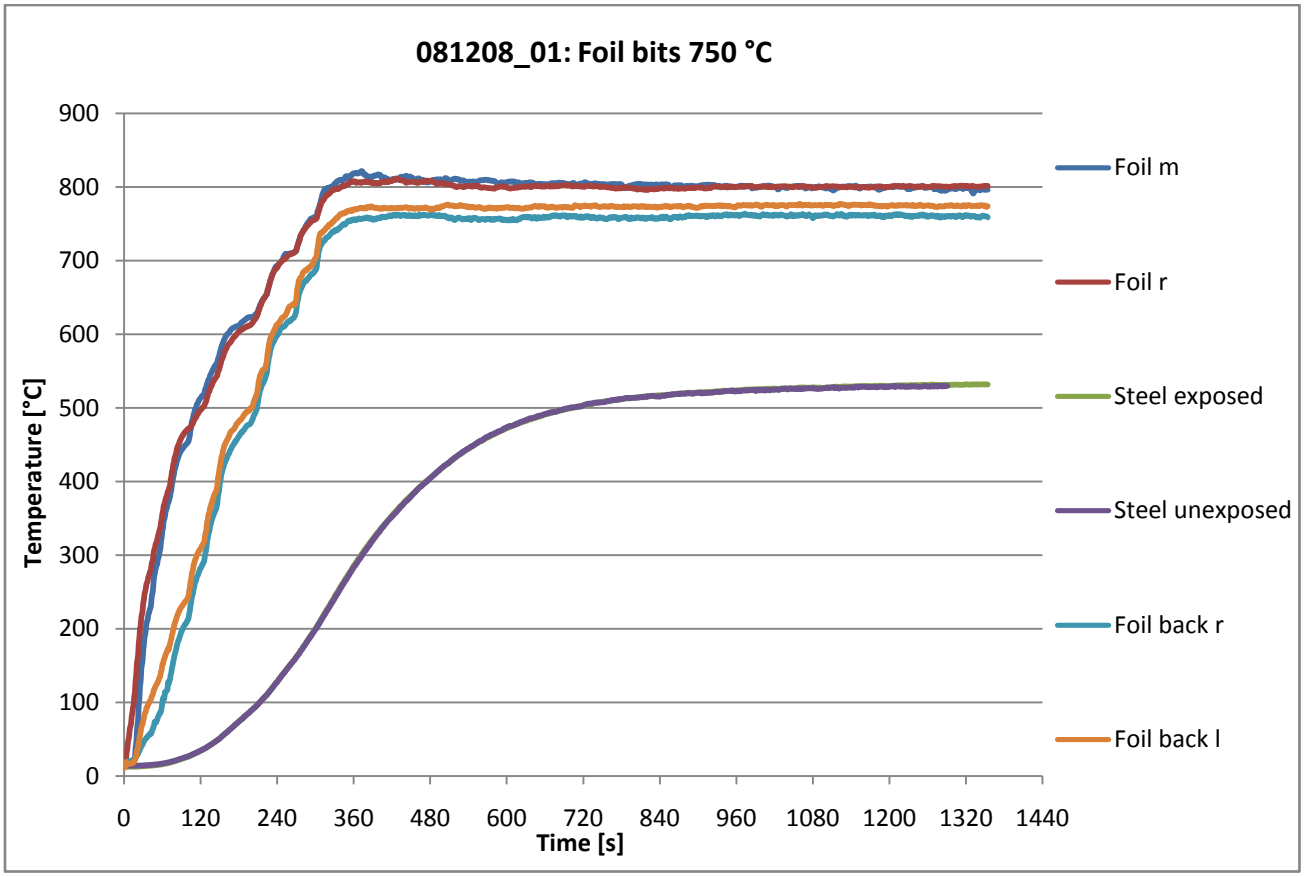

Figure 77 shows experimental values from 081208_01

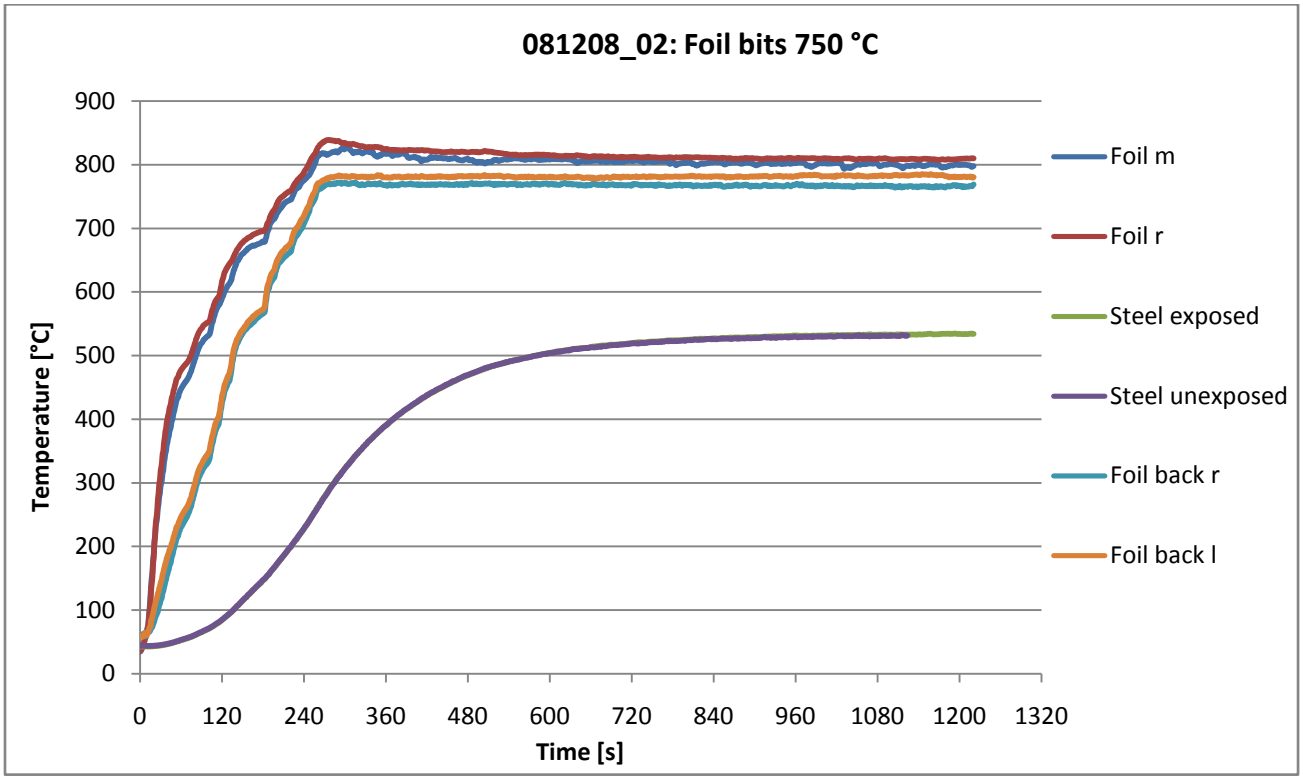

Figure 78 shows experimental values from 081208_02

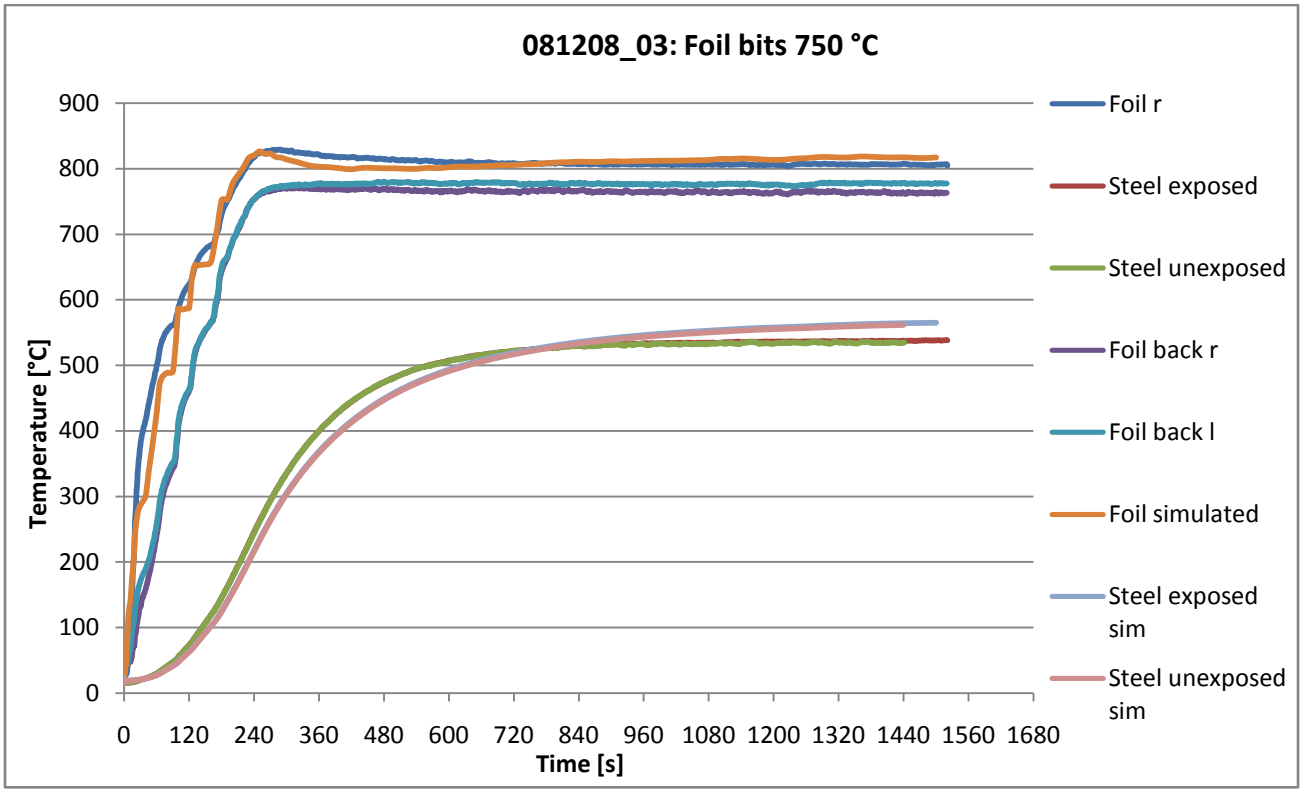

Figure 79 shows both experimental and simulated values from 081208_03

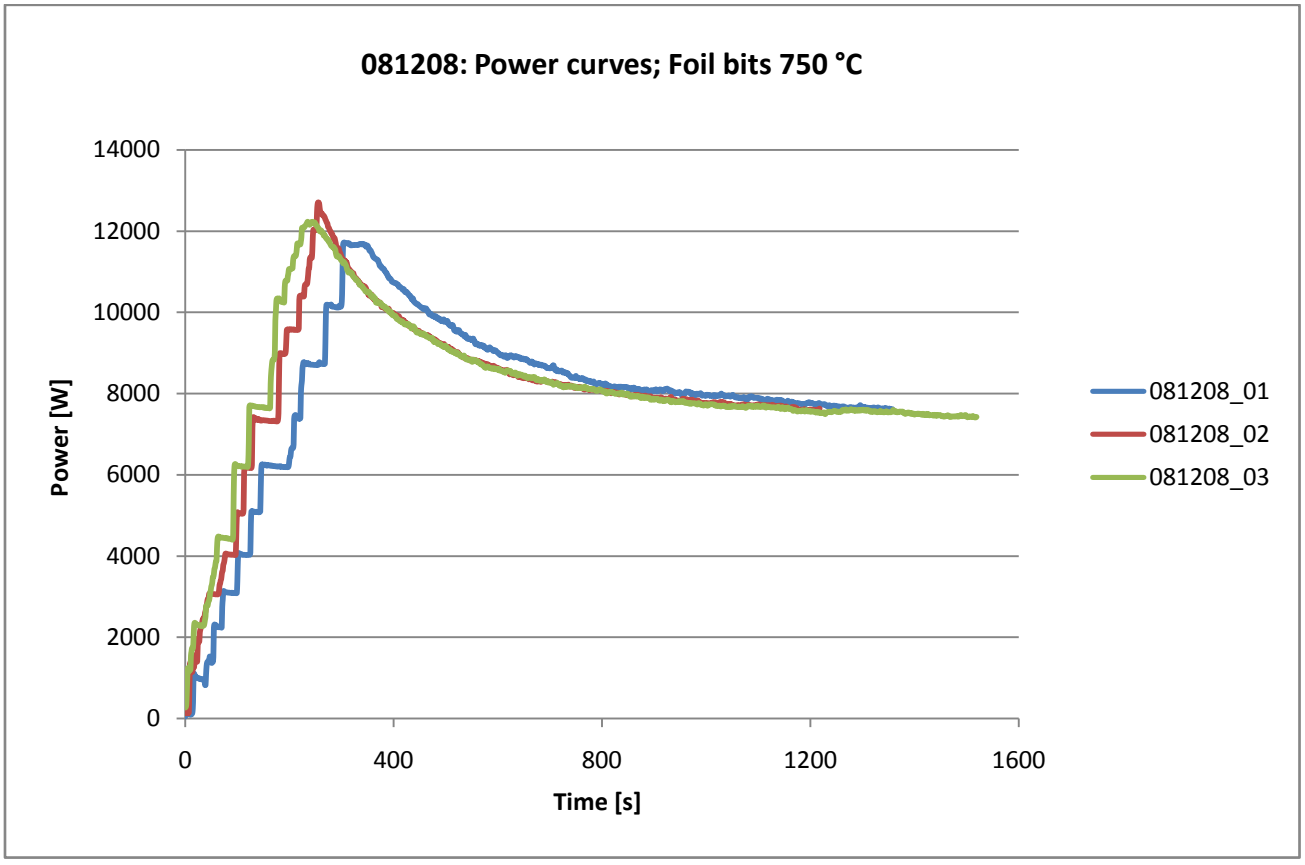

Figure 80 shows the power curves from 081208_01, 081208_02 and 081208_03

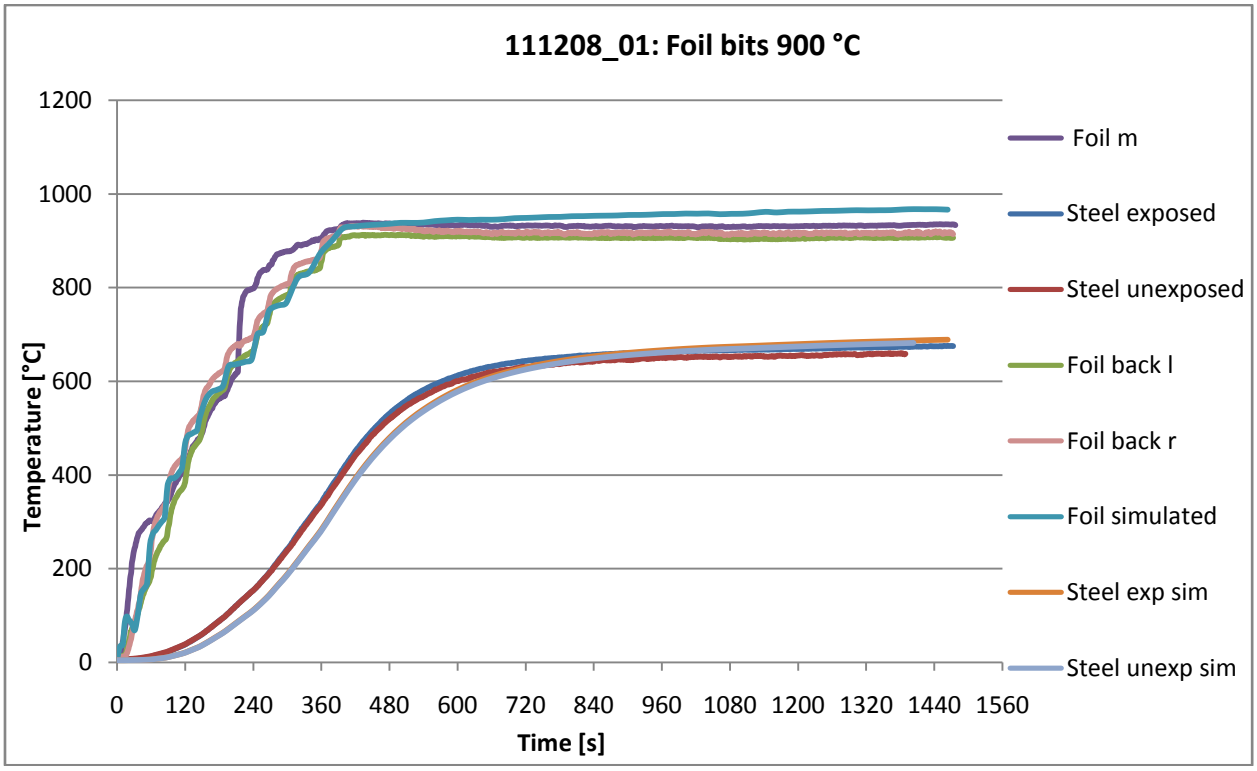

Figure 81 shows both experimental and simulated values from 111208_01

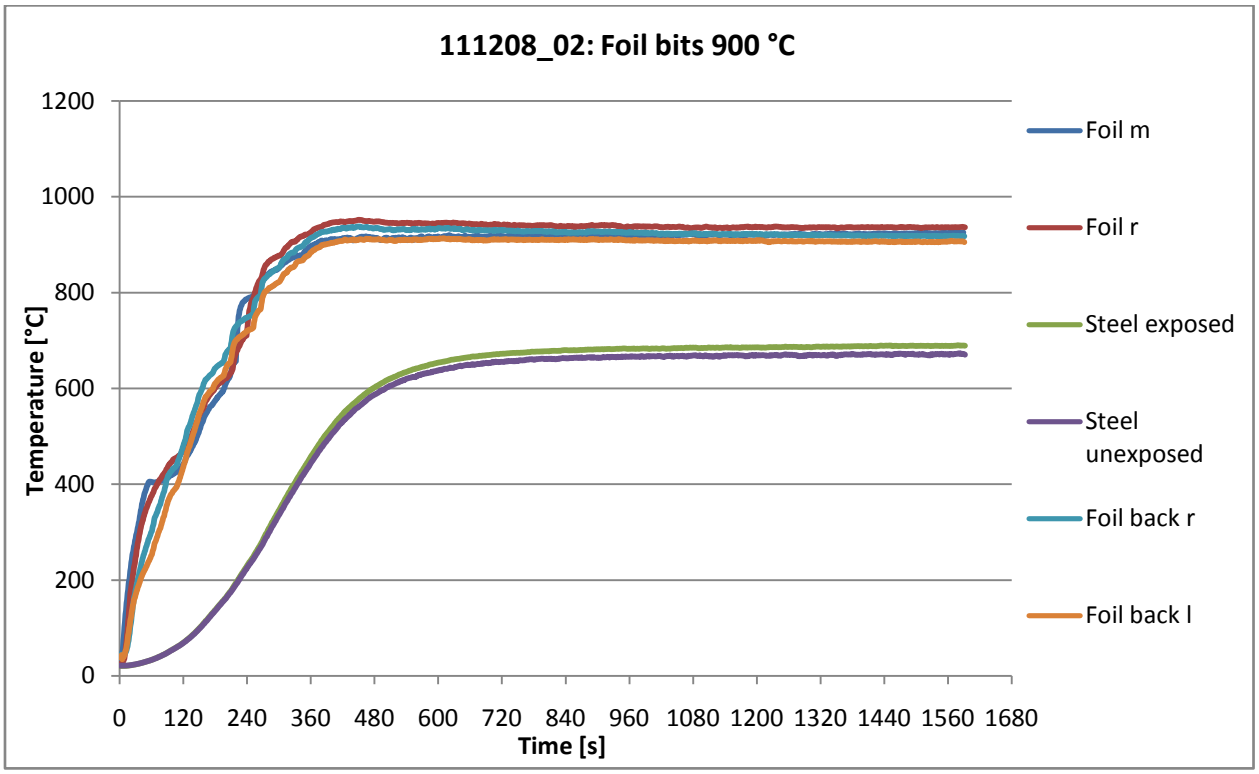

Figure 82 shows experimental values from 111208_02

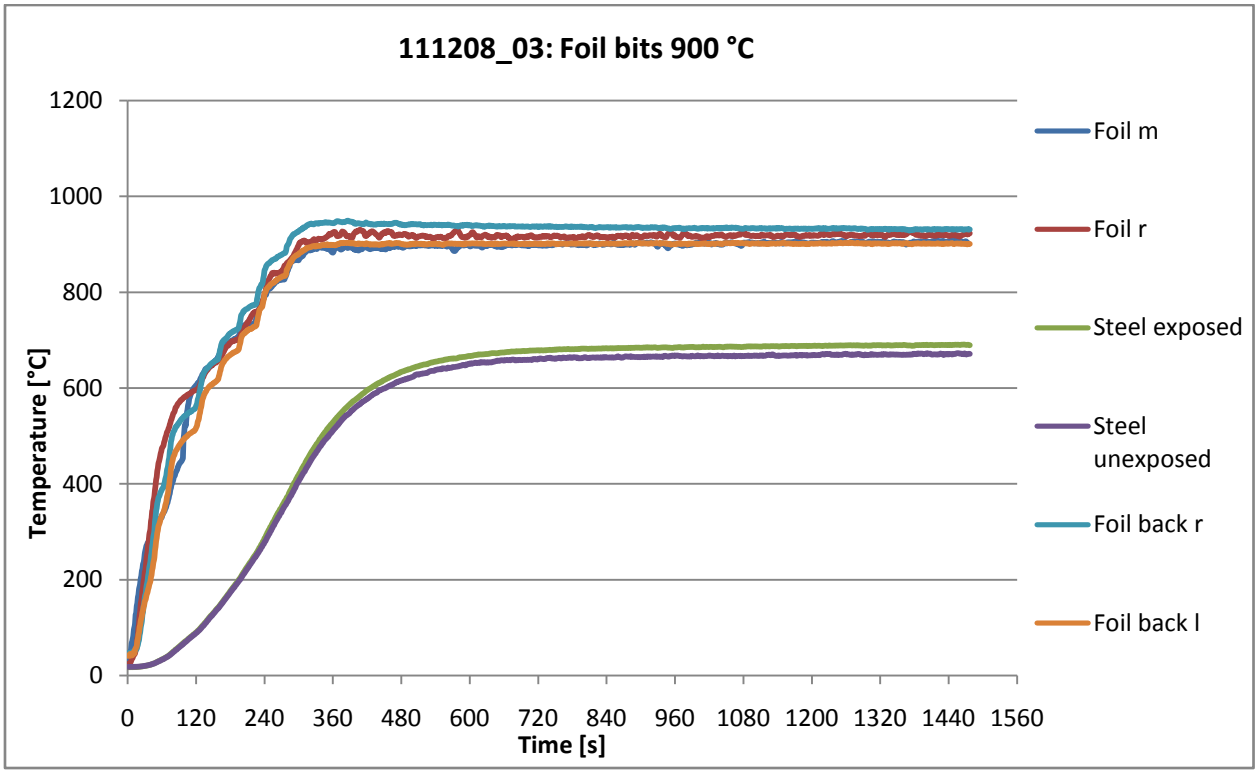

Figure 83 shows experimental values from 111208_03

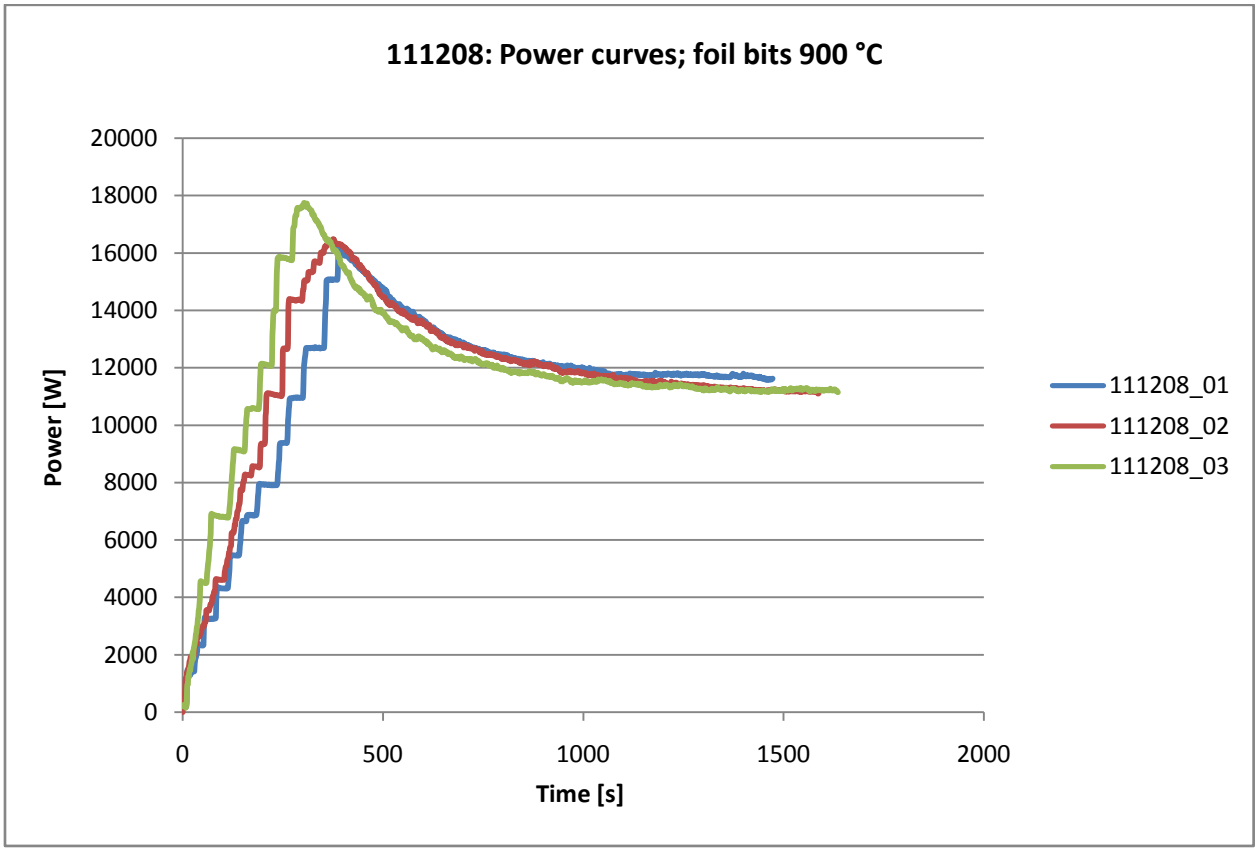

Figure 84 shows the power curves from 111208_01, 111208_02 and 111208_03

B.2 Dead materials

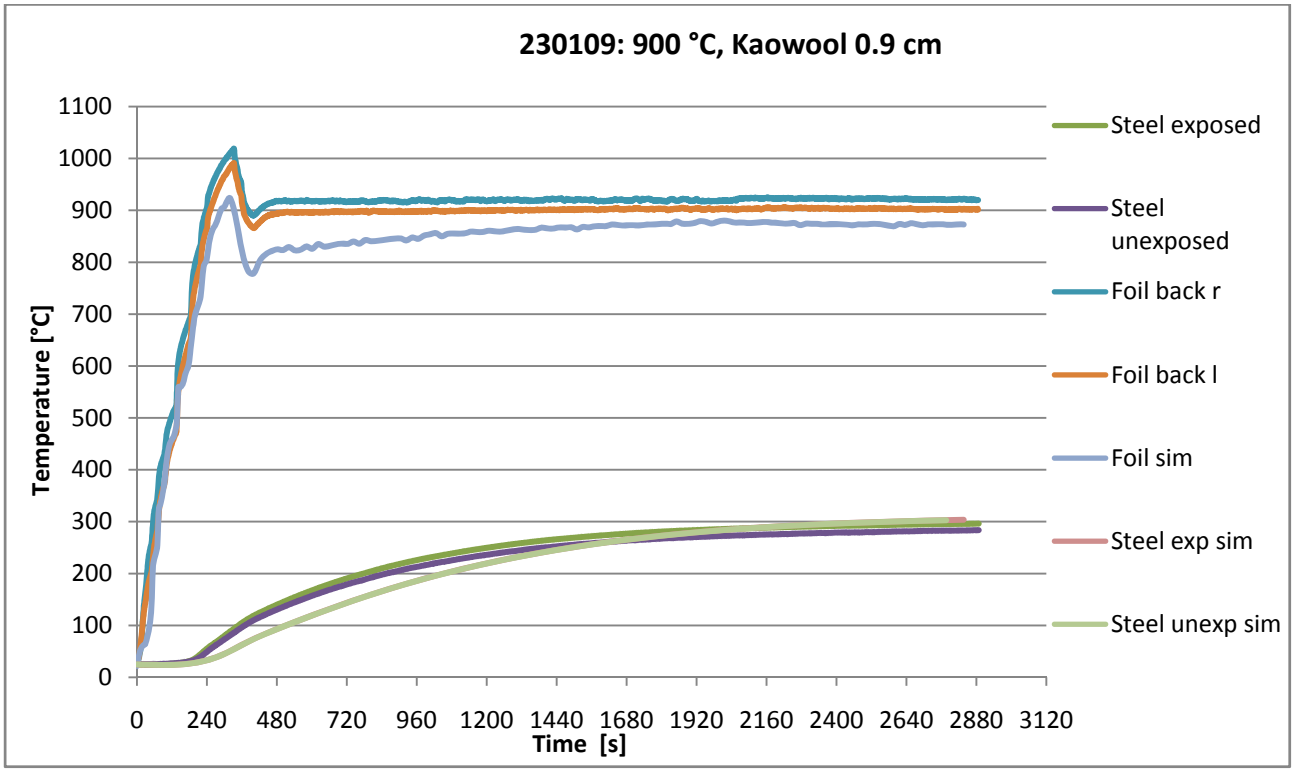

Figure 85 shows both experimental and simulated values from 230109

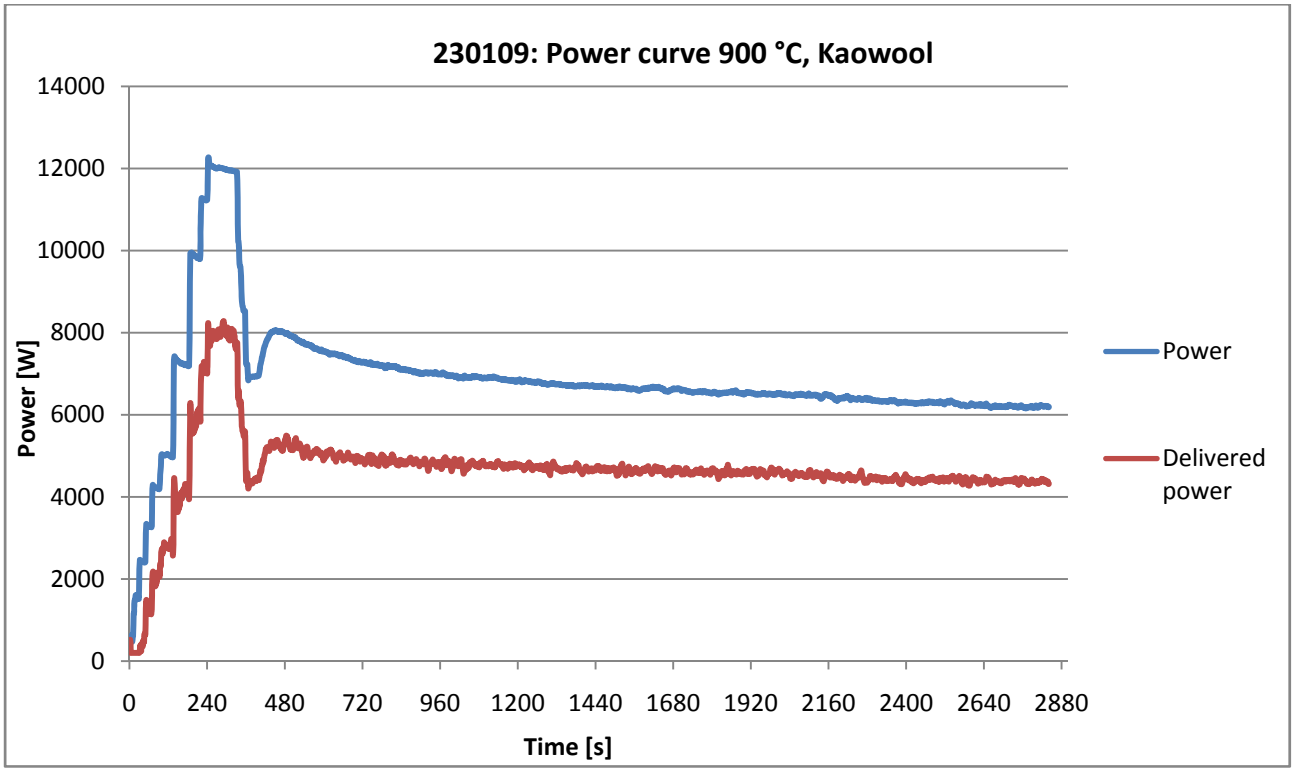

Figure 86 shows the power curve from experiment 230109

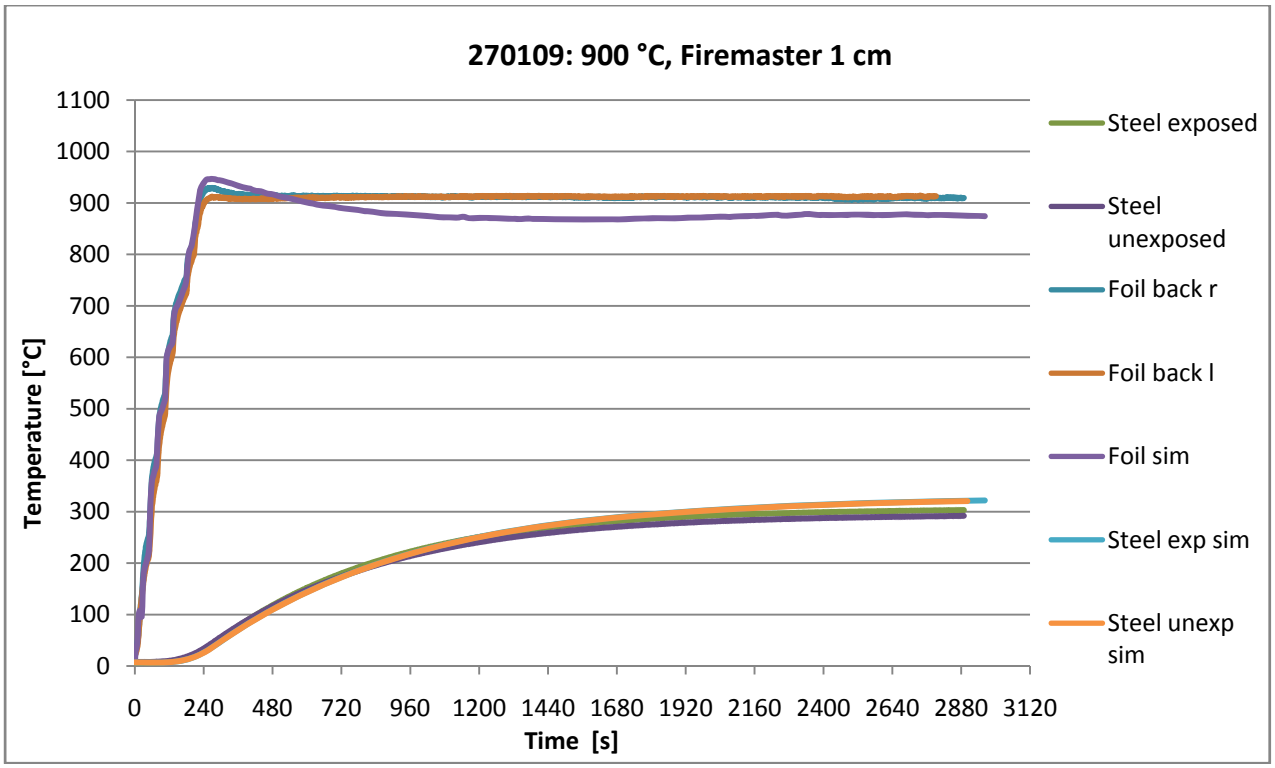

Figure 87 shows experimental and simulated values from 270109

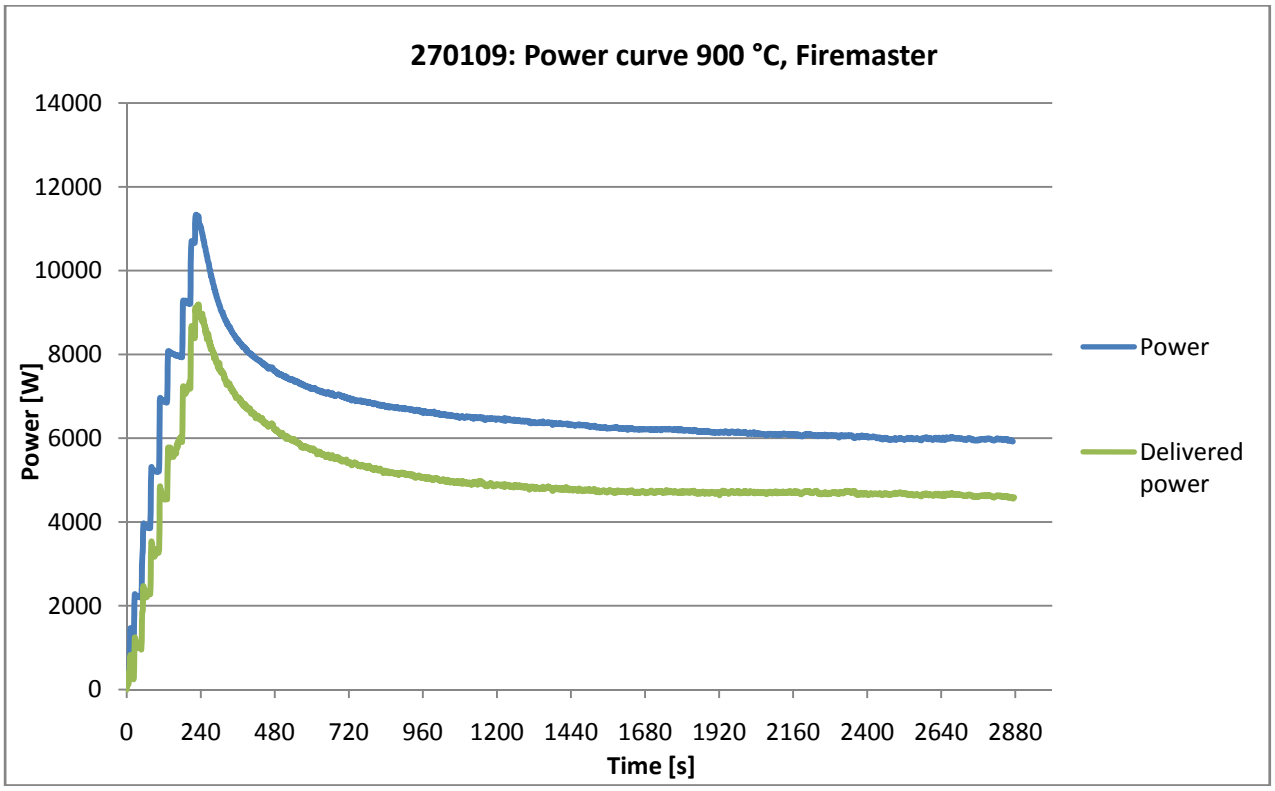

Figure 88 shows the power curve from 270109

B.3 Intumescing materials

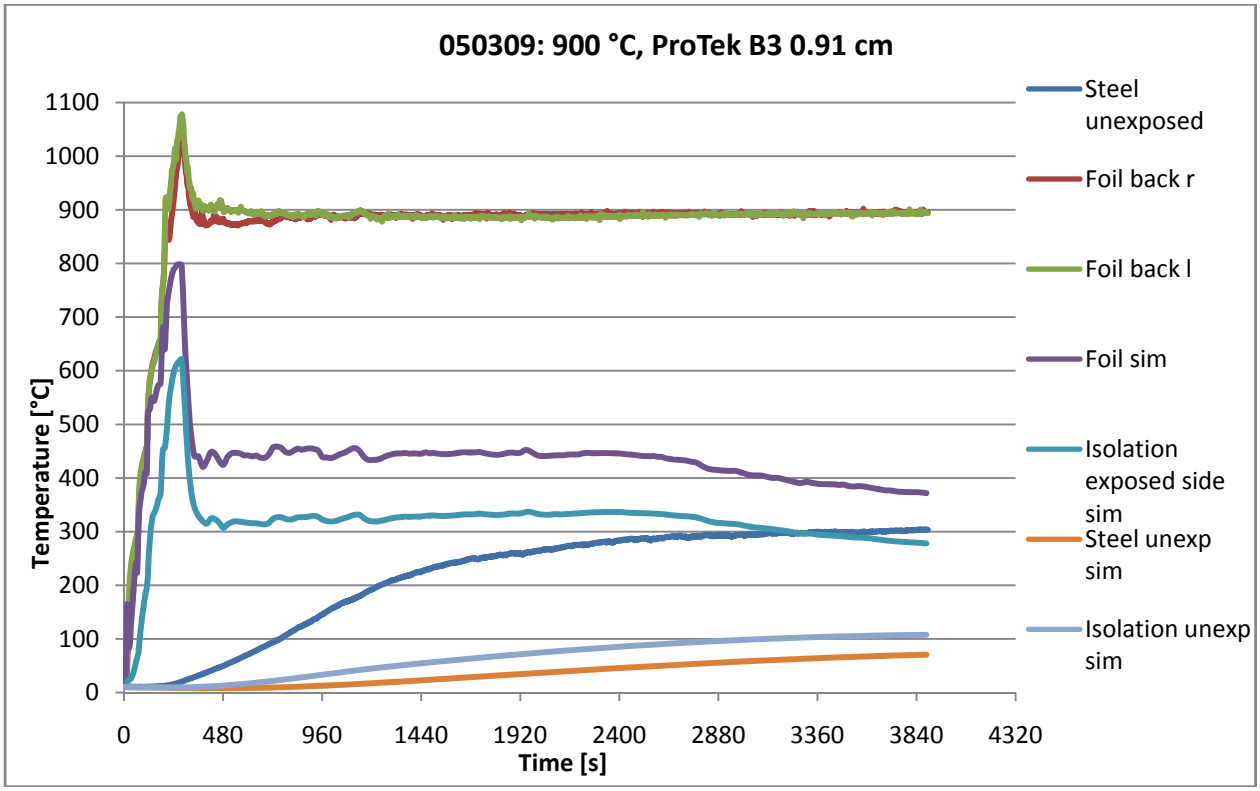

Figure 89 shows both measured values and simulated values from experiment 050309 using the delivered power from the control panel as input for the power in the simulation programme Brilliant

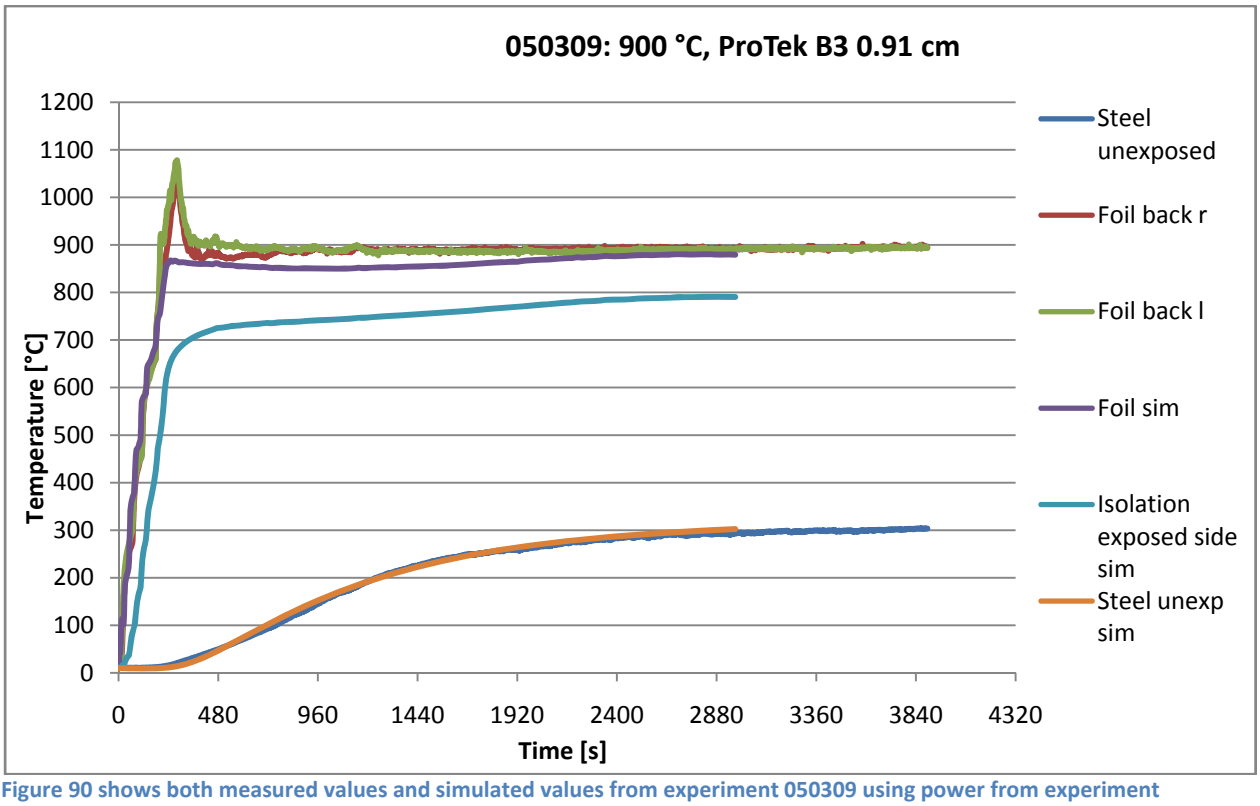

Figure 90 shows both measured values and simulated values from experiment 050309 using power from experiment 270109_02 and k-values called ProTek5

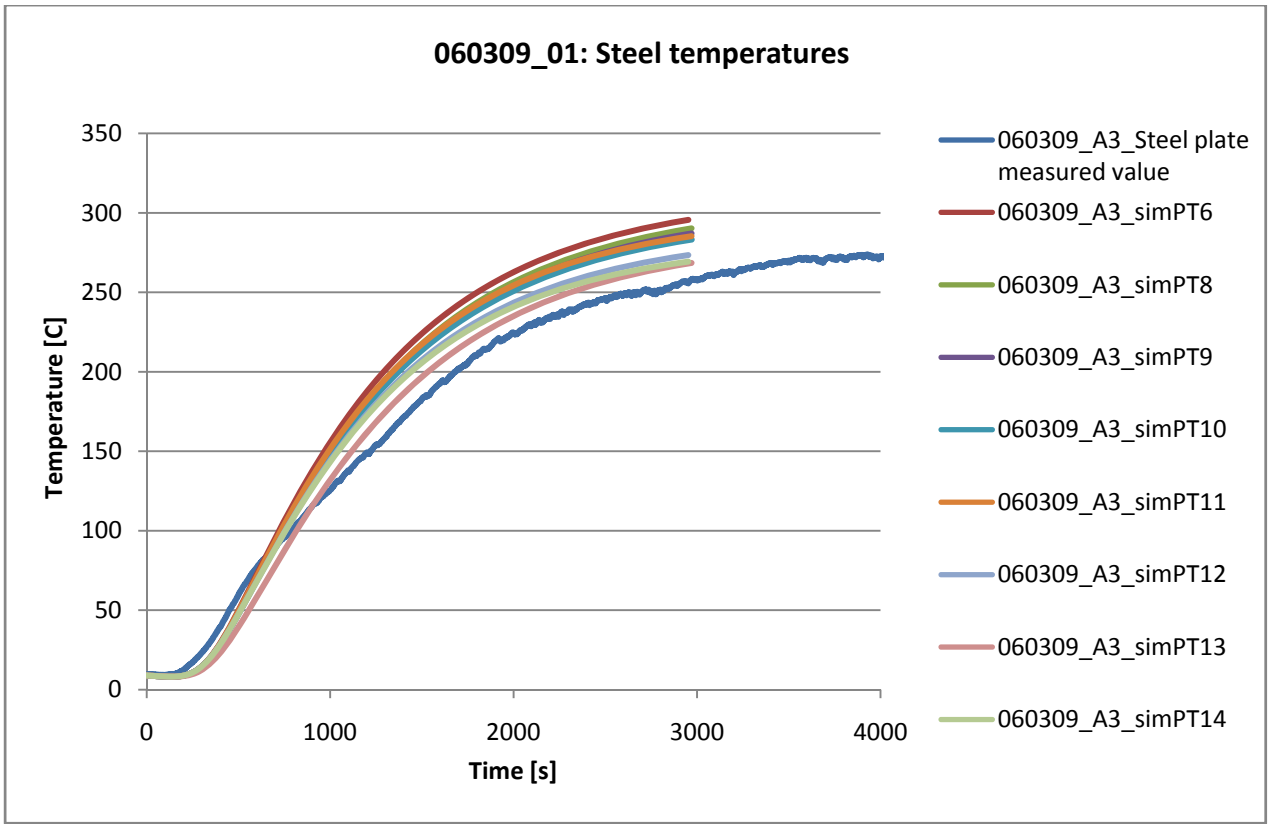

Figure 91 shows both measured steel temperature from experiment 060309_01 and all the different simulated steel temperatures done on this experiment, where the k-values on the tested isolation material were changed

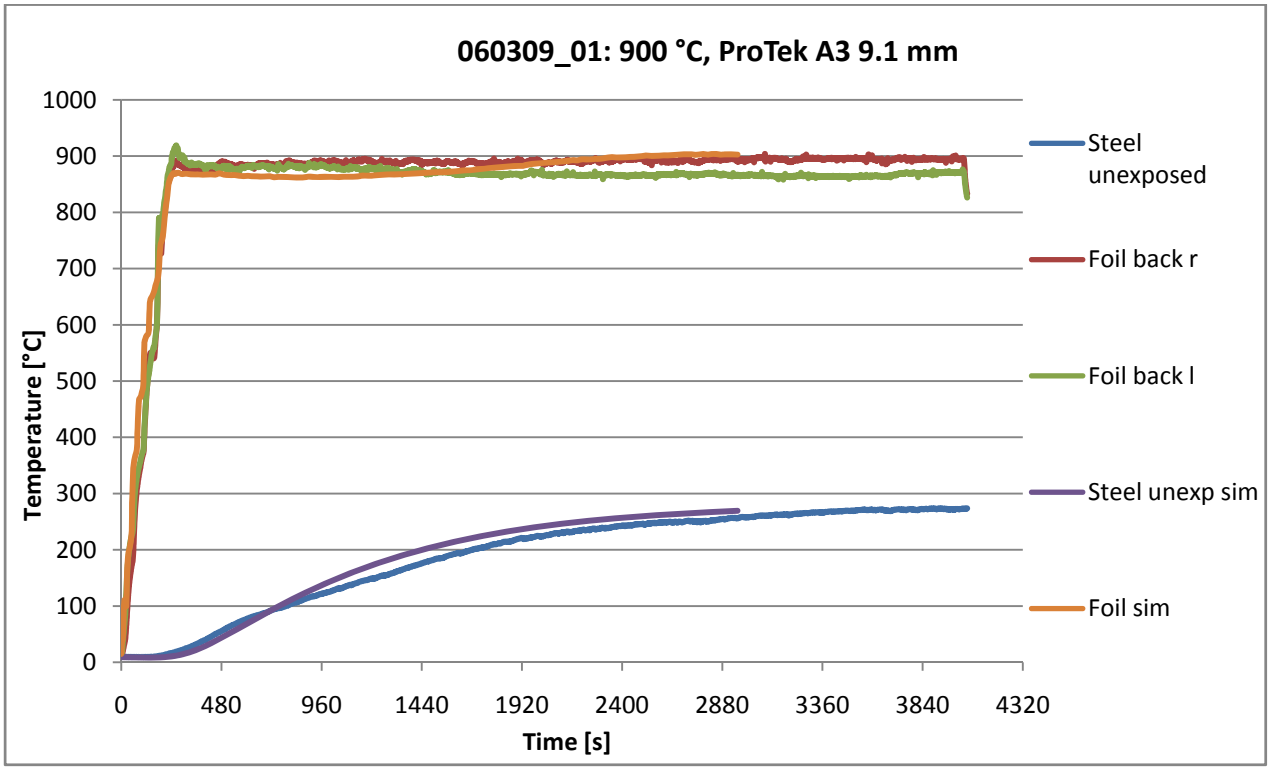

Figure 92 shows both simulated and measured values from experiment 060309_01. The simulation was carried out with power curve from experiment 270109_02 and k-values called ProTek14 as listed in Appendix G.

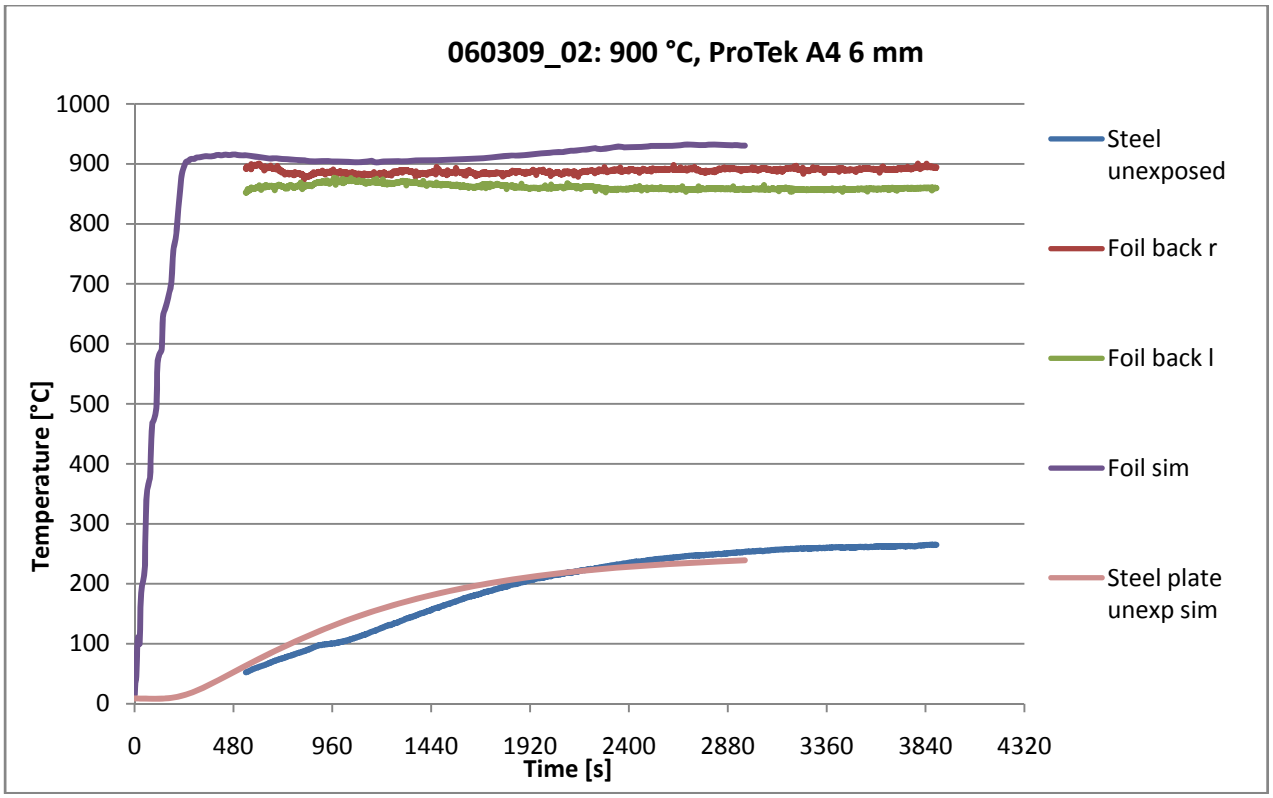

Figure 93 shows both simulated values and measured values from experiment 060309_02. In the simulation power curve from experiment 270109_02 has been used and k-values called ProTek16 in Appendix G have been used.

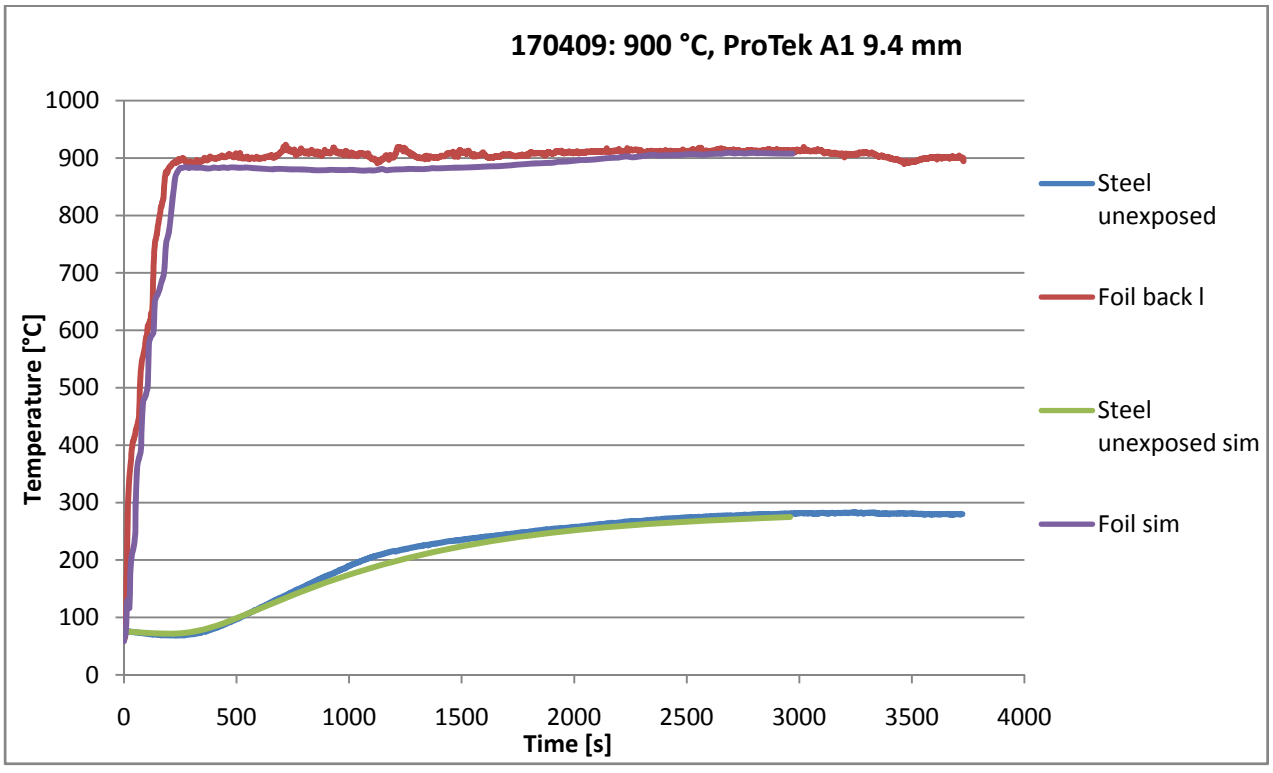

Figure 94 shows both measured values and simulated values from experiment 170409. The simulation uses the power curve from experiment 270109_02 and k-values called ProTek12 described in Appendix G.

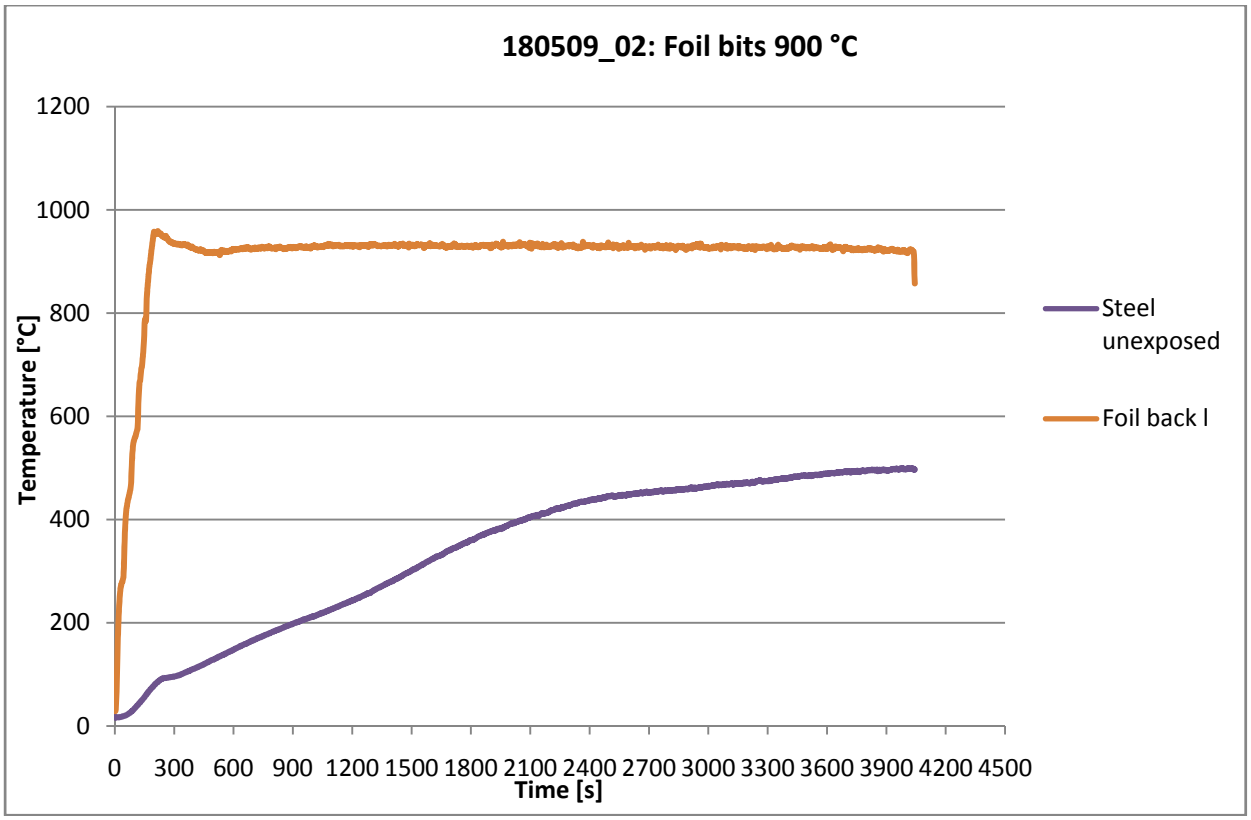

Figure 95 shows measured values from experiment 180509_02

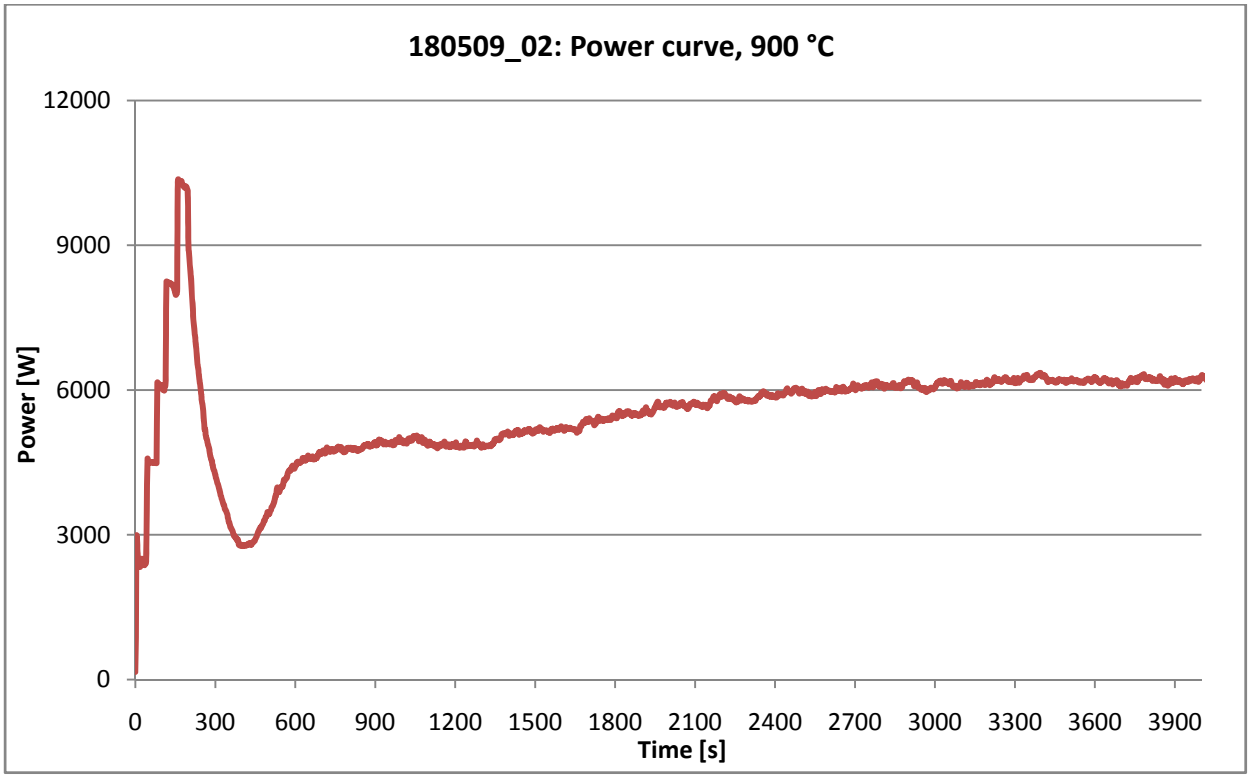

Figure 96 shows the power curve from experiment 180509_02

Appendix C – Power logging system

This appendix shows a schematic of the power logging system used when calibrating the power.

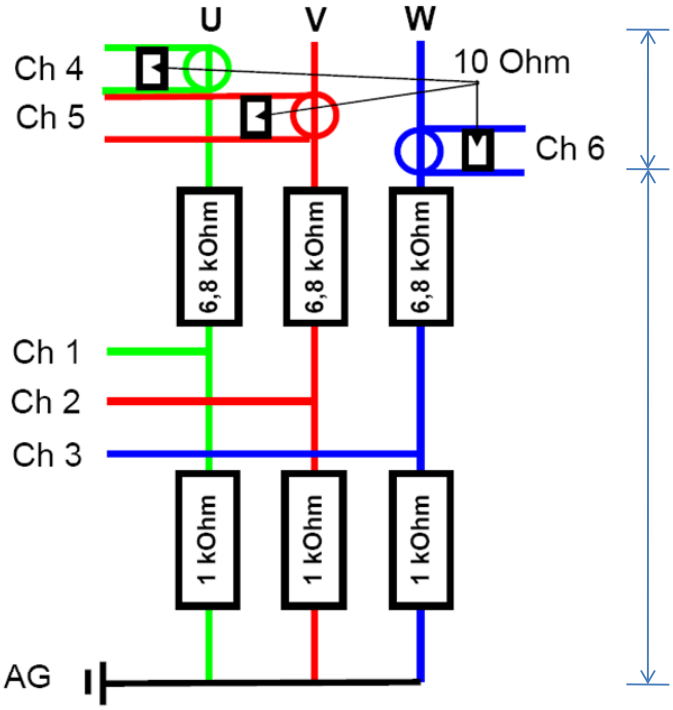

Indirect measurement of current by means of voltage measured over a resistor linked to a 5000/5 measuring transformer

Measuring voltage by means of voltage over a resistor connected in series between two phases

Appendix D – Temperature calibration data

Temperature calibration data from the calibration instrument Promac Calibrator DHT 740:

Channel	Description	Temperature	Volt signal	Temperature	Volt signal	Temperature	Volt signal
2	Foil middle	20	0,739	500	2,253	1000	3,829
3	Foil left	20	0,737	500	2,253	1000	3,829
4	Steel exposed	20	0,745	500	2,257	1000	3,83
5	Steel unexposed	20	0,741	500	2,253	1000	3,826
6	Air top	20	11,1	500	492	1000	991
7	Air bottom	20	11,4	500	492	1000	991
8	Copper T1	20	0,734	500	2,248	1000	3,822
9	Copper T2	20	0,742	500	2,256	1000	3,831
10	Copper inside	20	0,72	500	2,336	1000	3,8072
11	Foil back r	20	11,7	500	492,3	1000	991,6
12	Foil back m	20	11,5	500	492,3	1000	991,6
13	Foil back l	20	10,3	500	491,2	1000	990,5

The calculation of the different A - and B – values for the different channels are shown underneath. The channel order is the same as above.

Volt difference between 500 °C and 20 °C	A=temp.difference/ volt difference (500 to 20)	Volt difference between 1000 and 500	A=temp.difference/ volt difference (1000 to 500)	Volt difference between 1000 and 20	A=temp.difference/ volt difference (1000 to 20)	A average
1,514	317,0409511	1,576	317,2588832	3,09	317,1521036	317,150646
1,516	316,6226913	1,576	317,2588832	3,092	316,9469599	316,9428448
1,512	317,4603175	1,573	317,8639542	3,085	317,6661264	317,663466
1,512	317,4603175	1,573	317,8639542	3,085	317,6661264	317,663466
						1
						1
1,514	317,0409511	1,574	317,6620076	3,088	317,357513	317,3534906
1,514	317,0409511	1,575	317,4603175	3,089	317,254775	317,2520145
1,616	297,029703	1,4712	339,8586188	3,0872	317,4397512	318,1093577
						1
						1
						1

B=Volt signal 20°C*A-20 °C	B=Volt signal 500°C*A-500°C	B=Volt signal 1000 °C*A-1000 °C	B average
214,3743274	214,5404054	214,3698234	**214,4281854**
213,5868766	214,0722294	213,5741528	**213,7444196**
216,6592822	216,9664428	216,6510749	**216,7589333**
215,3886283	215,695789	215,3804211	**215,4882795**
-8,9	-8	-9	**-8,633333333**
-8,6	-8	-9	**-8,533333333**
212,9374621	213,4106468	212,9250409	**213,0910499**
215,4009948	215,7205448	215,3924677	**215,5046691**
209,0387375	243,1034595	211,1059465	**221,0827145**
-8,3	-7,7	-8,4	**-8,133333333**
-8,5	-7,7	-8,4	**-8,2**
-9,7	-8,8	-9,5	**-9,333333333**

Appendix E – Power calibration data

This appendix gives the power calibration data.

Effort	Test 151008		Test 171008		Average		$P_{el\ avg}$^chosen factor/$P_{volt\ avg}$	P_{effect} calculated using the formula
	$P_{electricity}$	P_{volt}	$P_{electricity}$	P_{volt}	$P_{el\ avg}$	$P_{volt\ avg}$		
0 %	0,00	0	0,000151	0	0,0002	0		0
10 %	1,14	0,1950	1,477902	0,215895	1,3102	0,2054	5,724060278	1,03237254
20 %	2,46	0,3426	2,4219	0,344277	2,4424	0,3434	4,975849776	2,430654753
30 %	4,11	0,4821	4,109977	0,481762	4,1109	0,4819	4,845942192	4,275429064
40 %	6,26	0,6250	6,552199	0,619023	6,4077	0,6220	4,900305595	6,541483167
50 %	8,84	0,7740	8,976115	0,762845	8,9082	0,7684	4,833776598	9,303736998
60 %	11,52	0,9161			11,5170	0,9161	4,730216215	12,47048774
70 %	14,89	1,0710			14,8883	1,0710	4,719840593	16,17994789

Calculating effect

$4{,}96 \times Volt^{1{,}67}$

4,961 : average value P_{el}^0,6/P_{volt}

1,667 :1/manually chosen factor

0,6: Manually chosen factor

Appendix F – Drawings of the testing furnace

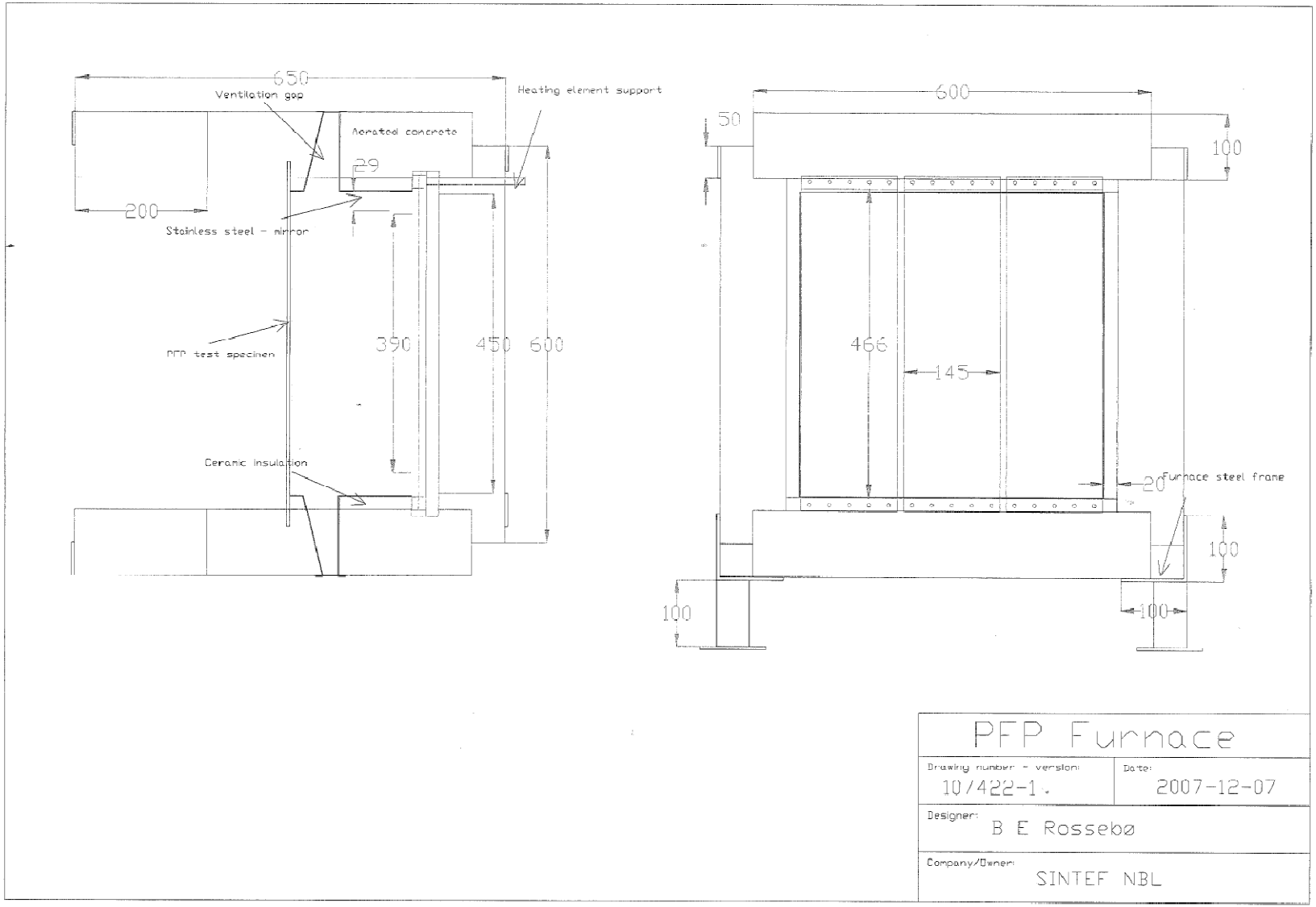

Appendix G – Overview of the k-values used in numerical simulations

This Appendix gives an overview of different k-values used in the numerical simulation programme Brilliant for the intumescing material ProTek.

ProTek 1 Temperature (K)	Conduction k (W/mK)	Density (kg /m^3)	Heat capacity (J/kgK)
293	0.03	1600	840
473	0.04		
673	0.05		
873	0.08		
1073	0.12		
1273	0.15		

ProTek 2 Temperature (K)	Conduction k (W/mK)	Density (kg /m^3)	Heat capacity (J/kgK)
293	0.04	1600	840
473	0.05		
673	0.07		
700	0.08		
773	0.085		
1073	0.12		
1273	0.2		

ProTek 3 Temperature (K)	Conduction k (W/mK)	Density (kg /m^3)	Heat capacity (J/kgK)
293	0.06	1600	840
473	0.07		
673	0.85		
700	0.09		
773	0.1		
1073	0.2		
1273	0.25		

ProTek 4 Temperature (K)	Conduction k (W/mK)	Density (kg /m^3)	Heat capacity (J/kgK)
293	0.03	1600	840
473	0.04		
673	0.07		
873	0.09		
1073	0.12		
1273	0.2		

ProTek 5 Temperature (K)	Conduction k (W/mK)	Density (kg /m^3)	Heat capacity (J/kgK)
293	0.08	1600	840
473	0.085		
673	0.09		
873	0.1		
1073	0.125		
1273	0.2		

ProTek 6 Temperature (K)	Conduction k (W/mK)	Density (kg /m^3)	Heat capacity (J/kgK)
293	0.08	1600	840
473	0.085		
673	0.09		
873	0.095		
1073	0.1		
1273	0.15		

ProTek 7 Temperature (K)	Conduction k (W/mK)	Density (kg /m^3)	Heat capacity (J/kgK)
293	0.08	1600	840
473	0.082		
673	0.085		
873	0.09		
1073	0.095		
1273	0.15		

ProTek 8 Temperature (K)	Conduction k (W/mK)	Density (kg /m^3)	Heat capacity (J/kgK)
293	0.08	1600	840
473	0.082		
673	0.085		
873	0.09		
1073	0.092		
1273	0.1		

ProTek 9 Temperature (K)	Conduction k (W/mK)	Density (kg /m^3)	Heat capacity (J/kgK)
293	0.08	1600	840
473	0.082		
673	0.085		
873	0.085		
1073	0.085		
1273	0.09		

ProTek 10 Temperature (K)	Conduction k (W/mK)	Density (kg /m^3)	Heat capacity (J/kgK)
293	0.08	1600	840
473	0.085		
673	0.085		
873	0.08		
1073	0.075		
1273	0.08		

ProTek11 Temperature (K)	Conduction k (W/mK)	Density (kg /m^3)	Heat capacity (J/kgK)
293	0.08	1600	840
473	0.085		
673	0.088		
873	0.09		
1073	0.05		
1273	0.06		

ProTek12 Temperature (K)	Conduction k (W/mK)	Density (kg /m^3)	Heat capacity (J/kgK)
293	0.08	1600	840
473	0.085		
673	0.083		
873	0.075		
1073	0.04		
1273	0.05		

ProTek13 Temperature (K)	Conduction k (W/mK)	Density (kg /m^3)	Heat capacity (J/kgK)
293	0.08	1600	1000
473	0.085		
673	0.083		
873	0.075		
1073	0.03		
1273	0.05		

ProTek14 Temperature (K)	Conduction k (W/mK)	Density (kg /m^3)	Heat capacity (J/kgK)
293	0.08	1600	840
473	0.085		
673	0.083		
873	0.075		
1073	0.02		
1273	0.05		

ProTek15 Temperature (K)	Conduction k (W/mK)	Density (kg /m^3)	Heat capacity (J/kgK)
293	0,08	1600	840
473	0,07		
673	0,06		
873	0,04		
1073	0,02		
1273	0,04		

ProTek16 Temperature (K)	Conduction k (W/mK)	Density (kg /m^3)	Heat capacity (J/kgK)
293	0,06	1600	840
473	0,05		
673	0,04		
873	0,025		
1073	0,015		
1273	0,02		

Appendix H – Overview of IMP5000 channels used

This Appendix gives an overview of the channels used in the logging system IMP 5000 when adjusting the furnace, testing dead materials and when testing intumescing materials.

IMP 5000; channels used when adjusting the furnace and when testing dead materials

1: Volt signal

2: Foil middle

3: Foil left (sometimes the foil on the right side)

4: Exposed side of the steel plate

5: Unexposed side of the steel plate

6: Air top

7: Air bottom

8: Copper T2

9: Copper T1

10: Copper inside

11: Foil bit right side

12: —

13: Foil bit left side

IMP 5000; channels used when testing intumescing materials

1: Volt signal

2: —

3: —

4: Unexposed side of the testing material if a thermocouple had already been mounted on.

5: Unexposed side of the steel plate

6: —

7: Air bottom

8: Copper T2

9: Copper T1

10: Copper inside

11: Foil bit right side

12: —

13: Foil bit left side

Appendix I – Procedure for changing the radiation foils

This appendix gives a step by step procedure for changing the radiation foil. As a procedure, when one radiation foil burn off, all the foils should be replaced. As the foils get heated, the material's properties may change. By changing all the foils at once, the foils characteristics will be the same during an experiment.

1. Remove the fuses in the "Byggstrøm" drawer, and put them on top of the distribution locker.
2. Disconnect the power cables from the copper plates
3. Detach the foils from the copper plates
4. Polish the copper plates by means of a polishing machine
5. Cut three new foils in the right dimensions by means of a shearing device
6. Drill four holes in both upper and bottom part of the foils, where the screws shall be placed
7. Fasten the copper plates to the foils. Make sure they are completely fastened with no entrapped air
8. Place the foils in the furnace
9. Fasten the copper plates to the power cables